Regulation of mitochondrial function by Myocardin during cardiac development and disease

By

Wajihah Mughal

A Thesis submitted to the Faculty of Graduate Studies

University of Manitoba

In partial fulfillment of the requirements for the degree of

DOCTOR OF PHILOSOPHY

Department of Human Anatomy and Cell Science

University of Manitoba

Winnipeg

Abstract

Metabolic specific myogenic precursors in the splanchnic, somatic mesoderm, and the neural crest give rise to specialized cell types such as cardiac, skeletal, and smooth muscle cells. This initiation of muscle cell lineage is coordinated by a reinforcing networking of transcription factors that regulate gene expression during cell proliferation and differentiation. Myocardin is a transcriptional coactivator that binds to transcription factors to regulate gene expression specific to both cardiac and smooth muscle cells. It is previously shown that Myocardin interacts with transcription factors of the MADS-Box family proteins such as myocyte enhancer factor-2 (MEF2) and serum response factor (SRF), that are known regulators of cellular differentiation and metabolism. Conversely, the role of Myocardin as well as its regulation of MADS-Box transcription factors and mitochondrial function during development and disease is not well understood. Therefore, we chose to investigate a Myocardin-regulated genetic pathway that regulates mitochondrial function in cardiac muscle that becomes dysregulated during disease.

My thesis summarizes our evaluation of the hypothesis in two studies. In the first study we characterize a mechanistic pathway involving MEF2 and SRF, that regulates mitochondrial function in all three muscle lineages. This initial study demonstrates a genetic pathway in which Nix is a direct target of miR-133a, its role in regulating insulin sensitivity and metabolic dysfunction in myocytes. These novel findings lead to my second study that examines the role of Myocardin in regulating miR-133a and Nix in cardiac cells. I provide evidence that miR−133a is a direct transcriptional target of Myocardin that regulates mitochondrial permeability transition to preserve cell survival during cardiac development and following myocardial ischemic injury.

Together, these findings inform researchers about the vital role of a Myocardin-regulated pathway that maintains mitochondrial function to oppose cell death during development as novel pharmacotherapy targets. Ongoing investigation is required to further understand miR-133a function as a potential cardiometabolic biomarker or as a therapeutic intervention for the prevention and/or treatment of congenital heart defects, cardiometabolic disease and heart failure.

Dedication

This thesis is dedicated

to my parents, Dost and Rehana Mughal, to my siblings and loved ones

for their continuous love, encouragement, support and guidance,
whose sacrifices made it possible for me to complete this work,
and without whom none of my success would be possible.

to my chand, Jason Van Zwol

for being an incredible husband,
for being the rock in my life,
for always encouraging me to be myself,
for supporting me emotionally and mentally,
and for loving me unconditionally since the day we met.

to my supervisor Dr Joe Gordon and mentors

for supporting my research goals and enthusiasm for science

to my fellow trainees

for their friendship that will last beyond grad school

and lastly, this thesis is dedicated to
the women in science

we all move forward when
we recognize how resilient
and striking the women
around us are

- rupi kaur

Acknowledgements

I would like to express my deepest gratitude and sincerest appreciation to my doctoral supervisor, mentor and career advisor, Dr Joseph Gordon. His limitless support, guidance, motivation, and friendship has greatly inspired me throughout my journey as a grad student. However, his mentorship started four years earlier during my masters studies while he was completing his post-doctoral fellowship. Early on, I saw many qualities in him that would make him an outstanding investigator, not knowing that I would be become his trainee one day. It is an honour that he took me under his wing, saw potential in me and had confidence in my skills as his first PhD student.

Joe's outstanding supervision, leadership, honesty, research enthusiasm, down to earth and caring personality, combined with our shared amusement for corny science jokes ("it Hoechst don't it?") has made this difficult rollercoaster of a journey a fun and unforgettable one. I will be forever appreciative and thankful for his shared wisdom and knowledge of literally everything and for supporting my research directions. I am thankful for how he would challenge and push me beyond my boundaries to think critically. I am thankful that he saw my potential as a cell biologist that has allowed me to advance my technical skillset, research knowledge, writing and presentation style under his supervision.

My supervisor has inspired me to pursue my goals, work with dedication and determination no matter what hurdles I had to face. His confidence in me has allowed me to persevere through many challenges that has led to my personal growth and professional success. Under his supervision and mentorship, my research was provincially funded, published in prestigious journals, presented at multiple international conferences, which has allowed me

to complete my thesis within a timely manner. My supervisor has always allowed for my career growth which is best demonstrated by his full support when I was applying for my Mitacs position and how he helped me prep for my interview. Joe has taught me some incredible life lessons that I am forever grateful for: he has always emphasized the importance of balancing work and personal life, to recharge when needed, and encourage creativity. While being my advisor and good friend, I can strongly assert that each and every supervisor should have qualities like Joe; he is the most outstanding mentor any student at any academic level could ask for. The completion of this work would not have been possible without his continuous support and guidance.

I would like to extend my gratitude to my doctoral advisory committee members, Dr Thomas Klonish, Dr Ian Dixon, and Dr Saeid Ghavami, for their constant encouragement and support throughout my studies. I am also thankful to my external examiner, Dr Lynn Megeney, for his time in travelling to attend my defense and offer his valuable insight to my research project. It was an honour and a memorable experience to defend my thesis to such an esteemed committee panel.

The studies presented in this document were supported by many collaborators that made it possible to publish our research whom I am very thankful for. This includes Dr Michael Parmacek from the University of Pennsylvania, Dr Ian Dixon from St. Boniface Research Centre, and our multiple collaborators from the Children's Hospital Research Institute including Dr William Diehl-Jones, Dr Vern Dolinsky, Dr Richard Keijzer, Dr Grant Hatch, and Dr Adrian West.

I would also like to thank Research Manitoba (formerly MHRC), the Children's Hospital Research Institute (CHRIM), the University of Manitoba's Faculty of Graduate Studies, and the Diabetes Research Envisioned & Accomplished in Manitoba (DREAM), for financially supporting this research project. I was also fortunate to receive many poster, travel, and research awards from various funding organizations for which I am very grateful for.

For the past and present members of the Department of Human Anatomy and Cell Science administrative staff, including Jennifer Genest, Jacki Armstrong, and Martha Ericastilla, I am appreciative of their support and for keeping things fun between seminars/deadlines.

I am forever grateful for the healthy and supportive lab environment that has had a very positive impact on my quality of research, success and productivity. I am fortunate to belong to a lab family that has gone above and beyond in supporting this work. I greatly appreciate our easy-going and exceptionally skilled technician, Donald Chapman, for his friendship and for being an integral part of the research presented in this thesis. I appreciate the days we spent in the cold room crushing tissues and I still remember our first time isolating neonatal hearts together (we are heart breakers). I appreciate all the times I spent with a good friend and fomer technician, Dr Yan Hai, for her kind heart and patience in teaching me highly difficult skills; whose presence and positivity brightened up the lab every day.

I am grateful for my lab mates, Matthew Martens and Jared Field, for their friendship, and random lab banter that always kept things interesting in the lab. I am grateful for the time we spent at our first conference in San Diego at EB, all the work they put into getting the

Myocardin manuscript out, and how they spent time awat from their research to help me prepare for my dissertation. We didn't get a long at first, but I am grateful for their support, friendship, and for making the lab such an enjoyable environment to learn in. I am thankful to Simone da Silva Rosa for her work ethic, her enthusiasm for science and for being among my first summer students in the lab. I am also appreciative of many past members of the Gordon lab including Adrian Ancheta, Alyssa Archibald, Lucas Nguyen, Steven Piotrowski, Tayna Fiuza, and Adel Rezai Moghadam, for being wonderful colleagues and their contributions towards this work.

I am extremely appreciative of Stephanie Kereliuk, my PhD soul sister, for her unconditional friendship, guidance, and continuous support. Every grad student should have a friend like her; she has always encouraged me to do my best, and always reminded me that I could do anything, but I just had to be myself. There aren't enough words to describe how she has been such an important and exceptionally positive part of my grad school experience, and I know our friendship will last for many years ahead. I am very fortunate that I had someone like her to lean on as a colleague, a friend, and a confidant. I am also thankful for her constant enthusiasm and support once I started working full-time off campus, and how she was always there for me when it came to prepare for my dissertation and defense #womeninscience. It was a pleasure to work alongside with Stephanie on the DREAM Trainees committee and organize research events together; our best ideas always came from our coffee breaks at Starbucks or during our infamous happy hour events on campus. I am also grateful to my fellow DREAM trainees for their friendship and the fun memories made we made over the years, especially during the DREAM-Eve networking events.

The pillar in my life that has given me the strength and encouragement to pursue this work is my family and my loved ones. There are no words to truly express how thankful I am for my parents, for their love, sacrifices, and for their constant support in my life that has allowed me to reach my goals and do things I didn't think I could. Mom, my Ammi, thank you for your unconditional love, your duaas and prayers, and for always being proud of me no matter what. Thank you for always encouraging me to do my best, and most importantly, for always believing in me. Thank you for always nurturing and looking after me, for making sure I was fed when I was so focused on my studies. Dad, I hope you are proud to see the woman I have become today and everything that I have accomplished. Thank you for everything you have taught me since I was a little girl and for always supporting my education at every stage. Your constant motivation continues to inspire me to be the best I can be; thank you for seeing my potential when I couldn't. To my parents, I hope I have made you as proud as I am to call you my parents; I love you so much.

My parents have always supported and acknowledged my success, but my siblings have done a wonderful job at keeping me grounded. Thank you to my sister, Madiha, and my brother, Samad, for always roasting me whenever you had the opportunity (there weren't many). But in all seriousness, thank you to both for tolerating me as your annoying older sister, but also for being there for me through the ups and downs. Samad, thank you for being the bratty brother you have always been, but also for sharing your food and supporting me at every turn. Madiha, you are my best friend and hold a very special place in my heart: thank you for being my strength in life and for being the person I could turn to for anything. Thank you for listening to my practice presentations, and for coming to the lab late at nights or on the weekends with me so I wouldn't have to be there alone. Thank

you for being there through all the tears and laughter, for taking care of our cats; I couldn't have accomplished this without you.

I am extremely fortunate to have found my soul mate, my life partner and my number one supporter as my husband, Jason Van Zwol. Your unconditional love, dedication to our relationship and utmost understanding has allowed me to pursue both my academic and personal goals. Completing my studies with you by my side as my right hand has made this journey so fun and I cannot thank you enough for all that you have done for me. Jason, thank you for always telling me to focus on school because it came first that has allowed me grow into the woman I am today. I will always remember and appreciate you for all the dinners you cooked for us that I couldn't help with because I had to study. Thank you for taking the time to watch me in action during my thesis defense; it was such an honour to see you in the crowd and that smile. Thank you for always loving me through the thick and thin, and for always finding ways to make me smile no matter what. As your wife I look forward to the future waiting for us and TBX5.

Table of Contents

List of Figures

Literature Review

Manuscript I

Manuscript I - Supplemental

Manuscript II

Manuscript II – Supplemental

Dissertation Summary

Additional Data

List of Tables

List of Abbreviations

AIF	Apoptosis inducing factor
ANF	Atrial natriuretic factor
Bcl-2	B-cell lymphoma-2
CDKO	Cardiac specific double knockout
CML	Cardiomyocyte-like
Co-IP	Co-immunoprecipitation
DCM	Dilated cardiomyopathy
DGKδ	Diacylglycerol kinase-δ
DNMT	DNA-methyltransferase
Dox	Doxorubicin
EMSA	Electrophoretic mobility shift assay
ERK1/2	Extracellular regulated kinases-1/2
FGF	Fibroblast growth factor
FOXO	Forkhead box, class O
GMT	GATA4-MEF2C-TBX5
GSK3β	Glycogen synthase kinase-3β
HAND2	Heart and neural crest derivate-2
HAT	Histone acetyltransferases
HDAC	Histone deacetylases
HERP1	Homocysteine-responsive endoplasmic reticulum-resident-1
HFS	High fat and sucrose diet
HMT	Histone methyl transferase
JAG1	Jagged-1
JAK-STAT3	Janus kinase inhibitor – signal transducer and activator of transcription-3
JMJ-KDM	Jumonji-domain-containing demethylases
KDM	Histone lysine demethylase
KLF4	Kruppel-like transcription factor-4
MADS-box	Mcm1Agamous Deficiens SRF
MAM	Mitochondrial associated membrane
MASTR	MEF2-activating SAP transcriptional regulator

MEF2	Myocyte enhancer factor-2
miR-133a	microRNA-133a
MKL1	Megakaryoblastic leukemia-1
MRTF	Myocardin related transcription factor
Myocd	Myocardin
NFATc3	Nuclear factor of activated T-cells c3
Nix/Bnip3L	BCL2/adenovirus E1B 19 kDa protein-interacting protein 3-like
Nkx2.5	Nk2 homeobox-5
Pax	Paired-box transcription factor
PKCδ	Protein kinase C δ
PTP	Mitochondrial permeability transition pore
SIK1	Salt-inducible kinase-1
SM-MHC	Smooth muscle myosin heavy chain
SM22	Smooth muscle protein-22
SMA	Smooth muscle α-actin
SRC3	Steroid receptor coactivator-3
SRF	Serum response factor
SUMO	Small ubiquitin-like modifiers
TAD	Transactivating domain
TBX5	T-box 5
Tg	Transgenic
$TGF\beta_1$	Transforming growth factor-$beta_1$
TMRM	tetramethylrhodamine
UBR5	Ubiquitin ligase E3 component n-recognin-5
UPR	Unfolded protein response
VSMCs	Vascular smooth muscle cells

CHAPTER I: Literature Review

1.1 Mammalian Cardiac Development

By some estimations, 221 infants born in Manitoba over the past year are affected by congenital heart defects, including underdeveloped cardiac chambers and atrial/ventricular septal defects impairing infant circulation. These cardiac anomalies can range from acute or non-life threatening that can sometimes go undiagnosed, to the most severe requiring surgical intervention contributing to the national Canadian infant mortality rate (1). With medical advancements in the last two decades greatly improving rates of infant survival, these children are able to transition from adolescence to adulthood. However, these young adults are at a greater risk of developing a variety of disabilities requiring multiple hospitalizations and make up to two thirds of the population living with congenital heart disease in US and Canada (1,2).

Advancements in our understanding of the pathology and treatment of congenital heart defects have been made in both basic and clinical research improves patient health and quality of life (3,4). However, the cause of congenital heart defects still remains unknown and medical therapies fail to prevent the progression of congestive heart disease to heart failure. Therefore, to improve cardiomyocyte function and treat congestive heart disease, researchers must investigate the dysregulation of molecular signals that occurs during cardiac development (5-8).

1.1.1 Cardiac development

The heart undergoes early embryonic cellular differentiation that is conserved among mammals; however my timeline outlines the beginnings of mouse cardiac development (5,9). Myogenic precursors in the splanchnic and pharyngeal mesoderm, and neural crest are responsible for the initiation of multiple cell lineages. This includes specialization of cardiac progenitor cells

or myocardial cells as early as embryonic day 6.5 (E6.5) that differentiate to form a 4-chambered heart (Figure 1) (5,7). Myocardial cells migrate and differentiate at embryonic regions referred to as the first and second heart fields (5,7). At E7.5, the first heart field forms the cardiac crescent that is positioned laterally to the second heart field; with contribution from the secondary heart field, the cardiac crescent fuses to form a linear heart tube by E8.0. The heart tube consists of cardiomyocytes and endothelial cells that begin to initiate a primitive heart beat (comparable to the third week of human gestation). In contrast, myocardial cells from the second heart field migrate to form the right ventricle and cardiac outflow tract. Similarly, neural crest-derived cells also contribute to form the outflow tract. Rightward looping of the heart tube at E8.5 brings the inflow and outflow components towards the anterior pole of the heart. This is followed by uneven cardiac growth and remodelling to form the primitive chambers at E10.5. Cardiomyocytes continue to proliferate and begin to have a strong electrical conduction velocity by E12.5. At E15, both myocardial and neural crest-derived cells contribute to cardiac septation, differentiate into vascular smooth muscle cells to form the aortic arch arteries, contributing to heart maturation (comparable to the seventh week of human gestation) (5-7).

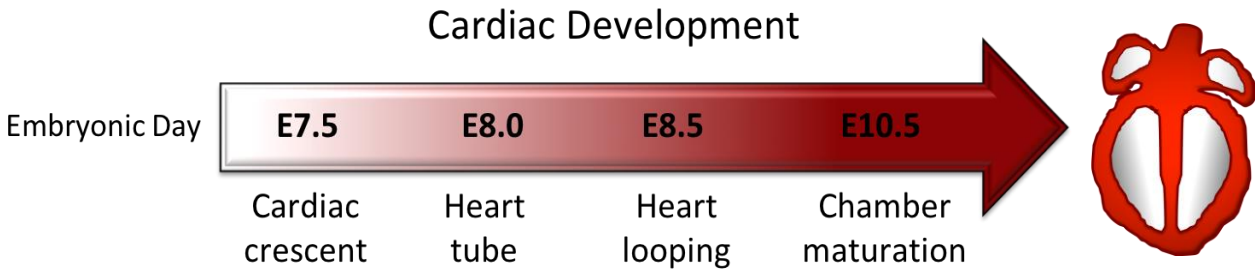

Figure 1: Stages of mammalian embryonic cardiac development to a 4-chambered heart.

1.1.2 Cardiac Transcription Factors

Development of the heart is a process coordinated by a precise network of transcription factors that orchestrate cardiac induction, specialization and heart maturation (7,10). Inductive cardiogenic signals including bone morphogenetic protein (BMP), Notch, Wnt and sonic hedgehog (SHH) activate downstream cardiac transcription factors (Figure 2) (7,10). Other induction signals such as Wnt, BMP, and fibroblast growth factor (FGF) trigger downstream activators including paired box 3-7 (Pax3/5) for inducing neural crest-derived cells during cardiogenesis (11). In the first heart field, cardiogenic signals activate GATA4, Nk2 homeobox-5 (Nkx2.5) and T-Box 5 (TBX5) that regulate downstream genes involved in cardiac muscle growth and differentiation. Mutations in this transcription factor triad have been reported to cause various human congenital heart defects such as ventricular septal defects (6,12). With a dual function, GATA4 also activates regulates transcription factors involved in the secondary heart field, including heart and neural crest derivate-2 (HAND2) and myocyte enhancer factor-2 isoform C (MEF2C). Together these transcriptional signals regulate cardiac muscle genes that promote the cardiac outflow tract formation and cardiac chamber maturation (5-7).

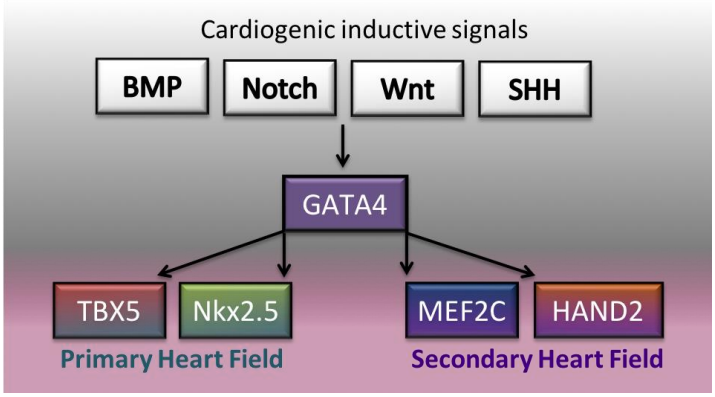

Figure 2: Cardiogenic transcription factors underlying mammalian heart development

1.1.3 Cardiac Reprogramming

As the heart is maturing into a 4-chambered organ, it consists of cardiomyocytes that have a limited regenerative capacity. To compensate for this limited cellular life span, an emerging technology called direct cardiac reprogramming is being used to generate new and functional cardiomyocytes. A transcriptional cocktail of GATA4, MEF2C and TBX5 (referred to as GMT) was first shown to reprogram mouse fibroblasts into cardiomyocyte-like (CML) cells but results in a low expression of contractile proteins (13). To overcome this limitation, GMT in the presence of Myocardin was found to greatly enhance cardiac reprogramming, and induce a broader range of cardiac genes including contractile proteins in comparison to the original GMT cocktail (Figure 3) (14). The addition of Myocardin with GMT induces a more efficient reprogramming of human adult fibroblasts into CML cells (15), and directs the cardiac differentiation program in both human dermal fibroblasts (16) and adult cardiac stem cells (17).

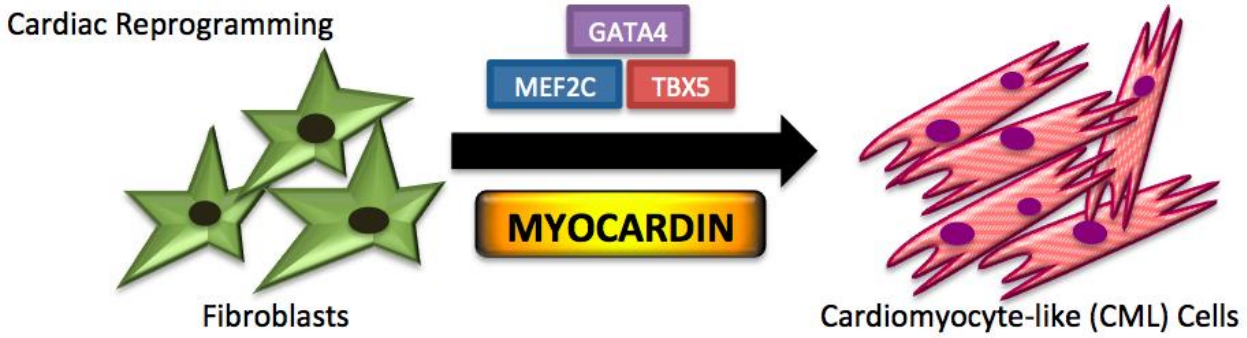

Figure 3: Molecular cocktail (GMT + Myocardin) reprogramming of human fibroblasts into cardiomyocyte-like cells

Such evidence highlights Myocardin as a molecular player in mediating cardiac reprogramming of fibroblasts but its ability to regulate fibroblast function is not well understood.

Recent studies report Myocardin overexpression mediates myofibroblast differentiation and regulates collagen expression in liver fibroblasts, yet these observations have not been documented in cardiac fibroblasts. (18,19). In contrast to Myocardin's limited role in fibroblasts, the Myocardin-related transcription factors (MRTFs), members of the Myocardin family discussed in a latter section, have a well reported role in regulating fibroblast function (20,21). Due to its limited function and lack of expression in fibroblasts, Myocardin has been most extensively studied in cardiac and smooth muscle cells.

1.2 Myocardin Biology

1.2.1 Discovery

The pioneering work on Myocardin's role during development was orchestrated by two independent research laboratories. In 2001, Eric Olson's post-doctoral fellow at the time, Dha-Zhi Wang, performed a bioinformatics screen using a BLAST search on expressed sequence tag databases on mouse cardiac muscle cDNA (17). Wang's computational approach led to the discovery of a new cardiac protein named Myocardin, for its specific expression in adult mouse myocardium and embryonic mouse cardiac tissue, as visualized by northern blots and in situ hybridization. The seminal findings demonstrate Myocardin expression as early as E7.75 in the cardiac crescent and linear heart tube, that progressed to the atrial and ventricular chambers by E11.5. Myocardin is also expressed in vascular smooth muscle tissue including the aortic arch arteries and pulmonary outflow tract from E13.5 to E15.5. In contrast, there were no detectable levels of Myocardin in skeletal muscle (17), further validating its specific expression in cardiac and smooth muscle.

1.2.2 Characterization of a Co-Activator

To extend the findings of Myocardin expression in the embryonic heart, domain mapping studies reveal Myocardin belongs to family of nuclear proteins consisting of a SAP-domain (named for nuclear scaffold attachment factors A/B), a 35-amino acid motif that recognizes chromosomal regions to regulate gene expression (17). Mutational analysis of the transactivating domain (TAD) combined with luciferase assays and GAL4-fusion constructs reveal Myocardin's ability to act as a potent transcriptional co-activator: a C-terminus Myocardin mutant containing the TAD (541-807 region; MyocdΔCT) has a 60-fold promoter activation in comparison to Myocardin wild-type, as assessed by luciferase fold activation normalized to B-galactosidase (17). Since then, transcriptional studies have led to Myocardin being described as "one of nature's titanic transcriptional coactivators" (22,23). Alternatively, generating mutations within the TAD region reversed this effect. Wang et al were able to map the TAD and illustrate Myocardin's transcriptional coactivation of CArG-Box dependent promoters with 1) Gal4, and 2) CArG luciferase studies (CArG-Box will be defined in a latter section) (17).

As Myocardin does not bind DNA, protein-DNA analysis using electrophoretic mobility shift assays (EMSA) combined with protein interaction assays using co-immunoprecipitations (co-IPs) confirm Myocardin's role as a transcriptional co-activator. Using radioactive labeled oligonucleotides during an EMSA, authors show serum response factor (SRF) binding to CArG-box, but Myocardin expression alone had no effect. With co-expression of Myocardin and SRF, an antibody shift was visualized: a larger complex was formed that migrated slower or ran higher, resulting in an upward shift, detecting a ternary complex of Myocardin/SRF/CArG-Box (17). In contrast, using a Myocardin mutant reversed the antibody shift. These findings reveal Myocardin co-activation is mediated in the presence of SRF to form a ternary complex with DNA. Protein

interaction analysis further confirm Myocardin's interaction with SRF: the N-terminus of Myocardin binds to the MADS-box region of SRF (17).

Studies first identified Myocardin's role in co-activating SRF, a muscle-enriched, but ubiquitous transcription factor involved in early gene expression during cardiogenesis (24,25). SRF belongs to the MADS-Box family [named for its four founding eukaryotic members: MCM1 (yeast), Agamous (plant), Defa (plant) and SRF (human)] and homodimerizes to a specific DNA sequence called the CArG-Box [$CC(A/T)_6GG$] (17). SRF directly binds DNA to regulate genes in multiple cell types including skeletal, smooth and cardiac muscle. This is driven by the recruitment of various transcriptional cofactors forming a ternary complex with SRF and the CArG-Box (17). As a co-activator, Myocardin binds SRF and serves as a central hub for the regulation of cardiac muscle (atrial natriuretic factor, ANF) and vascular smooth muscle (smooth muscle protein-22, SM22) gene expression (Figure 4) (17). It is important to note that SRF does not form a CArG-Box dependent complex with other cardiogenic transcription factors such as Nkx2.5 or GATA4 (17).

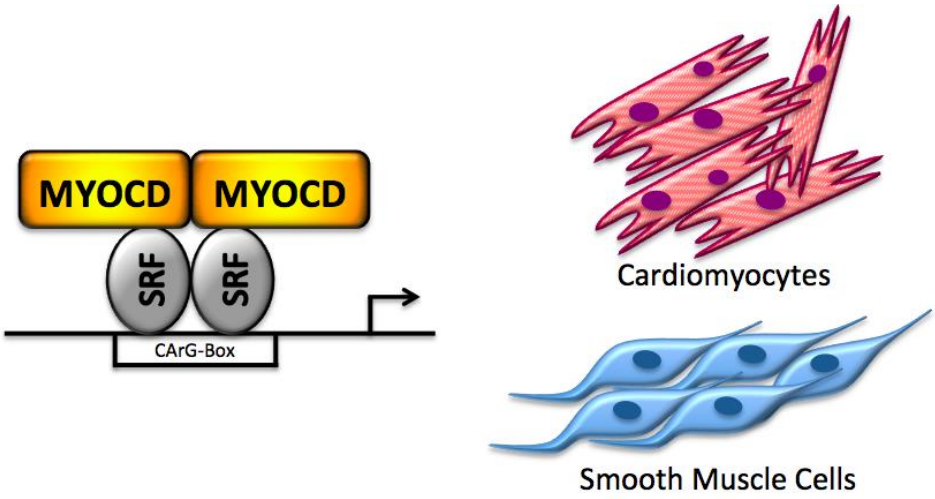

Figure 4: Myocardin, a transcriptional co-activator, forms a ternary molecular complex with SRF and CArG-Box to regulates gene expression in cardiac and smooth muscle.

1.2.3 Alternatively Spliced Isoforms

To elucidate the dual role of Myocardin in regulating cardiac and smooth muscle-specific gene expression, Creemers *et al.* identified two alternatively spliced isoforms: Myocd-856 and Myocd-935 coactivate SRF to regulate CArG-Box dependent target genes (Figure 5) (26). The inclusion of exon 2a of the Myocardin gene generates a downstream stop codon and an alternative ATG start codon in exon 4, resulting in a shorter 856-amino acid variant (Myocd-856 or Myocd-B) that is smooth muscle specific (26). In contrast, the exclusion of exon 2a generates a longer 935-amino acid isoform (Myocd-935 or Myocd-A) that coactivates both SRF and MEF2 to regulate cardiac gene expression (Figure 5) (26).

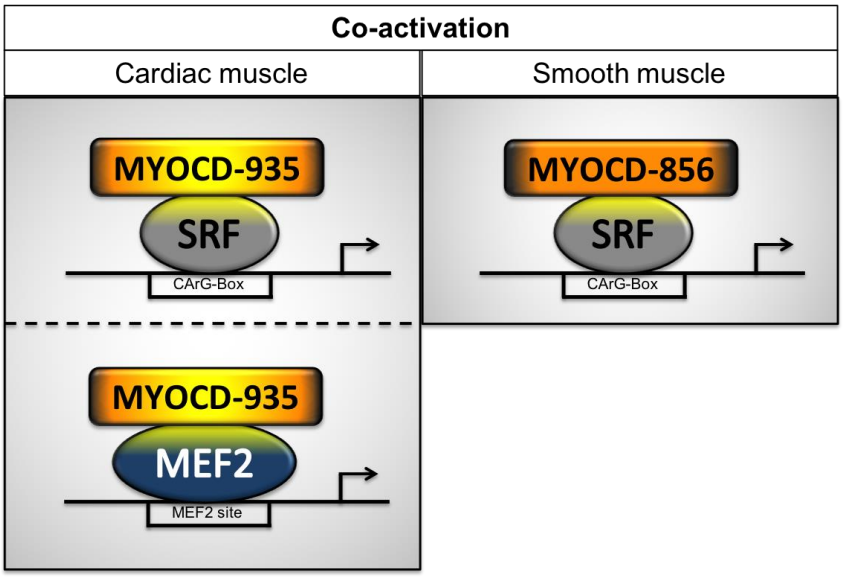

Figure 5: Myocardin isoforms co-activate SRF and MEF2 in cardiac or smooth muscle.

The authors also identified another variant, MEF2-activating SAP transcriptional regulator (MASTR) that specifically coactivates MEF2 but not SRF, in multiple tissue types and will be discussed in a latter section (26). To date, a total of four conserved Myocardin isoforms in mouse,

rat and human have been identified (27): MYOCDv1 (983-aa) and MYOCDv2 (935-aa) (26) are cardiac specific variants while MYOCDv3 (904-aa) and MYOCDv4 (856-aa) (26) are smooth muscle specific. However, this recent nomenclature has yet to be adopted by the rest of the scientific community.

1.2.4 Functional role of Myocardin during development

Prior to identifying spliced isoforms, the role of Myocardin during development was evaluated with expression of a dominant negative mutant (deletion of the carboxyl terminus containing the TAD; MyocdΔDN) in 8-cell blastomeres (17). Using a co-injection of GFP-mRNA as a control, authors were able to detect a reduced expression of cardiac actin, troponin-I and Nkx2.5 in *Xenopus* embryos. The MyocdΔDN mutant inhibited myocardial gene expression but had no effect on embryogenesis (17), highlighting Myocardin's novel role to convey specific myogenic activity. These observations were continued independently, confirming Myocardin as a regulator of smooth muscle differentiation and validating lack of Myocardin expression in skeletal muscle (28).

In contrast to seminal findings of Myocardin as a novel co-activator expressed in cardiac tissue, Michael Parmacek's laboratory published a parallel story detecting *in vivo* levels of human Myocardin expression in smooth muscle containing tissues such as the heart, aorta, bladder and small intestine (29). Analysis of mouse embryos reveal a regulated pattern of Myocardin expression in both vascular and visceral smooth muscle tissue, ranging from the heart at E9.5 to the esophagus and intestinal tracts by E14.5. Du *et al.* provided the first evidence of human Myocardin gene on chromosome 17 and to report Myocardin could not transactivate genes in SRF knock out embryonic stem cells. Similarly, loss of Myocardin function with small interfering RNA

(siRNA) reduced smooth muscle specific promoters in smooth muscle cells. Alternatively, forced expression of Myocardin activated the same promoters in undifferentiated mouse embryonic stem cells (29).

Fundamental studies by two independent research laboratories serve as the platform for understanding the developmental role of Myocardin with subsequent *in vivo* studies. Genetic deletion of exons 8 and 9 of the Myocardin gene containing the domains required for SRF binding, led to the generation of Myocardin mutant mice (30). Mouse embryos homozygous for this loss of function mutation of Myocardin (Myocardin$^{-/-}$ null) exhibited delayed development, abnormal pale yellow yolk sacs with severe vascular defects and died by E10.5 (30). Although the embryos expessing the global genetic deletion of Myocardin had underdeveloped aortas but completed normal cardiac looping, it is suggested other cardiac transcription factors may be dominant during early cardiogenesis that requires further investigation. Thus these findings reveal Myocardin as a requirement for embryogenesis (30).

Similarly, gain and loss of function approaches reveal Myocardin as a necessity for cardiac gene expression and myocardial differentiation during *Xenopus* development (31). With the established role of Myocardin in animal cells, Vantuyn *et al*. reported that the forced expression of Myocardin strongly activates cardiac and smooth muscle genes in primary human stem cells and human fibroblasts (32). Conversely, Myocardin did not activate skeletal muscle specific genes (32), confirming previous findings in animal models (23,28). Recent findings show that Myocardin interacts with MyoD, an essential skeletal muscle transcription factor (33). Using lineage-tracing studies, the authors show Myocardin prevents MyoD from binding to DNA, thus acting as a transcriptional repressor to block the skeletal muscle program while promoting smooth muscle differentiation (33).

1.3 Myocardin Family

As an established coactivator mediating cardiac and smooth muscle differentiation, Myocardin is the founding member of the Myocardin family that consists of Myocardin-related transcription factors A and B (MRTF A/B) and MEF2-activating SAP transcriptional regulator (MASTR) (Figure 6).

1.3.1 Myocardin Related Transcription Factors (MRTFs)

A year after the discovery of Myocardin expression in cardiac and smooth muscle, MRTFs were first reported as coactivators of SRF-dependent gene transcription, but in a broad range of embryonic and adult tissues (20). MRTF-B is the longer protein at 1080 amino acids compared to MRTF-A at 929 amino acids, but both MRTFs interact with SRF to form a ternary complex with the CArG-Box. In contrast to Myocardin, MRTFs have a functional role in modulating cell growth, myogenesis, and mediate changes in actin dynamics (34). MRTFs contain three RPEL domains (a functional domain described in section 1.5.1) that interact with actin, resulting in cytosolic sequestration of MRTFs (35): upon actin polymerization via growth factor stimulation, MRTFs shuttle between cytoplasm and nucleus to regulate gene expression (34,36). In contrast, Myocardin is constitutively nuclear and contains RPEL domains that do not bind to actin as efficiently suggesting the diverse functions of MRTFs (23,34,35).

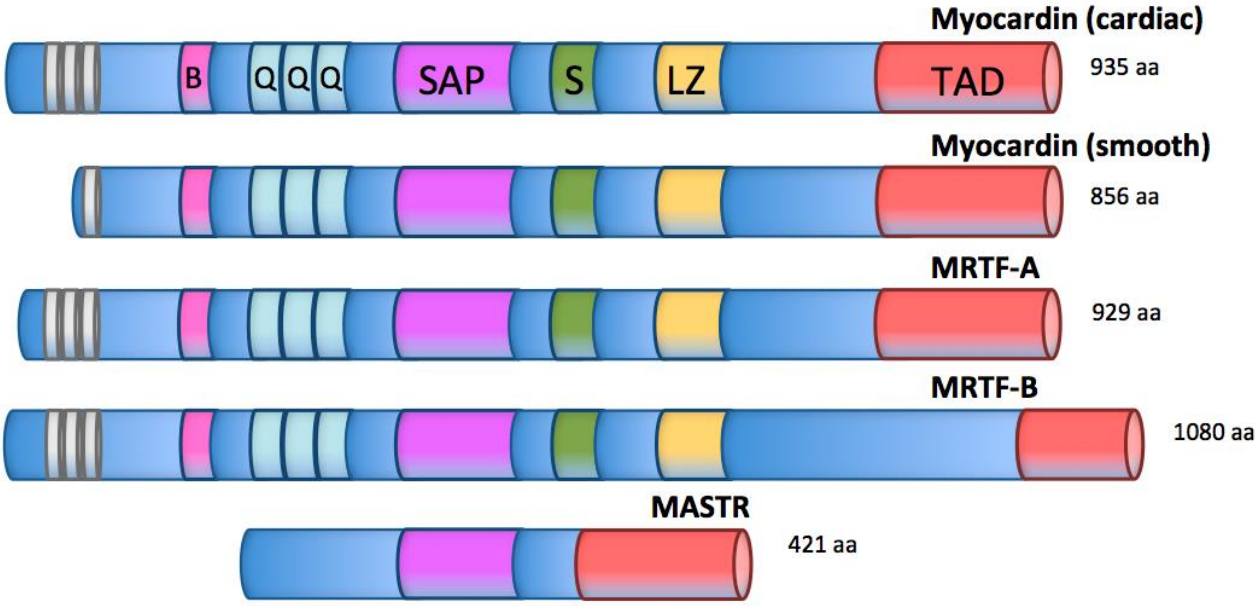

Figure 6: Myocardin family of transcription factors

Formerly described as Megakaryoblastic leukemia-1 (MKL1; also known as MAL), MRTF-A physically interacts with Myocardin via the leucine zipper domain, is co-expressed with Myocardin in the adult heart and smooth muscle (37) and regulates cardiac remodeling and fibrosis (21). As MRTF-A is broadly expressed in cardiac muscle tissue, viable mice with the genetic loss of MRTF-A do not exhibit cardiac defects (38), in contrast to Myocd$^{-/-}$ mice that resulted in embryonic lethality (30). Unlike the viable MRTF-A$^{-/-}$ mice, MRTF-B$^{-/-}$ mice exhibited defective cardiac outflow tracts, resulting in embryonic death or survival until post-natal day 1, succumbing to death from irregular differentiation in cardiac neural crest and smooth muscle cells (39). Furthermore, both MRTFs were shown to regulate cell migration and coronary vessel maturation (40).

With reports investigating the role of MRTFs during cardiac development, Mokalled and colleagues were the first to show that both MRTFs are required for cardiac structure and function

(41). The majority of cardiac-specific double knockout (CDKO) of MRTF-A and MRTF-B ($MRTF^{cdKO}$) mice resulted in post-natal death at 2 weeks. The mice that survived to 3 weeks, exhibited left ventricular dilation, fibrosis, an estimated 50% reduction in fractional shortening and irregular sarcomere structure, signs of cardiomyopathy and progression to heart failure (41). Using RNA Seq data, multiple cytoskeletal genes were dysregulated in the $MRTF^{cdKO}$ mice, suggesting that although not essential, MRTFs play a vital role during cardiac structural development (41). Despite their molecular homology, it is clear that the Myocardin and MRTFs have unique functions and expression patterns in various myogenic tissues. In contrast to Myocardin, recent evidence illustrates that both MRTF-A and MRTF-B are required for skeletal muscle development (42), but are not involved with MEF2 co-activation.

1.3.2 MASTR

Alternative to MRTFs, MASTR is a 421-amino acid variant that co-activates MEF2 and is detected in a broad range of tissues including skeletal muscle, brain, lung and aorta (43). Meadows *et al.* were the first to provide evidence of MASTR activating the MyoD enhancer to drive skeletal muscle gene expression in a *Xenopus* embryo model (44). These findings were validated by generation of $MASTR^{-/-}$ null mice that exhibited an impaired ability to repair skeletal muscle after injury (45). This effect was further enhanced in combination with MRTF-A deletion, resembling a similar phenotype to $MyoD^{-/-}$ null mice (45). These findings are compelling but further work is required to understand the myogenic function of MASTR; whether it acts as a molecular switch to inhibit smooth muscle differentiation and activate skeletal muscle differentiation, and how it synergistically works with MRTF-A. As the various members of the Myocardin family regulate gene expression in multiple cell types (46,47), the regulation of cardiac and smooth muscle gene expression has been most extensively characterized in Myocardin.

1.4 Myocardin: An Essential Cofactor for Cardiac Development

Similar to Nkx2.5, Myocardin is one of the earliest conserved cardiac markers required for cardiogenesis (48). Similar to the murine (30) and frog embryo models (31), Myocardin is sufficient to activate smooth and cardiac muscle gene expression in chick embryos: loss of function studies illustrate the transcriptionally inactive Myocardin dominant negative mutant inhibits chick cardiogenesis (48). Global loss of Myocardin in embryonic mice results in fetal death by E10.5 due to a lack of vascular muscle differentiation (30). This early lethal phenotype provides a clue as to the essential role of Myocardin in cardiac development and embryogenesis, but also poses a challenge for researchers investigating Myocardin's role during post-natal development.

1.4.1 Cre-Lox Recombinase Animal Models

In an effort to address the limitations of global knockout models and to investigate the function of Myocardin post-natally, Parmacek's laboratory generated a conditional knock out mouse model and inactivated the Myocardin gene in a tissue specific manner. This occurs by Cre-Lox recombinase excision of the Myocardin gene. Using conditional gene-targeting constructs, exon 8 is flanked by lox P sites (Floxed), containing the basic and poly-glutamine rich domains of Myocardin ($Myocd^{F/F}$) (23,49). Next, the $Myocd^{F/F}$ mice are interbred with CMV-driven Cre-transgenic (Tg) mice to generate Myocardin mutant mouse embryos ($Myocd^{F/F}$/CMV-Cre) that exhibit an exon 8 deletion of the Myocardin gene (49). The $Myocd^{F/F}$/CMV-Cre mice display a similar phenotype to the $Myocardin^{-/-}$ null mice (30) and survive until E10.5 (49). Wnt is a transcription factor involved in neural crest cell induction during embryogenesis (as mentioned in an earlier section), $Myocd^{F/F}$ mice were also interbred with Wnt1-Cre-Tg mice to generate a conditional deletion of Myocardin in neural crest-derived cells ($Myocd^{F/F}$/Wnt1-Cre) (30).

Based on these Tg mouse models, Myocardin is selectively deleted in cardiac neural crest cells that differentiate into smooth muscle cells to form the cardiac outflow tract (49). Pax3 is another transcription factor expressed in neural crest cells during early development. The authors interbred $Myocd^{F/F}$ with Pax3-Cre mice to confirm the specific deletion of Myocardin in the $Myocd^{F/F}$/Wnt1-Cre mice is specific to neural crest-derived smooth muscle cells (49). Mice exhibiting a smooth muscle-specific deletion of Myocardin ($Myocd^{F/F}$/Wnt1-Cre) die before post-natal day 3 (49), in contrast to $Myocardin^{-/-}$ null mice that die at E10.5 (30). The $Myocd^{F/F}$/Wnt-Cre mice exhibit structural defects such as an open or patent ductus arteriosus (PDA), a common congenital heart defect. A PDA is required during fetal development to shunt blood away from embryonic lungs for proper fetal circulation that normally closes at birth (50).

To further understand the role of Myocardin in the heart, Parmacek recently generated $Myocd^{-/-}$ null transgenic mice by specifically deleting exon 8 of the Myocardin gene (51), to validate previous observations that deleted exons 8 and 9 (30). $Myocardin^{-/-}$ null embryos exhibited hypoplastic hearts and underdeveloped cardiac chambers at E9.5. The $Myocardin^{-/-}$ null mice embryos completed cardiac looping but echocardiographs revealed hearts with a reduced systolic function and ejection fraction (51). These embryos exhibit fluid around the hypoplastic hearts, another cardiac defect, that quickly progresses into heart failure, resulting in embryonic lethality observed at E10.5, validating previous findings (30). Uniquely, the cardiomyocytes isolated from $Myocardin^{-/-}$ null mice illustrated a loss in cardiomyocyte proliferation with a combined increase in cardiac apoptosis (51). This report provided new evidence linking the functional loss of Myocardin with an increase in cardiac programmed cell death.

Confirming the effects from the global loss of Myocardin function, Parmacek's group generated a conditional deletion of Myocardin in cardiac muscle tissue in a Cre-recombinase

excision manner: Myocd$^{F/F}$ mice are interbred with Nkx2.5-Cre-Tg mice. The transcription factor Nkx2.5 is expressed as early as E7.5 in the cardiac crescent and mediates an early Myocardin deletion specific to cardiomyocytes, resulting in Myocd$^{F/F}$/Nkx2.5-Cre mutant mice. The Myocd$^{F/F}$/Nkx2.5-Cre mutant embryos exhibit no aortic tract defects (such as PDA) and survived till E13.5-E14.5 in comparison to Myocd$^{F/F}$/Wnt1-Cre conditional mutant mice that died by P3 (51). This observation suggests Myocardin expression in cardiac muscle is a necessity that is activated during the earlier stages of cardiogenesis in comparison to Myocardin expression in smooth muscle. The Myocd$^{F/F}$/Nkx2.5-Cre mutant mice exhibit similar defects as the Myocardin$^{-/-}$ null embryos including hypoplastic hearts and signs of heart failure. Interestingly, these conditional mutant embryos also exhibit a decrease in cardiac myocyte proliferation and uniquely developed a ventricular septal defect (VSD) by E13.5 (51). VSD is a common congenital heart defect that results in abnormal mixing of oxygenated and deoxygenated blood due to improper chamber formation. With the development of cardiac defects and an unexpected decrease in cardiac myocyte proliferation mediated by disruption of BMP10 signalling, the Myocd$^{F/F}$/Nkx2.5-Cre mutant hearts also exhibit a marked increase in cell death (51).

Adult mice with a cardiac specific deletion of Myocardin post-natally via cardiomyocyte specific α-myosin heavy chain (αMyHC) promoter (Myocd$^{F/F}$/αMyHC-Cre mutant mice) develop lethal dilated cardiomyopathy (DCM), a form of cardiac disease, by 10 months of age (52). Similarly, Myocardin deletion in the heart of adult mice using a tamoxifen-inducible αMyHC-Cre (αMHC-MerCreMer) leads to lethality within 6 days from heart failure associated with elevated levels of programmed cell death (52). Collectively these studies evaluating the complete loss of Myocardin function and the conditional loss of Myocardin (in either smooth or cardiac muscle) demonstrate Myocardin preserves cardiomyocyte survival. The embryonic loss of Myocardin

leads to congenital heart defects that can rapidly progress into heart failure in both the developing and post-natal heart. Such profound effects could be mediated by binding of various transcriptional regulators to the Myocardin domain.

1.5 Myocardin Domains

1.5.1 Functional Domains

The functional domains of murine Myocardin consist of: 1) the RPEL domain located at the amino terminus that mediates actin binding and nuclear localization (26); 2) a basic domain; 3) poly-glutamine rich region; 4) the SAP domain that mediates chromatin remodeling (17); 5) serine-rich domain; 6) coiled-coil motif that resembles a leucine-zipper that mediates Myocardin homodimerization (53); 7) and the TAD located at the carboxyl terminus that mediates transcriptional activity (Figure 7) (23,54).

1.5.2 Transcription Factor Binding Domains

Following domain organization, multiple studies have reported transcription factor binding domains of Myocardin that regulate cardiac gene transcription (Figure 7). At the amino terminus of Myocardin, coactivation of MEF2 is mediated by a stretch of amino acid residues located at the end of RPEL1 domain (26). This motif of Myocardin interacts with the MADS-Box domain of MEF2. After Myocardin domain mapping, co-IPs reveal a direct interaction of Myocardin and MEF2 that was validated with GST-pull down assays (30). The smooth muscle specific variant Myocd-856 did not interact or confer MEF2 activity while the cardiac variant Myocd-935 specifically co-activates MEF2 and SRF (30). Interestingly, deletion of the MEF2 binding region of Myocardin inhibits MEF2 coactivation and conversely, had no effect on SRF coactivation (30)

Mutational analysis of the amino terminus of Myocardin illustrates the basic and poly-glutamine rich domains interact with SRF (17). Co-IP assays reveal that the MADs-box

domain of SRF is required to interact with Myocardin to confer myogenic activity. Although highly conserved, the SAP domain of Myocardin does not interact with SRF to regulate cardiac gene transcription mediated by the TAD (17). Thus, the amino terminus of Myocardin binds to the MADS-Box of SRF while the carboxyl terminus mediates transcriptional activity of CArG-Box dependent genes.

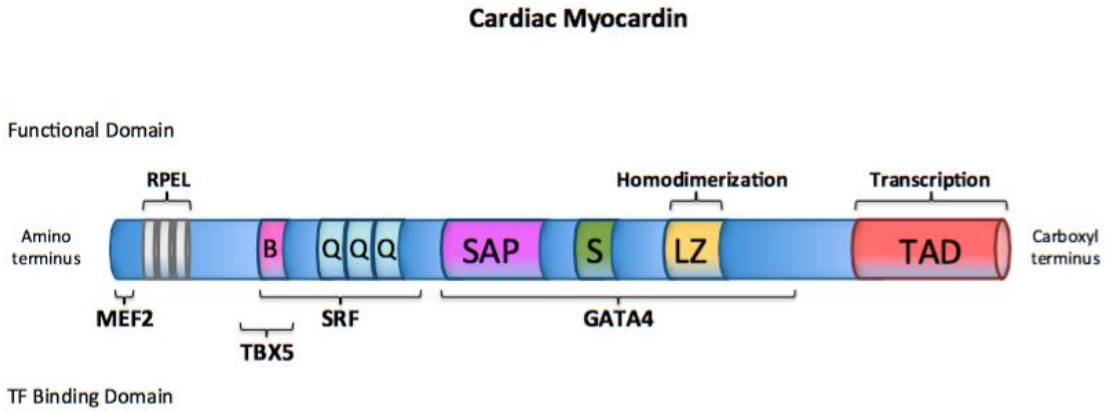

Figure 7: Cardiac Myocardin (Myocd-935) domain schematic: functional domains and transcription factor (TF) binding domains of murine Myocardin.
Cardiac Myocardin (Myocd-935) domain schematic: functional domains and transcription factor (TF) binding domains of murine Myocardin. The functional domains of Myocardin include: RPEL domain; basic domain (B); poly-glutamine rich region (Q); SAP domain (SAP); serine-rich region (S); leucine-zipper like motif (LZ) that mediates Myocardin homodimerization; and the transactivation domain (TAD) that mediates transcriptional activity. The binding regions required to interact with TFs such as: myocyte enhancer factor-2 (MEF2); T-box transcription factor-5 (TBX5); serum response factor (SRF); and member of the GATA family of zinc finger TF (GATA4).

With respect to cardiogenic transcription factors, not only does GATA4 regulate SRF-target genes, GATA4 also interacts with Myocardin to regulate cardiac gene expression (55). The regions of Myocardin that bind with GATA4 include the SAP and the leucine zipper-like (coiled-coil) domains. Once bound, GATA4 mediates a dual effect on Myocardin activity: the DNA binding domain of GATA4 interacts with Myocardin to stimulate cardiac gene expression. However, this stimulatory function does not require the TAD of GATA4. In contrast, the binding

of the TAD of GATA4 to Myocardin has an inhibitory effect and represses cardiac gene expression (55). This reveals GATA4 as a modulator of Myocardin activity that maintains a precise balance of cardiac gene transcription during different stages of development (22,55).

Another cardiogenic transcription factor that directly interacts with Myocardin to activate cardiac specific genes is TBX5. Dha-Zhi Wang's laboratory recently reported the interaction is mediated by the TBX5 binding region of Myocardin (containing the basic and coiled-coil domain) to activate cardiac genes and not activate smooth muscle specific genes (56). Interestingly, a TBX5 mutation, TBX5G80R, could neither bind to Myocardin nor activate cardiac gene transcription (56). This mutation is of key interest as it results in the Holt-Oram Syndrome that is associated with congenital heart defects in humans (56,57). Collectively, the domain mapping studies of MEF2, SRF, GATA4 and TBX5 binding regions highlight that Myocardin determines cell fate by transcriptional interactions to direct cardiac or smooth muscle signals during cardiovascular development.

1.6 Regulators of Myocardin Activity & Expression

1.6.1 Transcriptional Regulators

As Nkx2.5 is required for mouse cardiogenesis, it was the first reported factor required to transactivate the cardiac-specific Myocardin promoter (54). Initial observations reveal a reduced level of cardiac-specific Myocardin mRNA expression in $Nkx2.5^{-/-}$ null mouse hearts as assessed by in situ hybridization and northern blot analysis. After determining the primary sequence of the mouse Myocardin cardiac isoform, mutational analysis of the Myocardin promoter reveal a specific motif in the Nkx2.5 responsive element, NKE. This motif is required for Myocardin promoter activation driven by Nkx2.5 during cardiogenesis (54). As Myocardin was reported to activate the Nkx2.5 promoter (17), these findings suggest that Nkx2.5 and Myocardin co-regulate

their expression during early murine cardiac development that might require additional cofactors that remain to be reported.

To assess the regulatory elements that drive Myocardin transcription in embryonic and post-natal mouse development, Olson's lab reported a Myocardin enhancer region (43). A combination of factors including MEF2, Tead, and forkhead box class O (FOXO) proteins are required for Myocardin enhancer activation (43). Interestingly, Myocardin interacts with MEF2 to regulate its own enhancer in a SRF-independent manner for both cardiac muscle and smooth muscle expression *in vivo* (43). Both Tead and FOXO proteins are upstream regulators for Myocardin expression in cardiomyocytes while Tead2 is specific to neural crest-derived smooth muscle cells (43). Identifying the Myocardin enhancer provides insight into the various signals that mediate expression of Myocardin and how muscle lineages are established but further investigation is required. Such signalling pathways that control developmental genetic programs and cell differentiation are mediated by epigenetic changes.

1.6.2 Epigenetic Regulators

Genetic medicine has led to advancements to better understand epigenetics during development and its correlation to various human diseases including heart failure, as recently reviewed (58). Epigenetics is the study of inheritable changes to gene expression that are affected by external factors (such as various exposures during development, environment and diet), independent of DNA sequence. These inheritable or acquired modifications result in chromatin remodelling to control gene expression (59), that have recently shown to regulate Myocardin expression.

1.6.2A DNA Methylation

Modification of DNA by methylation occurs at a dinucleotide site where a cytosine follows a guanine, commonly referred to a CpG island, which becomes methylated to form a 5-methylcytosine, an attractive site that dominantly mediates chromatin remodelling (60,61). This condenses DNA and prevents transcription factors from accessing promoter regions resulting in gene inactivation. Recent studies have identified differential methylated regions that controls gene expression that does not always result in gene silencing. Hypomethylation of the 5' promoter region results in activation of gene expression while in contrast, hypermethylation of the gene body near the 3' untranslated region results in an inactivation of gene expression. Animal models have identified two enzymes DNA-methyltransferase (DNMT) and DNA-demethylase that modulate the methylated status of DNA (60).

Recently, Zhuang *et al.* reported the first link of DNA methylation to Myocardin in vascular smooth muscle cells to drive cell differentiation (62). Although DNA methylation patterns on the promoter region of Myocardin is not well understood, rat smooth muscle cells treated with a DNMT inhibitor, 5'-aza-2'deoxycytidine (5'-aza) result in global DNA hydroxymethylation. Treatment with 5'-aza restores Myocardin expression [and markers of smooth muscle genes including smooth muscle actin (SMA) and smooth muscle myosin heavy chain (SM-MHC)], driving smooth muscle dedifferentiation into a contractile phenotype and prevent vascular remodelling (62). These are the first findings that demonstrate the effect of DNA methylation on Myocardin expression, suggesting inhibition of DNMTs can serve as a potential therapy for the prevention of arterial remodelling and vascular disease (61). These findings have yet to be validated by independent researchers and inhibition of DNA methylation on Myocardin expression in cardiac muscle has yet to be shown.

1.6.2B Histone Modification: Acetylation

In contrast to DNA methylation regulating gene expression, another epigenetic mechanism is mediated by histone modifications. Post-translational modifications to amino acid residues on histone proteins, resulting in the rearrangement of DNA and transcriptional state. Histone core proteins (H2A, H2B, H3, H4) exist as an octamer that wrap DNA into a nucleosome, the building block of chromatin (61). Histone modifications are mediated by the catalytic activity of histone acetyltransferases (HAT) that promote unwinding of histone coiled DNA, resulting in a "relaxed" state. HATs transfer acetyl groups to the lysine resides on histones, thus unwrapping DNA (63). This facilitates binding of transcriptional factors to DNA thus promoting gene transcription. Extensively studied HATs include p300 and CREB-binding protein (CBP) that promote gene expression (64). In contrast to HATs turning genes on by acetylating histone lysines, removal of acetyl residues is mediated by histone deacetylases (HDAC). Antagonistic to HATs, HDACs promote coiling or condensation of DNA to repress gene transcription or turn genes off.

Based on sequence and domain homology, HDACs are characterized into three classes. Class IIa HDACs include HDAC4 and HDAC5, were first shown to interact with MEF2, a transcription factor, resulting in a reduction of myogenic gene transcription in skeletal muscle (65). Interestingly, studies implicate a salt-inducible kinase-1 (SIK1) that phosphorylates HDAC4-5, resulting in nuclear export (66,67). In contrast, direct phosphorylation of SIK1 by PKA inactivates SIK1 function, resulting in the nuclear localization of HDAC and repression of skeletal gene expression (66). Collectively, these findings illustrate the nuclear repressive function of class II HDACs and their regulation on MEF2 to control gene expression in myogenic cells.

With reports on the repressive function of HDACs in skeletal and smooth muscle cells, investigators demonstrate a repressive HDAC5/MEF2 complex that regulates mitochondrial

function in the heart (68) and a HDAC5/Myocardin repressive complex that inhibits fetal gene activation during pathological remodelling of the heart (64). Class IIa HDAC kinases that act as depressors to phosphorylate and promote the nuclear export of HDAC5 include calcium/calmodulin dependent kinase CaMK-I-II-IV and protein kinase D-1 (PKD1), have been characterized in the heart (69-71); however, the role of SIK1 in mediating the nuclear export of HDAC5 to remove the molecular brake on Myocardin in the heart has yet to be shown.

Furthermore, changes in chromatin acetylation enhance or repress gene expression regulated by Myocardin (64). Addition of acetyl groups on lysine residues on the amino terminus of Myocardin is mediated by p300, a HAT that is required to activate smooth and cardiac muscle genes (72). Uniquely, p300 binds to the transactivation domain of Myocardin and enhances the ternary complex of Myocardin-SRF binding to the CArG-Box, promoting myogenic activity (64,69). In contrast, removal of the acetyl groups is mediated by the interaction of histone deacetylase-5 (HDAC5) with Myocardin. The poly-glutamine domain of Myocardin interacts with HDAC5 that inhibits smooth muscle gene expression. As the HDAC5 inhibitory effect on Myocardin was suggested to be a dominant influence, it is proposed that HDAC5 represses Myocardin activity by default (64). Activation by p300 removes this molecular brake and subsequently mediates transcriptional activation of smooth muscle genes (64). Collectively, these findings illustrate the epigenetic regulation of Myocardin transcriptional activity as determined by the opposing influences of HATs and HDACs.

An additional repressor of the Myocardin-SRF complex that reduces smooth muscle gene expression is mediated by the Kruppel-like transcription factor-4 (KLF4) (73). Not only does KLF4 prevent CArG-Box binding of the Myocardin-SRF complex on the smooth muscle alpha-actin promoter, KLF4 also modulates Myocardin expression in response to vascular injury and

induced cardiac hypertrophy (73,74). This repressive function of KLF4 also involves chromatin regulation that recruits HDAC2, a class I HDAC. Thus, similar to repression of HDAC5, the HDAC2-KLF4 complex compacts the CArG-Box region and reduces the transcriptional ability of Myocardin to regulate smooth muscle genes (75). This repressive complex involving HDAC2 mediated regulation of cardiac muscle gene expression still remains unknown.

Olson's lab continued to dissect the repressive effects of Myocardin by evaluating a transcription factor of the FOXO family that inhibits Myocardin activity (43). The basic and SAP domain of Myocardin interact with FOXO4 that inhibits smooth muscle differentiation (43). However, phosphorylation of FOXO4 results in a nuclear translocation to the cytosol, thus removing the nuclear repression on Myocardin. Although the report indicates an interaction between FOXO4 and SRF, it is proposed that FOXO4 forms a ternary complex with Myocardin-SRF (73). This complex might recruit additional repressive factors such as HDACs to inhibit smooth muscle gene expression. It would be interesting to determine if these reported antagonistic modulators have similar effects on cardiac muscle gene expression. Recent evidence from the Schwartz lab show a HAT known as CSRP2BP, co-activates a transcription factor, CRP2, and directly interacts with Myocardin-SRF to activate smooth muscle gene transcription (76). However, the authors failed to assess HDAC repression of this complex.

More evidence is required to understand the role of HATs/HDACs on Myocardin transcriptional activation. Sun *et al.* recently demonstrate an interaction between a chromatin-remodelling complex and Myocardin: the embryonic deletion of Baf60c, an ATP-dependent chromatin-remodelling complex subunit, resulted in hypoplastic hearts (similar to a Myocardin null embryos), cardiac dysfunction, and dysregulated target genes of Myocardin (77). A yeast hybrid two-hybrid screen and GST-pull down assays reveal an interaction between Myocardin and

Baf60c, but a genetic interaction between Baf60c and the cardiac or smooth muscle isoform of Myocardin in the presence of MEF2 or SRF has yet to be shown (77). As evidence surrounding chromatin modulation requires independent validation, reports of histone methylation of Myocardin activity has been of recent interest.

1.6.2C Histone Modification: Methylation

Another epigenetic modification includes methylation of histone amino acid residues that regulate gene transcription. These changes are catalyzed by histone lysine (K) methyl transferases (HMTs) that methylate histone lysines that are antagonized by histone lysine demethylase (KDMs) (61). The abundance and localization of methylated histones alter chromatin structure to activate or repress gene transcription. Different degrees of methylation include mono- (me1), di- (me2) and tri- (me3) that methylate commonly documented residues including K4,-9,-37 on histone H3 and K20 on histone H4 (78). One well-investigated site includes H3K4me3, trimethylated lysine 4 on histone H3. Changes to histone methylation status have been well documented during cardiac cell differentiation and development, yet in contrast, methylation changes to H3K4me3 and H3K9me3 have been reported during the progression to heart failure, as reviewed by Zhang and Liu (79).

The removal of methyl groups on histone 3 such as H3K4me3 is mediated by KDMs that contain a conserved domain known as the jumonji-domain-containing demethylases (JMJ-KDM). Such KDMs include JMJD1A, JMJD2A (KDM4A), JMJD3 (KDM6B) and UTX (KDM6A). Histone H3K27 demethylases, UTX and JMJD3, were shown to regulate cell differentiation (80) and regulate specific enhancer sites for activating cardiac gene transcription during development (81). Another histone H3K9 demethylase, JMJD1A, interacts with Myocardin and MRTFs (as evident by GST-pull down analysis) in regulating smooth muscle gene expression (82). Although JMJD1A interacts with multiple Myocardin family members, promoter activation of

differentiating smooth muscle genes (including SM22 and alpha-actin) is strongly driven by the interaction between JMJD1A and MRTF-A (82).

Other members of the jumonji family of KDMs include the JMJD2 (KDM4A) protein, the first KDM discovered to regulate gene expression (83), that catalyzes demethylation of H3K9me3 and H3K36me3. Recent reports indicate JMJD2A demethylates H3K9 to activate fetal cardiac genes and promotes pathological cardiac hypertrophy (84). Elevated levels of JMJD2A were clinically observed in patients with hypertrophic cardiomyopathy while selective deletion of JMJ2DA in adult mouse hearts attenuated transverse aortic constriction-induced hypertrophy (84). In response to hypertrophic stimuli JMJD2A binds to a fetal gene promoter to upregulate gene expression that is enhanced by the interaction of Myocardin/SRF: JMJD2A recruits the Myocardin/SRF complex to regulate SRF-target genes (84). Based on these findings, it would be beneficial to evaluate whether JMJD2A affects the binding affinity of the Myocardin/SRF complex on additional cardiac or smooth muscle promoters during cardiovascular disease.

1.6.3 Post-Translational Modification of Myocardin in Smooth Muscle

Initial discovery of Myocardin expression and its potent role as a co-activator in mediating myocardial gene expression *in vivo* has led to subsequent research that evaluates the role of another co-activator, ELK-1, on smooth muscle biology (85). ELK-1 is a transcriptional coactivator that belongs to the E-twenty-six (ETS) transcription family that acts as an antagonistic cofactor to SRF: ELK-1 displaces Myocardin from SRF as it competes for the same SRF binding site, the MADS-Box. Thus, binding of ELK-1 to Myocardin inhibits transcription of smooth muscle genes (85). Similar to the competitive nature of cofactor ELK-1 to repress Myocardin activity, GATA6 competes with Myocardin for the same binding site on SRF (86). GATA6 displaces Myocardin from SRF, which selectively inhibits telokin expression, an abundant intestinal smooth muscle

protein. Alternatively, GATA6 increases the expression of vascular smooth muscle proteins such as myosin heavy chain (MHC) but does not affect SRF-Myocardin interaction (86). Although GATA6 can modulate smooth muscle specific genes, it highlights the complexity of regulatory machinery involved in the Myocardin-SRF complex.

Contributing towards the complexity of Myocardin regulation, Notch signalling was recently demonstrated to block smooth muscle differentiation and is associated with Alagille Syndrome, a genetic disorder caused by a mutation in the Jagged-1 (JAG1) ligand (87,88). JAG1 activates Notch1 signalling that represses Myocardin activity and blocks the smooth muscle differentiation program (84). This repressive signalling mechanism is mediated by a primary target of Notch known as homocysteine-responsive endoplasmic reticulum-resident-1 (HERP1), which physically binds to SRF and blocks the Myocardin-SRF complex (89).

As previous reports assess the Myocardin-SRF complex, Qiu and colleagues published the first report illustrating Myocardin coactivation in a CArG-Box independent manner (90). Stimulation with transforming growth factor-beta$_1$ (TGFβ_1) mediates direct interaction between Smad3 and Myocardin. Smad3 is an intracellular protein of the Smad family that communicates signals to the nucleus to regulate gene expression. Smad3 interaction with Myocardin activates smooth muscle genes including SM22, SM-MHC and SM-alpha actin. This interaction involves both TADs of Myocardin and Smad3, and in contrast to the CArG-Box, Smad3 binds to the Smad-binding element (SBE) on target genes (90). Thus, Myocardin can coactivate smooth muscle genes in a CArG-Box-dependent or SBE-dependent manner. Conversely in a recent report, Smad3 also inhibits expression of Myocardin during early phases of the smooth muscle differentiation program (91). Collectively, these findings highlight Smad3 as a dual regulator of Myocardin activity for directing smooth muscle gene transcription.

During smooth muscle development, the differentiation program favours a contractile muscle phenotype. Conversely in response to vascular injury, growth factors regulate smooth muscle cell plasticity, switching to a proliferative state of smooth muscle cells that inhibit smooth muscle gene transcription (73). As multiple reports have established Myocardin as a transcriptional cofactor, Li *et al.* identified steroid receptor coactivator-3 (SRC3) as a Myocardin coactivator (92). This novel cofactor is required for vascular smooth muscle transcription and differentiation into the contractile phenotype (92). The interaction between SRC3 and Myocardin involves the TAD of Myocardin that enhances its myogenic activity on SRC3 via CArG-Box dependent promoters (92). This effect is reversed by a loss of SRC3 function in cultured smooth muscle cells.

These findings provide clues to the receptor-mediated modulation of Myocardin that direct the proliferative or contractile phenotypes of smooth muscle. A recent report illustrated a direct interaction between Myocardin and signal transducer and activator of transcription-3 (STAT3) (93). This implicates the Janus kinase inhibitor (JAK)-STAT3 signalling pathway, which communicates extracellular signals to the nucleus and modulates the phenotype switching of vascular smooth muscle cells (VSMCs) (93). The nuclear p65 subunit of NF-κB is previously shown to interact with Myocardin to inhibit the SRF-ternary complex (94), Singh and Zhang demonstrate a dual role of tumor necrosis factor-alpha (TNFα, an inflammatory cytokine) in regulating Myocardin mRNA expression mediated by NF-κB (95). Reports show TNFα treatment decreases endogenous Myocardin expression and reduces VSCMs contractility in proliferative VSMCs, but in contrast stabilizes Myocardin mRNA in differentiated or contractile VSCMs (95). Another regulator of smooth muscle phenotype switch includes the fibroblast growth factor-12 (FGF-12) that induces the contractile phenotype (96). Treatment with FGF12 inhibits cell proliferation as mediated by p38 kinase activation while increasing Myocardin and SRF expression

(96). These findings illustrate various mechanisms that module the VSCM phenotypic switch by modulating Myocardin expression.

To better understand the mechanisms that stabilize Myocardin activity during smooth muscle differentiation, a yeast two-hybrid screen identified ubiquitin ligase E3 component n-recognin-5 (UBR5) as a potential protein that could regulate Myocardin activity (97). Independent of its protein degradation E3 ligase activity, UBR5 was revealed to localize to the nucleus and interact with the amino terminus of Myocardin. UBR5 was also reported to prevent degradation and stabilize Myocardin to enhance smooth muscle expression and differentiation (97). However, the authors failed to report if UBR5 binds to Myocardin as a ternary complex with SRF to drive smooth muscle gene expression.

Interestingly, the extracellular regulated kinases-1/2 (ERK1/2) directly phosphorylates the smooth muscle variant, Myocd-835 at four sites: $Ser^{812\text{-}859\text{-}866}$ and Thr^{893} (98). Phosphorylation of these sites within the TAD of Myocardin inhibits transcriptional activity of smooth muscle genes (98). This post-translation modification by ERK1/2 also reduces the interaction of Myocardin with cAMP-binding protein (CBP), an enhancer of Myocardin activity (98). As Myocardin undergoes phosphorylation, dephosphorylation of Myocardin via phosphatases in smooth muscle cells remains to be illustrated.

Furthermore, Yin and colleagues reported Myocardin degradation is required to transcriptionally activate Myocardin and regulate vascular smooth muscle genes (99). With the use of proteosome inhibitory drugs such as lactacystin, Myocardin protein levels increased as visualized by a higher molecular weight protein band. Consequently, the authors failed to report the size of this higher molecular protein. As lactacystin treatment increased Myocardin protein expression, it conversely reduced the transcriptional activity of Myocardin, which led to the

reduction of smooth muscle contractile markers. Interestingly, this repressive effect of proteosomal inhibition on Myocardin transcriptional activity was independent of other reported Myocardin repressors such as ELK-1, KLF4 and HDACs (99).

Recent findings describe Myocardin ubiquitylation as another post-translational modification required to transactivate Myocardin (100). This process is mediated by Atrogin-1, an E3 ligase that promotes the proteosomal degradation of Myocardin required for transcriptional activation (100). Co-IPs and GST-pull down assays confirmed a direct interaction between Atrogin-1 and Myocardin while immunostaining experiments illustrated Atrogin-1 and Myocardin nuclear localization (100). These findings highlight the continuous complexity surrounding ubiquitylation/degradation required for Myocardin transactivation. Future studies need to assess key missing points from these reports including 1) Myocardin domains that ubiquitin molecules bind to; 2) the size of Myocardin protein prior to degradation; 3) the specific domains of Myocardin that are degraded and 4) whether the cardiac Myocardin variant also undergoes similar post-translational changes of inactivation.

1.6.4 Post-Translational Modification of Myocardin in Cardiac Muscle

As Myocardin is phosphorylated in smooth muscle cells (98), glycogen synthase kinase-3β (GSK3β) phosphorylates Myocardin in cardiac myocytes (101). With the use of *in vitro* kinase assays, GSK3β phosphorylates Myocardin at four serine residues and reduces the cardiac hypertrophy gene program (101), thus altering the transcriptional activity of Myocardin. Additionally, this effect is reversed by phosphorylation of GS3Kβ by lithium chloride treatment that inhibits GS3Kβ activity and induces cardiac hypertrophy (101). Collectively these findings reveal GS3Kβ as a negative modulator of Myocardin activity that has yet to be reported with endogenous Myocardin.

Conversely, the bone morphogenetic protein-2 (BMP2) signaling pathway that is involved in cardiac cell differentiation enhances Myocardin activity and drives the transcriptional cardiac program (102). This process is driven by the synergistic interaction between Smad1 and Myocardin as assessed by biochemical assays. In contrast to the Smad3 regulation of smooth muscle genes, interaction of Smad1 and Myocardin is SBE-independent and does not interfere with the Myocardin-SRF ternary complex in cardiomyocytes (102). The CArG-Box is required to mediate this interaction between Myocardin and Smad1, which is completely inhibited by deletion of the basic domain of Myocardin. Interestingly, mutations in the SAP and poly-glutamine domain reduce the Smad1-Myocardin binding ability (102). The experimental evidence is compelling and provides a platform for validation with *in vivo* studies.

As BMP2 and Smad1 enhance Myocardin activity, sumoylation also enhances the cardiogenic activity of Myocardin in non-cardiac cells (103). Sumoylation is a post-translational modification mediated by small ubiquitin-like modifiers (SUMO). This process is mediated by SUMO-1 that modifies Myocardin at lysine residue 445 and enhances Myocardin transactivation (103). Co-IPs revealed that PIAS1, an E3 ligase, was also revealed to interact with Myocardin that stimulated Myocardin sumoylation. Due to this modification, sumoylated Myocardin also runs at higher position on a protein gel ~98kDa, compared to its non-sumoylated form. Both translational modifications of Myocardin by SUMO-1 and PIAS1 were illustrated to occur in an SRF-dependent manner via SRE sites (103). These findings highlight the sumoylation pathway that enhances Myocardin transcriptional activity that may contribute to cardiogenesis and direct cardiac muscle cell fate, but whether these changes are observed during cardiovascular disease are unknown.

1.7 Myocardin in Heart Disease

The presence of congenital heart defects in childhood can develop into congestive heart disease, contributing to dilated cardiomyopathy (DCM), hypertension, and ischemic heart disease that can deteriorate to heart failure (104). A study led by Mikhailov's lab was the first to report elevated levels of Myocardin expression in human biopsies with DCM (105). Myocardin mRNA expression was increased in left ventricular samples from humans with end stage heart failure in comparison to normal donor hearts (105). A similar increase in Myocardin expression in both left and right ventricle (LV/RV) myocardium was illustrated in a Doxorubicin (DOX)-induced model of CM in neonatal pigs (105). Interestingly, the forced expression of the cardiac isoform of Myocardin in neonatal pig hearts activated the fetal gene program and impaired cardiac function. Two days post Myocardin gene delivery, the piglet hearts exhibited impaired LV systolic function, abnormal echocardiograms and left and right ventricular remodelling *in vivo*, implicating Myocardin expression in human cardiovascular disease.

Myocardin is also implicated in stress-induced hypertrophy: mouse hearts with transverse aortic banding (TAB)-induced cardiac hypertrophy and human heart patients with idiopathic dilated cardiomyopathy (IDM) had an increasing expression of Myocardin (106). Hypertrophic stimulation in cultured neonatal cardiomyocytes increased Myocardin activation, which activated hypertrophic genes in a CArG-Box dependent manner. The forced expression of Myocardin activated hypertrophic and fetal genes including ANF, BNP, β-MHC (106). SRF expression was elevated as to enhance Myocardin target gene expression but no changes in GATA4 or MEF2 transcription factors were detectable, yet expression of HDAC5, a repressor of Myocardin activity, was able to inhibit Myocardin-induced hypertrophy (106). In regard to chromatin changes, the role of HATs in the Myocardin-induced hypertrophic program is currently unknown.

Cardiac hypertrophy also implicates a transcriptional member from the KLF family. In rat cardiomyocytes, KLF15 is a potent competitive inhibitor of Myocardin that becomes dysregulated during cardiac disease (106). KLF15 interacts with the basic domain of Myocardin and displaces Myocardin from SRF by competing for the same binding site. However, specific to left ventricular pathological hypertrophy, the loss of KLF15 expression results in non-repression of Myocardin activity, thus activating fetal genes and contributing to heart failure (106). Furthermore, the nuclear factor of activated T-cells c3 (NFATc3) transcriptional activates Myocardin during myocardial hypertrophy (107). Thus, multiple independent findings add to the complexity surrounding the regulation of Myocardin activity during cardiac hypertrophy.

Interestingly, a rare genetic mutation (1 out of 1137 control individuals) in the Myocardin gene has been described in a patient with congenital heart disease (108). This rare variant (K259R) in Myocardin is also hypomorphic, as it causes a partial loss in Myocardin function and reduces the ability of Myocardin to interact with SRF. However, this Myocardin mutation is specific to cardiac muscle tissue (108). The K259R mutation also acts as an auto-inhibitor to Myocardin and prevents stimulus-induced cardiac hypertrophy (108). Generating an animal model with a K259R Myocardin mutation will further clarify if it contributes to the embryonic or post-natal development of congenital heart disease.

Torrado *et al.* recently reported the *in vivo* delivery of a gene silencer targeted to Myocardin in a Dox-induced model of diastolic heart failure (Dox-DHF) in neonatal piglets (109). After illustrating high levels of Myocardin expression in hearts exhibiting DHF, short hairpin (sh) sequences targeting Myocardin mRNA degradation were generate: two days post sh-Myocardin gene delivery (via intra-myocardial injections) results in a decrease in Myocardin levels with a partial rescue towards normalization of the impaired diastolic function, contributing to a higher

neonatal survival rate (109). This study provides evidence that Myocardin serves as a potential therapeutic target for the treatment of heart failure.

1.8 Micro-RNA (miR) Regulation

As cardiomyocytes have a limited regenerative capacity, Myocardin plays a vital role in cardiac reprogramming to induce-cardiomyocyte-like (iCML) cells as an alternative to repairing a damaged heart (as described earlier). Christofou *et al.* have shown that a combination of micro-RNA/miRs such as miR-1 and miR-133a, with a cardiogenic transcriptional cocktail consisting of GMT + Myocardin (110) + Nkx2.5, reprogrammed human dermal fibroblasts into iCLM cells (111). Such evidence implicates miRs as important components during cardiac reprogramming and serve as potential therapies for cardiovascular disease (112,113). With the accumulating evidence on miRs in the heart (114), reports have illustrated miRNA regulation of the 3' un-translated region of Myocardin (115,116).

Dual expression of miR-145 and miR-143 regulate Myocardin/SRF in a CArG-Box dependent manner to activate smooth muscle differentiation (115). Concurrent with this positive effect, miR-145/143 also inhibits multiple repressive factors of Myocardin including ELK-1 and KLF4 that reduce proliferation of smooth muscle cells (115). These findings are the first evidence of miRNAs regulating coactivators and corepressors to dictate Myocardin-mediated smooth muscle cell fate. With respect to smooth muscle differentiation, Myocardin is also regulated by miR-1 that inhibits smooth cell proliferation (116,117). Interestingly, Myocardin positively regulates a cluster of miR-1/miR-133a to determine cardiac muscle or smooth muscle cell lineage (118). Thus, these independent reports illustrate Myocardin as a downstream target for miR regulation during heart development. Notably, miR-9 is able to repress Myocardin expression in cultured cardiomyocytes while miR-9 mimicking molecules inhibit cardiac hypertrophy in adult

mouse hearts (107). In a recent study, NF-κB (p65) elevated levels of miR-1 expression and inhibited Myocardin-mediated cardiomyocyte hypertrophy (119). Conversely, the use of antagomiRs, miR inhibitors, targeted muscle specific miR-133a that triggers cardiac hypertrophy, mediated by miR-133 modulation of the β-adrenergic signalling pathway (120). Whether miR-133 regulates Myocardin expression during hypertrophy or whether miR-133a is a downstream target of Myocardin to protect cardiomyocytes from cell death is currently unknown.

1.9 Regulated Cell Death

Traditionally, the process of cell death has been described as programmed or apoptotic versus accidental or non-programmed necrotic death (121). Apoptosis is a programmed mechanism of cell death without an inflammatory response that can be inhibited by use of pharmacological or genetic intervention (122,123). In contrast, necrosis is regarded as a morphologically distinct form of accidental or unregulated cell death that causes swelling and inflammation. During the last two decades, genetic studies combined with use of pharmacological agents has revealed that multiple forms of cell death are not by accident but occur via regulated signalling pathways, known as regulated cell death (RCD) (124,125).

Regulated Cell Death	Mechanism	Pharmacological Inhibition
Apoptosis	Caspase-dependent Mitochondrial outer membrane permeabilization (MOMP) - Apoptosome	caspase inhibitor (zVAD-fmk)
MPT-driven necrosis	MPT-pore opening Inner mitochondrial membrane (IMM) permeabilization	Cyclosporine A (CsA) NIM811
Necroptosis	RIP1/RIP3K Inflammation - Necroptosome	necrostatin-1 (Nec)
Pyroptosis	Inflammatory caspase-dependent Pyroptosome/inflammasome	caspase-1 inhibitor
Ferroptosis	Iron-dependent Lipid peroxidation and reactive oxygen species	ferrostatin-1
Autophagy-Dependent	Autophagolysosomes	3-methyladenine (3MA)

Table 1: Mechanisms of regulated cell death

As novel cell death pathways are characterized, the Nomenclature Committee of Cell Death 2018 recommends defining multiple pathways of RCD as exhibiting either apoptotic or necrotic morphology (non-apoptotic), and in contrast, recommends programmed cell death as a mode of RCD that occurs during physiological conditions (126,127). RCD can be defined by key characteristics including morphological features and biochemical features, as highlighted in Table 1. During apoptosis, external or internal signals via mitochondrial outer membrane permeabilization (MOMP), result in the formation of an apoptosome (128). This caspase-dependent process triggers formation of apoptotic bodies of contained cellular material that can be delayed by caspase inhibitors such as zVAD-fmk (129).

In contrast, mitochondrial permeability transition (MPT)-driven regulated necrosis involves permeabilization of the inner mitochondrial membrane (IMM) (130,131); process of MPT-pore opening is dependent upon a mitochondrial matrix protein, cyclophilin D, which can be pharmaceutically inhibited by cyclosporine A (CsA) or NIM-811 (129,132). MPT-pore opening

triggers organelle swelling, resulting in cellular rupture and necrotic death. As the cell ruptures it induces an inflammatory response, a morphological feature absent during apoptosis; associated with elevated levels of high mobility group box-1 (HMGB1), a nuclear protein that gets released in the cytoplasm of necrotic cells (133); recently implicated as a mediator of cellular damage in ischemia/reperfusion injury in the heart (134).

Similar to MPT-regulated necrosis, necroptosis (previously known as programmed or regulated necrosis) results in cellular swelling and plasma membrane, triggering an inflammatory response (135). This form of RCD is mechanistically dependent upon dimerization of receptor interacting protein kinases (RIPK) that form a necroptosome that can be inhibited by the presence of necrostatin-1 (136). Similar to necroptosis and MPT-driven necrosis, the pryoptosome also results in membrane rupture and inflammation (137). Ferroptosis is another form of non-apoptotic RCD that is iron-dependent and occurs through the loss of a lipid repair enzyme. This results in lipid peroxidation that can be inhibited by ferrostatin-1 (138).

Another non-apoptotic form of cell death is autophagy-dependent cell death or 'self-eating' (127). This consists of autophagic vacuoles known as autophagosomes, that degrade unwanted cellular contents in autophagolysosomes that can be inhibited by 3-methyladenine (139). It was recently reported by Ghavami and colleagues that simvastatin-induced apoptotic cell death (discussed in a latter section) in human atrial fibroblasts that was co-regulated by various modes of pro-survival mechanisms including autophagy and ER stress (139). Interestingly, the balance of pro-death and pro-survival proteins that initiate apoptosis were also implicated in simvastatin-induced cell death. Autophagy is a highly debated process, considered by some as a pro-survival response activated as a default mechanism to return to homeostasis, but can also trigger a mode of RCD termed autophagy-dependent cell death.

Determining which type of RCD is activated as a default mechanism or as a back-up plan currently requires further clarification and has been recently discussed elsewhere (127). Current literature suggests that impaired mitochondrial function is implicated in multiple pathways of cell death, yet execution of various pathways remains unknown. It is this curiosity that fuels the continued exploration of understanding how various mechanisms of RCD (such as apoptosis and regulated necrosis) are altered by mitochondrial dysfunction.

1.9.1 Apoptosis

Apoptotic cell death is coordinated by a network of caspases. Initiator caspases (caspase-8/9) activate downstream executioner caspases (caspase-3/6/7) that regulate two arms of apoptosis classified by the origin of death signal. Death signals with an extracellular input are extrinsic or receptor-mediated; signals that originate from within the cell initiate intrinsic or mitochondrial-mediated apoptosis. However, regardless of the source of the signal, caspases play a critical role in mediating the cellular events that ensue. The extrinsic pathway receives signals from the extracellular environment including death signals or ligands such as tumor necrosis factor-alpha (TNFa), which bind and activate death receptors located at the plasma membrane. Upon receptor activation, the cytoplasmic domain of the death receptors recruit adaptor proteins such as Fas-associated death domain (FADD) or TNF-receptor associated death domain (TRADD). This form a protein death inducing signalling complex (DISC) that recruits caspase-8 to activate executioner caspases and trigger apoptosis (122,141).

In contrast to death receptors receiving external signals, intrinsic apoptosis is mediated by internal signals via mitochondria (142). Key regulators of mitochondrial function include members of the Bcl-2 family. In the balance between life and death, anti-apoptotic factors are opposed by pro-apoptotic factors; the Bcl-2 family falls on both sides of this balance (143,144). During basal

conditions, anti-apoptotic proteins, Bcl-2 or Bcl-XL, inhibit pro-apoptotic members such as Bcl-2 associated X protein (BAX) and Bcl-2 antagonist or killer (BAK) (145-147). Upon cellular stress such as hypoxia, ER stress or DNA damage the balance is weighted towards cell death. The Bcl-2 homology-3 (BH3)-only pro-apoptotic proteins, can either directly activate BAX and BAK or counter the effects of Bcl-2, endogenous inhibitors of both BAX and BAK function, to bring about cell death (147,148). Conformational changes to activated BAX/BAK at the mitochondria creates a pore triggering MOMP, an essential response observed during intrinsic apoptosis (149-152). In response to intrinsic death signals, cells devoid of both BAX and BAK were unable to trigger MOMP nor induce apoptotic cell death (147). Permeabilization of the outer membrane results in leakage of apoptogenic factors from the mitochondrial intermembrane space including the release of cytochrome c.

In the cytosol, cytochrome c forms a protein complex consisting of activated caspase-9 and the apoptotic protease activating factor-1 (APAF1), known as the apoptosome, which activates downstream executioner caspases to mediate apoptosis (128,143,153). Although caspase-8 has a pivotal role during extrinsic apoptosis, it has also been reported to activate BID, another pro-apoptotic Bcl-2 protein, providing evidence of crosstalk between the extrinsic and intrinsic pathways via MOMP activation (147,154-156). Apoptosis is also mediated in a caspase-independent manner that increases expression of a nuclear enzyme, poly(ADP-ribose) polymerase-1 (PARP-1), and promotes the expression of PAR that mediates translocation of apoptosis inducing factor (AIF) to the nucleus, recently coined as parthanatos (127,157,158). Whether apoptotic cell death is mediated in a caspase-dependent or independent manner, both pathways results in nuclear condensation, DNA fragmentation, formation of apoptotic bodies, and

membrane blebbing that maintains plasma membrane integrity; triggering key cellular events that are absent during necrosis.

1.9.2 Necroptosis

Often associated with diseases of the immune response, programmed necrosis has become a controversial topic. Scientists now understand that necroptosis is a specific pathway of regulated cell death that is caspase-independent and mediated by two key members of the receptor interacting protein kinase family, RIPK1 and RIPK3 (125,135,159). Activation of RIPK1 can be triggered by multiple death receptors including tumor necrosis factor-alpha receptor-1 (TNFR1), a receptor that also mediates extrinsic apoptosis (as previously mentioned), that forms a receptor complex. Deubiquitinase enzymes such as A20 or CYLD, remove the polyubiquitin chains from RIPK1, thus promoting the dissociation from the receptor complex. In the absence of caspase activity, RIPK1 autophosphorylates and interacts with RIPK3, forming a necrosome (159,160). It has been suggested that necroptosis occurs when apoptosis or caspase activity is inhibited (by caspase inhibitor zVAD-fmk). Further phosphorylation of RIPK3 triggers phosphorylation of mixed lineage kinase like protein (MLKL). Phosphorylated MLKL translocates to the plasma membrane, resulting in membrane rupture in a calcium-dependent manner and tissue inflammation (161). It was recently shown that RIP3K activates STAT3, thus translocating STAT3 to the mitochondria, resulting in mitochondrial ROS generation (162). Such observations implicate impaired mitochondria as important mediators of TNF-induced necroptosis, but further experimental evidence is required.

The use of pharmacological inhibition by necrostatin-1 (NEC1), specifically inhibits RIPK1 activation while necrosulfonamide (NSA) specifically inhibits RIP3K, thus inhibiting necroptosis. However, NEC1 also has been reported to inhibit the ripoptosome, a multi-protein complex that

consists of RIPK and caspases, that activate apoptosis. Thus, NEC1 inhibits necroptosis through the necrosome, and certain forms of apoptosis dependent on the ripoptosome. Because NEC1 also targets the immune response, NEC1 analogues have been used to selectively inhibit RIPK1 activity. To further understand the mechanistic pathways underlying necroptosis, combination targeting of RIPK3 and MLKL must be taken into consideration to avoid overlap with apoptosis. Many studies suggest that the mitochondria are dispensable for necroptosis, as recently reviewed by Marshal and Baines (163).

1.9.3 Mitochondrial Permeability Transition-Regulated Necrosis

Mitochondria have dual roles in the cell life cycle: generating energy for cellular homeostasis and mediating cell death. Traditionally associated with apoptosis, recent evidence demonstrates that mitochondria permeability transition (MPT) results in a necrotic morphology (164,165). Based on genetic studies, this process has recently been coined as MPT-regulated necrosis, in efforts to replace the highly debated 'programmed necrosis' process. Permeabilization of the inner mitochondrial membrane, by formation of the mitochondrial permeability transition pore (MPTP) is a hallmark feature that occurs during MPT-regulated necrosis, in contrast to MOMP during apoptosis (164). During physiological conditions, the MPTP is thought to be open transiently to regulate mitochondrial calcium loading and metabolism (130,165). However, excessive mitochondrial calcium levels or elevated reactive oxygen species (ROS) results in prolonged or severe MPTP opening, creating a non-selective channel that allows exchange of molecules (up to 1.5 kDA) to move between the mitochondrial matrix and cytosol (166).

As the mitochondrial inner membrane-matrix proton gradient dissipates, the membrane potential across the inner membrane diminishes. This is followed by uncoupling of mitochondrial respiration and decreased ATP synthesis, key events that are absent during apoptosis. The

reduction in ATP combined with the disruption of calcium influx and osmotic pressure trigger mitochondrial swelling and outer membrane rupture. This results in cytochrome c release and caspase activation; a mechanistic overlap suggests necrosis is often associated with late apoptosis. One way to consolidate these pathways is the understanding that apoptosis is a caspase-dependent form of RCD that requires ATP to activate caspases. However, ATP synthase is dysregulated during MPTP, resulting in little or no ATP supply. With dysfunctional mitochondrial, cells ultimately rupture causing inflammation and MPTP-driven necrosis (165).

Since its functional characterization by Hunter and Haworth, the structure of MPT-pore continues to remain elusive, as it involves proteins from both inner and outer mitochondrial membranes and the mitochondrial matrix. Historically, MPT-pore was suggested to consist of three core proteins: cyclophilin D (CYPD), a mitochondrial matrix protein; a voltage-dependent adenine channel (VDAC) and adenine nucleotide transferase (ANT), an inner mitochondrial membrane transporter protein. However studies over the past decade propose an evolving model of MPTP, implicating ATP synthase within a multi-protein complex at the inner and outer mitochondrial membrane (167). With the use of genetic mice with CYPD deletion or use of pharmacological inhibition by cyclosporine A (CsA), NIM811 or Sanglifehrin A, the matrix protein CYPD remains as the undisputed regulator of MPTP (129,132,168,169). Although VDAC and ANT are not essential for MPT-pore opening (170,171), ANT is required for ATP synthesis yet also binds to CYPD (165,172).

Many proteins involved with the MPTP also interact with MOMP molecular machinery: mitochondria isolated from BAX/BAK double knock out mice (DKO) were resistant to MPT-pore opening but sensitive to apoptotic inducing factor (AIF). Although MPT-pore opening at the inner membrane also results in MOMP via BAX/BAK, opening of the MPT-pore does not result in

apoptotic cell death (173). Thus, the current model of MPTP consists of ATP synthase and CYPD that generate ATP to maintain mitochondrial function, until calcium or elevated ROS trigger a conformational change in ATP synthase, reducing ATP production (174). This results in mitochondrial swelling while BAX/BAK perforate the outer mitochondria membrane, triggering MPTP opening (131,167,175,176). Independent genetic studies demonstrate CYPD and BAX/BAK as essential components of MPT-pore, yet researchers require further evidence to validate ATP synthase as a key regulator of MPT-pore.

1.10 BH3-only proteins in the heart

Modulation of MPT-pore maintains cellular homeostasis and mitochondrial function that becomes dysregulated by effects of pro-death proteins: Bcl-2 homology3 (BH3) only proteins have been most demonstrated to activate different modes of cardiac cell death (165, 166). In cardiac cells Bcl-2 19kDa interacting protein-3, Bnip3, is highly responsive to hypoxic signals following ischemic injury to trigger cell death while Bnip3-like (Bnip3L) or Nix, is highly responsive to hypertrophic signals including adrenergic activation (177). It has been reported that both Bnip3 and Nix can regulate mitochondrial function and activate different arms of regulated cell death based on the subcellular localization.

Gary Isom's lab was the first to show that Bnip3 could trigger different cell death pathways when localized to the endoplasmic reticulum (ER) or mitochondria: Bnip3 targeted to the ER elicited an increase in calcium uptake by the mitochondria, triggering caspase-independent necrosis (178). Conversely, apoptosis involving MOMP was induced when Bnip3 was targeted to the mitochondria. Similarly, Gerald Dorn and colleagues showed mitochondrial targeted-Nix, could also activate caspase-dependent apoptosis; in contrast, ER targeted-Nix altered ER calcium levels, triggering MPT-regulated necrosis (164). Studies demonstrate that localization of pro-

apoptotic Bcl-2 family members promote crosstalk between ER and mitochondrial calcium flux during regulated cell death with potential therapeutic intervention for promoting cell survival.

This close relationship between the two organelles have led to advancements in understanding the functional role of the ER during cell death. The ER performs diverse roles within mammalian cells including protein synthesis and calcium handling (179,180). Disruption of ER function or ER stress triggers the unfolded protein response (URR) that activates machinery to maintain homeostasis but is also associated with various forms of cell death (181,182). ER stress and autophagy trigger necrosis in cells lacking BAX/BAK (183,184), employing a necrotic cell death mechanism when cells cannot die by apoptosis, further adding complexity towards the relationship between the ER and mitochondria. An overlap suggested to include MOMP, caspase activation, and ER stress has made it difficult for researchers to differentiate between apoptosis and MPT-regulated necrosis. Based on the current literature reviewed here, it is quite clear that some but not all forms of regulated cell death mechanistically overlap and implicate disruption of mitochondrial and ER function by BH3-only proteins.

1.11 Summary

The literature presented in this review serves to illustrate the established role of Myocardin as a transcriptional coactivator restricted to the cardiovascular system. Myocardin activity and expression is modulated by molecular regulators including microRNAs, that drive muscle differentiation in cardiac or smooth muscle tissue. Loss of Myocardin function in mouse embryos results in multiple congenital heart defects, associated with elevated levels of cell death; rapidly transitioning into heart failure that results in embryonic lethality. There is evidence that Myocardin has cardioprotective effects, but little is known about the role of Myocardin in preserving mitochondrial function and whether it opposes regulated cell death pathways mediated by BH3-only proteins in the heart.

CHAPTER II: Thesis rationale and specific aims

Members of the MADS-box family, MEF2 and SRF, are core transcription factors that regulate myogenic differentiation pathways; genetic studies reveal that loss of MEF2 results in mitochondrial deficiency while lack of SRF results in structural defects of the heart (185,186). Unpublished work from my supervisor's previous lab during his PhD suggest MEF2 and SRF are implicated to alter mitochondrial function; such observations contribute to reported findings of MEF2 regulation of a miR-1/miR-133a cluster and miR-133a regulation of mitochondria in the heart (187-189). However, the collaborative role of MEF2 and SRF regulation of miR-133a and its implication on regulating mitochondrial function during myogenic differentiation is unknown.

Myogenic properties of MEF2 and SRF are conveyed through Myocardin co-activation, regulating specific gene expression in cardiac and smooth muscle tissue (26,190). The functional loss of Myocardin results in congenital heart defects and embryonic lethality, while the specific cardiac deletion of Myocardin is associated with elevated levels of cell death and heart failure *in vivo* (30,49,52), However, the role of Myocardin to preserve mitochondrial function and oppose cardiac cell death during development and disease is unknown. Therefore, the purpose of my thesis is to investigate *a Myocardin-regulated genetic pathway that regulates mitochondrial function in cardiac muscle*. This would greatly contribute to the field of cardiovascular cell biology and identify the molecular machinery underlying mitochondrial function and cardiac cell survival during development; in hopes to develop novel pharmacotherapy strategies for preventing cardiac defects and reversing the progression to heart failure. This purpose is addressed experimentally by hypotheses presented in Manuscript I and Manuscript II:

1) Phosphorylation site on MADS-box motif of MEF2 regulates miR133a

2) miR133a regulates mitochondrial function through death gene Nix in three muscle cell lineages
3) Expression of Nix and cardiac necrosis is elevated in Myocardin null mouse embryos
4) Myocardin regulates a genetic pathway and mitochondrial function in cardiac muscle
5) Myocardin regulates mitochondrial permeability transition pore and calcium homeostasis through Nix repression.

In the first series of experiments, we investigated a genetic pathway that regulates muscle differentiation and mitochondrial function. I evaluated the role of MEF2 and SRF in cooperatively activating miR-133a that regulates muscle differentiation in skeletal, cardiac and smooth muscle: miR-133a preserves mitochondrial function and represses a cell death protein, Nix. This pathway becomes dysregulated in a rodent model of offspring exposed to gestational diabetes exhibiting elevated levels of Nix expression. Thus, I provide a mechanistic pathway that involves MEF2 and SRF regulation of mitochondrial function through miR-133a inhibition of Nix in all three muscle lineages, with implications in metabolic diseases.

With a reported genetic pathway of MEF2 and SRF activating miR-133a to oppose Nix and mitochondrial dysfunction, I next focused on the upstream molecular regulators. Myocardin serves as a potential molecular candidate for it co-activate MEF2 and SRF to regulate cardiac genes. Due to the lack of evidence evaluating the role of Myocardin to oppose cardiac necrosis, I investigated Nix expression in mouse embryos exhibiting the global loss of Myocardin function. I show loss of Myocardin increases Nix expression in a miR-133a dependent mechanism and confirm a Myocardin-regulated genetic pathway that preserves mitochondrial function in cardiac muscle. With a function in promoting cardiac cell survival, I demonstrate Myocardin preserves the

mitochondrial permeability transition pore and calcium homeostasis through Nix inhibition to prevent cell death via miR-133a activation in cardiac myocytes. I further demonstrate that the Myocardin genetic pathway is dysregulated in the infarcted border zone following ischemic heart injury but not during cytotoxicity-induced cardiac necrosis highlighting the specificity of this pathway to metabolic disease, with further implication in offspring exposed to gestational diabetes.

CHAPTER III: Manuscript I

3.1 Rationale

Core transcription factors coordinating muscle lineage include MEF2 and SRF regulate genes involved in muscle differentiation: these transcription factors belong to a family of proteins that contains a MADS-Box sequence that mediates factor dimerization, bind to DNA, and are co-activated by Myocardin (68,191,192). Interestingly, MEF2 is previously reported to regulate miR-133a in the heart but the role of SRF on miR regulation has yet to be evaluated. Despite the myogenic defects exhibited in $SRF^{-/-}$ null animals, or the mitochondrial deficiency and defective cell differentiation in $MEF2^{-/-}$ null animals, little is known about the cooperative role of MEF2 and SRF during myogenic differentiation or the impact of Myocardin during development. Therefore, my first manuscript presents evidence of a genetic pathway that promotes myogenic differentiation and mitochondrial function during fetal metabolic programming. This manuscript addresses the two experimental objectives outlined in the Thesis Rationale, which are: 1) Phosphorylation site of MADS-box motif on MEF2 activates miR-133a; 2) miR-133a preserves mitochondrial function through death gene Nix in three muscle cell lineages. These objectives are evaluated primarily in immortalized myogenic cells including skeletal myotubes (C2C12), cardiac myocytes (H9C2) and airway smooth muscle cells (ASMC).

A conserved MADS-box phosphorylation motif regulates differentiation and mitochondrial function in skeletal, cardiac, and smooth muscle cells.

Wajihah Mughal[1,6], Lucas Nguyen[6], Sofia Pustylnik[8], Simone Cristina da Silva Rosa[1,6], Steven Piotrowski[1,6], Donald Chapman[5,6], Min Du[8], Nezeka Ali[8], Jorg Grigull[8,9], Andrew J. Halayko[3,7], Michel Aliani[4], Matthew K. Topham[11], Richard M. Epand[12], Grant M. Hatch[2,6], Troy J. Pereira[2,6], Stephanie Kereliuk[2,6], John C. McDermott[8], Christof Rampitsch[10], Vernon W. Dolinsky[2,6] , Joseph W. Gordon[1,5,6*].

Departments of Human Anatomy and Cell Science[1], Pharmacology and Therapeutics[2], Physiology and Pathophysiology[3], Human Nutritional Sciences[4], College of Nursing[5], The Diabetes Research Envisioned and Accomplished in Manitoba (DREAM) Theme[6] and the Biology of Breathing Theme[7] of the Children's Hospital Research Institute of Manitoba, University of Manitoba, Winnipeg, Canada

Departments of Biology[8], and Mathematics and Statistics[9],York University, Toronto, Canada and Agriculture and Agrifood Canada[10], Morden, Manitoba Canada.

Huntsman Cancer Institute[11], University of Utah, Salt Lake City, United States

Department of Biochemistry and Biomedical Sciences[12], McMaster University, Hamilton, Canada

Author contribution:

WM: wrote manuscript, created figures, designed experiments, data analysis and interpretation, transfection, immunoblot, immunoprecipitation (IP), fluorescent microscopy, mitochondrial respiration, animal tissue protein extracts, and ImageJ analysis.
LN: fluorescent microscopy (Figure 4: I), assisted with Figure 4.
SP: Computational screen and MCK-luciferase assays (Supplemental)
SCSR: glucose uptake assay (Figure 6: E-F)
SP: telokin-luciferase assays (Supplemental)
DC: in vitro kinase assay (Figure 1: D-F; Figure 2), quantitative real-time polymerase chain reaction (qRT-PCR; Figure 3: D-E; Figure 4: E; Figure 7: B-E), IP (Figure 4: F)
MD: MCK-GFP experiments (Supplemental)
NA: MEF2A and SRF mutagenesis
JG: Computational screen (Supplemental)
AJH: generated hTERT human airway smooth muscle cells (hASMC; Figure 4: D)
MA: LC-MS metabolomics (Figure 7A)
MKT: Generated DGK null cells (Figure 4F)
RME: Generated DGK null cells (Figure 4F)
GMH: Technical assistance with DGK null cells (Figure 4F) and mitochondrial respiration (Figure 6A-D)
TJP and SK: isolated cardiac and soleus tissue from the gestational diabetes rodent model (Figure 7) and for metabolomics (Figure 7: A)
JCM: Supervision of SP, NA, and MD and financial support for their projects.
CR: phospho-peptide mapping with mass spectrophotometry analysis (LTQ ion-trap; Figure 1: D-

F; Figure 2).
VWD: generated diet-induced gestational diabetes rodent model (Figure 7), supervision and financial support of TJP and SK.
JWG: designed experiments, transfection experiments (Figure 1: A-B; Figure 3B, E), bioinformatics (Figure 1: C; Figure 5: A), phospho-peptide mapping (Figure 1: D-F; Figure 2), luciferase assay (Figure 3A and supplement), fluorescent microscopy (Figure 5F), advisor and corresponding author: conceptualized and wrote manuscript.

3.2 Abstract

Exposure to metabolic disease during fetal development alters cellular differentiation and perturbs metabolic homeostasis, but the underlying molecular regulators of this phenomenon in muscle cells are not completely understood. To address this, we undertook a computational approach to identify cooperating partners of the myocyte enhancer factor-2 (MEF2) family of transcription factors, known regulators of muscle differentiation and metabolic function. We demonstrate that MEF2 and the serum response factor (SRF) collaboratively regulate the expression of numerous muscle-specific genes, including microRNA-133a. Using tandem mass spectrometry techniques we identify a conserved phosphorylation motif within the MEF2 and SRF MADS-box that regulates microRNA-133a expression and mitochondrial function in response to a lipotoxic signal. Furthermore, reconstitution of MEF2 function by expression of a neutralizing mutation in this identified phosphorylation motif restores microRNA-133a expression and mitochondrial membrane potential during lipotoxicity. Mechanistically, we demonstrate that microRNA-133a regulates mitochondrial function through translational inhibition of a mitophagy and cell death modulating protein, called Nix. Finally, we show that rodents exposed to gestational diabetes during fetal development display muscle diacylglycerol accumulation, concurrent with insulin-resistance, reduced microRNA-133a and elevated Nix expression, as young adult rats. Given the diverse roles of microRNA-133a and Nix in regulating mitochondrial function, and proliferation in certain cancers, dysregulation of this genetic pathway may have broad implications

involving insulin resistance, cardiovascular disease, and cancer biology.

Key Words: MEF2, SRF, microRNA-133a, muscle differentiation, mitochondrial function.

Abbreviations: MEF2, myocyte enhancer factor-2; SRF, serum response factor; miR-133a, microRNA-133a; MADS domain/box, Mcm1 Agamous Deficiens SRF; PKCδ, Protein Kinase-Cδ; HFS, high fat and sucrose diet; Nix/Bnip3L, BCL2/adenovirus E1B 19 kDa protein-interacting protein 3-like; PTP, mitochondrial permeability transition pore; DGKδ, diacylglycerol kinase-δ.

3.3 Introduction

Extensive cell and molecular analysis has identified numerous extracellular cues that regulate skeletal, cardiac, and smooth muscle myogenesis (193-195). However, the impact of nutrient availability and metabolic excess on myogenesis has been less studied. One of most important periods of myogenesis is during gestation and fetal exposure to metabolic diseases dramatically alters the development and post-natal metabolism of muscle. For example, the offspring of overweight pregnant rats have reduced muscle fibers and nuclei (196). In addition, fetal exposure to diabetes during pregnancy increases the risk for early-onset insulin resistance in the offspring (197); however, the key molecular regulators responsible for fetal metabolic programming have not been characterized in muscle tissues.

During mammalian development, myogenic precursors derived mostly from mesenchymal populations, commit to one of three main muscle lineages: skeletal, cardiac, and smooth muscle (194,198-200). Amongst the core muscle transcriptional regulators is the myocyte enhancer factor 2 (MEF2) family of transcription factors, where gene-targeting studies in both *Drosophila* and

mammals have reported essential roles for the MEF2 family in the development and post-natal remodeling of all muscle lineages (201).

The MEF2 family is composed of four transcription factors, MEF2A to -D, which have both overlapping and non-redundant functions. The amino terminus of MEF2 proteins contains a highly conserved 58-amino acid MADS-box that mediates dimerization and binding to a cognate *cis* element, (T/C)TA(A/T)$_4$TA(G/A) (191). The transcriptional activity of MEF2 proteins, along with their ability to bind DNA is highly regulated by post-translational modification, including phosphorylation (202-204). In mammalian cells, the only other MADS-box containing transcription factor is the serum response factor (SRF), which binds to a similar cognate *cis* element, CC(A/T)$_6$GG (191), and has also been implicated in smooth muscle and striated muscle differentiation (131,186,192). Given their similar structure and overlapping function, surprisingly little is known regarding the cooperation between MEF2 and SRF proteins during muscle differentiation, and whether these MADS-box factors serve to coordinate aspects of mitochondrial function.

MEF2 proteins regulate metabolism and muscle fibre-type by direct transcriptional activation of numerous enzymes and transporters important for muscle metabolism, as well as the mitochondrial biogenesis inducer PGC-1α (68). Furthermore, MEF2 has been demonstrated to regulate the expression of several microRNA clusters, including microRNA-133a (miR-133a), that operate during muscle differentiation and regulate mitochondrial function (187,188). In skeletal muscle, mice harboring deletions in the miR-133a alleles display a severe myopathy, accompanied by impaired mitochondrial respiration (188). Furthermore, miR-133a has been shown to regulate smooth muscle phenotype by altering proliferation (205).

Diacylglycerol levels are chronically elevated in muscle tissues of obese and diabetic rodent

models, and contribute to the lipotoxic and insulin resistant state (206,207). Therefore, one possible intracellular signaling pathway linking muscle metabolism with myogenesis is the diacylglycerol-protein kinase C (PKC)δ pathway. This pathway has been implicated in aberrant vascular smooth muscle growth, and can be viewed as an integrator of both metabolic and mitogenic cues (67). Interestingly, in human neonatal fibroblasts, PKCδ can inhibit SRF function by direct phosphorylation of threonine-160, which impairs SRF DNA binding leading to cell senescence (208). Furthermore, PKCδ signaling is reinforced by the proteolytic cleavage of a small constituently active PKCδ catalytic fragment from full-length PKCδ (208). However, whether this pathway regulates MEF2 or SRF in muscle tissues is untested.

In this report, we present the findings of an unbiased bioinformatics screen, utilizing position weight matrices. This computational approach predicted the co-occurrence of *cis* elements and a functional interaction between MEF2 and SRF. Experimentally, we demonstrate MEF2C and SRF cooperatively activate the expression of miR-133a. Furthermore, we identify a conserved MADS-box phosphorylation motif, targeted by PKCδ, that serves to regulate endogenous miR-133a expression and mitochondrial function in all three muscle lineages. Finally, our data reveals that this signaling module is regulated by lipotoxicity to control mitochondrial function through the regulation of Nix, a known mitophagy and programmed cell death mediator (209).

3.4 Materials/Methods

Bioinformatics screen to predict functional transcription factor interactions. Muscle gene expression data was compiled from the profile published by Zhang et al (210). Genomic sequence representing the proximal promoter region (-1000 to +200 bp) of 46 muscle genes was extracted from the Database of Transcriptional Factor Start Sites (DBTSS) and used for this analysis.

Position weight matrices of all known mouse transcription factors were collected from the TRANSFAC and Wasserman-Fickett databases. We determined the conserved index (Ci) by calculating the degree of conservation of individual nucleotides in the matrix as a numerical value. In this model, Ci varies between 0 and 100, where 100 represents a position with total conservation of one nucleotide, and 0 represents equal distribution of all four possible nucleotides. Using this approach, we defined a core binding region as a region with four consecutive nucleotide positions with the highest Ci values, and used this core binding region to reduce the number of matches in the position weight matrices. We calculated the optimized matrix threshold and screened the promoter regions of the target sequences with the position weight matrices and optimized matrix threshold to detect interacting partners of MEF2 proteins based on the co-occurrence of *cis*-regulatory elements.

Plasmids. The MEF2 plasmids were described previously (211-213). The plasmid expressing the PKCδ catalytic fragment was kindly provided by K. Wheaton. The miR-133a expression plasmid was purchased from Addgene (Principal Investigator David Bartel, plasmid 26326) (214). The shRNA targeting SRF was based on the targeting sequence previously described by Medjkane et al (5'-CTGCAGCCCATGATCACCA-3') (215). Sense and antisense oligonucleotides containing the target sequence were purchased from Sigma, annealed, and ligated into pSilencer 3.0 H1 (Ambion). The Nix (Bnip3L), shNix, and Bcl-2 plasmids were purchased from Addgene (Principal Investigator Wafik El-Deiry, plasmid 17467, 17469, and Principal Investigator Clark Distelhorst, plasmid 18003) (216,217).

Cell culture and transfections. All cell lines were maintained in Dulbecco's modified Eagle's

medium (DMEM; Hyclone), containing penicillin, streptomycin, and 10% fetal bovine serum (Hyclone) at 37 degrees celsius and 5% CO_2. Generation of the hTERT senescent-resistant human airway smooth muscle cells (hASMC) was described previously (218), as were the DGKδ-null fibroblasts (162). C2C12 and hASMCs were transfected using JetPrime Polyplus reagent, and the H9c2 cell line was transfected using Qiagen's Polyfect reagent, as per the manufacturer's instructions. C2C12 were differentiated by re-feeding cells in 2% fetal bovine serum (Hyclone) for to 2-5 days, as indicated in the figure legends, while H9c2 cells were differentiated in 1% fetal bovine serum (Hyclone) for 24-48 hours. Palmitate conjugation and treatments were performed as described by Chavez et al. (219).

In vitro kinase assay. Synthetic peptides (Fisher Scientific) were resuspended in molecular biology grade water at a concentration of 1 mg/ml. Peptide sequences used were MEF2 wild-type amino acids 14-27: ERNRQVTFTKRKFG, MEF2 Threonine-20 mutation: ERNRQV**A**FTKRKFG, SRF amino acids 154-167: KLRRYTTFSKRKTG. These peptides were used as the substrate in a PKCδ kinase assay kit (SignalChem) according to the manufacturer's instructions, with the exception that [^{32}P]-ATP was replaced with fresh molecular biology grade ATP. The manufacturer's CREBtide synthetic peptide substrate (KRREILSRRPSYR) was used as a positive control in each assay. Following incubation at 30 degrees Celsius for 15 minutes, reactions were frozen at -80 degrees Celsius prior to mass spectrometry analysis.

Phospho-peptide mapping. Prior to mass spectrometry analysis, kinase assays were prepared using C_{18} ZipTips (Millipore), according to the manufacturer's protocol, to desalt and concentrate peptides. Samples in 50% acetonitrile, 0.1% formic acid were introduced into a linear ion-trap

mass spectrometer (LTQ XL: ThermoFisher, San Jose CA) via static nanoflow, using a glass capillary emitter (PicoTip: New Objective, Woburn, MA). All spectra were acquired using the ZoomScan setting. For MS^2, collision-induced dissociation (CID) or electron-transfer-dissociation (ETD) were used. For the former, collision energy was set to 25%; for the latter a reaction time of 100 ms with fluoranthane was set. Spectra were sequenced de novo manually.

Immunoprecipitation and immunoblotting. Protein extractions were achieved using a RIPA lysis buffer containing proteases inhibitors and phosphatase inhibitors (Santa Cruz). Protein concentrations were determined using a Bio-Rad Protein assay kit. Extracts were resolved using SDS-PAGE and transferred to a PVDF membrane. Immunoblotting was carried out using appropriate primary antibody in 5% powdered milk or BSA in TBST. Appropriate horseradish peroxidase-conjugated secondary antibody (Jackson; 1:4000) was used in combination with chemiluminescence to visualize bands. Immunoprecipitations utilized the Immunocruz kit (Santa Cruz), described previously (213), and complexes were probed by immunoblot using the RXRXXpS/T or RXXpS/T phospho-antibodies from Cell Signaling Technology.

Fluorescent staining. MitoTracker Red CMXRos was purchased from Cell Signaling Technology and applied to cells for 30 minutes. Following incubation, cells were re-fed standard DMEM. TMRM, Calcein-AM, MitoView Green, and Hoechst 33342 were purchased from Biotium. PTP imaging was performed by quenching the cytosolic Calcein-AM signal with 5 μM cobalt chloride during the incubation period. All imaging was done on an Olympus IX70 inverted microscope with QImaging Retiga SRV Fast 1394 camera using NIS Elements AR 3.0 software. Quantification, scale bars, and processing was done on ImageJ software.

Mitochondrial respiration and glucose uptake. Mitochondrial respiration was determined on a Seahorse XF-24 Extracellular Flux Analyzer, as described previously (220). Calculated respiration rates were determined as per manufacturer's instructions (Mito Stress Kit; Seahorse). Insulin-stimulated glucose uptake was evaluated in differentiated H9c2 cells incubated the presence or absence of 10 nM insulin in phosphate-buffered saline (PBS) for 15 minutes, followed by 15 minutes with the inclusion the fluorescent D-glucose analog 2NBDG (200 µM; Molecular Probes). Cells were imaged by standard techniques and quantified using ImageJ.

Diet-induced gestational diabetes model. All procedures in this study were approved by the Animal Welfare Committee of the University of Manitoba, which adheres to the principles for biomedical research involving animals developed by the Council for International Organizations of Medical Sciences. Female Sprague-Dawley rats were obtained at 4 weeks of age (University of Manitoba Colony) and randomly allocated to a low-fat diet (10% fat, Research Diets D12450B) or a high-fat and sucrose diet (45% fat, Research Diets D12451) for 6 weeks to induce pre-gestational glucose intolerance (197,221). The female rats continued on their respective diets throughout pregnancy and weaning. The high-fat/sucrose-fed female rats developed hyperglycemia characteristic of gestational diabetes (GDM) while pregnant. Pups were weaned at 3 weeks of age and randomly assigned to either low-fat or high-fat and sucrose diets for 12 weeks, creating four experimental groups: the offspring of lean mothers fed low-fat or high-fat/sucrose diets and the offspring of GDM mothers fed low-fat or high-fat/sucrose diets. For tissue analysis, rats were euthanized by overdose of sodium pentobarbital, and the heart and soleus muscles were dissected, rinsed in PBS, and immediately clamp frozen in liquid nitrogen.

Quantitative PCR. Total RNA was extracted from cultured cells and pulverized frozen tissue by TRIzol method. For microRNA analysis all primers were purchased from Quanta BioSciences. cDNA was generated using QScript MicroRNA cDNA Synthesis kit (Quanta BioSciences) and q-RT-PCR performed using PerfeCTa SYBR green super mix on a ABI 7500 Real-Time PCR Instrument, and normalized to RNU6 expression. For mRNA analysis, following column purification using Qiagen RNeasy kit and DNase treatment, cDNA was generated with QScript cDNA super mix (Quanta BioSciences) and analyzed as described above, and normalized to β-actin expression. Primers used were PGC-1α total: Forward 5'-CAGCTTTCTGGGTGGATTGA-3' and Reverse 5'-GCTCATTGTTGTACTGGTTGGA-3', Mitofusin-2: Forward 5'-CTCTCAAGCACTTTGTCACTGC-3' and Reverse 5'-TGTATTCCTGTGGGTGTCTTCA-3', β-actin: Forward 5'-TTGCTGACAGGATGCAGAAG-3' and Reverse 5'-TAGAGCCACCAATCCACACA-3'.

Mass spectrometry metabolomics analysis. Analysis of total soleus lipids was performed using a lipid soluble extraction, and analysis was performed as described previously (197). Briefly, lipid extracts were reconstituted with 100 µL of 80% acetonitrile prepared in deionized water. Metabolomics analysis was performed on a 1290 Infinity Agilent high-performance liquid chromatography (HPLC) system coupled to a 6538 UHD Agilent Accurate Q-TOF LC/MS equipped with a dual electrospray ionization source. A 3 x 50 mm, 2.7µ Agilent Poroshell column was used to separate metabolites while the column temperature was maintained was at 60°C. The mass detection was operated using dual electrospray with reference ions of m/z 121.050873 and 922.009798 for positive mode; and m/z 119.03632 and 980.016375 for negative mode. The

workflow utilized for data processing comprised several algorithms used by Agilent Mass Hunter Qualitative (MHQ, B.05) and by Mass Profiler Professional (MPP, 12.6).

3.5 Results

Computational Screen to Predict Transcription Factor Cooperation During Muscle Differentiation. To identify factors that collaborate with MEF2 proteins during muscle differentiation, we performed a bioinformatics screen that combined position weight matrices, conservation index, and optimized matrix threshold approaches. Since combinations of transcription factors regulate gene expression through their respective *cis* elements, this computational approach is founded on the hypothesis that one could predict functionally interacting factors based on the co-occurrence of their *cis* elements, within evolutionary conserved genomic regions. This analysis revealed that MEF2 is predicted to have target-genes in common with seven other transcription factors (Supplemental Table 1). Among these was a predicted functional interaction between MEF2 and SRF. Since both MEF2 and SRF contain MADS-box domains, we investigated the hypothesis that MEF2 and SRF functionally cooperate during muscle differentiation and that this cooperation is regulated by a common intracellular signaling pathway.

MEF2 and SRF cooperatively activate select muscle-specific promoters. In order to experimentally validate the results of our bioinformatics screen, we initially studied the activation of the muscle creatine kinase (MCK) promoter as an index of muscle gene expression (222). We also evaluated representative cardiac (atrial natriuretic factor, ANF) and

Figure 1.

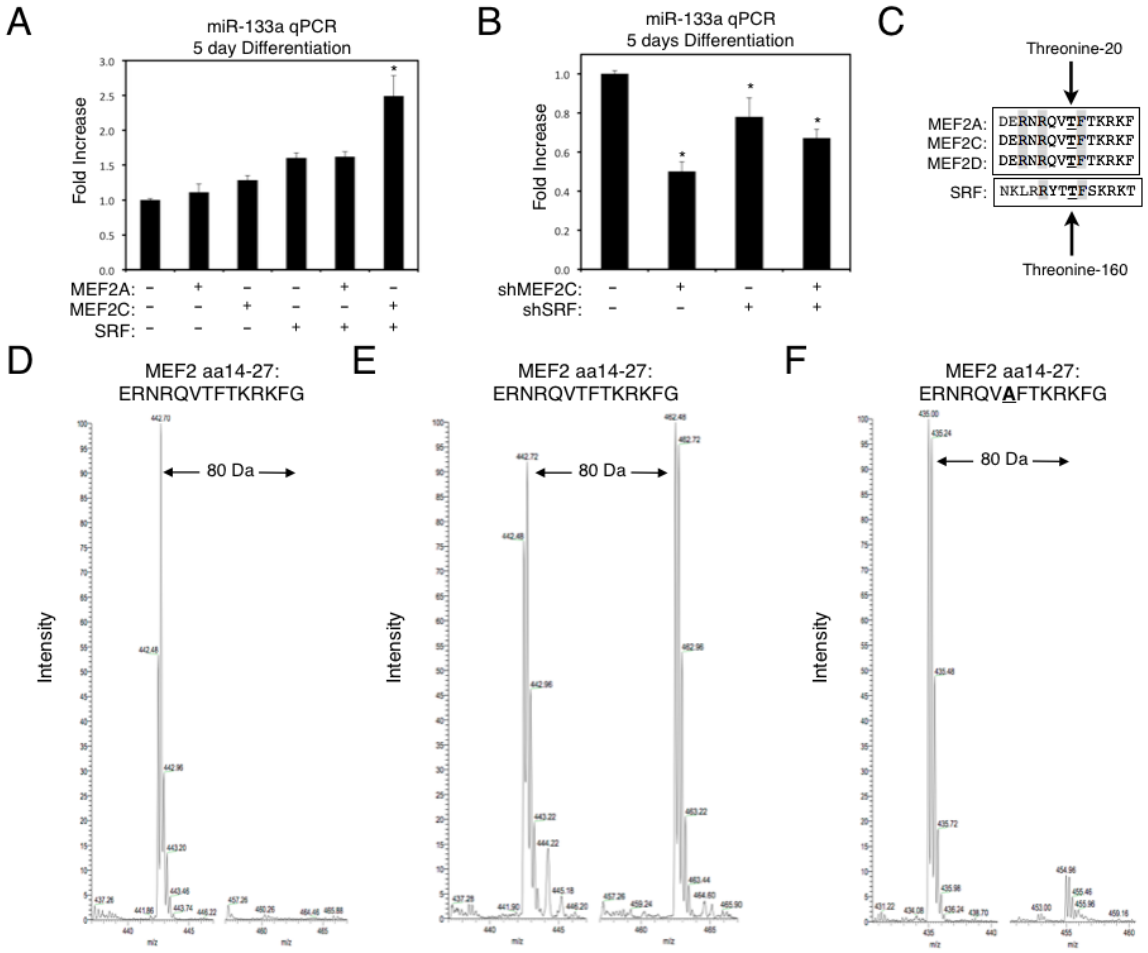

I - Figure 1: PKCδ inhibits the cooperation between MEF2 and SRF by direct phosphorylation.
A. C2C12 myoblasts were transfected with MEF2A, MEF2C, or SRF, as indicated. Following recovery, cells were differentiated in low serum media for 5 days and harvested for RNA. Quantitative PCR assays were performed using the ΔΔCT method, where RNU6 was used as an internal control. B. C2C12 cells were transfected with short-hairpin RNAs targeting MEF2C (shMEF2C) or SRF (shSRF), as indicated. Following 5 days for differentiation, cells were harvested and assayed as described above. C. Schematic demonstrating the conservation surrounding the MEF2 threonine-20 and SRF threonine-160 phosphorylation motif. D-F. Single ion monitoring (SIM) scans of the wild-type peptide (D and E) spanning the MADS-box motif of MEF2A. The unphosphorylated peptide (left) has a 442 m/z, while the putative phosphorylation (right in B) showing an increased m/z of 20 that corresponds to PO_3 (M = 80.00 Da). Panel F shows a SIM scan of a mutated peptide where threonine-20 is replaced with alanine. On the right, phosphorylation of this mutate peptide is negligible at the predicted m/z that corresponds to the addition of a PO_3 (M = 80.00 Da). Both peptides are quadruply charged ($z = 4^+$). Data are represented as mean ± SEM. * $p<0.05$ compared to control.

smooth muscle (telokin) promoters. As predicted by our bioinformatics screen, MEF2A and SRF co-operatively activated these promoters in Cos7 cells (Supplemental Figure 1). Next, we systematically engineered mutations in these promoters in order to understand how preventing MEF2 or SRF binding impacts promoter activity. For these experiments, the promoters were transfected into C2C12 cells, H9c2 cells, or a senescent-resistant human airway smooth muscle cell line (hASMC), to represent skeletal, cardiac, smooth muscle myoblasts. Mutation of either the MEF2 or SRF *cis* element reduced the activity of the MCK, ANF, and telokin promoters (Supplemental Figure 1). Interestingly, mutation of the MEF2 *cis* element rendered the ANF and telokin reporter-genes less responsive to mutation of the SRF site. Furthermore, mutation of all three *cis* elements simultaneously in the MCK promoter did not reduce promoter activity further than mutation of either MEF2 site alone. Collectively, these observations demonstrate a degree of functional dependency between MEF2 and SRF in the activation of these promoters in three different muscle cell lines.

MEF2C and SRF regulate the endogenous expression of miR-133a. Next, we focused our studies on the endogenous expression of a single MEF2 and SRF target gene that is expressed in all muscle lineages. For this we chose miR-133a, given that it has been recently identified as a regulator of muscle growth and metabolic function (187,188,205). We began with a gain of function approach, where C2C12 myoblasts were transfected with MEF2A, MEF2C, and SRF, alone and in combination. The combination of MEF2C and SRF induced endogenous miR-133a expression in differentiating C2C12 myotubes (Figure 1A), and we confirmed that ectopic expression of MEF2C and SRF was maintained at this time-point (Supplemental Figure 2). Importantly, either factor alone had no effect, and MEF2A did not activate miR-133a expression. Interestingly,

miR-133a has been shown to target both SRF and MEF2C, which suggests an element of feedback controlling the expression of this microRNA (223,224). Next, C2C12s myoblasts were transfected with plasmids encoding short-hairpin-RNAs (shRNAs) targeting MEF2C and SRF. Knock-down of MEF2C or SRF individually, reduced the endogenous expression of miR-133a in differentiating myotubes (Figure 1B). Interestingly, simultaneous knock-down of both MEF2C and SRF did not additively reduce miR-133a expression (Figure 1B). Furthermore, knockdown of MEF2C and SRF was confirmed by qPCR at this time-point (Supplemental Figure 2). These findings suggest a degree of functional dependency between MEF2C and SRF in the regulation of miR-133a expression that is consistent with our promoter analysis in Supplemental Figure 1.

Peptide-mapping of PKCδ phosphorylation of MEF2 and SRF by mass spectrometry. Previously it was demonstrated that PKCδ phosphorylates SRF at threonine-160 to inhibit DNA binding[24]. Since threonine-160 lies within the MADS-box of SRF, we aligned the amino acid sequence of the MEF2 and SRF MADS-domains and found a high degree of conservation surrounding this phosphorylation site (Figure 1C), suggesting that this is a conserved MADS-box phosphorylation motif. To determine if PKCδ directly phosphorylates this conserved MADS-box motif in MEF2 proteins, we performed *in vitro* kinase assays using engineered peptides representing amino acids 14-27 of MEF2. Following exposure to a kinase reaction with purified PKCδ, peptides were analyzed by mass spectrometry. Shown in Figure 1D, a single ion monitoring (SIM) scan of the the control peptide displayed a predominant peak at m/z of 442.74 ($z=4^+$); however, following kinase incubation the peptide showed an increased m/z of 20, corresponding to the addition of a phosphate (PO_3) to the peptide (Mass = 80.00 Da; Figure 1E). Although an 80 Da mass shift is consistent with phosphorylation, it is not unequivocal, nor does it permit localization of the

phosphorylated amino acid. For location, we engineered an additional peptide where the residue representing threonine-20 was mutated to a neutral alanine. Mutation of threonine-20 substantially reduced the 80 Da mass-shifted (Figure 1F). These findings support the notion that threonine-20 is phosphorylated by PKCδ.

Next, we analyzed the MS^2 spectra produced by collision-induced dissociation (CID) of the precursor ion with m/z = 462.98 ($z=4^+$; shown in Figure 2A). CID typically fragments phosphopeptides (pS or pT) by breaking the labile O-phosphodiester bond. This results in the neutral loss of H_3PO_4, and a prominent neutral loss product-ion dominates the resulting MS^2 spectrum. CID of the wild-type phosphopeptide yielded a product-ion with m/z = 438.42 (delta = 24.56), consistent with phosphorylation (98.0/4 = 24.5; Figure 4A). Furthermore, the precursor ion, (m/z = 462.98, $z=4^+$) was selected for electron transfer dissociation (ETD). This technique breaks peptide bonds, but retains side-chain modifications, such as phosphorylation. MS^2 spectra following ETD definitively identified threonine-20 of MEF2 as the phosphorylation residue (Figure 2B). Similar findings were observed for peptides spanning threonine-160 of SRF (Figure 2C, -D, -E).

Site-directed mutagenesis of the PKCδ phospho-acceptor site on MEF2 and functional analysis.
In order to ascertain the cellular significance of PKCδ-dependent phosphorylation of threonine-20 of MEF2 and threonine-160 of SRF, we generated neutral alanine (MEF2A-T20A and SRF-T160A) and phospho-mimetic aspartic acid (MEF2A-T20D and SRF-T160D) mutations at these residues. Shown in Figure 3A, the MEF2A-T20A mutation displayed a modest increase in activity compared to wild-type MEF2A on a concatemerized MEF2-driven promoter (MEF2-luc), while the phospho-mimetic MEF2-T20D mutant provided no activation of

Figure 2.

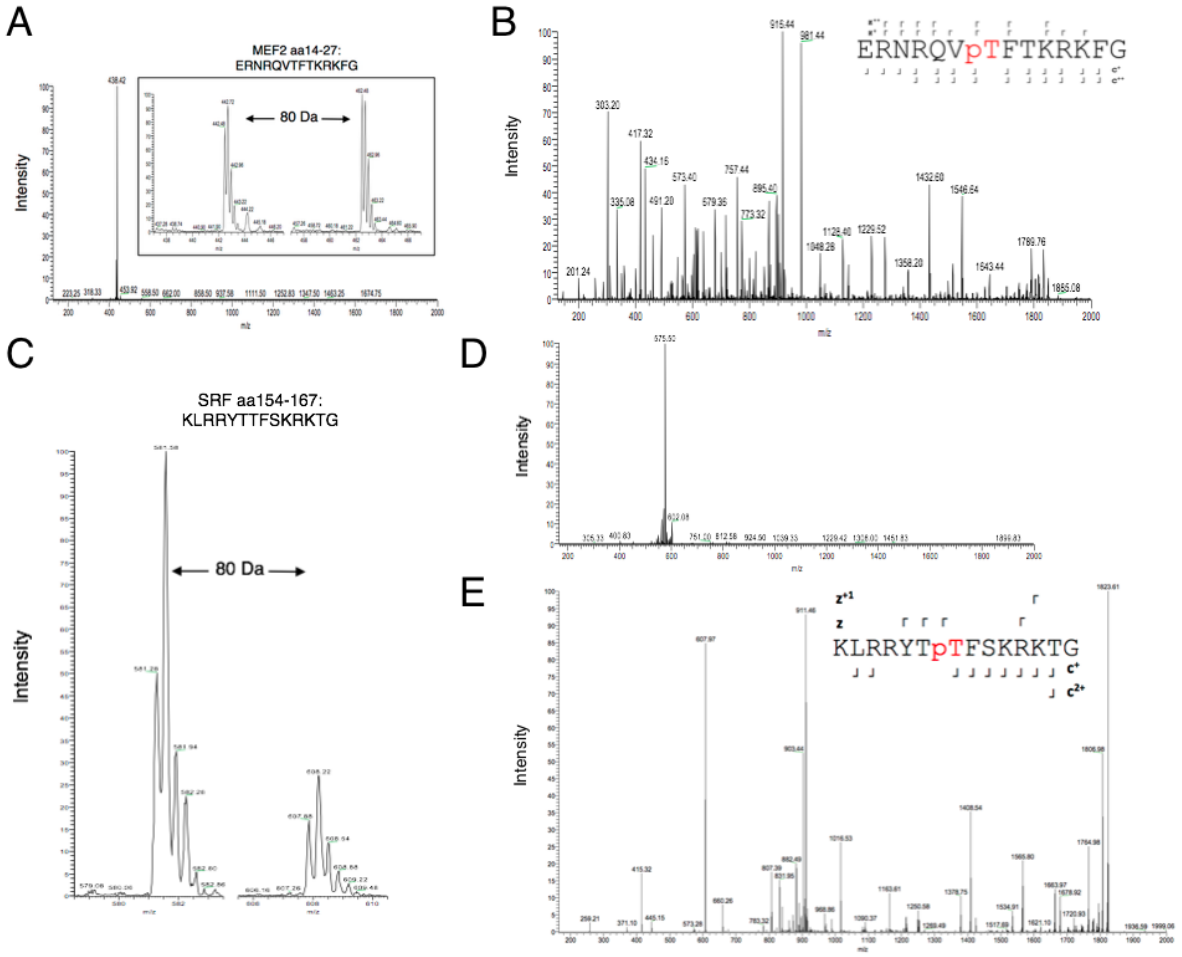

I - Figure 2: Identification of Threonine-20 as a putative PKCδ phosphorylation residue.
A. Inset: SIM scan of native peptide (442.72, z=4^{+}) and putative phospho-peptide (462.48, z=4^{+}), as shown in Figure 1. The mass shift of +19.76 m/z is consistent with of a quadruply charged peptide ion. Both threonine-20 and threonine-22 are possible sites of phosphorylation. Main Figure: CID MS^{2} spectrum of the native peptide showing a prominent neutral loss ion at 438.42 m/z with z=4^{+}. This represents a -24.56 Da shift consistent with a neutral loss of phosphate from threonine-20 or threonine-22 of the native peptide. B. Fragmentation of the phospho-peptide (462.48, z=4^{+}) by electron transfer dissociation (ETD) produced a near-complete c and z ion series with some y ions also present. Analysis of this fragmentation spectra confirmed that threonine-20 is the preferred phosphorylation residue. Inset: Schematic illustrating the z and c ions detected by ETD. C. Single ion monitoring (SIM) scan of a peptide spanning the MADS-box motif of SRF (amino acids 154-167). The unphosphorylated peptide (left) has a 581.58 m/z (z=3^{+}), while the putative phosphorylation (right in A, m/z of 608.22) showing an increased m/z of 26.64 that corresponds to PO_3 (M = 80.00 Da). D. CID MS^{2} spectrum of the phospho-peptide in (C) with m/z of 608.22, showing a prominent neutral loss ion at 575.5 m/z with z=3^{+}. E. ETD MS^{2} spectrum of SRF confirming phosphorylation of threonine-160.

this reporter-construct. The expression of these mutants was confirmed by western blot to ensure that the introduced mutations did not alter MEF2 stability (Figure 3A). Similar findings were observed using a MCK-GFP reporter gene in differentiating C2C12 cells (Supplemental Figure 3C). Furthermore, we generated alanine and aspartic acid mutations of threonine-20 in a MEF2-VP16 fusion construct, where the MADS-box and adjacent MEF2 domain (amino acids 1-91 of MEF2A) is fused to the viral VP16 transcriptional activation domain (67,162). These expression plasmids demonstrated similar activation pattern in a luciferase assay as the MEF2A mutations (Supplemental Figure 3). Finally, we determined that the phosho-mimetic mutations in MEF2A and SRF could disrupt the functional cooperation between these factors on the telokin promoter (Supplemental Figure 3D).

Next we evaluated whether the endogenous expression of miR-133a by MEF2C and SRF was regulated by PKCδ. When the catalytic fragment of PKCδ was co-expressed with MEF2C and SRF, the induction of miR-133a was inhibited in differentiating C2C12s (Figure 3B). To determine the effect of an endogenous activator of PKCδ on miR-133a expression, we exposed cells to the saturated fatty acid palmitate (206). This treatment increased the active catalytic fragment of PKCδ (Figure 3C). Concurrently, we observed reduced expression of miR-133a (Figure 3D). Furthermore, when C2C12 cells were transfected with T20A-VP16, palmitate treatment was unable to inhibit miR-133a expression (Figure 3E). To further define the role of diacylglycerols and PKCδ activation in the phosphorylation of the MADS-box motif, we utilized mouse embryonic fibroblasts genetically deficient in diacylglycerol kinase-δ (DGKδ) (162). These cells display defective lipogenesis and reduced levels of diacylglycerols[29]. Compared to wild-type cells, DGKδ-null fibroblasts have reduced PKCδ activity, determined by expression of the active catalytic

Figure 3.

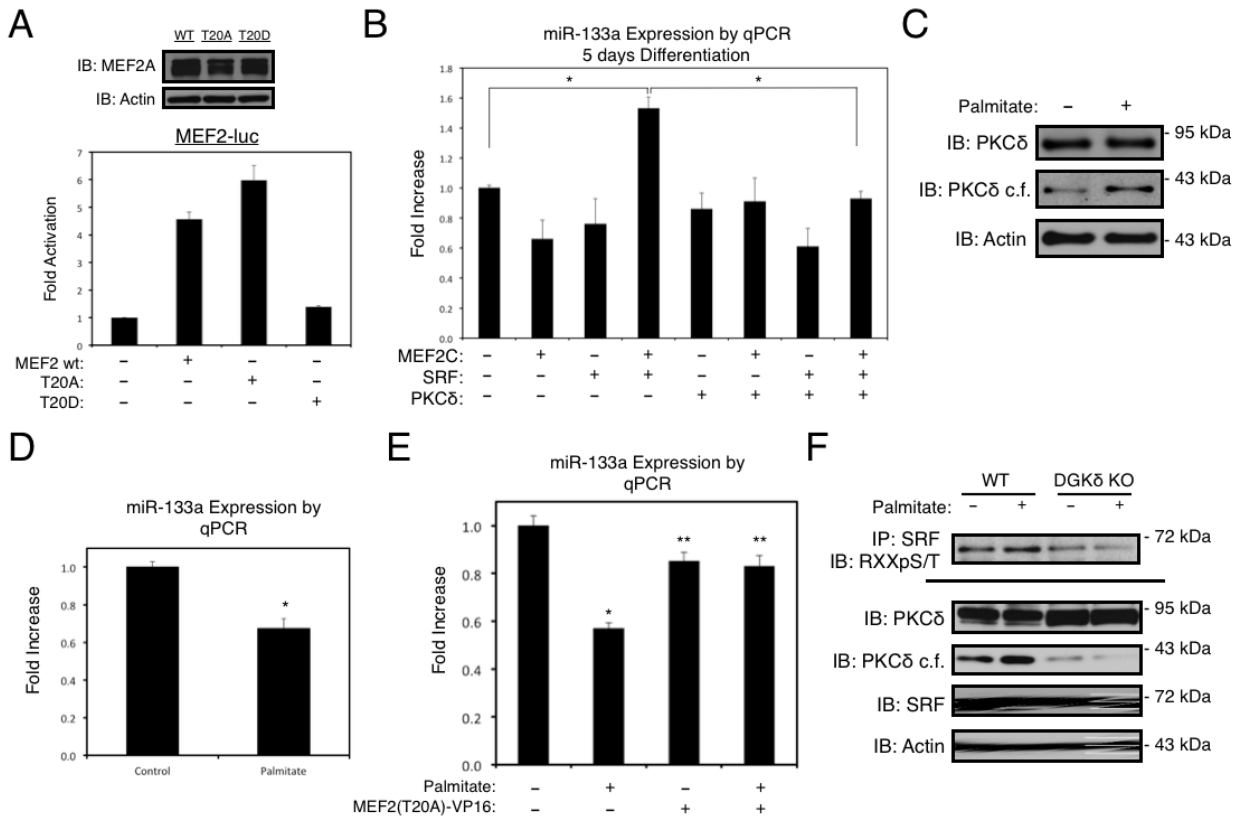

I - Figure 3: Mutational analysis of Threonine-20.

A. HEK293 cells were transfected with MEF2A (MEF2 wt), or a plasmid containing MEF2A where threonine-20 is mutated to a neutral alanine (T20A) or phospho-mimetic aspartic acid (T20D), as indicated, and subjected to western blot (above). 10T1/2 cells were transfected, as above, along with MEF2-driven luciferase reporter gene (MEF2-luc). Extracts were subject to luciferase assay, where β-galactosidase assay was used to correct for transfection efficiency (below). All assays were done in triplicate. B. C2C12 myoblasts were transfected with MEF2C, SRF, or PKCδ, as indicated. Following recovery, cells were differentiated in low serum media for 5 days, harvested for RNA, subjected to qPCR assay. C and D. Following 5 days of differentiation, C2C12 myotubes were treated with 200 μM palmitate conjugated to 2% albumin in low glucose media overnight. Control cells were treated with 2% albumin alone. Myotubes were harvested for RNA or protein,and assayed by immunoblot (C) or qPCR (D). E. C2C12 myoblasts were transfected with MEF2-VP16 fusion where threonine-20 is mutated to a neutral alanine [MEF2(T20A)-VP16], or control plasmid. Cell were differentiated for 5-days and treated with 200 μM palmitate, as indicated. Myotubes were harvested for RNA and assayed by qPCR. F. Wild-type (WT) or diacylglycerol kinase-δ knock-out (DGKδ KO) embryonic fibroblasts treated with palmitate, as described above. Extracts were immunoprecipitated (IP) with SRF antibody and probed using an antibody that recognizes phospho-serines/threonines with arginines at the -3 position (RXXpS/T), or immunoblotted (IB), as indicated. PKCδ = catalytic fragment of PKCδ. Data are represented as mean ± SEM. *$p<0.05$ compared to control. **$p<0.05$ compared to palmitate treatment.

fragment, in both vehicle and palmitate treated conditions (Figure 3F). Furthermore, we observed that phosphorylation of threonine-160 of SRF is reduced in the DGKδ-null fibroblasts, and phosphorylation of this site is not enhanced by exposure to palmitate, as it is in wild-type fibroblasts (Figure 3F). These findings strongly implicate *de novo* diacylglycerol production and subsequent PKCδ activation in the phosphorylation of this MADS-box motif.

Palmitate-induced mitochondrial depolarization involves PKCδ and inhibition of miR-133a expression. Given the recently described role of miR-133a in regulating muscle mitochondrial respiration (188), we hypothesized that palmitate-induced mitochondrial dysfunction involves PKCδ-dependent miR-133a inhibition. To test this hypothesis, we differentiated C2C12 cells and hASMCs, followed by overnight treatment with palmitate, and stained cells with fluorescent mitochondrial dyes. Palmitate treatment reduced TMRM staining in both cell lines (Figure 4A). Interestingly, palmitate treatment had little effect on MitoView Green staining in C2C12 myotubes, indicating a loss of mitochondrial membrane potential without a substantial loss of mitochondrial content (Figure 4A, -B, -C). However, treatment of C2C12 cells and hASMCs with the PKCδ inhibitor rottlerin, abrogated the palmitate-induced loss of mitochondrial membrane potential (Figure 4A, -B, -C). Correspondingly, palmitate treatment reduced miR-133a expression, which was reversed by PKCδ inhibition by rottlerin (Figure 4D). Finally, we evaluated MEF2C phosphorylation at threonine-20 by immunoprecipitating endogenous MEF2C and western blotting the eluted proteins with a phospho-specific antibody that recognizes phospho-serines or phospho-threonines with arginine residues at the -3 and -5 positions (RXRXXpS/T) (225). Shown in Figure 4F, palmitate exposure increased MEF2C phosphorylation, which was reversed by rottlerin treatment.

Figure 4.

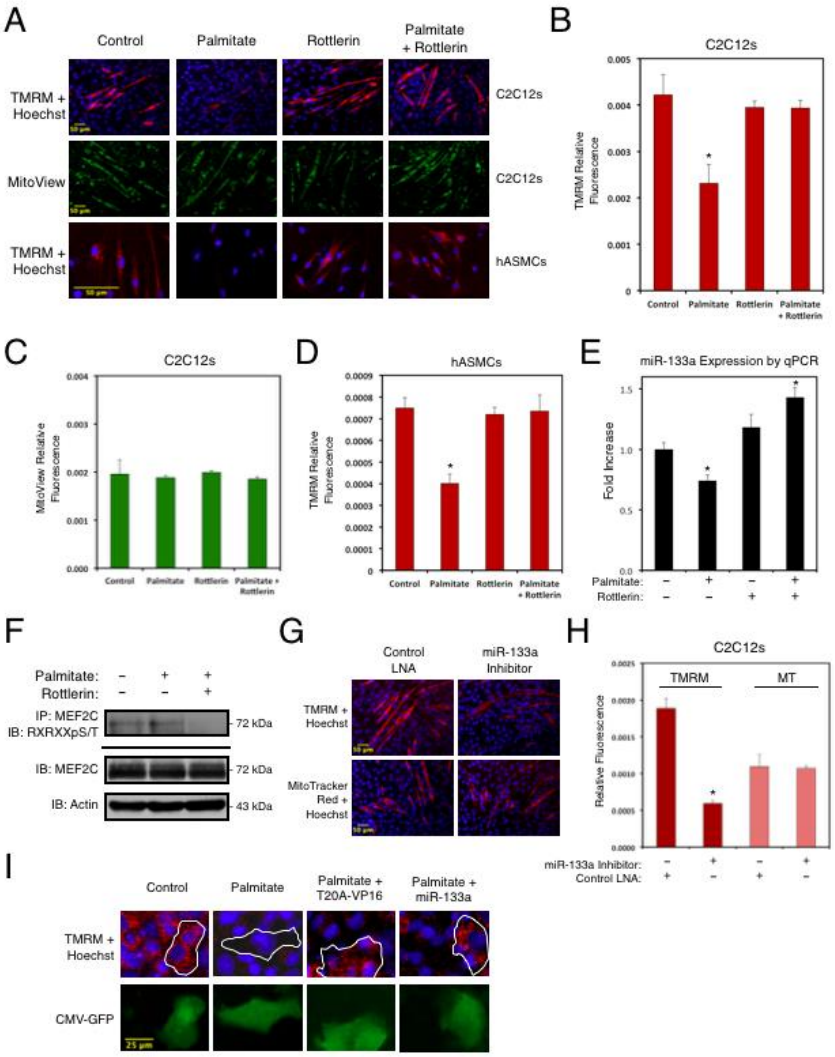

I - Figure 4: Palmitate-induced PKCδ activation regulates mitochondrial membrane potential through miR–133a.

A. C2C12 myotubes were differentiated for 5-days (above), or hASMCs were differentiated for 2-days (below), and treated with 200 µM palmitate conjugated to 2% albumin in low glucose media with or without rottlerin (5 µM) overnight. Control cells were treated with 2% albumin alone. Cells were stained with TMRM, Hoechst, and MitoView Green, as indicated, and imaged by standard fluorescence techniques (20x for C2C12s; 40x for hASMCs). B-D. Fluorescent intensities from myotubes in (A) were quantified using ImageJ software. E. hASMCs were treated as described in (A), harvested for RNA and subjected to qPCR analysis for miR-133a. F. Differentiated C2C12 myotubes were treated as in (A). Protein extracts were immunoprecipitated (IP) with an MEF2C antibody, and probed using an antibody that recognizes phospho-serines/threonines with arginines at the -5 and -3 positions (RXRXXpS/T), and immunoblotted (IB), as indicated. G. C2C12 cells were transfected with a miR-133a inhibitor oligonucleotide, or a control oligonucleotide. Cells were differentiated for 5 days and imaged at 20x with TMRM, Hoechst, or MitoTracker Red CMXRos, as indicated. H. Quantification of myotube fluorescence in (G). I. H9c2 myoblasts were transfected with MEF2-T20A-VP16 (T20A-VP16) or miR-133a. Following 2 days of differentiation, cells were treated with 200 µM palmitate conjugated to 2% albumin or 2% albumin alone as a control. CMV-GFP was included to visualize transfected cells. Data are represented as mean ± SEM. *p<0.05 compared to control.

To assess the role of miR-133a in palmitate-induced mitochondrial depolarization mechanistically, we transfected C2C12 myoblasts with an inhibitory oligonucleotide targeting miR-133a. Control cells were transfected with a scrambled oligonucleotide. Following differentiation, cells were stained with either TMRM or MitoTracker Red CMXRos. Shown in Figure 4E, myotubes transfected with the miR-133a inhibitor displayed a reduced TMRM fluorescence, but an equivocal MitoTracker fluorescence, compared to control myotubes (Figure 4G, -H). Next, we transfected myoblasts with a plasmid encoding miR-133a in order to reconstitute this microRNA's function in palmitate-treated cells. Shown in Figure 4I, cells expressing miR-133a were resistant to palmitate-induced disruption of mitochondrial membrane potential. We also transfected cells with T20A-VP16. Reconstitution of MEF2 function by this construct also enabled cells to be resistant to palmitate-induced mitochondrial depolarization (Figure 4I).

miR-133a regulates mitochondrial function through the mitophagy and death gene Nix. In order to identify a mechanism by which miR-133a regulates mitochondrial function, we performed an *in silico* screen in an attempt to identify novel mRNA targets of miR-133a. This screen identified a conserved miR-133a target sequence in the 3'-untranslated region of the human and rodent Nix mRNA (Figure 5A). Thus, we expressed miR-133a in cultured myoblasts, and observed reduced protein expression of Nix, where a short-hairpin RNA targeting Nix (shNix) was used as a positive control (Figure 5B). In addition, when miR-133a was expressed in myoblasts, we did not detect a change in Nix mRNA, suggesting that miR-133a inhibits Nix expression by translational block rather than mRNA degradation. To perform the reciprocal experimentation, we utilized a miR-133a inhibiting oligonucleotide, and observed increased

Figure 5.

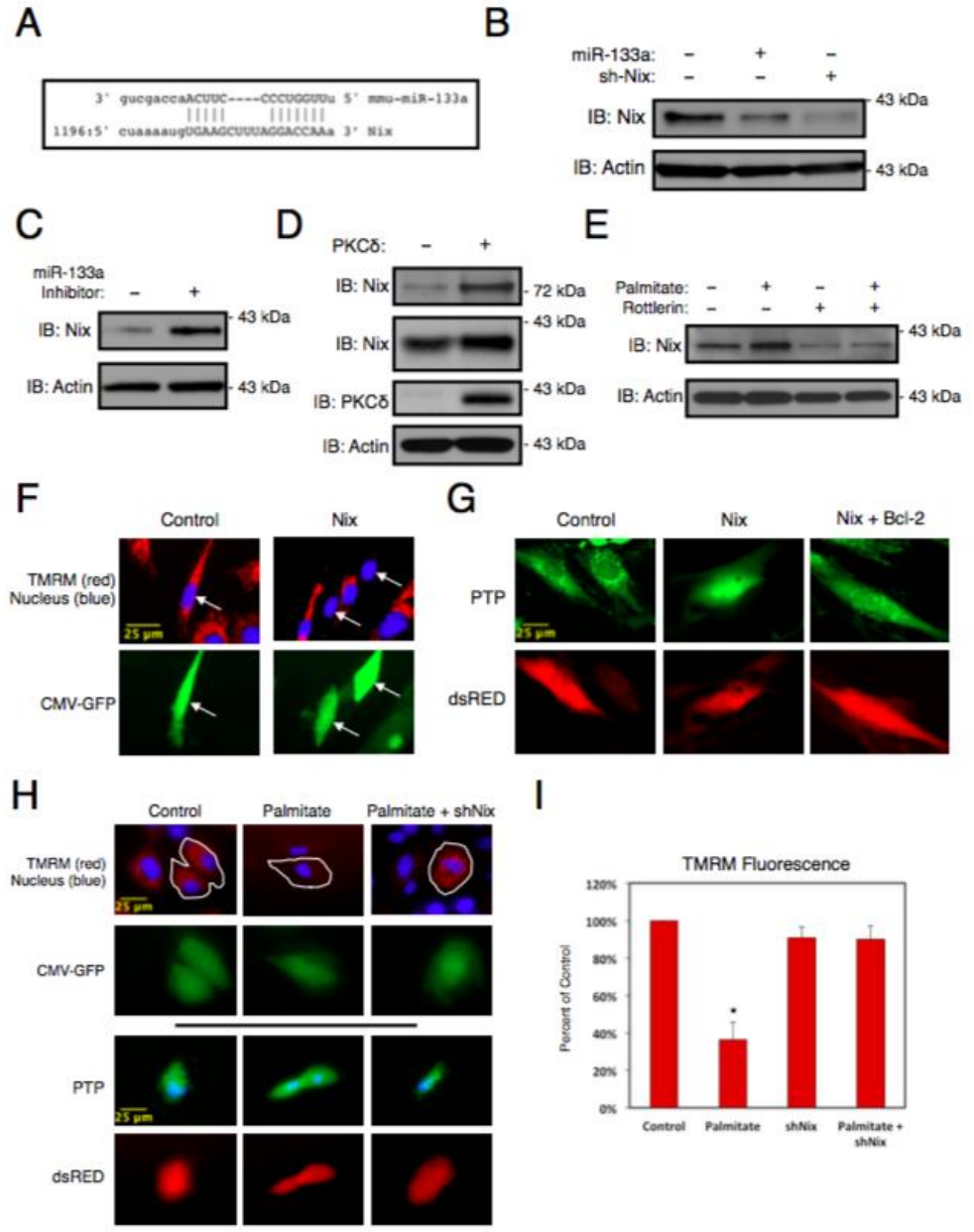

I - Figure 5: miR-133a regulates mitochondrial membrane potential through Nix.

A. Sequence alignment of mouse miR-133a and the 3' UTR of Nix. B. H9c2 myoblasts were transfected with miR-133a or a short-hairpin RNA targeting Nix (sh-Nix). Following protein extraction, samples were immunobloted as indicated. C. H9c2 cells were transfected with a miR-133a inhibitor (50 μM), or a scrambled control oligonucleotide. Extracts were immunoblotted, as indicated. D. C2C12 cells were transfected with the catalytic isoform of PKCδ. Extracts were immunoblotted, as indicated. E. 5-day differentiated C2C12 cells were treated with 200 μM palmitate conjugated to 2% albumin, or 5 μM rottlerin overnight, as indicated. Protein extracts were immunoblotted, as indicated. F. C2C12 myoblasts were transfected with Nix, or an empty vector control. CMV-GFP was included to identify transfected cells. Cells were stained with TMRM and Hoechst and imaged by standard fluorescence microscopy. Arrows indicate GFP positive cells. G. H9c2 cells were transfected with Nix and Bcl-2, as indicated. CMV- dsRed was used to identify transfected cells. Cells were stained with calcein-AM with cobalt chloride (5 μM) to assess PTP opening. H. H9c2 cells were transfected with shNix, or a scrambled control shRNA. Following recovery, cells were treated with 200 μM palmitate conjugated to 2% albumin overnight, and stained with TMRM and Hoechst to evaluate mitochondrial membrane potential (above) or with calcein-AM with cobalt chloride (5 μM) to assess PTP opening (below). I. Quantification of myotube fluorescence in (H). Data are represented as mean ± SEM. *$p<0.05$ compared to control.

expression of Nix protein (Figure 5C). Previous studies have shown that Nix can form a SDS-resistant dimer with a predicted molecular weight of 80 kDa[31]. Ectopic expression of the catalytic fragment of PKCδ increased the protein expression of both monomeric and dimeric Nix (Figure 5D). Consistent with these findings, overnight palmitate treatment increased the protein expression of both monomeric and dimeric Nix, which was reversed by the PKCδ inhibitor rottlerin (Figure 5E). To investigate the role of Nix in mitochondrial function, we transfected C2C12 cells with Nix, and stained cells with TMRM. We observed reduced mitochondrial membrane potential in C2C12 myoblasts that expressed Nix compared to control (Figure 5F). In addition, we observed that expression of Nix opened the mitochondrial permeability transition pore (PTP) when transfected into the cardiac H9c2 myoblasts, as evident by the loss of green mitochondrial puncta, where this effect was reversed by co-expression of the pro-survival gene Bcl-2 (Figure 5G). Finally, to establish the role of Nix in palmitate-induced mitochondrial dysfunction, we transfected H9c2 myoblasts with shNix and evaluated mitochondrial PTP opening and membrane potential following palmitate exposure. Shown in Figure 5H, exposure to palmitate opened the mitochondrial PTP and reduced mitochondrial membrane potential; however, the shNix restored both mitochondrial puncta, and reversed the effect of palmitate on mitochondrial membrane potential (Figure 5I).

To determine the role of miR-133a on mitochondrial physiology, we evaluated oxygen consumption rate in cultured H9c2 cells. Shown in Figure 6A, overnight exposure to palmitate reduced oxygen consumption, as well as the calculated basal and maximum respiration rates when cells were stressed with oligomycin (A), FCCP (B), and antimycin A and rotenone (C)(Figure 6C)[32]. However, when cells were transfected with a miR-133a mimicking oligonucleotide, the palmitate-induced drop in oxygen consumption was prevented (Figure 6B), where control cells

were transfected with a scrambled oligonucleotide. Furthermore, the calculated basal and maximum respiration rates were increased when miR-133a-mimic treated cells were exposed to palmitate (Figure 6D), suggesting that improved mitochondrial function enabled cells to metabolize the available palmitate. Finally, we determined if restoration in mitochondrial function translated into improved insulin-stimulated glucose uptake. Shown in Figure 6E, -F, overnight exposure to palmitate prevented insulin-stimulated glucose uptake in differentiated H9c2 cells, determined by the fluorescence glucose analog 2NBDG, which was restored when cells were treated with a miR-133a-mimic. Interestingly, basal glucose uptake was also increased in cells treated with the miR-133a-mimic and exposed to palmitate.

Evaluation of miR-133a and Nix expression in vivo.

In order to determine the *in vivo* relevance of this genetic pathway in muscle tissues, we utilized a rodent model of gestational diabetes, as fetal exposure to diabetes during pregnancy increases the risk for early-onset insulin resistance in the offspring and may program metabolism (196,197). Rats exposed to diabetes during gestation become insulin resistant by 15 weeks of age, a phenotype that is exacerbated by the postnatal consumption of a high-fat and sucrose diet (HFS) (197). To further define the metabolic alterations induced by exposure to gestational diabetes in muscle tissue, we performed metabolomics analysis by mass spectrometry using extracts enriched for lipid-soluble metabolites. This screen identified 44 species of diacylglycerols varying in the composition of their fatty acid chains (Supplemental Table 2). In the offspring of normoglycemic lean dams, numerous diacylglycerol species were increased by the HFS diet (Fig. 7A). However, exposure to maternal diabetes increased diacylglycerols in the soleus muscle of both low fat (LF) and HFS-fed offspring, suggesting the presence of a programming

Figure 6.

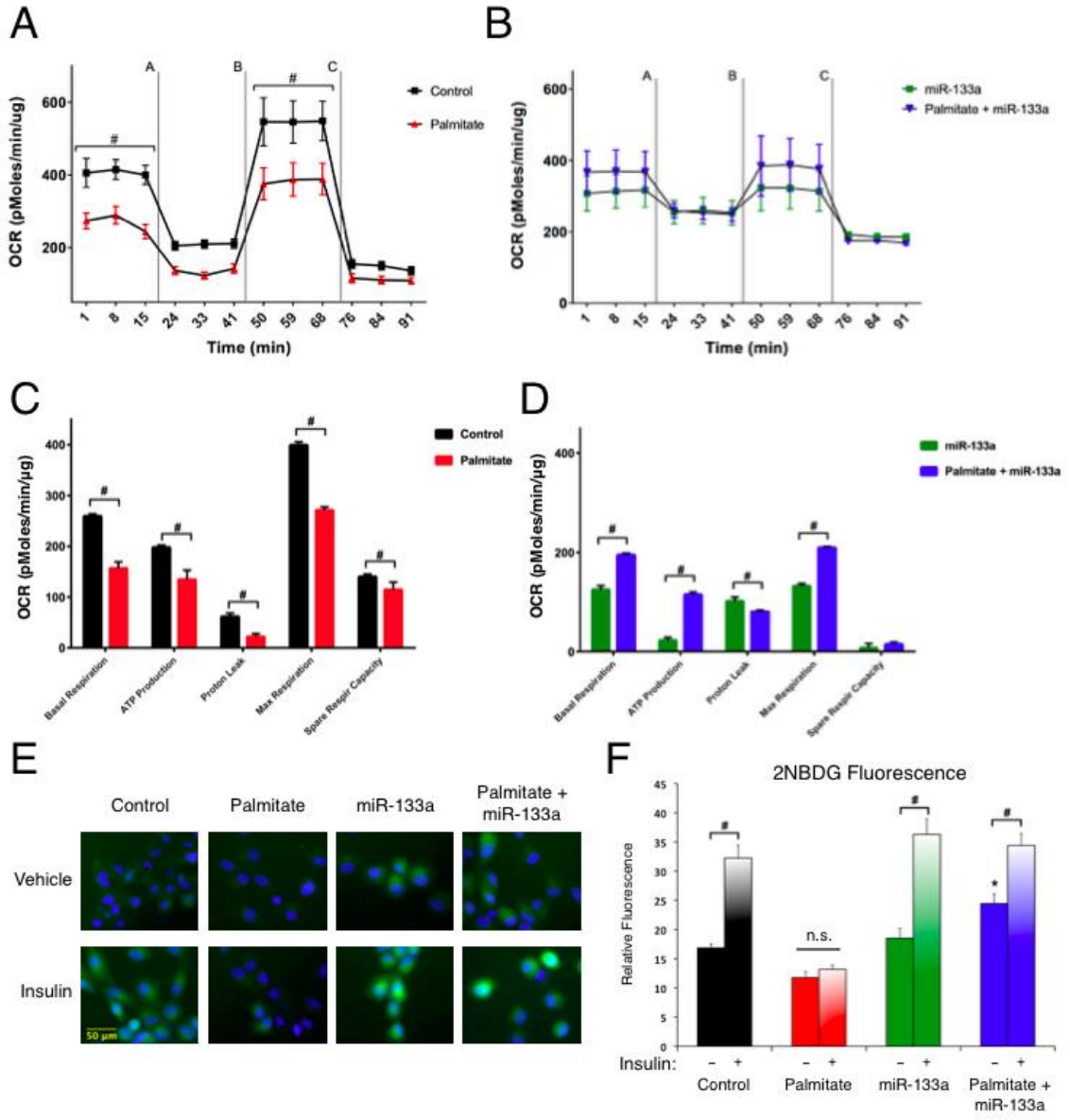

Figure 6: Evaluation of mitochondrial respiration and glucose uptake.
A. Differentiated H9c2 cells were treated overnight with with 200 µM palmitate conjugated to 2% albumin in low glucose media. Control cells were treated with 2% albumin alone. Oxygen consumption rate (OCR) was evaluated on a Seahorse XF-24. To evaluate mitochondrial function, cells were injected with oligomycin (1uM) [A], FCCP (1uM) [B], and antimycin A (1uM) and rotenone (1uM) [C] B. H9c2 cells were transfected with a miR-133a mimic (50 µM), or a scrambled control oligonucleotide. Following recovery, OCR evaluated as in (A). C-D. Calculated respiration rates from (A) and (B), respectively. E-F. H9c2 cells were transfected as in (B) and treated as in (A). Insulin stimulated uptake (10nM) was determined by 2NBDG fluorescence and quantified in (F). Data analyzed by 2-way ANOVA and represented as mean ± SEM. #p<0.05 between groups, *p<0.05 compared to control.

effect on soleus muscle (Figure 7A). Thus, we hypothesized that the accumulation of diacylglycerol species would provide an activating stimulus for PKCδ. In support of this, we observed that miR-133a expression was reduced by 40% in the soleus and heart of animals exposed to both gestational diabetes and a HFS diet (Figure 7B, -C). In addition, we evaluated the expression of mitochondrial marker genes in the soleus muscle of our rodent model. PGC-1α expression was reduced by both the postnatal consumption of the HFS diet and fetal exposure to gestational diabetes, and the consumption of HFS diets by the offspring of diabetic dams caused an additive suppression of PGC-1α expression (Figure 7D). Moreover, mitofusin-2 expression was also reduced in the gestational diabetes offspring fed HFS diets (Figure 7E). In addition, we observed an increased expression of Nix in the soleus of rats exposed to the HFS diet or gestational diabetes (Figure 7F), concurrent with increased expression of the catalytic fragment of PKCδ. These findings suggest that developmental programming of diacylglycerol metabolism and miR-133a expression influences mitochondrial markers, and Nix expression, in the offspring.

3.6 Discussion

PKC signaling has been implicated in lipotoxicity and diabetic complications in multiple cell types (207), although the precise molecular mechanisms have not yet been defined in muscle tissues. Previously, our research group demonstrated that novel PKC isoforms could activate the C-terminus of MEF2 proteins utilizing Gal4-DNA binding domain fusion proteins (226). In addition, novel PKC isoforms activate a PKD-dependent signaling cascade resulting in liberation of MEF2 from HDAC5 repression during cardiac growth (69). However, during the course of our investigations, we observed that expression of PKCδ could inhibit MEF2 activity in some cellular contexts. Utilizing three independent muscle cell lines, an *in vivo* model, and mouse embryonic

fibroblasts genetically deficient in DGKδ, we characterized a novel pathway initiated by PKCδ signaling during lipotoxicity that converges on MEF2 and SRF transcription factors to regulate muscle gene expression and mitochondrial membrane potential. Detailed mass spectrometry analysis revealed that PKCδ phosphorylates MEF2 proteins at threonine-20 and SRF at threonine-160, a conserved MADS-box residue. Downstream, collaborative regulation of miR-133a expression by MEF2C and SRF is attenuated by PKCδ phosphorylation of these transcription factors. Importantly, expression of either miR-133a or an active MEF2 fusion protein, which cannot be phosphorylated by PKCδ, reverses palmitate induced mitochondrial dysfunction.

Recently, phosphorylation of *Drosophila* MEF2 at threonine-20 was shown to direct MEF2 activity between immune activation or metabolic function (225). In flies, MEF2 is normally phosphorylated at threonine-20 to promote anabolic gene expression. However, during infection MEF2 is dephosphorylated and targeted to genes involved with immune function at the expense of anabolic nutrient storage. At first these results may seem contrary to the findings of the present study. However, regulation of MEF2 and SRF by phosphorylation at the conserved MADS-box motif, and its downstream effects on miR-133a and Nix, may have evolved to limit mitochondrial metabolism and divert nutrients to anabolic storage or cell growth during differentiation. Thus, the novel genetic pathway identified in the present study, may represent an anabolic survival pathway, maintained through evolution in part due to the conservation of the MADS-domain.

One of the most intriguing findings of the present study is the identification of Nix as a miR-133a target. Previous studies have implicated both Nix and miR-133a in the regulation of mitochondrial function and programmed cell death in multiple cell types (188,189,227,228), and our data strongly suggest that miR-133a is dependent on Nix for mitochondrial membrane potential regulation in muscle tissues. Furthermore, both Nix and miR-133a are involved in pathological

Figure 7.

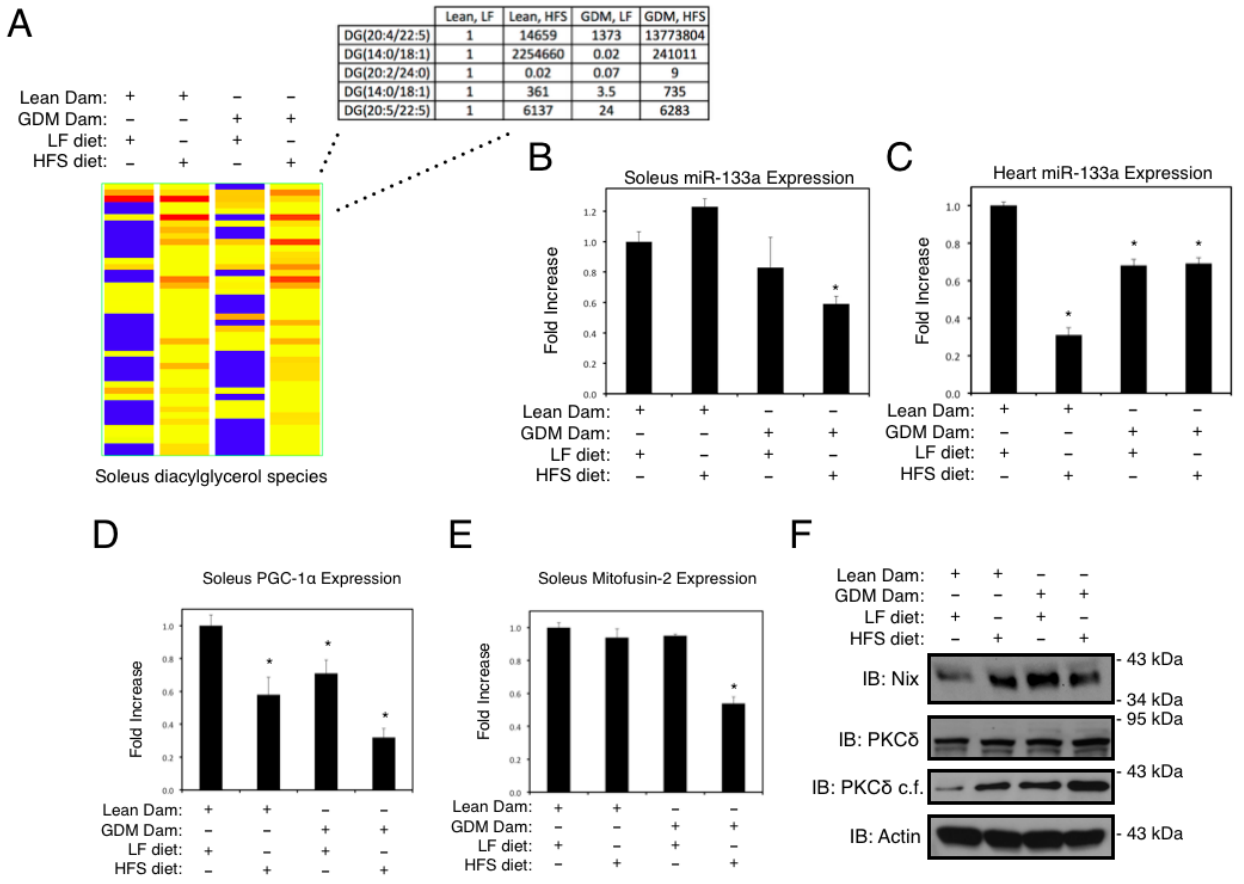

	Lean, LF	Lean, HFS	GDM, LF	GDM, HFS
DG(20:4/22:5)	1	14659	1373	13773804
DG(14:0/18:1)	1	2254660	0.02	241011
DG(20:2/24:0)	1	0.02	0.07	9
DG(14:0/18:1)	1	361	3.5	735
DG(20:5/22:5)	1	6137	24	6283

I - Figure 7: miR-133a expression *in vivo*.
A. Metabolomics analysis of 44 species of diacylglycerols from soleus muscle excised from low fat diet (LF), or high fat and sucrose diet (HFS), and a normal pregnancy (Lean Dam), or gestational diabetes (GDM Dam) during development, as indicated. Blue = low abundance, yellow = medium low abundance, orange = medium high abundance, red = high abundance. B-E. Rat soleus muscle or heart tissue was excised and total RNA was extracted, from rodents treated as described in (A). qPCR analysis was performed using the ΔΔCT method, where RNU6 was used as an internal control for miR-133a, and β-actin was used as a control for PCG-1α and mitofusin-2. F. Protein extracts from rat soleus muscle was subjected to immunoblot analysis, as indicated. PKCδ catalytic fragment (PKCδ c.f.). Data are represented as mean ± SEM. *$p<0.05$ compared to control.

cardiac remodeling (229-231). Thus, our findings may represent an important mechanism involved in diabetes-induced heart disease and play an important role in the progression to heart failure following cardiac injury.

In summary, these studies document a novel signaling cascade triggered by lipotoxicity, and converging on MEF2 and SRF transcription factors to regulate the expression of miR-133a during muscle development and post-natal remodeling. Repression of miR-133a expression ultimately regulates mitochondrial function, through the Bcl-2 family member Nix, which may have implications to pathological states such as insulin resistance and cardiovascular disease.

3.7 Acknowledgements

We thank Drs. Keith Wheaton and Robert Perry for providing the PKCδ and MEF2-VP16 fusion plasmids, respectively. We also thank Tao Fan for MS technical support, Dr. Laura Cole and Edward Mejia for technical assistance with respiration experiments, and Dr. William Diehl-Jones for technical assistance and helpful comments on the manuscript. JWG is supported by NSERC Canada, and VWD, AJH, GMH, and JCM are supported by CIHR. GMH is supported by the Heart and Stroke Foundation of Canada. Seed funding for this project was provided by the Manitoba Medical Service Foundation, Children's Hospital Foundation of Manitoba, and the Manitoba Health Research Council to VWD and JWG. VWD is the Dr. J.A. Moorhouse Fellow of the Diabetes Foundation of Manitoba. AJH and GMH are supported through the Canada Research Chairs program, and JCM is a McLaughlin Research Chair. JWG is a member of the Endocrinology and Metabolic Disease (E&MD) research group. WM, LN, and SP are supported by scholarships from the Children's Hospital Foundation of Manitoba. TJP was supported by a studentship from the Manitoba Health Research Council.

3.8 Supplemental Figures for Manuscript I

Supplemental Figure 1.

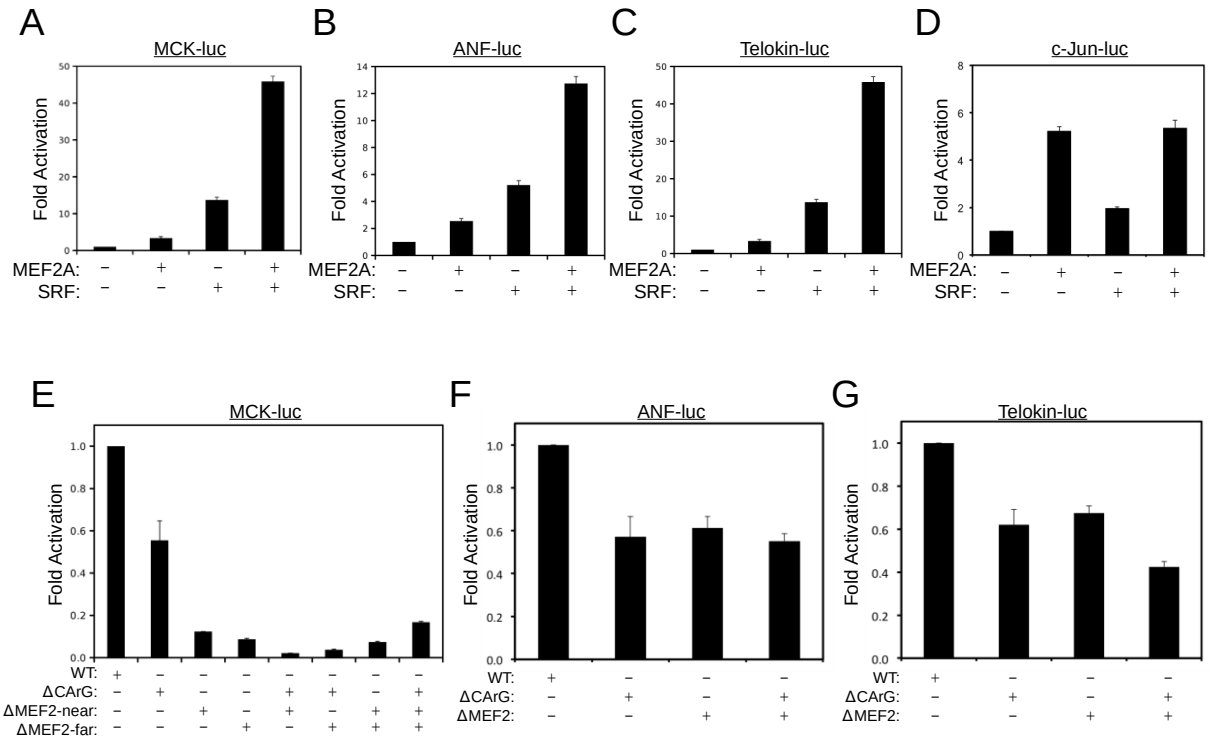

I - Supp Figure 1: MEF2A and SRF cooperatively activate select muscle- specific promoters.
A-D. Cos7 cells were transfected with MEF2A and SRF, as indicated, along with luciferase-driven promoters for muscle creatine kinase (MCK-luc), atrial natriuretic peptide (ANP-luc), telokin (telokin-luc), or *c-jun*. Extracts were subject to luciferase assay, where β-galactosidase assay was used to correct for transfection efficiency. E-G. C2C12 (E), H9c2 (F) and hASMC (G) myoblasts were transfected with the wild-type (WT) promoters, or constructs where the SRF binding site is mutated (ΔCArG) or the MEF2 sites are mutated (ΔMEF2). Cells were allowed to differentiate for 2-days in low serum media prior to harvesting for luciferase and β-galactosidase assay. All assays were done in triplicate.

Supplemental Figure 2.

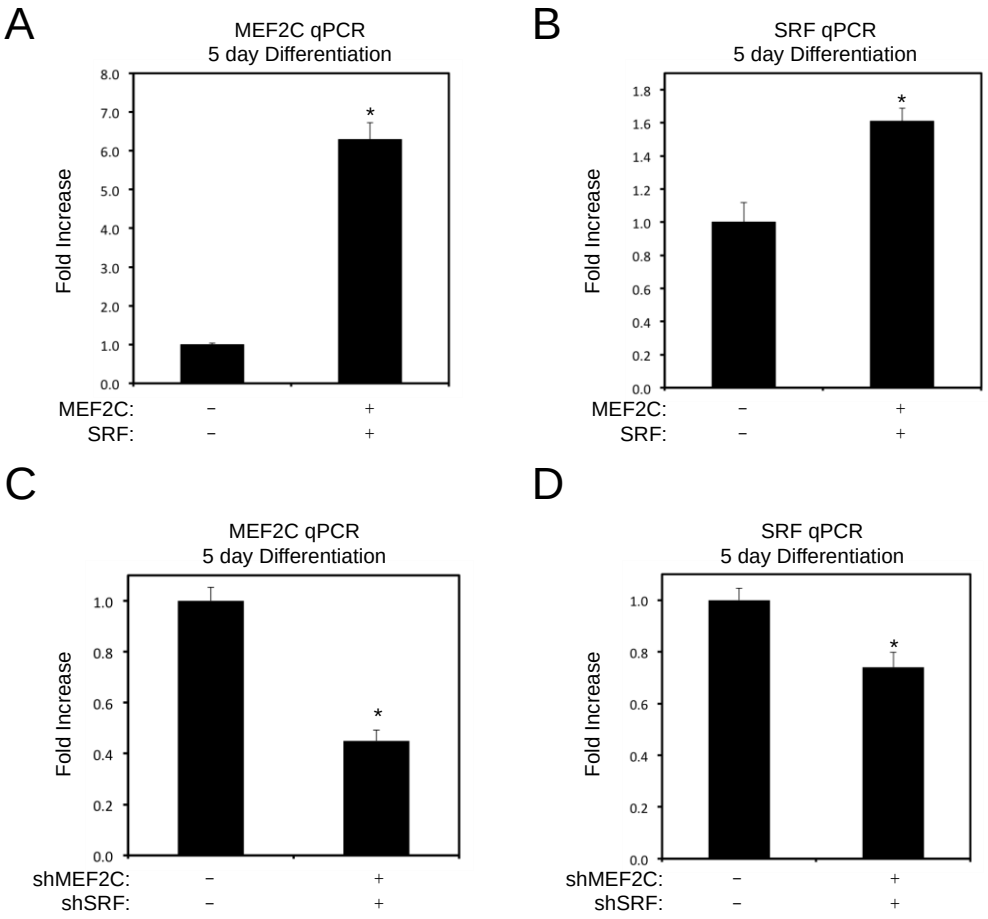

I - Supp Figure 2: Over-expression and knockdown control experiments.
A-B. C2C12 cells were transfected with MEF2C and SRF (Shown in Figure 1A). RNA extracts were analysed for MEF2C and SRF expression by qPCR to ensure over- expression was maintained following differentiation. C-D. C2C12 cells were transfected with shMEF2C and shSRF (Shown in Figure 1B). qPCR was performed to ensure knockdown was maintained throughout differentiation.

Supplemental Figure 3.

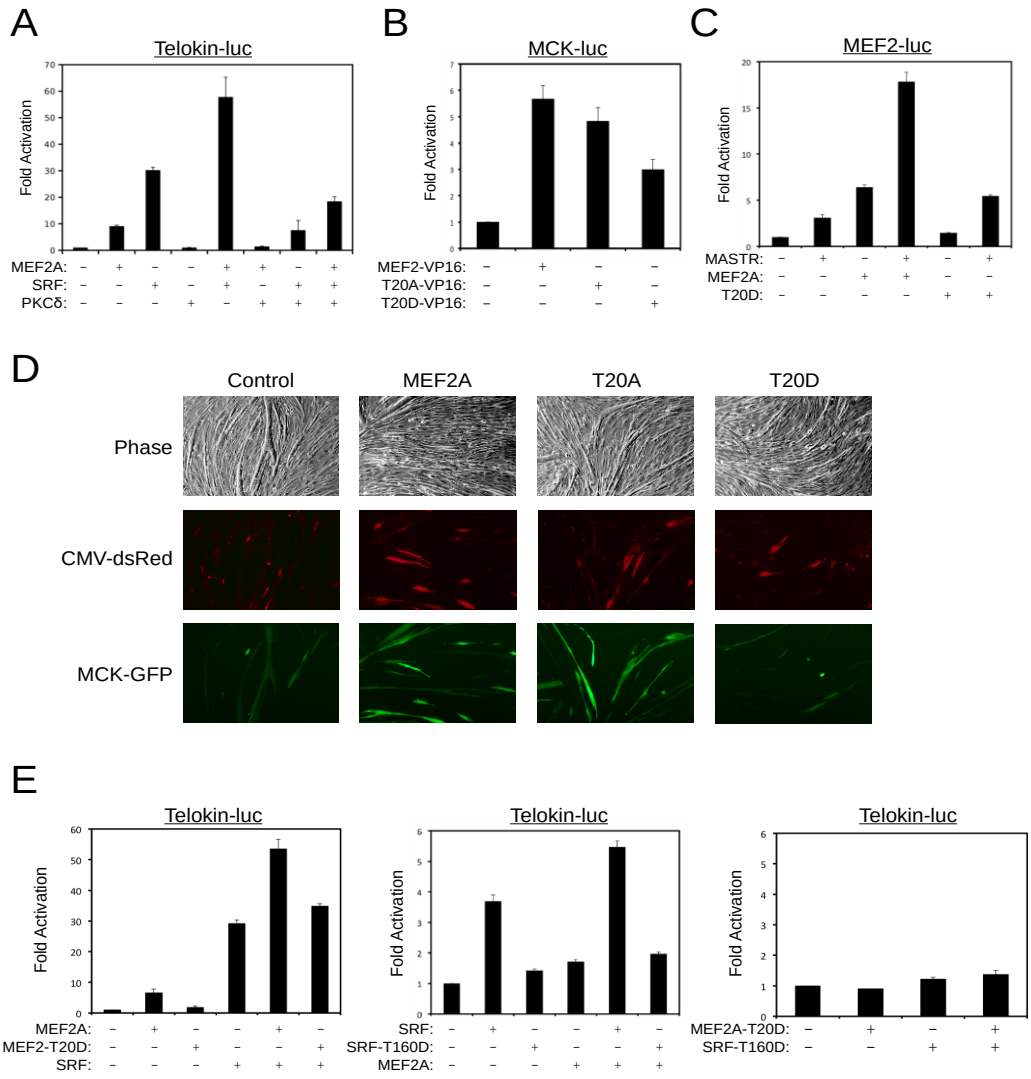

I - Supp Figure 3: Mutational analysis of Threonine-20.
A. 10T1/2 cells were transfected with MEF2A, SRF, or PKCδ, as indicated. Extracts were subject to luciferase assay, where β-galactosidase assay was used to correct for transfection efficiency. B. 293 cells were transfected with MEF2A-VP16 fusion protein, or a construct where threonine-20 is mutated to a neutral alanine (T20A-VP16) or phospho-mimetic aspartic acid (T20D-VP16), as indicated, along with MCK promoter (MCK-luc). Extracts were subject to luciferase assay as in (A). B. 293 cells were transfected with MASTR, MEF2A, and MEF2A-T20A (T20A), as indicated. Extracts were assayed as described above. C. C2C12 myoblasts were with MEF2A, MEF2A- T20A and MEF2A-T20D, as indicated, along with a MCK-GFP reporter-gene and CMV- dsRed to identify transfected cells. Following recover cells were differentiated in low- serum media for 96-hours and imaged by standard fluorescent techniques. D. 293 cells were transfected with MEF2A, SRF, or plasmids containing phospho-mimetic aspartic acid mutations in MEF2A and SRF (T20D and T160D), as indicated, along with the telokin promoter (Telokin-luc). Extracts were assayed as described above.

CHAPTER IV: Manuscript II

4.1 Rationale

After establishing the cooperative role of MEF2 and SRF in regulating miR-133a to preserve mitochondria function during muscle differentiation, the second manuscript published in the journal of Cell Death and Differentiation, focuses on understanding the upstream regulation of the miR-133a, and the mechanisms mediating mitochondrial calcium homeostasis to preserve cardiac function. The transcriptional co-activator, Myocardin, interacts with MEF2 and SRF to drive cardiac gene expression and cardiomyocyte differentiation (18,21). Despite the genetic loss of Myocardin in mouse embryos exhibiting congenital heart defects and embryonic lethality, or the specific cardiac deletion of Myocardin implicating cardiac cell death *in vivo* (30,49,52), the role of Myocardin to preserve mitochondrial function and oppose cardiac necrosis during development and disease is unknown. Thus, this second manuscript addresses the last three experimental objectives outlined in the Thesis Rationale, which are: 1) Expression of Nix and subendocardial necrosis is elevated in the heart of Myocardin null mouse embryos; 2) Myocardin regulates a genetic pathway regulating mitochondrial function in cardiac muscle; and 3) Myocardin regulates mitochondrial permeability transition pore and calcium homeostasis through Nix.

Myocardin regulates mitochondrial calcium homeostasis and prevents permeability transition.

Wajihah Mughal[1,7], Matthew Martens[1,7], Jared Field[4,7], Donald Chapman[1,7], Jianhe Huang[11], Sunil Rattan[2,9], Yan Hai[6,7], Kyle G. Cheung[3,7], Stephanie Kereliuk[3,7], Adrian R. West[2,8], Laura K. Cole[3,7], Grant M. Hatch[3,7], William Diehl-Jones[4,10], Richard Keijzer[2,5,8], Vernon W. Dolinsky[3,7], Ian M. Dixon[2,9], Michael S. Parmacek[11], and Joseph W. Gordon[1,6,7,*].

Departments of Human Anatomy and Cell Science[1], Physiology and Pathophysiology[2], Pharmacology and Therapeutics[3], Biological Science[4], and Surgery[5], Colleges of Medicine and Nursing[6], Rady Faculty of Health Science, and The Diabetes Research Envisioned and Accomplished in Manitoba (DREAM) Theme[7] and the Biology of Breathing Theme[8] of the Children's Hospital Research Institute of Manitoba, Institute of Cardiovascular Sciences[9], University of Manitoba, Winnipeg, Canada.

Faculty of Health Disciplines, Athabasca University, Edmonton, Canada[10].

Department of Medicine, Penn Cardiovascular Institute, Hospital of the University of Pennsylvania, Philadelphia, USA[11].

Author contribution:

WM: designed experiments, wrote manuscript, cardiomyocyte isolation, transfection, transduction, immunofluorescence, immunoblot, fluorescent microscopy, mitochondrial respiration, sh-Myocd cell fractionation, animal tissue protein isolation, MTT cell viability assay, and ImageJ analysis.
MM: fluorescent microscopy (Figure 4: F, Figure 5: A), animal tissue immunoblot densitometry (Figure 7: D, H), targeted-Nix fractionation (Figure S2: G)
JF: sh-Myocd with miR-133a immunoblot (Figure 1: G), fluorescent microscopy (Figure 6: A)
DC: qPCR-based array (Figure 1, H), real-time quantitative polymerase chain reaction (RT-qPCR; Figure 7: A, B, E, F), animal tissue protein isolation (Figure 7: C, G)
YH: technical and cloning supervision, generation of targeted Nix constructs
JH: fixed and mounted Myocd null mouse embryonic tissue (Figure 1: A-B)
MSP: generated Myocd null mouse model (Figure 1: A-B)
SR: coronary ligation and isolation of cardiac tissue in rodent model of myocardial infarction (Figure 7: A-C)
IMD: generated rodent model of myocardial infarction (Figure 7: A-C)
KC: isolated cardiac tissue from doxorubicin-induced cardiotoxicity mouse model (Figure 7: E-G)
SK: cardiomyocyte isolation, fluorescent microscopy (Figure S2: D)
VD: generated doxorubicin-induced cardiotoxicity mouse model (Figure 7: E-G)
ARW: fluorescent microscopy (Figure 2: K)
LC and GMH: technical expertise on mitochondrial respiration (Figure 2: I-J; Figure 5: F-G)
WDJ: reviewed and edited manuscript, supervision of MM and JF.
RK: confocal immunofluorescence on Myocd null mouse embryonic tissue (Figure 1:A-B).

JWG: designed experiments, confocal microscopy (Figure 1: A-B), fluorescent microscopy (Figure 2: K), generation of Myocardin and SRF shRNAs, advisor and corresponding author: conceptualized and wrote manuscript.

4.2 Abstract

Myocardin is a transcriptional co-activator required for cardiovascular development, but also promotes cardiomyocyte survival through an unclear molecular mechanism. Mitochondrial permeability transition is implicated in necrosis, while pore closure is required for mitochondrial maturation during cardiac development. We show that loss of Myocardin function leads to subendocardial necrosis at E9.5, concurrent with elevated expression of the death gene Nix. Mechanistically, we demonstrate that Myocardin knockdown reduces microRNA-133a levels to allow Nix accumulation, leading to mitochondrial permeability transition, reduced mitochondrial respiration, and necrosis. Myocardin knockdown elicits calcium release from the endo/sarcoplasmic reticulum with mitochondrial calcium accumulation, while restoration of microRNA-133a function, or knockdown of Nix rescues calcium perturbations. We observed reduced Myocardin and elevated Nix expression within the infarct border-zone following coronary ligation. These findings identify a Myocardin-regulated pathway that maintains calcium homeostasis and mitochondrial function during development, and is attenuated during ischemic heart disease. Given the diverse role of Nix and microRNA-133a, these findings may have broader implications to metabolic disease and cancer.

Keywords: Myocardin, Nix, microRNA-133a, mitochondria, necrosis

4.3 Introduction

The formation of the mammalian heart during embryogenesis is orchestrated by a core set of cardiomyocyte-enriched transcription factors that govern the cellular phenotype by regulating the expression of genes involved in lineage specification, differentiation, patterning, and cell survival (5). This highly conserved genetic network is reinforced by transcriptional co-activators that modulate cardiac gene expression and dictate target-gene specific activation (232). Myocardin is a cardiomyocyte- and smooth muscle cell-restricted transcriptional co-activator that physically interacts with several core cardiac transcription factors, including SRF, MEF2C, GATA4, and Tbx5, to regulate gene expression during both cardiovascular development and post-natal cardiovascular remodeling (23,26,55,56). Cell programming experiments have demonstrated that a transcription factor 'cocktail' comprised of GATA4, MEF2C, and Tbx5 (ie. GMT) can directly convert fibroblasts to functional cardiomyocyte-like cells (233). Interestingly, the addition of Myocardin to the GMT and Hand2 cocktail enhances the conversion of human fibroblasts by up to 40% (110). These observations suggest that Myocardin plays a potent co-activator role during cardiomyocyte differentiation. Original gene targeting studies in mice harboring homozygous null alleles for Myocardin identified a critical role for this transcriptional co-activator during vascular smooth muscle differentiation and yolk sac vascularization[9]. More recently, Myocardin floxed mice were crossed with CMV-Cre and Nkx2.5-Cre transgenic mice, and offspring display exacerbated cardiomyocyte cell death and defects in proliferation, resulting in hypoplastic ventricles, heart failure, and embryonic lethality (51). Furthermore, the block in cardiomyocyte proliferation was due to a defect in Bone Morphogenetic Protein-10 (BMP10) expression and signaling; however, the direct cause of cell death in the developing ventricles was less clear. Moreover, the direct transcriptional targets of Myocardin that regulate this survival phenotype

remain unknown. However, electron microscopy identified cardiac nuclear condensation and apoptotic body formation, with the addition of mitochondrial swelling (51). Conditional cardiac deletion of Myocardin in adult mice using a tamoxifen-inducible system led to rapid deterioration in cardiac function, sarcomeric disorganization, and lethal heart failure (52). Given the rapid deterioration of cardiac function in these animal models, combined with the degree of cell death in the myocardium, we hypothesized that multiple modes of cell death, in addition to apoptosis, were involved in the deterioration of cardiac function when Myocardin is genetically inhibited.

Cardiomyocytes rely on mitochondria as a primary source of ATP, and mature cardiomyocytes may contain as much as 35% cellular volume of mitochondria (234). These observations make cardiomyocytes ideally suited to study mitochondrial-related disease mechanisms. Mitochondrial permeability transition is a term describing the phenomenon where the inner mitochondrial membrane permeabilizes and allows passage of solutes surpassing a kilodalton in size. This results in rapid dissipation of the mitochondrial membrane potential, respiratory uncoupling, and mitochondrial swelling (165). If prolonged, mitochondrial permeability transition will lead to mitochondrial rupture and cell death resembling a necrotic phenotype. Although originally associated with apoptosis, mitochondrial permeability transition leading to cell death has been recently termed mitochondrial permeability transition-driven regulated necrosis to replace the previous controversial term ‘programmed necrosis’ (235). The components of the mitochondrial permeability transition pore (MPTP) have been historically elusive; however, recent studies implicate a conformational change in the mitochondrial ATP Synthase as the fundamental pore structure (175), where Bax and Bak serve as outer member modulators of permeability transition (236). Although these components are ubiquitously expressed in virtually all tissues, recent studies have defined a developmental role for the MPTP

in the heart, where pore closure is required for proper cardiac myocyte differentiation, accumulation of mitochondrial content, and mature mitochondrial cristae formation (130).

Accumulating evidence suggests that mitochondrial permeability transition and necrosis are intimately linked with ischemic and mitochondrial-related diseases (121,235,237). An important component of regulated necrosis involves permeability transition triggered by elevations in matrix calcium concentration and reactive oxygen species (235). Evidence supporting the important nature of regulated necrosis in models of heart disease comes from several studies, by independent laboratories, demonstrating that mice genetically deficient in the mitochondrial matrix protein cyclophilin D, or its pharmacological inhibition by cyclosporine A, are protected against permeability transition and necrosis triggered by cardiac ischemia (168,238). Furthermore, mice deficient in the mitochondrial calcium uniporter are protected from ischemia-reperfusion injury (239,240).

Nix (ie. Bnip3L) is an atypical BH3-only member of the Bcl-2 family that has been demonstrated to regulate apoptosis, necrosis, autophagy, and mitophagy in numerous cell types and several cancers (209). Nix function has been studied in the heart during pathological remodeling events that lead to heart failure (241,242). Since its discovery, it has been noted that Nix, and the homologue Bnip3, could induce cell context-dependent apoptotic or necrotic cell death (243,244). Newer findings suggest that Nix can be targeted to either the mitochondria or the endoplasmic/sarcoplasmic reticulum (SR), where mitochondrial-targeted Nix activates apoptotic cell death, and SR-targeted Nix induces necrosis (227,245). The mechanism responsible for this alternative cellular targeting remains unknown, as does the exact mode of killing in these different subcellular locations. However, *in vivo* studies suggest that Nix preferentially localizes to the SR during pressure overload-induced cardiac remodeling (245).

We recently identified microRNA-133a (miR-133a) as an important regulator of mitochondrial function and insulin sensitivity through the repression of Nix expression (246). Previous reports observed that miR-133a is downregulated in human heart failure and in animal models (229,231). These findings prompted us to examine the regulation of miR-133a and Nix expression by Myocardin in both the developing heart and in animal models of necrotic cardiac injury, where mitochondrial permeability transition has been demonstrated to play a critical biological role.

In this report, we present evidence of subendocardial necrosis in Myocardin knockout embryos, concurrent with elevated Nix expression. Through detailed gain-of-function and loss-of-function approaches, we define a genetic pathway regulated by Myocardin that drives mitochondrial function, maintains calcium homeostasis, and reduces cardiomyocyte sensitivity to permeability transition-driven necrosis. Moreover, we provide evidence that this genetic pathway is attenuated within the infarct border-zone following coronary ligation, but not during doxorubicin-induced cardiac necrosis. These findings highlight the specificity of this genetic pathway and suggest that necrosis within the infarct border-zone is uniquely regulated compared to toxicity-induced necrosis in the heart.

4.4 Materials/Methods

Myocardin-null embryos and Confocal Immunofluorescence:

Myocardin-null mice were generated using the homozygous Myocardin conditional mutant mice ($Myocd^{F/F}$), which were intercrossed with CMV-Cre (BALB/c-Tg(CMV-cre)1Cgn/J) transgenic mice, as described previously (51). Embryos at day 9.5 (E9.5) were dissected, fixed, and mounted as described previously (51). Sections were prepared for immunofluorescence using antibodies for

Nix (Bnip3L, CST #12396), or HMGB1 (CST #3935), as per manufacturer's protocols, and nuclei were stained with Dapi. Confocal microscopy was performed on a Zeiss Laser Scanning LSM 700.

Plasmids and microRNA mimic:

The Myocardin-935 plasmid was provided by E. Olson, and described previously (67,213). The shRNA targeting Myocardin was based on the targeting sequence previously described by Yoshida et al (5'-GTTCCGATCAGTCTTACAG-3') (247). Sense and antisense oligonucleotides containing the target sequence were purchased from Sigma, annealed, and ligated into pSilencer 3.0 H1 (Ambion) (Addgene #100768) and pLKO.1-puro (Addgene #100769). The Nix (Bnip3L pcDNA3.1) and shNix plasmids were a gift from Wafik El-Deiry (Addgene #17467, 17469) (216). Myc-tagged Nix was generated using Bnip3L pcDNA3.1 as a PCR template and ligating the subsequent amplicon into a pcDNA3 backbone containing an N-terminal Myc tag (EcoRI-XhoI)(Addgene #100795). Flag-Bcl-2, -Cb5, an -MaoB plasmids were gifted from Clark Distelhorst (Addgene #18003, 18004, 18005) (190). ER-targeted and mitochondrial-targeted Nix constructs were generating by using Myc-Nix, the ER-targeting domain of cytochrome B5 (from Bcl-2-Cb5), or the outer mitochondrial membrane-targeting domain of monoamine oxidase B (from Bcl-2-MaoB) in an overlapping PCR reaction, respectively. Primers were designed to replace the transmembrane domain of Nix (aa 186 to the stop codon) with the ER-targeting domain or the outer mitochondrial membrane-targeting domain (EcoRI-XhoI)(Addgene #100756, #100757). pcDNA3.2/V5 mmu-mir-133a-1 was a gift from David Bartel (Addgene plasmid # 26326) (214). ATeam1.03-nD/nA/pcDNA3 was a gift from Takeharu Nagai (Addgene plasmid # 51958) (248). CMV-mito-CAR-GECO1 and CMV-ER-LAR-GECO1 were a gift from Robert Campbell (Addgene plasmid # 46022, 61244) (249,250). Lentiviral mito-CAR-GECO1 was

generated by inserting EcoRI and XhoI restriction sites into a PCR amplicon and ligated into pLenti-puro (Addgene #100765). The miR-133a LNA mimic and control oligonucleotide were purchased from Exiqon, described previously (246).

Cell culture, transductions, and transfections:

All cell lines were maintained in Dulbecco's modified Eagle's medium (DMEM; Hyclone), containing penicillin, streptomycin, and 10% fetal bovine serum (Hyclone) at 37 degrees Celsius and 5% CO_2. The H9c2 cell line was transfected using Qiagen's Polyfect reagent or JetPrime reagent, as per the manufacturer's instructions. Rat neonatal ventricular myocytes were isolated with the Pierce Primary Cardiomyocyte Isolation Kit (#88281), as per manufacturer's protocol. Knockdown of Myocardin in primary cardiomyocytes was performed with rat Myocardin shRNA lentiviral particles (Santa Cruz; sc-72228-V), or a lentivirus generated in pLKO.1-puro (above), where control shRNA lentiviral particles-A (sc-108080) were used to control for transduction.

Fluorescent staining:

TMRM, Calcein-AM, ethidium homodimer-1, MitoView Green, and Hoechst 33342 were purchased from Biotium. MitoSox was purchased from Life Technologies. MPTP imaging was performed by quenching the cytosolic Calcein-AM signal with 5 µM cobalt chloride during the incubation period. All imaging, including ER and mitochondrial calcium imaging, was done on an Olympus IX70 inverted microscope with QImaging Retiga SRV Fast 1394 camera using NIS Elements AR 3.0 software. Quantification, scale bars, and processing including background subtraction, was done on ImageJ software. ER-LAR-GECO and mito-carmine imaging was performed 48-hours following transfection in H9c2 cells and 18-hours after FSK-I stimulation

(additional details are included in figure legends). Calcium imaging in ventricular myocytes was done 48-hours after viral transduction. ATeam 1.03 was imaged with a CFP and FRET (CFP-YFP) cube-set on an Olympus IX70 inverted microscope with QImaging. Images were analyzed and quantified using ImageJ software.

Immunoblotting:

Protein extractions were achieved using a RIPA lysis buffer containing proteases inhibitors and phosphatase inhibitors (Santa Cruz). From tissue, protein was extracted in RIPA buffer by homogenization. Protein concentrations were determined using a Bio-Rad Protein assay kit. Fractionation studies utilized the Qiagen QProteome mitochondrial isolation kit. Extracts were resolved using SDS-PAGE and transferred to a PVDF membrane. Immunoblotting was carried out using appropriate primary antibody in 5% powdered milk or BSA in TBST. Appropriate horseradish peroxidase-conjugated secondary antibody (Jackson; 1:4000) was used in combination with chemiluminescence to visualize bands. The following antibodies were used: Myocardin (Santa Cruz sc-33766), Nix (CST # 12396), PGC-1 (Santa Cruz sc- 13067), and Actin (Santa Crux sc-1616). Fractionation experiments used Qiagen's Q-Proteome kit.

Mitochondrial respiration:

Mitochondrial respiration was determined on a Seahorse XF-24 Extracellular Flux Analyzer, as described previously (246). Calculated respiration rates were determined as per manufacturer's instructions (Mito Stress Kit; Seahorse).

Quantitative PCR:

Total RNA was extracted from pulverized frozen tissue or from cultured cells by TRIzol method. For microRNA analysis all primers were purchased from IDT. cDNA was generated using QScript MicroRNA cDNA Synthesis kit (IDT) and q-RT-PCR performed using PerfeCTa SYBR green super mix on a ABI 7500 Real-Time PCR Instrument. microRNA was normalized to RNU6 expression (Quanta). For mRNA analysis, following column purification using Qiagen RNeasy kit and DNase treatment, cDNA was generated with QScript cDNA super mix (Quanta BioSciences) and analyzed as described above, and normalized to β-actin expression. The primers used were: Myocardin FWD 5'-GTGTGGAGTCCTCAGGTCAAAC-3'; REV 5'-TGATGTGTTGCGGGCTCTT-3'; Beta Actin FWD 5'-CTGTGTGGATTGGTGGCTCTA-3'; REV: 5'-AAAACGCAGCTCAGTAACAGTCC-3'. The SA Biosciences Cell Death Pathway Finder Array was purchased from Qiagen and used manufacturer's protocol.

Coronary Ligation and doxorubicin-induced cardiotoxicity:

All procedures in this study were approved by the Animal Welfare Committee of the University of Manitoba, which adheres to the principles for biomedical research involving animals developed by the Council for International Organizations of Medical Sciences. In the *in vivo* rodent model of myocardial infarction, the left coronary artery of Sprague Dawley rats was ligated approximately 2 mm from its origin, while sham operated rats serve as control (251,252). Following recovery for 4 or 8 weeks, animals are anesthetized, the heart excised, and the left anterior descending territory dissected for scar tissue and viable border-zone myocardium. For Dox-induced cardiotoxicity, C57BL6 mice received weekly intraperitoneal injections of Dox (8 mg/kg body weight) for 4 weeks (220). Mice were anesthetized and the heart excised for protein and RNA analysis.

4.5 Results

Silencing of Myocardin increases Nix expression through a miR-133a-dependent mechanism: Consistent with a role for Myocardin in the regulation of necrosis, in addition to apoptosis, examination of E9.5 Myocardin-null embryos revealed elevated Nix expression in the heart (Figure 1A). E9.5 is 1-day prior to the reported cardiovascular failure and embryonic lethality of Myocardin knock-out mice (51). Previous studies have implicated Nix in cardiac necrosis (227,245); therefore, we stained Myocardin-null embryos for an early and specific marker of necrosis, called HMGB1(125,133,253). HMGB1 is a chromatin-binding protein that is exported into the cytoplasm during necrosis, and is eventually released into the interstitium where it contributes to the inflammatory response (133). We observed cytoplasmic HMGB1 in the subendocardial region of hearts from Myocardin-null embryos, compared to a nuclear localization in control embryos, suggesting removal of Myocardin function during cardiac development leads to myocyte necrosis (Figure 1B).

Recently, we identified miR-133a as an important regulator of Nix expression in cardiac, skeletal, and smooth muscle cells (246). Thus, we tested the hypothesis that Myocardin regulates Nix expression through a miR-133a dependent mechanism. We knocked-down Myocardin expression in both primary neonatal rat ventricular cardiomyocytes and in the H9c2 myocyte cell line, using lentiviral and plasmid-based shRNA vectors, respectively. Knock-down of Myocardin in these cellular models resulted in simultaneous decreased expression of miR-133a and increased expression of Nix (Figure 1C-F). Since Myocardin does not bind to DNA directly, and regulates gene expression primarily through interaction with SRF, we knocked-down SRF and observed a comparable decrease in miR-133a expression, and no additional decrease in miR-133a expression when both SRF and Myocardin were knocked-down (Figure 1F). Furthermore, reconstitution of

miR-133a expression attenuated Nix expression following Myocardin knock-down (Figure 1G), suggesting that miR-133a is sufficient to repress Nix expression independent of Myocardin function. In addition, we performed a PCR-based gene expression array in H9c2 cells following Myocardin knock-down using a commercially available cell death pathway finder array (Figure 1H and Supplemental Table 1). Interestingly, few if any survival genes were reduced by 50% or more, and only three death genes were increased by 2-fold using this array. Although not exhaustive, this observation led us to speculate that the genetic pathway connecting Myocardin function to Nix expression was biologically relevant in cardiac myocytes.

Myocardin regulates mitochondrial function and permeability transition:

In order to understand how inactivation of Myocardin leads to cardiomyocyte necrosis, we used RNA interference in primary cardiomyoctes and H9c2 cells and assessed mitochondrial- and cell viability-parameters by fluorescent microscopy. In primary cardiomyocytes, knockdown of Myocardin led to loss of mitochondrial membrane potential and mitochondrial permeability transition, determined by the calcein-cobalt chloride staining method (Figure 2A-C). Similar findings were observed in the H9c2 cell line (Figure 2D, -E). Furthermore, knockdown of Myocardin increased the percentage of necrotic cells, determined by ethidium homodimer staining in both primary cardiomyocytes and H9c2 cells (Figure 2F-H). As a positive control, we treated primary cardiomyocytes with isoproterenol (100μM for 18 hours), as excessive β-adrenergic stimulation has been previously implicated as an important trigger for permeability transition and cardiac necrosis[37]. Shown in Supplemental Figure 1A-C, isoproterenol affected mitochondrial membrane potential, permeability transition, and ethidium homodimer staining in a comparable manner to Myocardin knockdown. We also evaluated respiration in cardiomyocytes using a metabolic flux analyzer (Seahorse, XF24). While Myocardin knock-down had no effect on basal

respiration in neonatal rat ventricular myocytes. When Myocardin knockdown cells were challenged with the mitochondrial uncoupler FCCP, reduced respiration was observed (Figure 2I and -J). In addition, knockdown of Myocardin reduced cellular ATP levels, determined by the ATeam1.03 ATP biosensor (Figure 2K). Finally, we observed that mitochondrial permeability transition, induced by Myocardin knockdown, was inhibited by the cyclophilin-D inhibitor (cyclosporine A ; 1μM), the inositol triphosphate receptor (IP3R) inhibitor (2APB; 10μM), and the mitochondrial calcium uniporter inhibitor (Ru360; 10μM)(Figure 2M); however, the ryanodine receptor (RyR) antagonist Dantrolene (Dan; 10μM) had no effect on permeability transition induced by Myocardin knockdown (Figure 2L). These findings suggest the involvement of an IP3R-dependent SR-to-mitochondria calcium transfer in the regulation of permeability transition when Myocardin expression is reduced.

In order to perform the reciprocal gain of function experiments, we used H9c2 cells transfected with Myocardin and evaluated the sensitivity of these cells to agents known to induce mitochondrial permeability transition and necrosis. Ionomycin is a calcium ionophore, previously demonstrated to induce MPTP-dependent necrosis (Supplemental Figure 1E-F) (236). Following Myocardin transfection, or empty vector control, we treated cells with ionomycin (2μM). Myocardin expression substantially reduced the number of ethidium homodimer-positive cells and reduced mitochondrial permeability transition (Figure 3A-D). As a control, we treated cells with cyclosporine A (1μM), and we observed a near complete reversal of permeability transition following ionomycin treatment (Figure 3E). We also treated Myocardin expressing H9c2 cells with staurosporine (2μM), previously shown to induce mitochondrial outer membrane permeability (MOMP) and caspase-dependent apoptosis (Supplemental Figure 1G-H) (236).

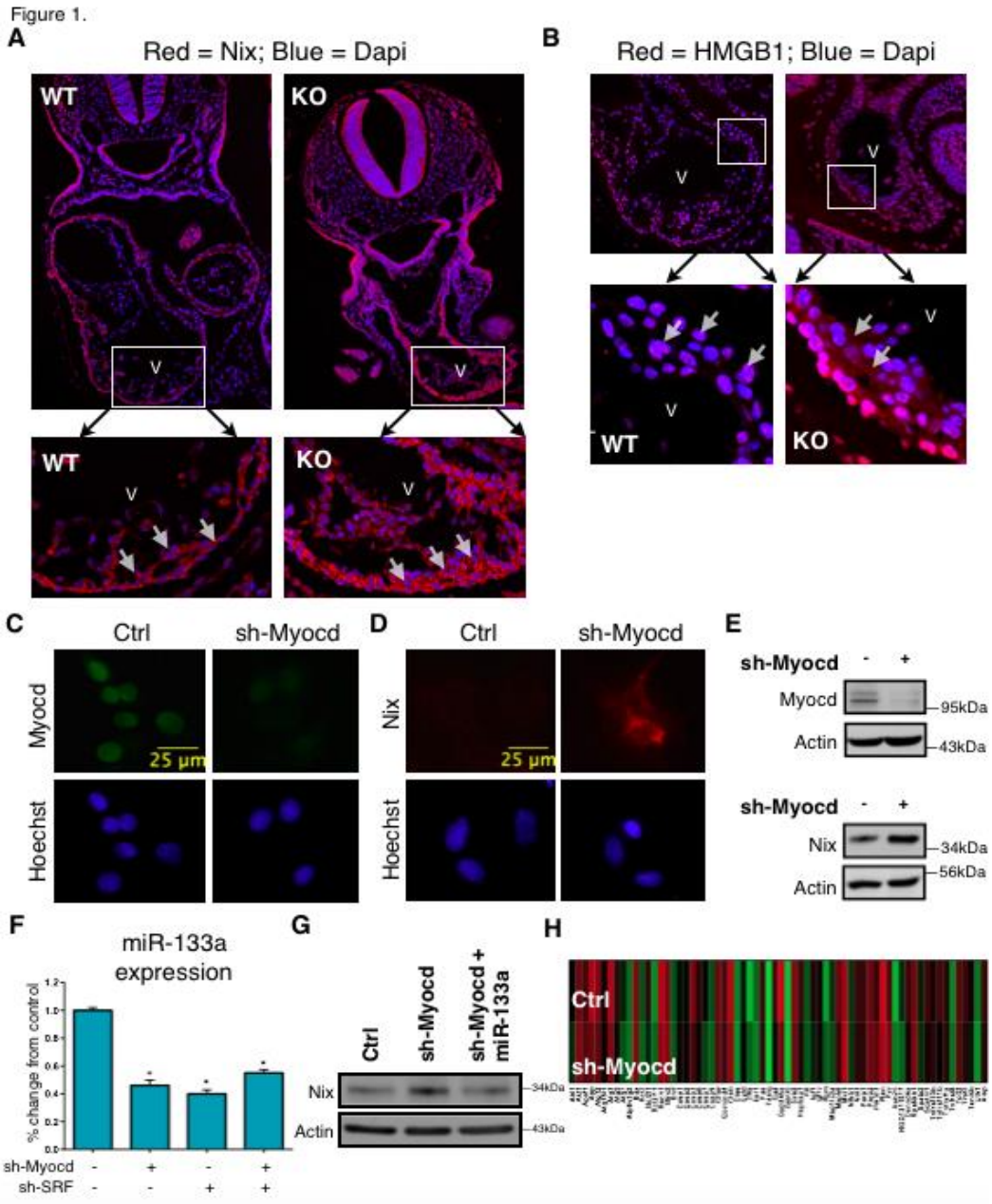

II - Figure 1: Silencing of Myocardin increases Nix expression through a miR-133a dependent mechanism. (A-B) E9.5 wild-type (WT) and Myocardin knock-out (KO) mouse embryos were fixed, mounted and stained for confocal immunofluorescence. Dapi (blue) identifies nuclei. Inserts identify myocardium. (C-D) Primary ventricular neonatal cardiomyocytes were infected with an shRNA targeting Myocardin (sh-Myocd) lentivirus or scrambled control. Cells fixed and stained, as indicated, and visualized by fluorescent microscopy. (E) H9c2 cells were transfected with sh-Myocd or scrambled control. Protein extracts were immunoblotted as indicated. (F) H9c2 cells were transfected with sh-Myocd, sh-SRF, as indicated, and RNA extracts were analyzed by real-time PCR for microRNA-133a (miR-133a). (G) H9c2 cells were transfected sh-Myocd or a scrambled vector, and miR-133a. Protein extracts immunoblotted for Nix expression. (H) H9c2 cardiac myocytes were transfected as in (E). Isolated RNA was analyzed by PCR-based array. Data are expressed as mean +/- SE. * p <0.05 compared to control, determined by 1-way ANOVA.

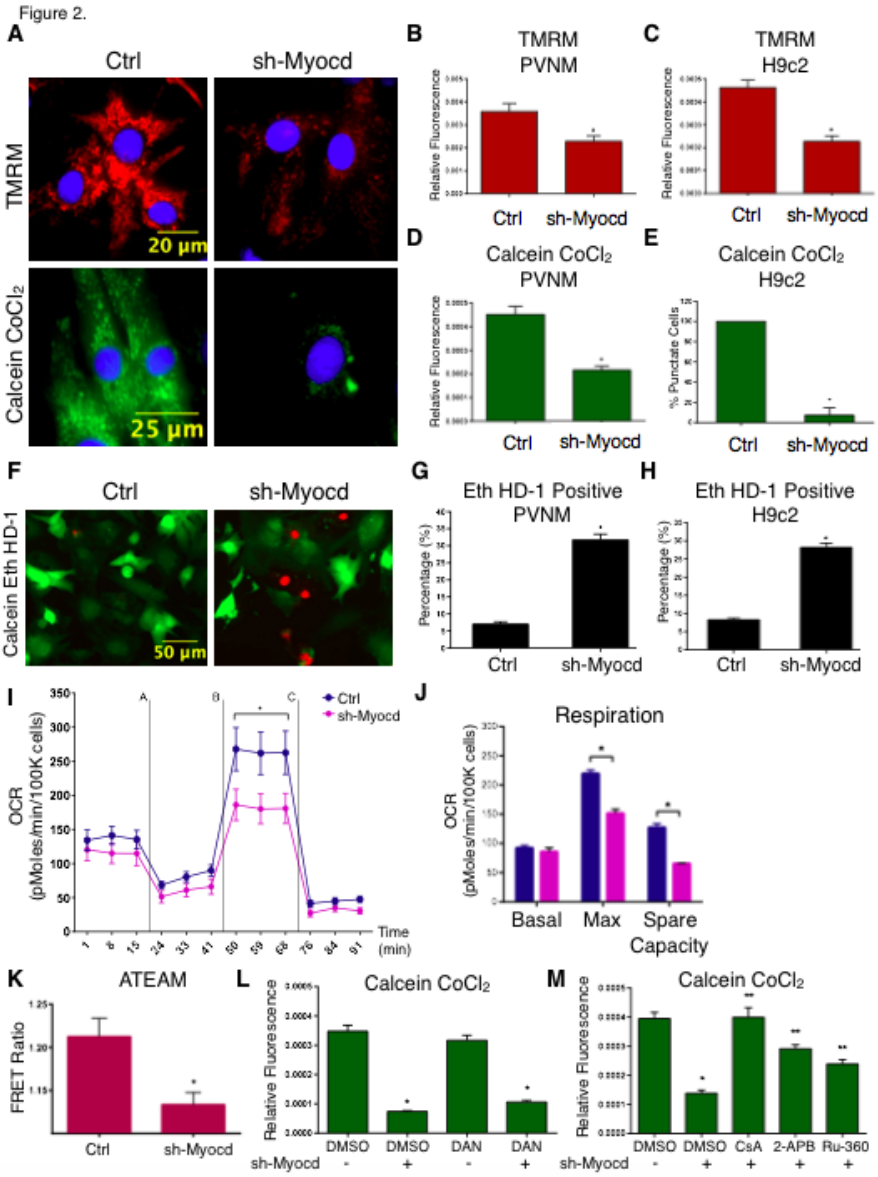

II - Figure 2: Myocardin regulates mitochondrial function and permeability. (A) Primary ventricular neonatal cardiomyocytes (PVNM) were infected with sh-Myocd or a scrambled control. Cells were stained with TMRM or with calcein-AM and cobalt chloride ($CoCl_2$, 5µM) to determine mitochondria permeability transition. (B) Quantification of TMRM; fluorescence signal normalized to cell area (relative fluorescence) quantified in 10 random fields and 30 cells/condition. (C) H9c2 cells transfected with sh-Myocd or scrambled vector; stained with TMRM and quantified. (D) PVNM treated as in (A); stained with calcein-AM and $CoCl_2$, and quantified (in 10 random fields and 30 cells/condition). (E) H9c2 cells treated as in (C); stained with calcein-AM and $CoCl_2$, and quantified. (F) PVNM treated as in (A), stained with calcein-AM and ethidium homodimer-1 (Eth HD-1) to identify living (green) and necrotic (red) cells, respectively. (G) Quantification of fluorescent images in (F) by calculating the percentage of necrotic cells (Eth HD-1 Positive) in 10 random fields and over 200 cells per condition. (H) H9c2 cells treated as in (C), Eth HD-1 Positive cells quantified. (I) PVNM treated as in (A); to assess oxygen consumption rate (OCR). PVNMs were injected with oligomycin (1uM) [A], FCCP (1uM) [B], and antimycin A (1uM) and rotenone (1uM) [C]. OCR was corrected by total cell number following analysis (n=9). (J) Calculated respiration rates from (I). (K) H9c2 cells were transfected as in (C), along with ATeam 1.03. Cells were analyzed by excitation of CFP and taking the emission ratio of YFP to CFP (FRET Ratio) in 15 random fields and 35 cells per condition. (L) PVNM treated as in (A), following treatment with Dantrolene (DAN, 10uM; 18 hours); DMSO used as a control vehicle. Cells stained with calcein-AM and $CoCl_2$ and quantified. (M) PVNM treated as in (A), following treatment with cyclosporine A (CsA, 1uM), 2-aminoethoxydiphenyl borate (2APB, 2uM), or Ruthenium360 (Ru360, 10uM; 18 hours). DMSO used as a control vehicle. Cells stained with calcein-AM and $CoCl_2$ and quantified. Data are expressed as mean +/- SE. * $p<0.05$ compared to control, ** $p<0.05$ compared to treatment, determined by 1-way ANOVA.

As determined by MTT assay, Myocardin expression had no effect on cell viability when H9c2 cells were exposed to staurosporine (Figure 3F).

Myocardin regulates myocyte calcium homeostasis:

To more fully investigate the role of cellular calcium in Myocardin-regulated permeability transition, we used organelle-targeted and genetically encoded calcium biosensors, called GECOs (Genetically Encoded Ca2+ indicators for Optical imaging)[38]. We used the mitochondrial matrix-targeted red GECO, known as Carmine (mito-carmine), and ER-targeted LAR-GECO (ER-LAR-GECO) (249,250). We rationalized that sustained activation of protein kinase-A (PKA) would trigger an intracellular calcium release from the SR that would be buffered by the mitochondrial. As a proof-of-concept experiment, we transfected these GECO constructs into H9c2 cells and treated cells with a combination of the adenylate cyclase activator forskolin (FSK; 10μM) and the pan-phosphodiesterase inhibitor IBMX (500μM), termed FSK-I. Shown in Figure 4A-C, FSK-I treatment reduced SR calcium and increased mitochondrial calcium, while the IP3R inhibitor 2APB blocked the effects of FSK-I. Interestingly, the RyR blocker dantrolene had no effect on FSK-I induced calcium release (Supplemental Figure 2A). Furthermore, transfection of cells with Myocardin prevented both the SR calcium release and the mitochondrial calcium accumulation triggered by FSK-I treatment (Figure 4D and -E). Consistent with our hypothesis that an SR-dependent calcium release leads to mitochondrial permeability transition, we observed that FSK-I treatment reduced mitochondrial membrane potential, reduced calcein-cobalt chloride staining, increased mitochondrial superoxide production, and the percentage of ethidium homodimer positive cells (Figure 4F-I).

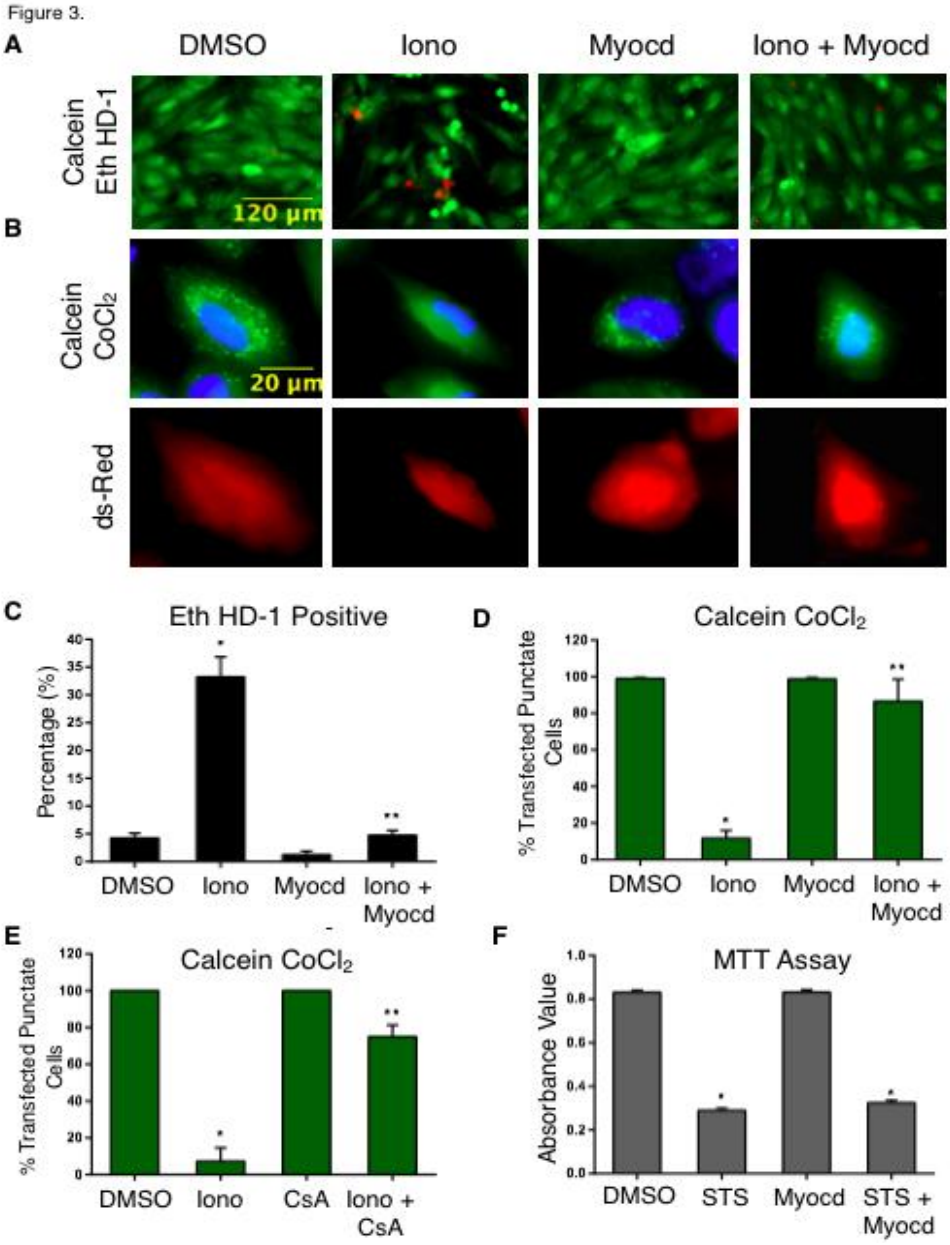

II - Figure 3: Myocardin opposes necrosis and mitochondrial dysfunction.
(A) H9c2 cells were transfected with Myocardin (Myocd) or an empty vector control, and treated with ionomycin (Iono, 2µM, 18 hours); DMSO used as a control vehicle. Cells stained with calcein-AM and Eth HD-1 to identify living (green) and necrotic (red) cells, respectively; (B) stained with calcein-AM and $CoCl_2$. CMV-dsRed identifies positive cells. C) Quantification of (A) by calculating the percentage of necrotic cells (Eth HD-1 Positive) and over 200 cells per condition and D) by calculating the percentage of transfected cells with mitochondrial puncta, in 10 random fields. (E) H9c2 cardiac myocytes were pre-treated with CsA (1uM, 2 hours) followed by ionomycin treatment (Iono, 2 µM, 18 hours). Cells stained with calcein-AM and $CoCl_2$; quantified. (F) H9c2 cardiac myocytes transfected with Myocd or an empty vector control, treated with staurosporine (STS, 2uM, 18 hours); cell viability assessed by MTT analysis (n=4). Data are expressed as mean +/- SE. * $p<0.05$ compared to control, ** $p<0.05$ compared to treatment, determined by 1-way ANOVA.

Moreover, expression of Myocardin rescued permeability transition and necrosis induced by FSK-I treatment (Figure 4F-I). In addition, FSK-I induced mitochondrial membrane depolarization and permeability transition were blocked by 2APB treatment, while isoproterenol increased mitochondrial calcium in primary cardiomyocytes (Supplemental Figure 2B-D). Myocardin expression also reduced the expression of Nix, without affecting other mitochondrial regulators, such as the mitochondrial biogenesis inducer PGC-1α or mitofusin-2 (Figure 4J). Finally, Myocardin knockdown increased mitochondrial calcium accumulation, determined by the mito-carmine biosensor (Figure 4K and -L). Collectively, these findings suggest that Myocardin can alter the sensitivity of the SR-dependent calcium release, which serves as a proximal event to mitochondrial calcium uptake and MPTP opening.

The Myocardin-dependent microRNA, miR-133a, regulates mitochondrial function and permeability transition:

To evaluate the role of miR-133a in mitochondrial permeability transition and necrosis, we transfected H9c2 cells with miR-133a and assessed cell sensitivity to FSK-I treatment. Shown in Figure 5A and -B, cells expressing miR-133a displayed improved mitochondrial membrane potential when exposed to FSK-I, and did not undergo permeability transition to the same extent as control cells. Furthermore, expression of miR-133a reduced the number of necrotic cells following FSK-I treatment (Figure 5C). Next, we expressed the SR- and mitochondrial-targeted calcium biosensors to assess if miR-133a expression could impact calcium homeostasis. Cells expressing miR-133a were desensitized to FSK-I induced SR calcium release, compared to control cells (Figure 5D). Furthermore, miR-133a expression prevented mitochondrial calcium accumulation triggered by FSK-I treatment (Figure 5E).

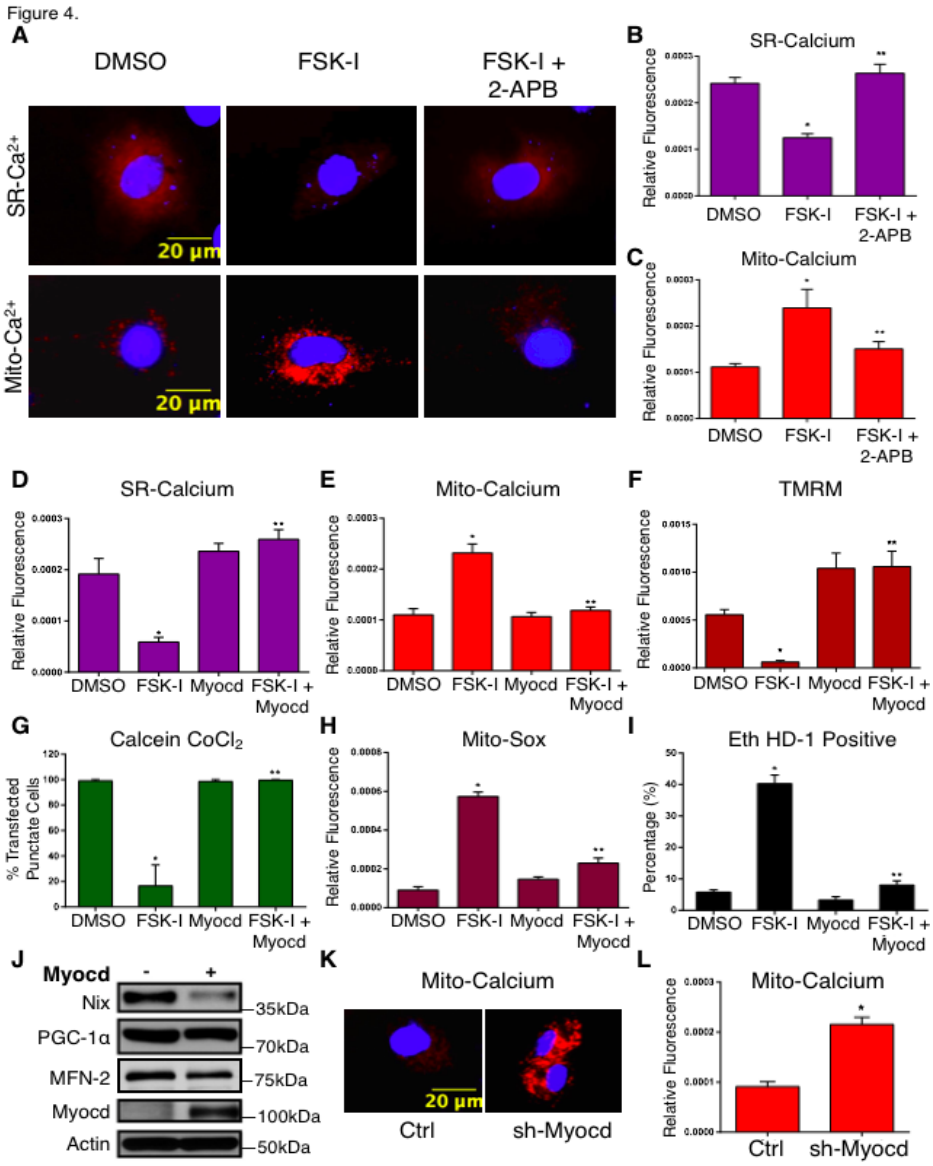

II - Figure 4: Myocardin regulates Mitochondrial Calcium homeostasis.
(A) H9c2 cells were transfected with a SR-targeted (above) or mitochondrial (mito)-targeted (below) calcium biosensor. Cells were pre-treated with 2APB (2uM, 2 hours) followed by co-treatment with Forskolin (FSK, 10uM) and 3-isobutyl-1-methylxanthine (IBMX, 500uM; FSK-I, 18 hours), or DMSO as a control vehicle. (B) Quantification of SR-calcium and (C) mito-calcium from (A). Fluorescence signal normalized to cell area (relative fluorescence) was quantified in 10 random fields. (D) H9c2 cardiac myocytes were transfected with Myocd or an empty vector, and a SR-targeted calcium biosensor or (E) a mito-targeted calcium biosensor; treated with FSK-I, and quantified. (F) H9c2 cardiac myocytes transfected with Myocd or an empty vector and treated with FSK-I; stained with TMRM, or (G) calcein-AM and $CoCl_2$, or (H) Mito-Sox to evaluate mitochondrial super oxide, or (I) calcein-AM and Eth HD-1; 10 random fields were quantified for each end-point. (J) H9c2 cells were transfected with Myocd or empty vector. Protein extracts analyzed as indicated. (K) H9c2 cells were transfected with sh-Myocd or scrambled control, with the mito-calcium biosensor and stained with Hoechst to visualize nuclei. (L) Quantification of (K). Data are expressed as mean +/- SE. * $p<0.05$ compared to control, ** $p<0.05$ compared to treatment, by 1-way ANOVA.

We also evaluated respiration in H9c2 cells treated with FSK-I. Shown in Figure 5F and -G, 18-hour treatment with FSK-I significantly reduced basal and maximal respiration in these cells; however, miR-133a attenuated the effects of FSK-I on mitochondrial respiration. Next, we performed a rescue experiment, where we determined if miR-133a expression could overcome mitochondrial calcium accumulation when Myocardin was knocked-down. Shown in Figure 5H, Myocardin knockdown increased mitochondrial calcium levels; however, when cells were co-transfected with miR-133a, mitochondrial calcium levels were restored to control levels. Finally, we reconstituted Nix function by expressing a Nix construct, which lacks the miR-133a 3'-UTR binding site, and demonstrate that FSK-I induced elevations in mitochondrial calcium were maintained, even in the presence of ectopic miR-133a expression (Figure 5I).

Myocardin regulates mitochondrial permeability transition and calcium homeostasis through Nix:

To further describe the role of Nix as a down-stream effector of Myocardin-regulated calcium homeostasis, we performed a double-knockdown experiment and evaluated mitochondrial calcium accumulation. Shown in Figure 6A and -B, knockdown of Myocardin increased mitochondrial calcium and induced permeability transition; however, simultaneous knockdown of Nix returned mitochondrial calcium to control levels and prevented permeability transition. Furthermore, expression of Nix in H9c2 cells induced mitochondrial permeability transition, which was inhibited by CsA treatment (Figure 6C). In addition, expression of Nix reduced SR calcium and increased mitochondrial calcium levels (Figure 6D and –E), and

Figure 5.

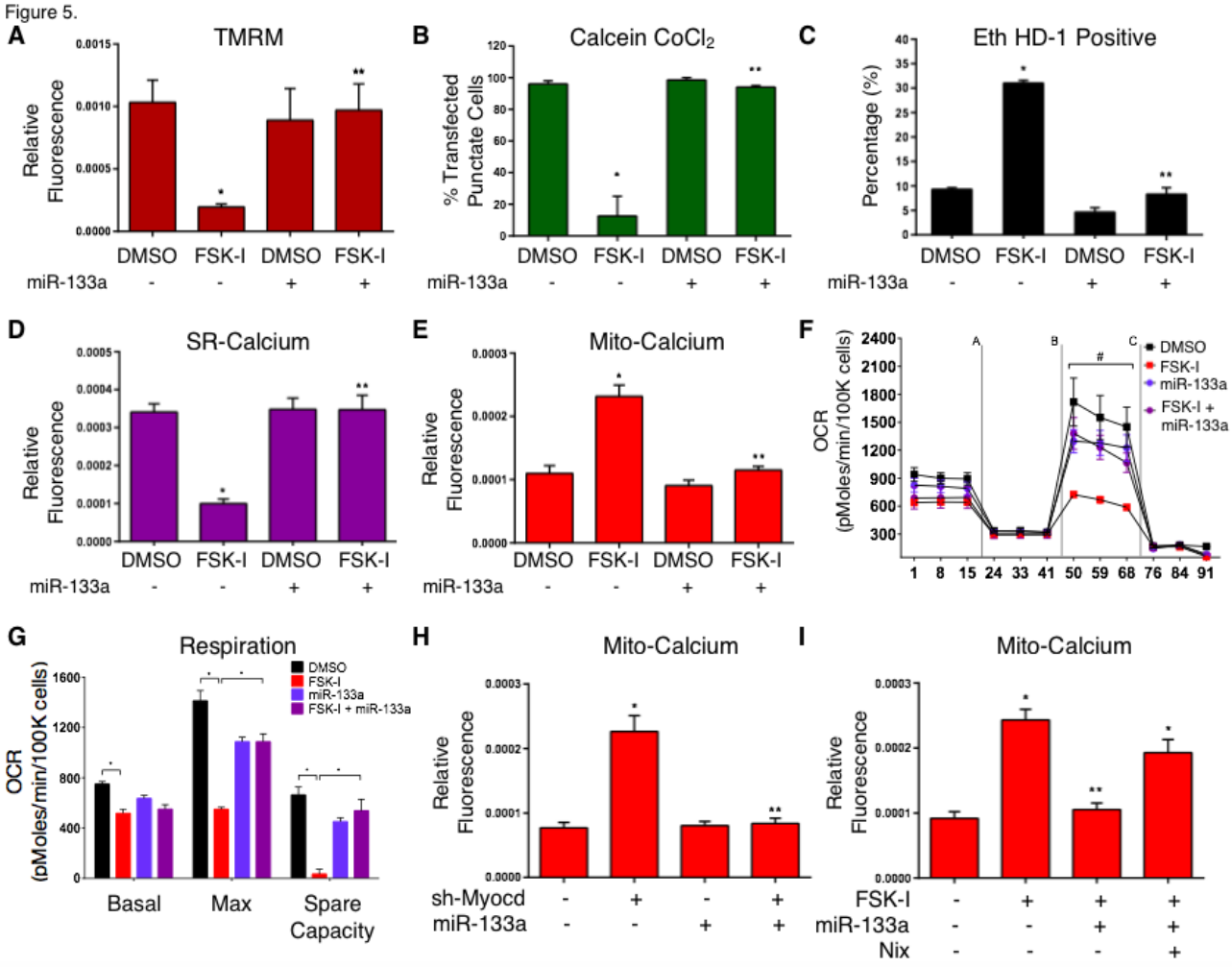

II - Figure 5: Myocardin-dependent micro-RNA, miR-133a, regulates mitochondrial function and permeability transition.
(A-C) H9c2 cells were transfected with miR-133a or an empty vector, and treated with FSK-I (18 hours), or DMSO as a control vehicle; stained with TMRM (A) or (B) with calcein-AM and $CoCl_2$, or (C) with calcein-AM and Eth HD-1. (D) H9c2 cells were transfected with a SR-targeted calcium biosensor, treated with FSK-I, and quantified. (E) H9c2 were transfected with miR-133a or an empty vector, a mito-targeted calcium biosensor, treated with FSK-I, and quantified. (F) H9c2 cells were transfected with a miR-133a mimic, and treated with FSK-I or vehicle control. Cells were injected with oligomycin (1uM) [A], FCCP (1uM) [B], and antimycin A (1uM) and rotenone (1uM) [C]. OCR was corrected by total cell number following analysis (n=4). (G) Calculated respiration rates from (F). (H) H9c2 cells were transfected with sh-Myocd or scrambled control, miR-133a, a mito-targeted calcium biosensor, and quantified. (I) H9c2 cells were transfected with miR-133a or an empty vector control, Nix and a mito-targeted calcium biosensor. Cells were treated with FSK-I (18 hours), or DMSO as a control vehicle and quantified. Data are expressed as mean +/- SE. * $p<0.05$ compared to control, ** $p<0.05$ compared to treatment, determined by 1-way ANOVA.

knockdown of Nix prevented FSK-I induced permeability transition and necrosis (Figure 6F and Supplement Figure 2E). Next, we performed cell fractionation studies following Myocardin knock-down. Although Nix expression is greater in the mitochondria fraction than in the ER/SR fraction, the primary induction of Nix following Myocardin knock-down occurred in the ER/SR fraction. The mitochondrial fraction remained relatively unchanged (Figure 6G). Taken together, our data suggests that suppression of Nix expression at the ER/SR is an important component of Myocardin-regulated calcium homeostasis and survival phenotype.

In order to further understand how Nix regulates mitochondrial permeability transition, we engineered SR- and mitochondrial-targeted Nix constructs (Supplemental Figure 2G) and evaluated mitochondrial calcium accumulation. Expression of wild-type Nix increased mitochondrial calcium levels (Figure 6H). Interestingly, mitochondrial-targeted Nix had no effect on mitochondrial calcium levels, while SR-targeted Nix increased mitochondrial (Figure 6H). These data implicate an SR-dependent calcium release as an important aspect of Nix-induced permeability transition. Previous studies have implicated Bcl-2 as a regulator of IP3-dependent calcium release, and Nix has been demonstrated to functionally interact with Bcl-2 (243,254,255). Thus, we utilized organelle-targeted Bcl-2 constructs to further interrogate mitochondrial calcium accumulation (190). Shown in Figure 6I and -J, expression of wild-type Bcl-2 attenuated Nix-induced calcium accumulation and permeability transition. Consistent with our organelle-targeted Nix constructs, only SR (ie. ER)-targeted Bcl-2 could prevent Nix-induced mitochondrial calcium accumulation and permeability transition, while mitochondrial-targeted Bcl-2 had no effect on these end-points (Figure 6I and -J).

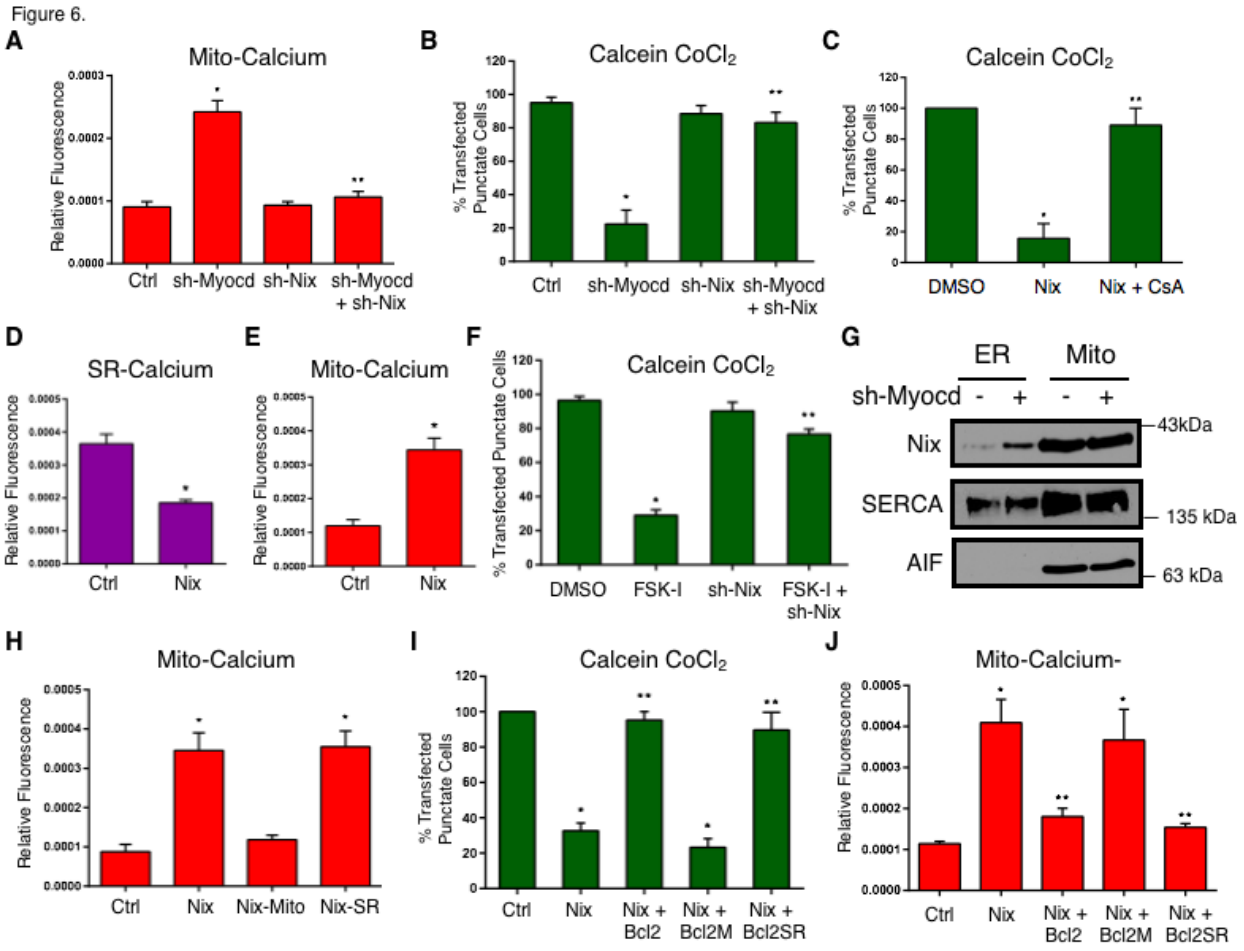

II - Figure 6: Myocardin regulates mitochondrial permeability transition and calcium homeostasis through Nix.

(A) H9c2 cells were transfected with sh-Myocd, sh-Nix, as indicated, a mito-targeted calcium biosensor and quantified (B). H9c2 cells were transfected with sh-Myocd, sh-Nix; as in (A) and stained with calcein-AM and $CoCl_2$ and quantified. (C) H9c2 cells were transfected with Nix or empty vector control, treated with cyclosporine A (CsA, 1uM, 18 hours); stained with calcein-AM and $CoCl_2$ and quantified. (D-E) H9c2 cells were transfected with Nix or empty vector control and (D) the SR-targeted calcium biosensor or (E) the mito-targeted calcium biosensor, and quantified. (F) H9c2 cells were transfected with sh-Nix or a scrambled control, treated with FSK-I (18 hours), or DMSO as a control vehicle; stained with calcein-AM and $CoCl_2$ and quantified. (G) H9c2 cells were transfected with sh-Myocd or scrambled control. Mitochondrial and ER fractions were immunoblotted as indicated. (H) H9c2 cells were tansfected with Nix, mitochondrial-targeted Nix (Nix-Mito), or SR-targeted Nix (Nix-SR), and the mito-targeted calcium biosensor, and quantified. (I) H9c2 cells were transfected with Nix, wild-type Bcl2, mitochondrial-targeted Bcl-2 (Bcl2-M), or SR-targeted Bcl-2 (Bcl2-SR), or empty vector control, stained with calcein-AM and $CoCl_2$ (J) or transfected with mito-targeted calcium biosensor, and quantified.

Myocardin expression is reduced in the border-zone following myocardial infarction:

To evaluate whether this pathway connecting Myocardin and Nix through miR-133a operates *in vivo*, we utilized two animal models of cardiac necrosis. First, we used a rat coronary ligation model, and dissected the infarct border-zone from the scar tissue, 4-weeks post-ligation (251). The border-zone is the area at risk within the left anterior descending territory, that does not infarct within the first 24-hours following coronary ligation. By 4-weeks post-ligation, this tissue is located immediately adjacent to the infarct scar tissue. Left ventricle tissue from sham-operated animals was used as control. We observed a 40% reduction in Myocardin mRNA within the infarct border-zone, and a concurrent 45% reduction in miR-133a expression (Figure 7A and -B). Consistent with our hypothesis, Nix expression was also increased within the border zone (Figure 7C and -D). However, these gene expression changes were returned to control levels by 8-weeks post-infarction (not shown). Second, we used a doxorubicin (Dox)-induced cardio-toxicity model[45]. C57BL6 mice received weekly intraperitoneal injections of Dox (8 mg/kg body weight) for 4 weeks. In contrast to the infarction model, we observed a modest increase in miR-133a expression and no change in Myocardin expression in Dox-treated animals (Figure 7E and –F). Furthermore, we observed a trend towards decreased Nix expression, but this was not statistically significant in Dox-treated hearts (Figure 7G and -H). These findings suggest that cardiac necrosis in the infarct border-zone and Dox models have unique features and the Myocardin-Nix pathway is specifically and temporally regulated within the infarct border-zone.

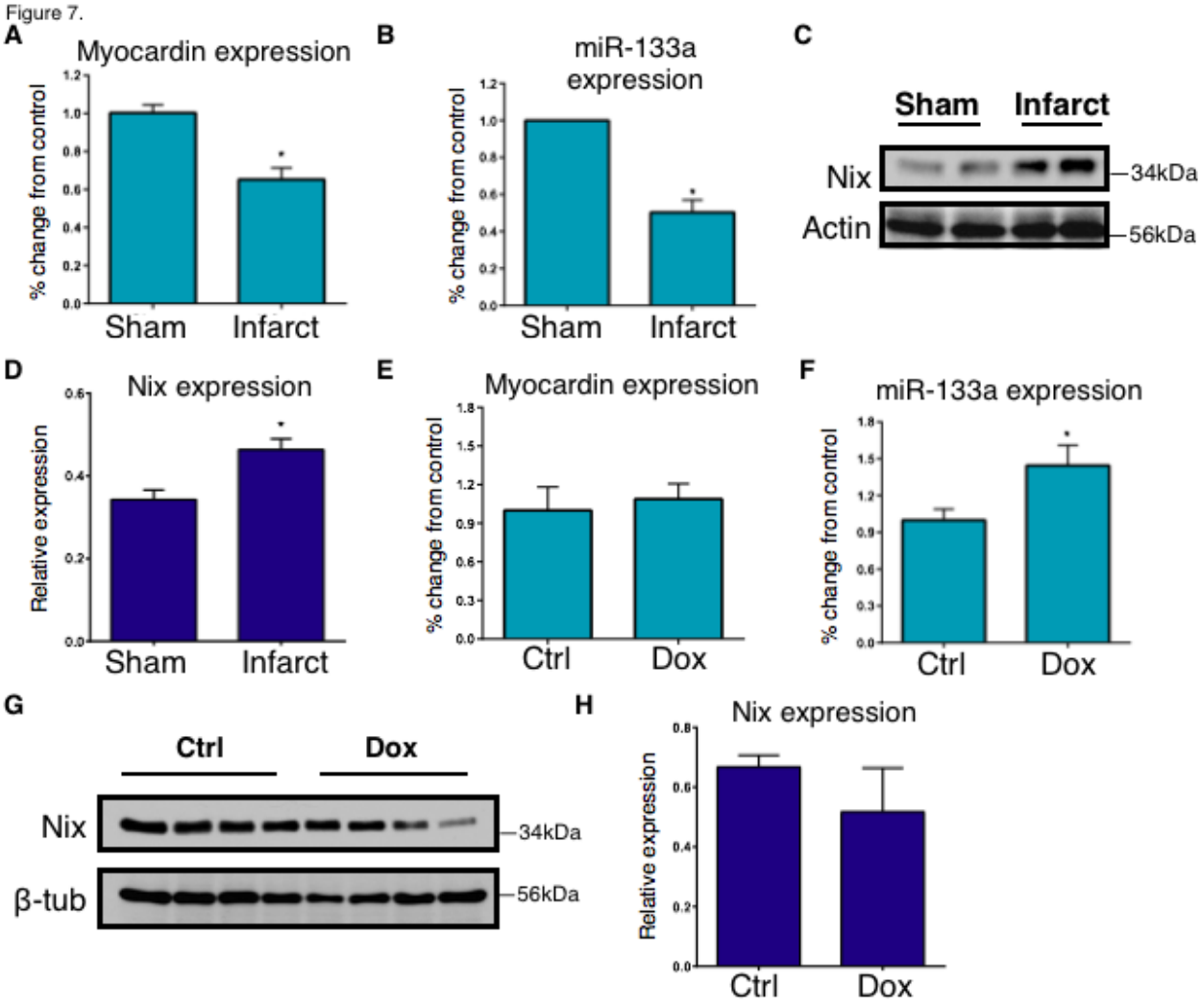

II - Figure 7: In vivo analysis of the Myocardin-miR133a-Nix pathway.
(A-D) Sprague Dawley rats were subjected to left coronary artery ligation, or sham operation as a control. Following 4-weeks of recovery, the viable infarct border-zone was harvested from the left ventricle. Extracts were analyzed by real-time PCR for Myocardin (A), or miR-133a (B) expression (n=4). Protein extracts were immunoblotted for Nix (C) expression and subjected to densitometry (D, n=3). (E-H) C57BL6 mice received weekly intraperitoneal injections of doxorubicin (Dox; 8 mg/kg), or vehicle control, for 4 weeks. Extracts were analyzed by real-time PCR for Myocardin (E), or miR-133a (F) expression (n=4). Protein extracts were immunoblotted for Nix (G) expression (n=4) and subjected to densitometry (H). Data are expressed as mean +/- SE. * $p<0.05$ compared to control, determined by students T-test.

4.6 Discussion

Mitochondrial permeability transition in cardiomyocytes has been implicated in both developmental processes and in regulated necrosis occurring during cardiac pathologies; however, the transcriptional regulation of these events remains poorly defined. Here, we describe a Myocardin-regulated pathway that opposes mitochondrial permeability transition through a calcium-dependent mechanism. We also demonstrate that this pathway is operational during embryonic cardiac development and within the infarct border-zone during the recovery from coronary ligation. To our knowledge, this is the first evidence of a direct Myocardin-target gene regulating cardiomyocyte survival.

Detailed evaluation of Myocardin expression during mouse embryogenesis previously documented that Myocardin transcripts are detectable as early as E9.5 in the embryonic heart, and are robustly expressed throughout the embryonic ventricles by E14.5 (29). This is temporally correlated with developmental closure of the MPTP[17]. Collectively, these findings are consistent with our data demonstrating Myocardin is a regulator of mitochondrial permeability transition. In addition, conditional Myocardin knockout mouse models have demonstrated that there are developmental and post-natal 'windows' where genetic inactivation of Myocardin produces lethal cardiac defects (51). For example, genetic removal of Myocardin using the Nkx2.5-Cre line results in lethality at E13.5 due to cardiac chamber maturation defects[10]. Furthermore, using MerCreMer line for the tamoxifen-inducible removal of Myocardin in the mature adult mouse heart, which is highly dependent on mitochondrial oxidative metabolism for ATP production, results in rapid deterioration to heart failure (52). Conversely, conditional knockouts generated with the αMHC-Cre line, which removes Myocardin function after chamber maturation and MPTP closure occurs,

results in a delay in mortality by up to 10 months, suggesting that loss of Myocardin function at this developmental stage can be partially compensated for, at least transiently (52).

Previous studies have implicated Myocardin as a regulator of pathological hypertrophy elicited by aortic banding (106). Myocardin expression is increased following aortic banding and produces hypertrophy when delivered to cultured cardiomyocytes (106). Our findings that Myocardin expression is reduced following coronary artery ligation may at first seem contradictory to this study. However, the infarct border-zone following coronary ligation is a unique pathological environment, where myocytes are exposed to metabolic stress induced by hypoxia/ischemia, adrenergic stimulation, and mechanical stretch, which is undoubtedly different than the afterload- and/or neurohumoral-induced stress imposed by aortic banding.

Our findings are consistent with several important developmental and post-natal cardiac remodeling studies involving miR-133a and Nix, and help consolidate these findings into a genetic pathway that operates during cardiac ontogeny and during ischemic heart disease, where Myocardin serves as a proximal regulator of this pathway. In this regard, miR-133a-1 and miR-133a-2 double knockout mice display evidence of abnormal mitochondrial cristae formation in the heart and aberrant smooth muscle gene expression[48]. Furthermore, miR-133a repression has been implicated in both rodent and human cardiac hypertrophy (231) and diabetes-related cardiac remodeling[31], while transgenic mice expressing miR-133a under control of the αMHC promoter display reduced levels of fibrosis during pathological cardiac remodelling[33]. Previously, we demonstrated that miR-133a was a direct transcriptional target of MEF2C and SRF in cardiac, skeletal, and smooth muscle cells (246). However, we also observed that the gene expression pattern of miR-133a was different in the heart than in skeletal muscle (246). Based on the observations in the present study, we content that the presence of Myocardin creates an addition

layer of regulation over miR-133a expression that is present in the heart, but not in myotubes or mature skeletal muscle. Nix expression is induced following pressure overload and in genetic models of heart failure, such as the transgenic Gαq mouse, while Nix knockout mice are protected from heart failure in these models (230,256). However, highly purified mitochondrial isolated from Nix knockout animals are identical to wild-type in terms of permeability transition determined triggered by exogenous calcium (245). In addition, Nix preferentially accumulates in the SR following aortic banding resulting in enhanced caffeine-induced calcium release (245). These findings are consistent with our data, and we provide addition insight into the function of Nix at the SR/ER, and demonstrate that Nix depletes the SR calcium content, which is buffered by mitochondria calcium uptake at the expense of MPTP opening.

Recent progress has been made regarding the mitochondrial components and regulators of the permeability transition pore, and several studies have defined the importance of MPTP-dependent necrosis in the pathophysiology of ischemic cardiac and cerebrovascular diseases (235). However, little is known regarding the transcriptional regulation of permeability transition, especially the tissue-specific regulation during developmental or during pathological conditions. The data presented here describe a genetic pathway that regulates MPTP function during cardiac development and within a discrete temporal period in the infarct border-zone following coronary ligation. Our data also suggests that the transcriptional regulation over permeability transition occurs through calcium homeostasis, where Nix expression dictates the sensitivity of the ER/SR to IP3R-activating stimuli. Furthermore, previous literature suggests that an ER-to-mitochondrial calcium transfer, occurring at the mitochondrial associated membrane of the ER, is an important regulatory component of mitochondrial function and cell death (257,258). Additional work is needed to determine if this pathway, or a similar pathway, is conserved in multiple tissues, and to

determine how MPTP and necrosis is regulated in other pathologies. Given the diverse roles of miR-133a and Nix in regulating mitochondrial function, proliferation, and autophagy, dysregulation of this genetic pathway may have broad implications involving cardiometabolic disease, insulin resistance, and cancer biology.

4.7 Acknowledgements

This work was support by the Natural Science and Engineering Research Council (NSERC) Canada, through a Discovery Grant to JWG. Seed funding was provided by the Thorlakson Foundation Fund and the Children's Hospital Foundation of Manitoba. MSP is support by NIH R01-HL102968 and R01-HL094520. IMD, VWD, and GMH are supported by the Heart and Stroke Foundation of Canada. RK is a Thorlakson Chair in Surgical Research, and GMH is a Canada Research Chair in Molecular Cardiolipin Metabolism. VWD is the Ken Hughes Young Investigator and the Allen Rouse Fellow of the Manitoba Medical Services Foundation. JWG, VWD, GMH, and RK are members of the DEVOTION Research Cluster. WM is supported by a scholarship from the Children's Hospital Foundation of Manitoba and Research Manitoba, JF is supported by a studentship from NSERC Canada, and LKC is supported by a CIHR Fellowship. We thank Fuqin Zhu for assistance with the confocal microscopy.

Author Contributions

Conceptualization, WM, ARW, VWD, IMD, and JWG; Methodology, YH, LKC, SR, KGC, VWD, ARW, GMH, RK, and IMD; Investigation, WM, JF, MM, DC, JH, SR, SK, KGC, ARW, JWG; Writing – Original Draft, WM and JWG; Writing – Review & Editing, WM, ARW, GMH, WD-J, VWD, IMD, MSP, JWG; Funding Acquisition, GMH, WD-J, VWD, IMD, MSP, JWG; Resources, YH, LKC, ARW, GMH, RK, VWD, IMD, MSP, JWG; Supervision, YH, LKC, WD-J, VWD, IMD, MSP, JWG.

4.8 Supplemental Figures for Manuscript II

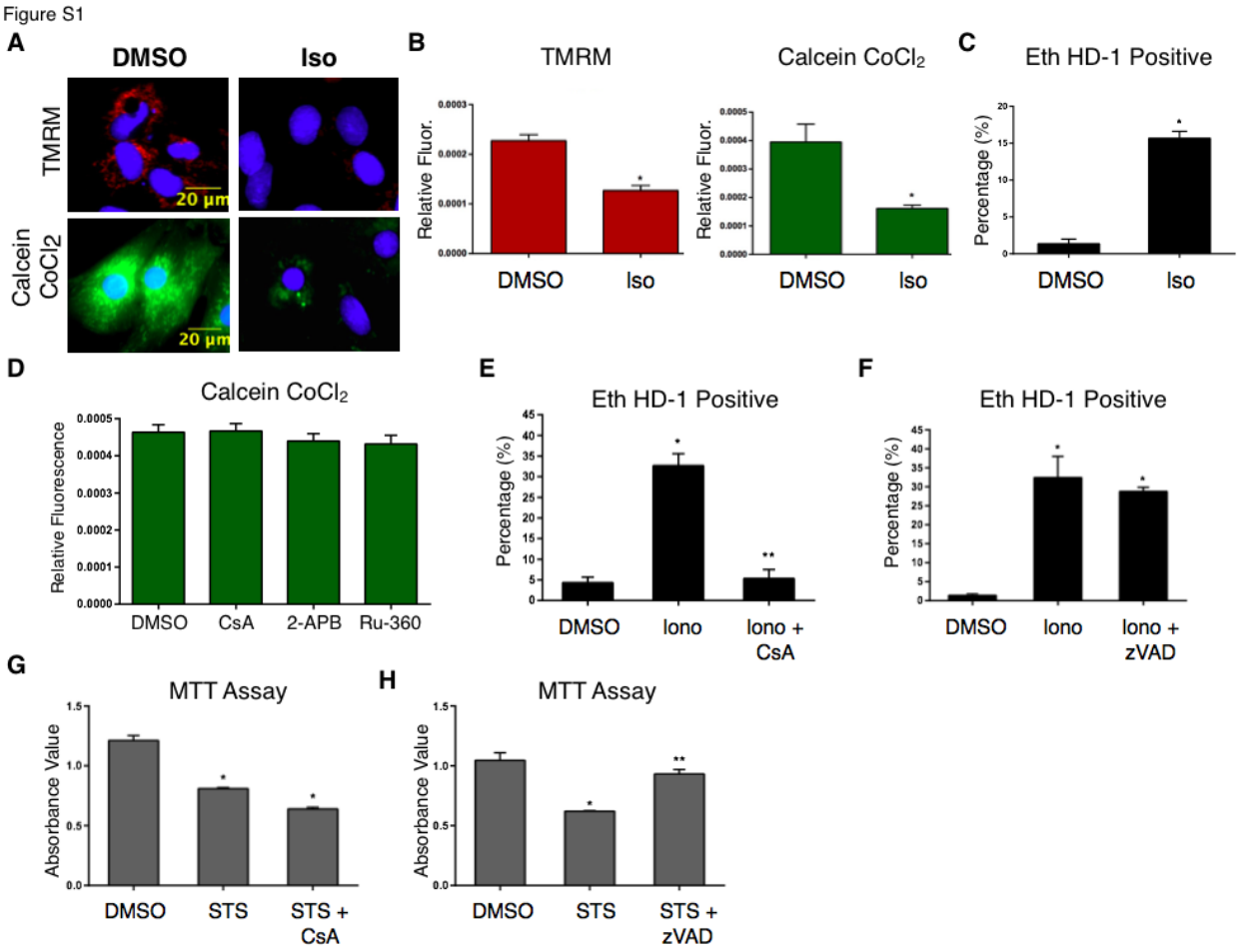

II - Supp Figure 1: Cell death pathways in cardiac cells.
(A-C) Primary ventricular neonatal cardiomyocytes (PVNC) were treated with isoproterenol (Iso; 100uM, 18 hours). Cells stained with TMRM to determine mitochondrial membrane potential or with calcein-AM and CoCl2 to determine mitochondrial permeability transition (A) and relative fluorescence quantified (in 10 random fields and 30 cells/condition) (B). (C) Cells stained with calcein-AM and Eth HD-1 to identify living (green) and necrotic (red) cells, respectively and quantified by calculating the percentage of necrotic cells (Eth HD- 1 Positive) and over 200 cells per condition; DMSO used as a control vehicle. (D) PVNCs treated with cyclosporine A (CsA, 1uM), 2-aminoethoxydiphenyl borate (2APB, 2uM), or Ruthenium-360 (Ru-360, 10uM) for 18 hours; DMSO used as a control vehicle. Cells were stained with calcein-AM and CoCl2 and quantified. (E-F) H9c2 cells pre- treated with cyclosporine A (CsA, 1uM, 2 hours) (E) or a caspase inhibitor (zVAD, 50uM, 2 hours) (F) followed by ionomycin treatment (Iono, 2 µM, 18 hours). Cells stained with calcein-AM and Eth HD-1 and quantified; DMSO used as a control vehicle. (G-H) H9c2 cells pre-treated with cyclosporine A (CsA, 1uM, 2 hours) (G) or a caspase inhibitor (zVAD, 50uM, 2 hours) (H) followed by staurosporine treatment (STS, 2uM, 18 hours); DMSO used as a control vehicle. Cell viability assessed by MTT analysis (n=4). Data are expressed as mean +/- SE. * $p<0.05$ compared to control, ** $p<0.05$ compared to treatment, determined by 1-way ANOVA.

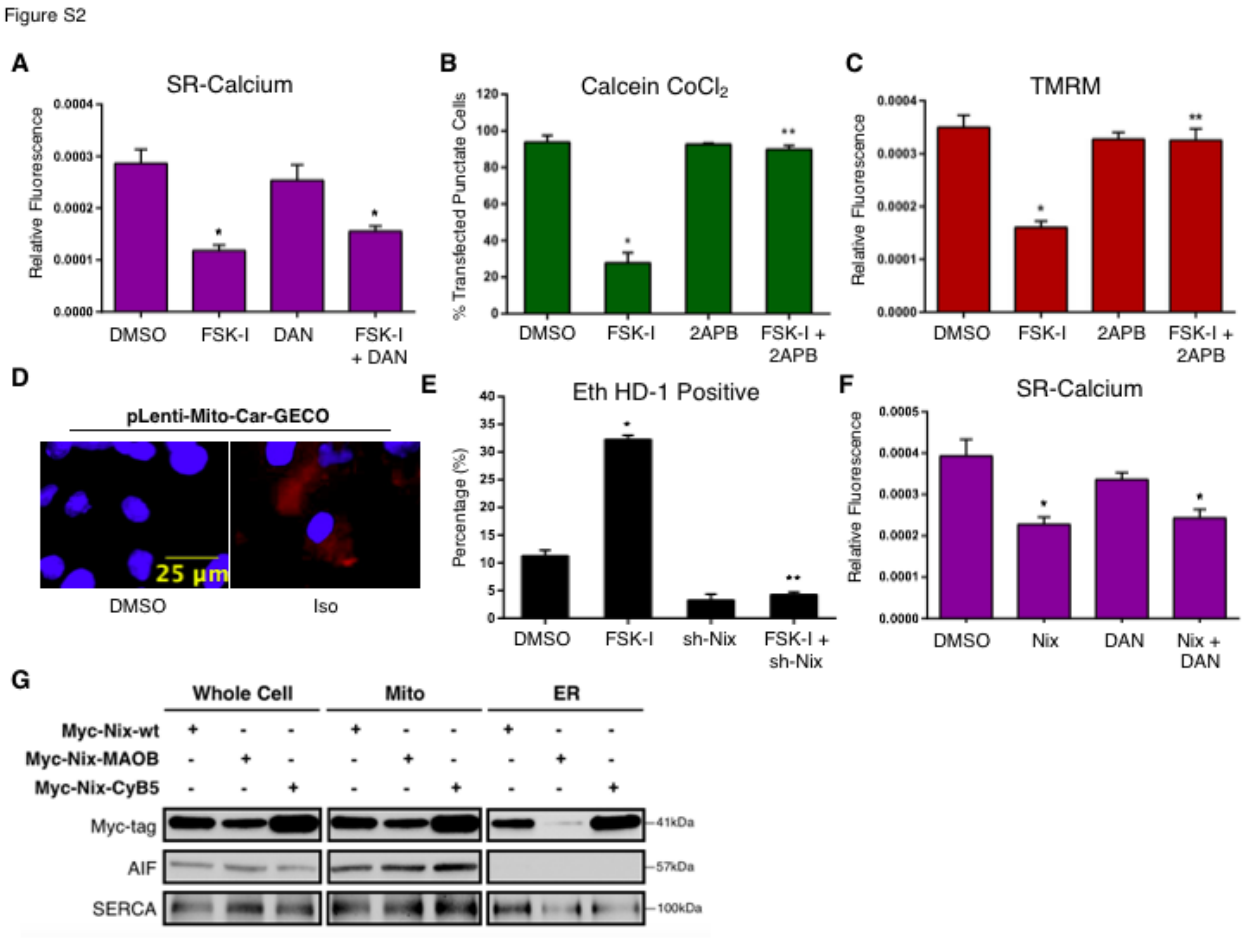

II - Supp Figure 2: Regulation of calcium homeostasis.
(A) H9c2 cells were transfected with a SR-targeted calcium biosensor, pre-treated with Dantrolene (DAN, 10uM; 2 hours) following treatment with Forskolin (FSK, 10uM) and 3- isobutyl-1-methylxanthine (IBMX, 500uM; FSK-I, 18 hours), or DMSO as a control vehicle. (B-C) H9c2 cells were treated with Forskolin (FSK, 10uM) and 3-isobutyl-1- methylxanthine (IBMX, 500uM; FSK-I, 18 hours), or DMSO as a control vehicle, along with 2-aminoethoxydiphenyl borate (2APB, 2uM). Cells were stained with calcein-AM and cobalt chloride ($CoCl_2$, 5µM) to determine mitochondria permeability transition (B) or TMRM to determine mitochondrial membrane potential (C). (D) Primary ventricular neonatal cardiomyocytes were transduced with a mito-carmine lentivirus (pLenti-Mito- Car-GECO) and treated with isoproterenol (Iso; 100uM, 18 hours) or DMSO as a control vehicle; nuclei were stained with Hoechst. (E) H9c2 cells were transfected with sh-Nix or a scrambled control, following treatment with FSK-I (18 hours), or DMSO as a control vehicle; stained with calcein-AM and Eth HD-1 and quantified. (F) H9c2 cells were transfected with Nix or an empty control vector, and SR-targeted calcium biosensor; following treatment with Dantrolene (DAN; 10uM, 18 hours), and quantified. (G) 3T3 cells were transfected with wild-type Nix, Nix-MaoB (Nix-mito), or Nix-CytoB5 (Nix-SR). Whole cell, mitochondrial, and ER cellular fractions were subjected to western blot, as indicated, to confirm the subcellular distribution of these engineered constructs. Data are expressed as mean +/- SE. * $p<0.05$ compared to control, ** $p<0.05$ compared to treatment, determined by 1-way ANOVA.

CHAPTER V: Dissertation Discussion

Initially identified as a transcriptional co-activator restricted to the cardiovascular system, animal models demonstrate Myocardin as an essential regulator of cardiac development: expression is detected as early as E7.75 in the primordial heart and throughout the pulmonary outflow tract, while loss of Myocardin results in congenital heart defects associated with increased cell death, heart failure, and lethality in mouse embryos (30,49,51). However, the molecular mechanisms by which Myocardin protects the heart is not understood. Tissue and animal models enabled me to evaluate a Myocardin-genetic pathway that preserves cardiomyocyte survival by regulating mitochondria through miR-133a inhibition of Nix (Figure 1).

First, we established a pathway in which MEF2 and SRF, reported to be co-activated by Myocardin, regulate miR−133a to preserve mitochondrial function through Nix inhibition during muscle differentiation. We provide evidence of miR-133a inhibition of Nix in human airway smooth muscle cells; however detection of miR-133a and Nix expression in mice exhibiting a smooth-muscle-specific deletion of Myocardin (MyocdF/F/Wnt1-Cre) would confirm if the Myocardin-genetic pathway is conserved in smooth muscle tissue (49). Reported upstream regulators of Myocardin function in smooth muscle including HDAC5, FOXO4, ELK1 and c-Jun, (43,64,67,75,85), are possible molecular candidates that may regulate this Myocardin-genetic pathway to mediate muscle differentiation during cardiac development. An additional potential regulator of this Myocardin-genetic pathway includes a RhoA/ROCK signalling mechanism that implicates c-Jun and CPI-17 as regulators of Myocardin expression and calcium sensitivity in vascular smooth muscle cells (213); c-Jun or CPI-17 regulation of Myocardin expression in cardiac muscle is currently unknown.

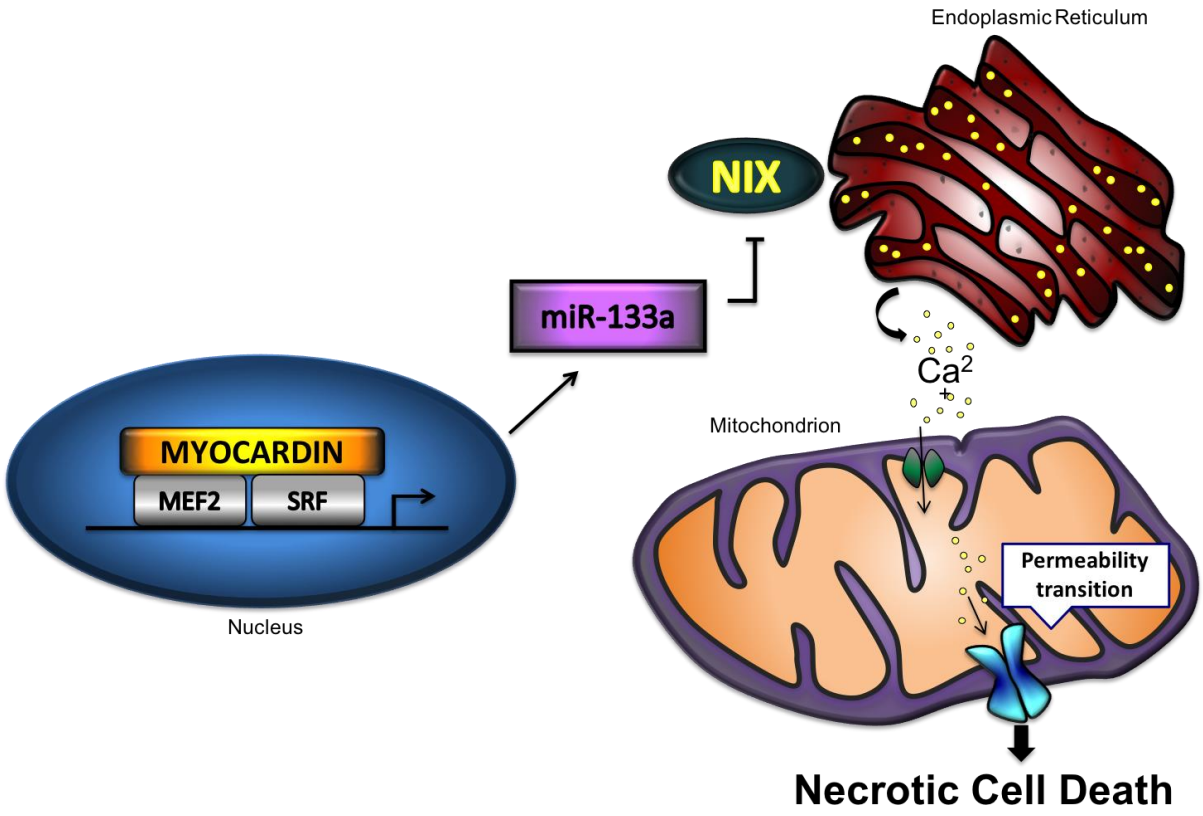

Summary: Figure 1: Dissertation graphical abstract.
Proposed mechanism of a Myocardin-genetic pathway that activates miR-133a to oppose Nix mediated MPT-pore-regulated cardiac necrosis. Myocardin co-activates MEF2 and SRF to regulate miR-133a inhibition of Nix to preserve cardiomyocyte survival.

In view of this genetic pathway conserved in three muscle lineages, we next provided evidence that Myocardin as an upstream co-activator that regulates miR-133a and opposes Nix in the heart using isolated primary neonatal cardiomyocytes and cultured H9C2 cardiac myocytes. Primary neonatal and adult cardiomyocytes contract but are sensitive cells that are difficult to isolate with a limited regenerative capacity. As an alternative strategy to reduce the number of research animals used to study molecular pathways in the heart, embryonic H9C2 rat cardiac myocytes are a well-established cell culture model that express cardiac genes and exhibit many biochemical similarities to primary cardiomyocytes were used in the studies described (259-261).

Certain limitations to the H9C2 cell line include its replicating nature compared to cardiomyocytes with a limited life span, its skeletal properties, and their inability to contract. Thus, our preliminary findings of the Myocardin genetic pathway were discovered in H9C2s and validated in primary neonatal cardiomyocytes. This pathway was further validated *in vivo* during embryonic mouse development that was demonstrated to become dysregulated in a model of ischemic heart disease. The demonstrated Myocardin genetic pathway remains to be investigated in the adult and human heart that may employ a strategy using human pluripotent embryonic stem cells-derived cardiomyocytes for further validation (262,263).

Our findings support previous reports of miR−133a regulating muscle differentiation (118,205,231,264,265); however, lineage tracing experiments detecting miR-133a expression in Myocd$^{-/-}$ null embryos will further validate this pathway during development. Shen and colleagues have recently reported miR-322/503 expression during early phases of cardiac looping as regulators of cardiac cell fate (266); whether miR-133a expression is detected in a similar pattern to Myocardin expression at E7.75 in the cardiac crescent, heart tube, cardiac loop, cardiac chambers and throughout the pulmonary tract at E15.5 is currently unknown.

Additional work is required to evaluate if this Myocardin-genetic pathway regulating miR−133a is conserved among other tissue types; however, this pathway could implicate other members of the Myocardin family that are not restricted to the cardiovascular system. Other members of the Myocardin family that are broadly expressed in embryonic and adult tissue that regulate MEF2 and SRF include MRTF-A, MRTF-B, and MASTR (20,26,46). Evidence from MRTF-B$^{-/-}$ mice exhibiting cardiac defects and embryonic death highly suggest MRTF-B may be implicated as an additional or alternative upstream regulator, that can be evaluated with a global or cardiac specific Myocd$^{-/-}$/MRTF-B$^{-/-}$ double knockout mouse model (39,41); in contrast, loss of

MRTF-A is not lethal, but may implicate miR-133a inhibition of Nix during cardiac fibrosis post myocardial infarction (21). Similar to MRTFs, MASTR is also broadly expressed in multiple tissues; both MRTFs and MASTR may serve as upstream regulators of miR-133a inhibition of Nix to oppose cell death in skeletal muscle has yet to be shown.

In contrast to previous reports on Myocardin regulating cardiac apoptosis (49), our findings provide the first evidence of Myocardin regulating the cardiac MPT-pore. Myocardin activation of miR-133a to oppose MPT–pore driven necrosis and not caspase-dependent apoptosis may appear contrary to the previous reports by our collaborators on Myocardin regulating apoptosis in the heart (51,52). However our data validates Myocardin as pro-survival regulator of cardiac cell fate: Myocardin may protect against both caspase-independent apoptosis and MPT–pore driven necrosis. This suggests an overlap between the two mechanisms of RCD, which may be better defined by detecting Nix and HMGB1 expression in the cardiac specific Myocardin knock out mouse model generated by our collaborators (51), combined with specific cell death assays to distinguish between caspase-independent apoptosis and other forms of regulated necrosis. I anticipate cardiac necrosis as the dominant form of cell death with loss of Myocardin function. This will validate the Myocardin-genetic pathway and provide new insight into the details of Nix mediated MTP-pore driven necrosis during development and the transition to heart failure.

Nix has been documented to regulate multiple forms of regulated cell death in various cell types (209); an overlap of multiple cell death pathways further adds complexity to understanding the mechanisms of Myocardin preserving cardiac function. Despite the elusive structure of MPT-pore implicated in ischemic heart disease (186), the findings of Myocardin maintaining mitochondrial calcium homeostasis support previous reports of Nix regulating 1) mitochondrial

calcium to trigger MPT-pore opening (164), and 2) ER and mitochondrial calcium crosstalk to mediate cell death (245,258).

The mitochondrial associated membrane (MAM) as the communication point between the mitochondria and ER includes tethering proteins such as dynamic related protein-1 (DRP-1), mitofusin-1/2 (MFN-1/2), to trigger MPT-pore by calcium transfer that may be influenced by the unfolded protein response (UPR) triggered by ER stress (267,268). Evidence of ER stress induced from the loss of Myocardin in smooth muscle cells combined with the reported upregulation of Nix in response to ER stress further implicates the UPR within the demonstrated Myocardin genetic pathway (269,270). However, ER stress in cardiac cells lacking Myocardin function and whether Nix interacts with UPR machinery in the heart is currently unknown.

Reports on Nix dysregulating calcium homeostasis have not addressed the mechanisms by which Nix or pro-death Bcl-2 proteins are directed to the ER; evidence suggests potential mediators of subcellular localization include pro-survival MCL-1, a member of the Bcl-2 family previously shown to regulate mitochondrial function and cell survival (271), that could involve a complex with 14-3-3 chaperone proteins that mediate protein-protein interactions to regulate cardiomyocyte function, cell death, and inhibition of a pro-death Bcl-2 member, BAX (272-274). Molecular players that promote Nix subcellular localization are unknown, but findings suggest miR-133a may mediate a 14-3-3/Nix interaction and ER localization that has yet to be evaluated. With Nix and other members of the Bcl-2 family (Bnip3) involved in mitophagy (209), Bcl-2 like-13 (Bcl2l-13; also known as Bcl-2-rambo) has recently been reported to mediate mitochondrial fragmentation, mitophagy, and apoptosis in human embryonic kidney cells (275,276). Whether Bcl-2-rambo is regulated by miR-133a in a similar manner to Nix regulation

in the heart is currently unknown, but our findings contribute to mitophagy research and highlight the various molecular regulators of mitochondrial function and cardiac cell survival.

Our findings provide mechanistic details underlying cell survival during cardiac development that are dysregulated during ischemic heart disease, with implications in insulin resistance, cardiac defects, pathological remodelling, hypertrophy, cardiac fibrosis, and diabetes induced heart disease (21,106,205,229,277). Reports on infant exposure to diabetes in utero are at a high risk of developing youth onset T2D, obesity, and cardiovascular disease (278-280), implicate miR−133a as a potential cardiometabolic biomarker assessed during fetal development and post-natally. With miRs currently being evaluated as biomarkers and targeted therapy for heart failure (281), evaluation of miR-mimicking molecules as a potential therapy to reverse cardiac dysfunction and metabolic reprogramming in offspring exposed to GDM and in models of ischemic heart disease is required to validate this Myocardin-genetic model in pre-clinical studies. Regulation of MPT-pore, miR-133a and Nix has also been implicated in cancer, thus evaluating miR−133a and mitochondrial function can advance our understanding of the dysregulation of cell death mechanisms underlying cancerous tumor cells (209,282,283).

Collectively the findings presented in this thesis advances the scientific knowledge to the field of cardiovascular cell biology regarding the role of Myocardin and the regulation of mitochondrial function during development and disease. Results of my dissertation provides evidence of a Myocardin-genetic pathway that activates miR-133a inhibition of Nix to oppose cardiac necrosis (Figure 1), with clinical implications in congenital heart defects, cardiometabolic disease, diabetes and cancer biology.

CHAPTER VI: Future Directions

Many experimental strategies were put aside during my PhD project to complete my dissertation. The findings presented here have transitioned into the basis for my future directions, presented under the following future experimental hypotheses.

1) Myocardin protects against cardiomyocyte necrosis
2) miR-mimics repress Nix in rodent infarction model
3) Offspring interbred with cardiac-specific Myocardin$^{-/-}$ mice with cardiac-specific Cyclophilin D$^{-/-}$/Nix$^{-/-}$ knockout mice will be protected from heart failure
4) Myocardin regulation by PKA is a SIK1 dependent mechanism

The experimental approach for each stated hypothesis is outlined: the complementary pre–clinical approach proposed in this section will help dissect this novel genetic pathway that regulates necrosis in cardiac myocytes. These innovative experiments will lay the molecular foundation to advance the understanding of regulated cell death in the heart, with the ultimate goal to develop a therapeutic strategy to preserve cardiac function.

6.1 Myocardin protects against cardiomyocyte necrosis

Elevated levels of apoptosis in the cardiac specific Myocardin knock out mouse model has been previously reported by our collaborators (49,51) As necrotic cell death was not assessed in this model, we recently reported Myocardin's role in protecting cardiomyocytes from PTP-dependent necrosis (ref). To further understand Myocardin's cell survival phenotype, we would extend our findings by analyzing the ratio of apoptosis and necrosis in loss of Myocardin experiments. Using flow cytometry, staining primary cardiomyocytes with Annexin-V (conjugated to APC) and propidium iodide (PI) would determine the percentage of apoptotic cells

(Annexin-V^+) and the percentage of necrotic cells (Annexin-V^+/PI^+). Based on our data, I predict loss of Myocardin function by shRNA knockdown (sh-Myocardin) will result in an increase in necrotic cells in comparison to scrambled control cells, that will be rescued by CsA treatment, a potent inhibitor of PTP-dependent necrosis. In contrast, cardiomyocytes expressing sh-Myocardin will not be protected by zVAD-fmk treatment, an inhibitor of caspase-dependent apoptosis.

To validate our cell culture findings *in vivo*, we would evaluate cardiac necrosis in an inducible Myocardin knock out model. Using tamoxifen-induced Cre-mediated deletion of Myocardin in adult mouse hearts and $Myocd^{F/F}$ as control (treated with vehicle injection), we would monitor cardiac necrotic serum markers such as lactate dehydrogenease (LDH) and cardiac troponin-I. Based on our findings on elevated levels of HMGB1 in Myocardin null embryos, we would also collect cardiac tissues for histological examination and measure HMGB1 expression by immunofluorescence. I predict tamoxifen-induced Myocardin knockdown will increase levels of cardiac necrotic serum markers and HMGB1 expression. Based on previous evidence of increased apoptosis with cardiac specific Myocardin deletion, apoptosis will also be monitored by TUNEL assays. I anticipate cardiac necrosis as the dominant form of cell death with loss of Myocardin function.

6.2. miR-mimics repress Nix in rodent infarction model

Locked nucleic acid delivery (LNA, Exiqon) of microRNA mimicking molecules is a new promising therapeutic strategy offering many advantages including low toxicity, high serum stability, and effective delivery/uptake in the heart (284,285). Therefore, to evaluate the genetic relationship between Myocardin, miR-133a and Nix *in vivo*, we would deliver miR133a-mimicking molecules to two adult rodent models of infarction or tamoxifen-induced Myocardin knock out. I will compare miR133a mimic LNA animals to control mimic-LNA animals at 4

weeks post-infarction. LNAs will be delivered by subcutaneous injections at 10mg/ml (dissolved in saline) for three consecutive days prior to infarction, while maintenance doses will be delivered weekly until end of the post-infarction timeline. In a similar manner, LNAs will be delivered for three consecutive days prior to tamoxifen treatment, while a "booster" injection will be delivered on the third day of tamoxifen treatment. In both rodent models receiving miR mimic LNAs, we would evaluate changes in Nix and HMBG1 expression, assess necrosis serum markers (LDH, cardiac troponin), measure mitochondrial respiration and monitor signs of cardiac dysfunction.

We have reported that expression of miR-133a inhibits Nix to promote cardiac cell survival. Based on such evidence, I predict miR-133a mimic LNAs will reduce cardiac Nix protein, reduce necrotic serum marks and improve cardiac function and cardiac performance in comparison to control mimic LNA treated animals. I also predict miR-133a mimic LNAs will improve survival rate following tamoxifen induced Myocardin knockdown. These future studies will help us understand this genetic relationship in vivo and its implication for miR-133a as a therapeutic strategy for ischemic heart disease and heart failure.

6.3. Genetic mouse models: cardiac-specific Myocardin transgenic mice with cardiac-specific Cyclophilin D /Nix knockout mice will be protected from heart failure

The evidence presented in this thesis outlines a genetic pathway linking Myocardin to activation of miR-133a that inhibits Nix expression, providing a molecular framework for my future studies in transgenic mice models. To validate the *in vivo* observations in the rodent infarction model, we would perform coronary ligation procedures in control and miR-133a transgenic mice and Nix knockout mice (231,256). I anticipate a decrease in cardiac necrosis when miR-133a expression is maintained or with the loss of Nix function. To clearly define Myocardin's

pro-survival phenotype and the impact on mitochondrial function, an inducible cardiac-specific Myocardin transgenic mouse model will have to generated.

Investigation into the role of Myocardin regulating the mitochondrial permeability transition pore will be further clarified by cross-breeding the tamoxifen inducible cardiac-specific Myocardin transgenic mouse model with Cyclophilin-D knockout mice, provided by Jackson labs. Based on the evidence provided in my thesis, I predict that the genetic deletion of Cyclophilin-D, the undisputed regulator of the MPT-pore, will have a cardioprotective effect and rescue heart failure when Myocardin deletion is induced by tamoxifen treatment. I also anticipate that this inducible Myocardin knockout mouse model will be protected when interbred with cardiac specific Nix-null mice (230).

6.4. Myocardin regulation by PKA is a SIK1 dependent mechanism

Recent studies implicate SIK1 as a HDAC repressor, mediating the nuclear export of HDAC4/5 in skeletal muscle that is inhibited by PKA phosphorylation (66,68). However, if SIK1 plays a similar function in cardiac muscle or prevent cardiac necrosis remains unknown; whether SIK1 mediates the nuclear export of HDAC5 to remove the molecular brake on Myocardin to promote cardiac gene expression has yet to be investigated. Based on my preliminary unpublished observations, I predict HDAC5 will suppress Myocardin activation of miR-133a expression, that will be reversed in the presence of SIK1. This will be confirmed with reciprocal loss-of-function studies: I predict the loss of SIK1 activity will decrease miR-133a expression, concurrent with elevated levels of cardiac necrosis. Based on our findings, I anticipate isoproterenol treatment and activation of β-adrenergic signalling, will increase phosphorylation of SIK1 that will be reversed by the PKA inhibitor H89 (10 μM). To determine if this pathway operates *in vivo* following myocardial infarction in a model of ischemic heart disease, we would evaluate SIK1 and HDAC5

phosphorylation throughout the animal model as previously described in this section. I predict that the decreased HDAC5 phosphorylation will correspond to decreased miR-133a expression, as dephosphorylated HDAC5 remains in the nucleus to repress target gene expression. Furthermore, to determine the role of SIK1 activity in preserving cardiac function following infarction, cardiac-specific SIK1 knockout mice will be generated and undergo coronary ligation experiments and be compared to control mice.

The pre-clinical studies proposed as my future directions will advance the understanding of a novel genetic pathway that regulates mitochondrial function in cardiac cells. The innovative studies using new technology and genetic animal models will extend the findings presented in this thesis, validate the Myocardin–genetic pathway and lay the molecular foundation for investigating regulated forms of cell death in the heart. My long-term goal is the development of a therapeutic strategy to preserve cardiac function during development and disease.

CHAPTER VII: Additional Data

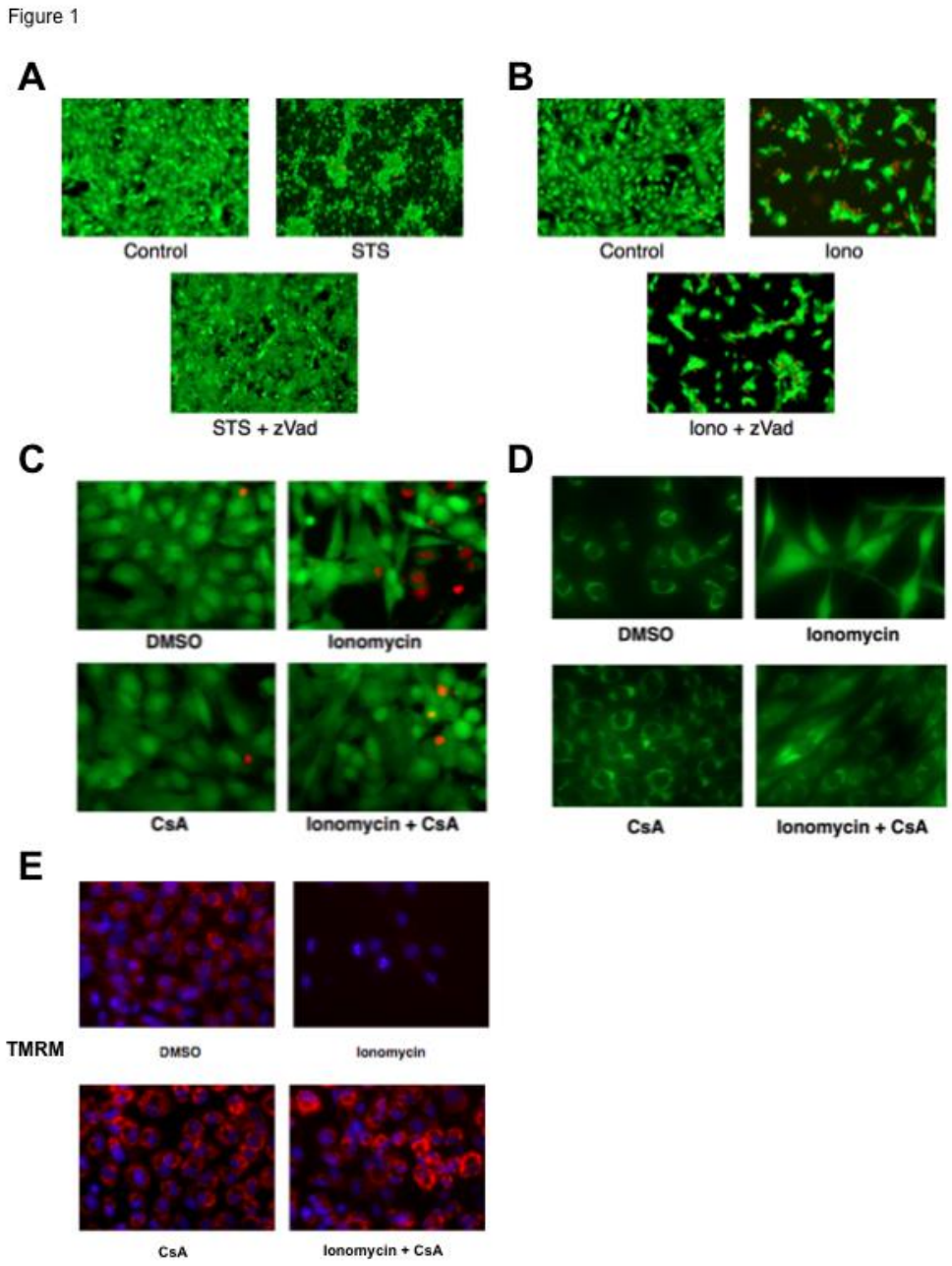

Additional Figure 1: Apoptotic and necrotic cell death assays
H9C2 cardiac myoctes were pre-treated with a caspase inhibitor (zVad, 50uM, 2 hours) following treatment with A) staurosporine (STS, 2uM, 18 hours) or B) ionomycin (Iono, 2uM, 18 hours); stained with cell viability fluorescent dyes (calcein-AM and Eth HD-1). H9C2 cardiac myoctes were pre-treated with cyclophilin D inhibitor (CsA, 1uM, 2 hours) following ionomycin treatment; cells were stained with C) cell viability fluorescent dyes, D) calcein-AM and cobalt chloride to measure PT-pore opening, or D) TMRM to measure mitochondrial membrane potential; DMSO was used as a control vehicle.

Figure 2

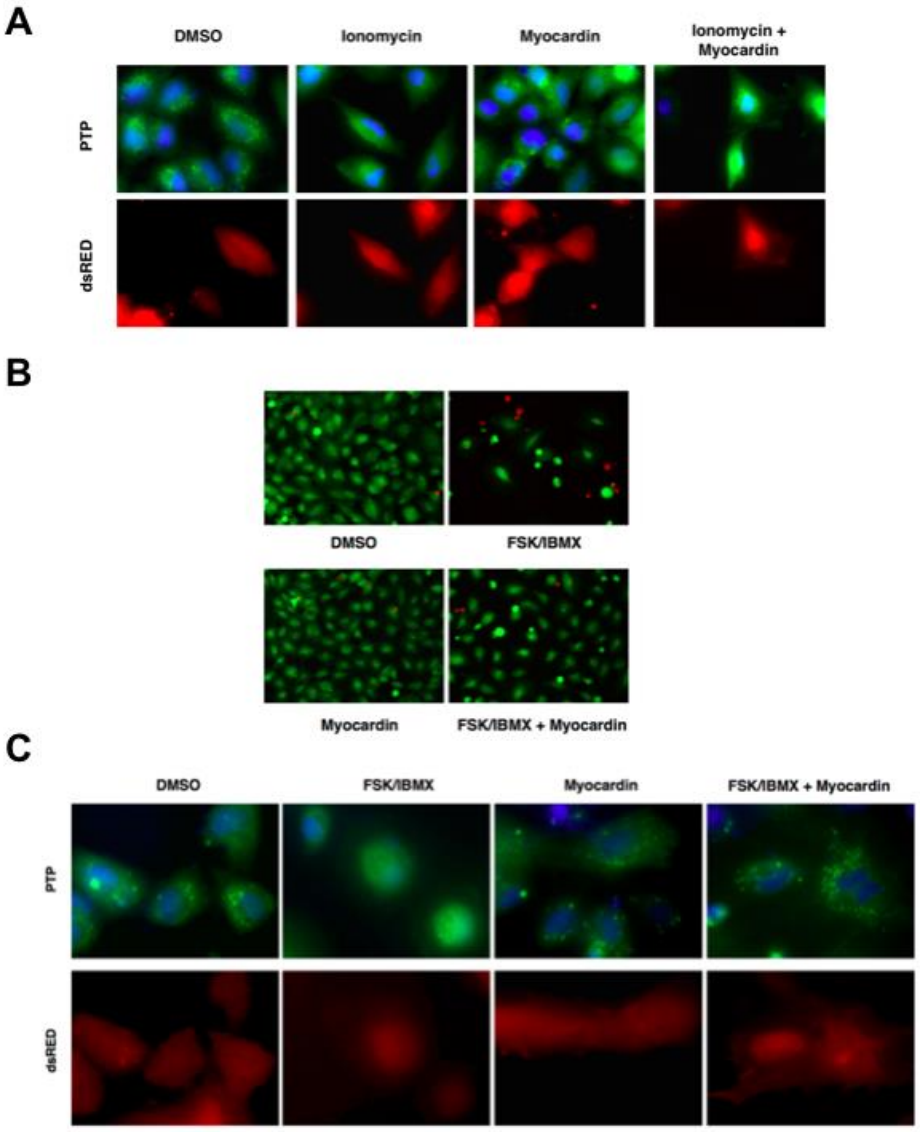

Additional Figure 2: Myocardin protects against induced mitochondrial PT-pore (PTP) opening and cardiac cell death

H9C2 cardiac myocytes were transfected with Myocardin or control expression vector, pcDNA3. Post transfection cells were treated with ionomycin (2uM, 18 hours) and stained with A) calcein-AM and cobalt chloride to measure MPT-pore opening, and B) cell viability fluorescent dyes; D) co-treated with FSK/IBMX and stained with calcein-AM and cobalt chloride to measure MPT-pore opening; DMSO was used as a control vehicle. Expression vector ds-RED was utilized for transfection efficiency for MTP-pore imaging.

Figure 3

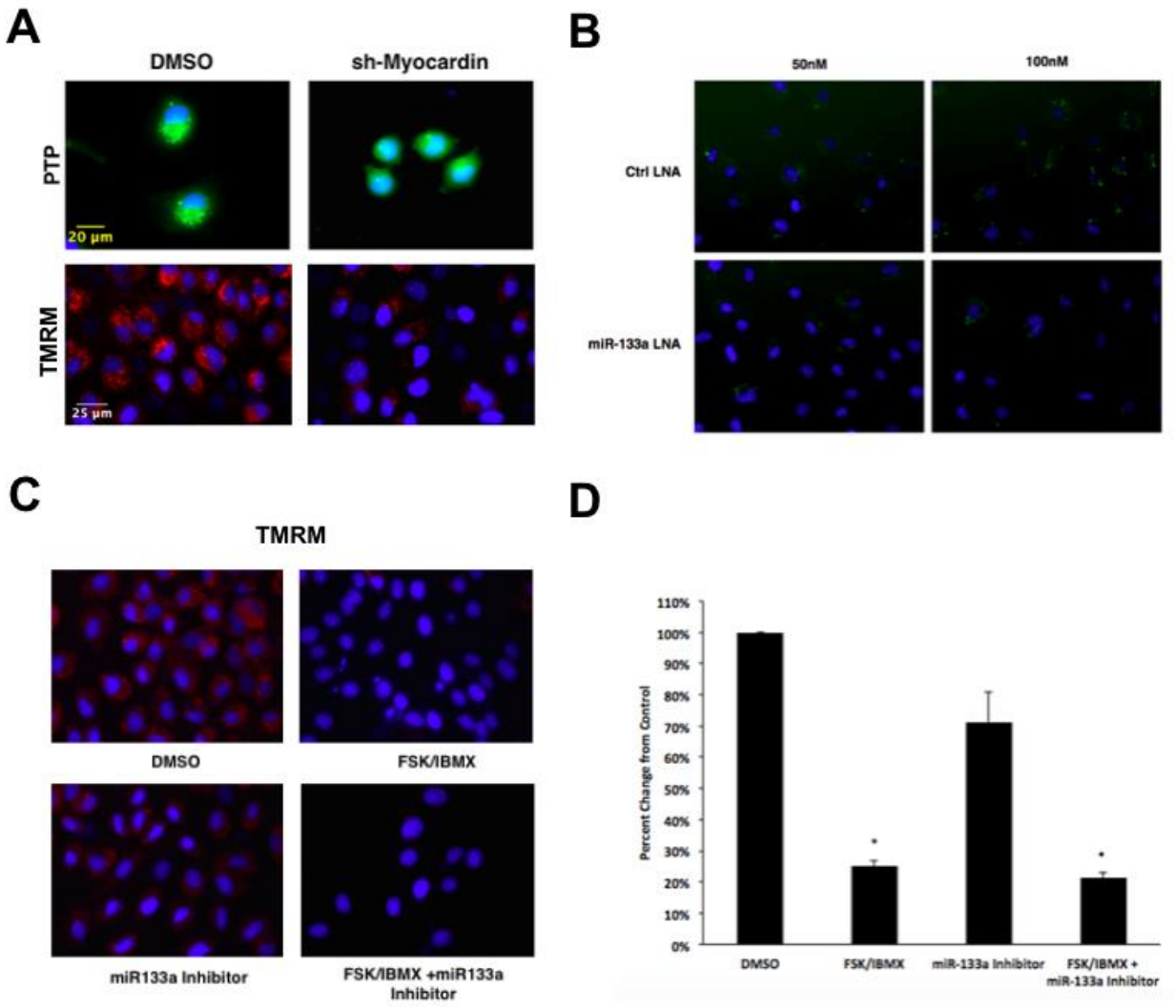

Additional Figure 3: Myocardin shRNA knockdown and miR-133a inhibitor studies.
A) Primary ventricular neonatal cardiomyocytes were infected with sh-Myocd or a scrambled lentivirus and stained with: calcein-AM and cobalt chloride to measure mitochondrial PTP opening, and TMRM to measure mitochondrial membrane potential. B) H9C2 cardiac myocytes were transfected with GFP-tagged miR-133a inhibitor locked nucleic acid (LNA; 50nM and 100nM) molecules and stained with nuclear dye Hoechst to determine optimal LNA dosage. C) H9C2 cardiac cells were transfected with miR-133a inhibitor (50nM), and treated with FSK/IBMX (18 hours), and stained with TMRM to measure mitochondrial membrane potential and nuclear stain Hoechst; D) TMRM fluorescent intensity percent change in relation to control treated cells quantified, DMSO was used as vehicle control. Data are expressed as mean +/- SE. * $p<0.05$ compared to control, determined by 1-way ANOVA.

Figure 4

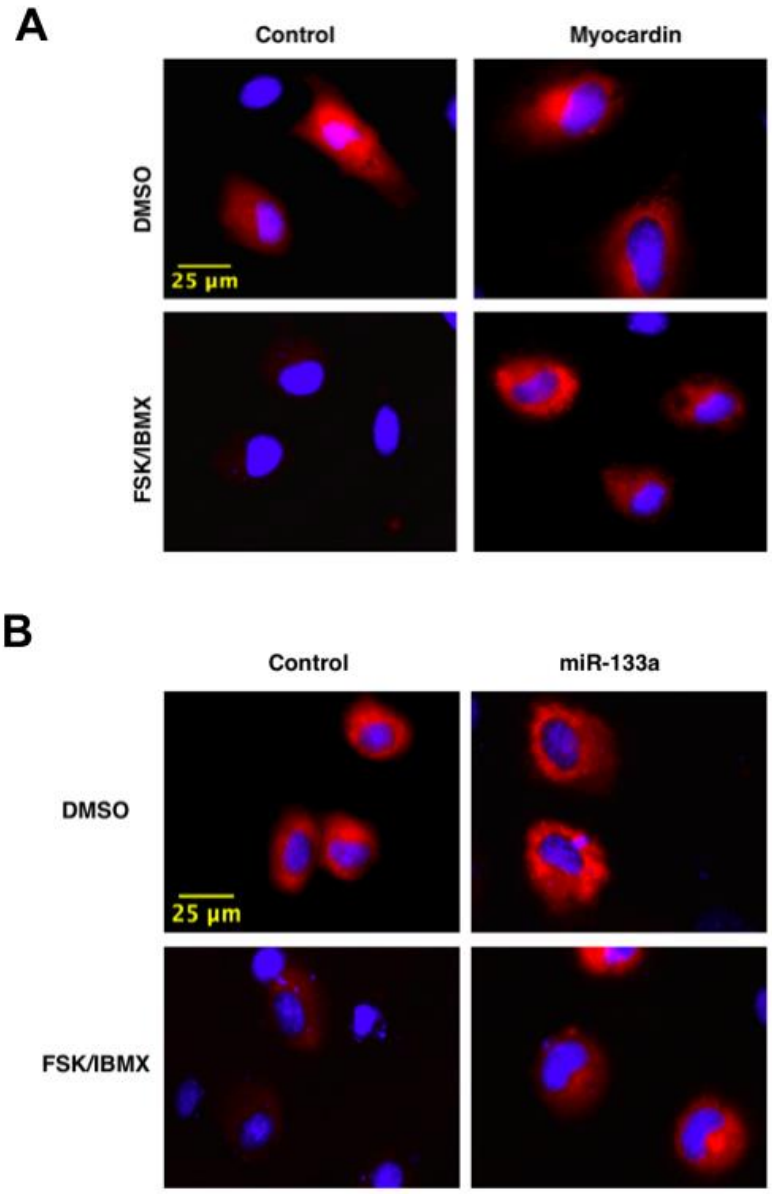

Additional Figure 4: Myocardin and miR-133a prevent forskolin (FSK)/IBMX induced ER-calcium release.
H9C2 cardiac myocytes were transfected with SR-targeted calcium biosensor, and with A) Myocardin or B) miR-133a; or an empty vector control and treated with FSK/IBMX (18 hours). Cells were stained with nuclear stain Hoechst and imaged.

Figure 5

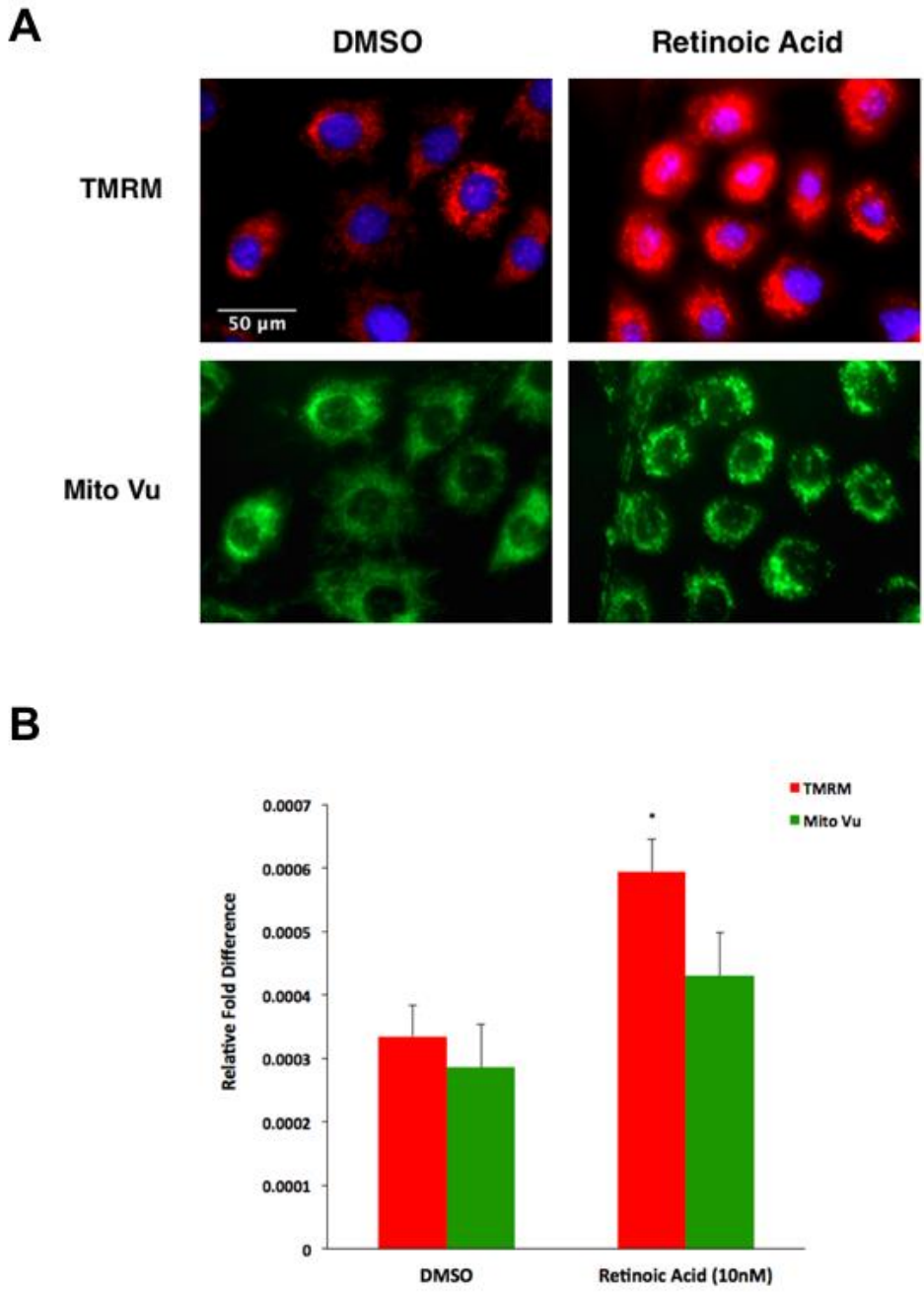

Additional Figure 5: Retinoic acid treatment hyperpolarizes mitochondria
A) H9C2 cardiac myocytes were treated with retinoic acid (10nM in 1% low serum/DMEM media) and stained with TMRM to measure mitochondrial membrane potential, Mito Vu to identify mitochondria, and nuclear stain Hoechst; (B) fluorescent intensity was quantified to determine relative fold difference between treatments, DMSO was used as vehicle control. Data are expressed as mean +/- SE. * $p<0.05$ compared to control, determined by 1-way ANOVA

Figure 6

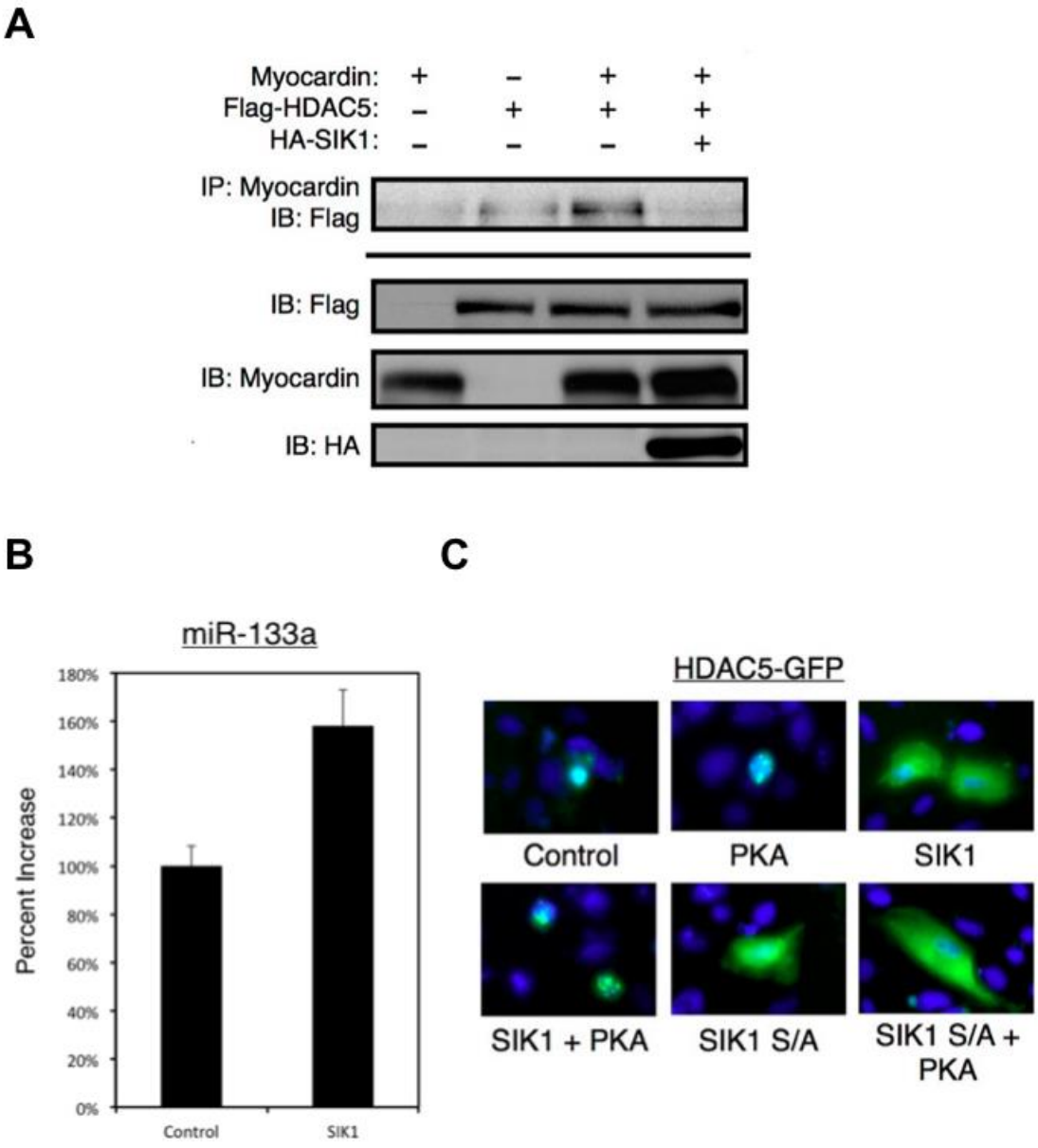

Additional Figure 6: Myocardin is regulated by HDAC5 and SIK1.
A) Human embryonic kidney (HEK) 293 cells were transfected with Myocardin, Flag-HDAC5 and HA-SIK1. Protein extracts were immunoprecipitated with an antibody targeting Myocardin. Immuno-complexes were subjected to SDS-PAGE and immunoblotted, as indicated. B) Cells were transfected with SIK1 or an empty vector control, as indicated. Total RNA was isolated by trizol method, and microRNAs were converted to cDNA with a reverse transcriptase kit from Quanta. miR-133a mRNA was detected by real-time PCR and graphed according to the ΔΔCT method; technical assistance was provided by Donald Chapman. C) H9C2 cardiac cells transfected with HDAC5-GFP, SIK1, and PKA, and SIK1 SA mutant; cells were visualized by standard epifluorescence techniques.

CHAPTER VIII: Extended Materials and Methods

8.1 Cell culture

Cell lines utilized in the aforementioned studies include rat cardiac cells H9c2, mouse skeletal muscle cells C2C12, human airway smooth muscle cells (hASMC), and diacylglycerol kinase-delta (DGKδ)-null mouse fibroblasts. The following are cell culture guidelines and recommendations by American Type Tissue Collection (ATCC) that were adhered to for all cell lines.

Reagents:

- Growth media: DMEM supplemented with Penicillin-Streptomycin (Gibco) and 10% fetal bovine serum (FBS; Hyclone); sterilized by passing through a 0.2um filter
- Freezing media: growth media with 10% DMSO
- Phosphate buffered saline (PBS; with Ca^{2+}/Mg^{2+})
- TrypLE Express dissociation solution (Gibco)

1. Passaging Cells

- Aspirate off existing media from established stock cultures and rinse the cell monolayer with 5 ml PBS; aspirate.
- Add 1 ml of TrypLE to 100mm culture dish of cells and incubate at 37C for 1-4 min. Tap plate to dissociate cells from plate. Collect cells with 5ml DMEM by pipetting the cells up and down 5-10 times, ensuring complete removal from plate and dissociation of clumps.
- Collect cell suspension volume in 15ml conical tube and pellet by centrifugation at 1100 x g for 4 min.

- Aspirate off media and agitate/tap bottom of tube to dislodge cellular pellet. Add 10 ml of media to resuspend cells and triturate cells up and down for a homogenous solution.
- Count cells using a haemocytometer (optional) and seed a dilution of cells according to desired tissue culture dish (100 mm, 6-well plate, 24-well plate), allowing for cell growth or for experimental procedure.
- If continuing cells for future passage, record cell line, passage #, date and initials on tissue culture 100 mm culture dish.

2. Freezing Cells

- Collect cells, centrifuge and tap to dislodge pellet as described above. After dislodging pellet, resuspend cells in freezing medium at a concentration of $1x10^6$ - $8x10^6$ cells/ml.
- Deliver 1 ml of cell suspension into labelled freezing vial (with cell type, passage, date, and initials)
- Wrap vials in a Kimwipe and place vials in a -80C freezer box or place in liquid nitrogen (long term storage)

3. Thawing Frozen Cells

- Remove frozen vial from -80C freezer or liquid-nitrogen storage and thaw in 37C water bath for 1-2 minutes in a microtube floater
- Using 1 ml warm growth media, collect cells using a Pasteur pipette and transfer to a 15 ml conical tube containing 5 ml of media: centrifuge 1100 x g for 4 minutes.
- Aspirate off media carefully and agitate tube with gentle tapping. Resuspend cells in 2 ml of growth medium.

8.2 Transfection of Mammalian Cells

For transient transfection, H9c2, C2C12 and hASMC cells were seeded at a 60-70% cell confluence and transfected with DNA using JetPRIME Polyplus reagent (1:2 ratio). Below are manufacturer's guidelines for transfecting cells seeded on 35 mm plates; reagents were scaled proportional to surface area for transfection of 100 mm plates.

Reagents:

- DMEM supplemented with Penicillin-Streptomycin (Gibco) and 10% fetal bovine serum (FBS; Hyclone); sterilized by passing through a 0.2um filter
- JetPRIME buffer
- JetPRIME reagent

1. JetPRIME Transfection

- Seed cells 24 hours prior to transfection so that they are 50-70% confluent at time of transfection.
- Add 0.2 ml of JetPRIME buffer to pre-labeled sterile microtube.
- Add 2ug DNA to JetPRIME buffer; vortex tube for 10 seconds and spin down
- Add 4 µl JetPRIME reagent to mixture; vortex for 10 seconds and spin down. Incubate mixture at room temperature for 10 minutes.
- During incubation, rinse cells with PBS and re-feed with complete growth media.
- Add transfection reagent and DNA mixture drop-wise to cells.
- Following 4 hours post transfection, wash cells with PBS and replace with fresh growth media.

H9c2 cells were also seeded at a 60-70% cell confluence and transfected with DNA using Qiagen's PolyFect reagent. Below are manufacturer's guidelines for transfecting cells seeded on 35 mm plates; reagents were scaled proportional to surface area for transfection of 100 mm plates.

Reagents:

- Serum free DMEM
- DMEM supplemented with Penicillin-Streptomycin (Gibco) and 10% fetal bovine serum (FBS; Hyclone); sterilized by passing through a 0.2um filter
- PolyFect reagent

2. PolyFect Transfection

- Seed cells 24 hours prior to transfection so that they are 60-70% confluent at time of transfection ($4x10^5$ cells/well on a 6-well plate)
- Add 100 ul serum free media to pre-labeled 5 ml polystyrene tubes.
- Add 1.5ug DNA to each tube.
- Add 12ul of PolyFect reagent; pipette to mix. Incubate mixture at room temperature for 10 minutes.
- During incubation, rinse cells with PBS and re-feed with complete growth media.
- Add transfection reagent and DNA mixture drop-wise to cells.
- Following 24 hours post transfection, wash cells with PBS and replace with fresh growth media.

8.3 Isolation of primary neonatal ventricular cardiomyocytes

Primary neonatal ventricular cardiomyocytes (PNVM) were isolated from rat pups using the Pierce Primary Cardiomyocyte Isolation Kit (#88281, Thermo Scientific). All tissue and reagents remained on ice unless stated otherwise, as per manufacturer's protocol.

Reagents:

- Growth media: Primary Cell Isolation DMEM media with 10% FBS and Penicillin-Streptomycin (Gibco)
- Hank's balanced salt solution (HBSS; without Ca^{2+}/Mg^{2+})
- Cardiomyocyte isolation enzyme 1 (with papain)
- Cardiomyocyte isolation enzyme 2 (with thermolysin)
- Cardiomyocyte growth supplement (1000x)

a) Harvesting neonatal hearts

- Anesthetize two-day old Sprague-Dawley neonatal rat pups were with isoflurane and sacrifice by cervical dislocation.
- Collect hearts in ice-cold HBSS: remove atria and aortic tissue. Place each heart in in microtube containing 0.5 ml cold HBSS.

b) Enzymatic digestion

- Using fine scissors, mince heart tissue into 1 – 3 mm^3 pieces directly in microtube. Wash twice with 0.5 ml HBSS to remove any additional blood.
- Tissue is enzymatically digested using 0.2 ml cardiomyocyte isolation enzyme I and 10 ul of enzyme II in 37C water bath for 30 minutes.
- Wash tissue twice with 0.5 ml cold HBSS to inactivate the enzymatic solution.
- Remove HBSS and add 0.5 ml warm growth media to digested tissue
- Break up tissue and triturate 20-30 times with a 1000ul pipette to achieve single cell suspension
- Add 1.0 ml growth media to each tube for a final volume of 1.5 ml per tube, mix gently to avoid damaging cells.

c) Cell viability determination

- Combine individual cell suspensions in microtubes into a 15 ml conical tube to determine cell yield: mix 25ul µl of cell suspension with 25 µl trypan blue in a fresh 1.5 ml tube.
- Transfer 10 µl of trypan-stained cells into haemocytometer and count the total number of cells and the number of trypan-stained cells to determine cellular viability.
- Seed cells for a density 5.0 x 10^5 cells/well in a 16 mm well of 24-well plate (Primaria treated tissue plate, Corning) and incubate at 37C at 5% CO_2.
- Replace growth medium after 24 hours and supplement with Cardiomyocyte growth supplement (1:1000 dilution in media).

8.4 Viral transduction of primary cardiomyocytes

The volume of lentivirus for transduction of 1 well (of 24-well plate) was determined empirically.

Reagents:

- Packaged lentiviral particles (suspended in cell growth medium)
- Control lentiviral particles (Santa Cruz)
- Polybrene (Santa Cruz)
- Growth media: DMEM media with 10% FBS and Penicillin-Streptomycin (Gibco)

<u>1. Lentivirus transduction</u>

- Add polybrene at 1:1000 dilution to tube with 1 ml growth medium
- Add 10 µl viral particles; mix virus-polybrene solution by pipetting up and down
- Aspirate medium from cells and rinse with PBS.
- Add virus-polybrene media solution drop-wise to cells and incubate for 16 -18 hour.
- Remove medium, rinse with PBS and re-feed cells with growth media.

8.5 Protein extraction

Keep protein samples cold at all times (unless otherwise directed). Whole cell extracts were prepared as follows:

Reagents:

- Cold PBS
- Cold PBS^+ (1 mM sodium vanadate, 1 mM PMSF, Protease inhibitor cocktail (Sigma, P-8340)
- $RIPA^+$ Lysis buffer (1 mM Sodium vanadate, 1 mM PMSF, Protease inhibitor cocktail (Sigma, P-8340)
- 2X SDS sample buffer (Biorad).
- β-mercaptoethanol (Sigma)

1. Protein extracts from adherent cells

- Aspirate media from cultured cells, wash twice with PBS. Place culture places on ice.
- Add 1.0 ml PBS^+ and gently scrape cells with cell scrapper. Collect into pre-chilled and pre-labeled microtubse. Centrifuge cells at 1500 x g for 3 min.
- Remove supernatant and approximate the cell pellet volume; dilute with five times that volume in $RIPA^+$ lysis buffer.
- Vortex cells briefly every 10 min for 30 – 60 minutes.
- Centrifuge cell lysate at high speed at 4C (>10 000xg). Transfer supernatant to newly labeled microtubes. These are stock protein extracts that will be used for long term storage in -80C freezer.
- Determine protein concentration using Bradford assay. Dilute protein samples with 2x SDS sample buffer and 5% β-mercaptoethanol

- Boil samples for 5 minutes. Chill on ice for additional five minutes and then spin down. Store at – 20C for short-term storage or until ready to run on a protein gel.

For isolating protein extracts from animals, use tissue crushing and homogenization procedure. Must use liquid nitrogen and dry ice for this protocol. Always wear freezer gloves and you can perform this procedure at the lab bench.

Reagents:

- Liquid nitrogen (in 2 doers; may fill up midway through procedure)
- Dry ice (for short-term tissue storage; comparable to storing at -80C)
- Two pairs of freezer gloves
- Tissue pulverizer (pre-chilled) + hammer
- Polytron tissue homogenizer
- Scoopula and long tongs (pre-chilled: throw into 1 liquid tank doer)
- Pre-labelled 5 ml polypropylene stubs
- RIPA Lysis buffer

<u>2. Protein extracts from animal tissue (hearts)</u>

- Prep RIPA Lysis Buffer with 20ul PI components/mL.
    - 12 hearts = 8 mL
    - 4 hearts = 4-5 mL
    - want extra as back up
    - approx 600 ul/heart
- Label 5ml PP tubes:
    - time point (ie 4 week) — animal # — condition (Sham vs Infarct/Viable)

- Add 250uL RIPA/tube (keep on ice)

- Collect N2 from cold room. Obtain animal tissue samples from -80C and keep in N2 doer to ensure it is frozen. Throw in scoopula and large tongs. Also throw in folded weigh paper if you will use it.
- Thoroughly clean the Pulverizer using 70% EtOH using Kim Wipes
    - carefully with freezer gloves, lower/raise pulverizer using the handles into N2 doer
    - pre-chill for 5 minutes
    - using the handle arms with freezer gloves, place frozen pulverizer onto paper towel (working surface)
- **With gloves and using the forceps, pick up a frozen tissue vial from N2 doer onto the centre of pulverizer**
    - push down the centre piece on top
    - using the arms, carefully lower the pulverizer onto the floor (with glove beneath it)
    - hammer down on pulverizer 3-6x — twist the top back and forth to grind tissue as finely as possible into a powder — hammer down again 3-6x.
    - want to grind tissue as much as possible to facilitate the homogenization process
    - using arms, carefully place the pulverizer back onto bench.
    - Repeat if necessary
- Use the pre-chilled scoopula, carefully collect the fine tissue powder into the appropriate pre-labelled 5mL tube (with RIPA). Scrape as much tissue as possible including surface edges.

    - Can also collect the fine powder onto a folded weigh paper for easier transfer into PP tube (it has a small diameter).
- Add another cold 250uL RIPA to tube (on top of tissue so it's sandwiched) - keep on ice. Can use pipette tip to scrape sides of the tube
- Clean Up:
    - Wipe down Scoopula - place in N2 doer
    - Clean the pulverizer: scrape off excess tissue with 70% EtOH - get in between edges etc.
- Using the arms with freezer gloves, carefully raise the pulverizer into N2 doer and pre-chill for 5 minutes
- Obtain a new tissue samples from N2 doer

8.6 Homogenize animal tissue in RIPA lysis buffer

- Wash thoroughly at medium (speed 4) to high (speed 6-7) for 20-sec. (Have a waste beaker nearby)
    - 5mL tube of "dirty" H2O
    - 5mL tube of 70% EtOH
    - 5mL tube of "clean" H2O(ensure it is clear).
    - Repeat this cleaning proess if any tissue fragments are found.
    - Wipe the probe with a paper towel
- Homogenize tissue:
    - at speed 4 for 20s
    - keep tubes on ice
    - clean probes inbetween samples as described above

- Vortex homogenize/lysed tissue samples every 10 min (total 30 min) to ensure a thorough lysis (on ice at all times).
    - Label fresh microtubes (1 set for tissue extracts that will contain the pellet; 2nd set for protein extracts).
- Collect tissue extracts in tube set 1:
    - spin at 13,000 rpm - 5 min in fridge (Halayko lab) - pellet cellular debris
- Collect protein extracts (supernatant; do not disturb pellet) in labelled tube set 2.
    - Store in -80C and run protein assay.
    - May want to dilute samples with 100-300ul RIPA (base it on the pellet) to have an average protein [ ] within the range of 3-6 ug/ul. May or may not need to dilute samples.

Additional Notes:

- Do not let tissue thaw, especially if isolating for RNA analysis. May want to homogenize in cold room if using for RNA purposes
- Carefully pick up and lower pulverizer with arms - use caution when using a glass-coated N2 doer.
- Always clean equipment in between samples with H2O and EtOH
- When wiping pulverizer, scrape off excess tissue and then wipe off. Then spray towel with 70% EtOH to wipe off. If you use too much EtOH, it'll get gummy, but just scrape off.

Mitochondrial and cytoplasmic extracts were made using the Q-proteome mitochondrial and cytoplasmic extraction kit (Qiagen). Thaw reagents at least two hours prior to extraction procedure

but keep on ice; add protease inhibitors to lysis buffer and disruption buffer, as described by manufacturer's procedure.

Reagents:

- PBS^+ (described in whole cell lysate section)
- Lysis Buffer
- Disruption Buffer
- Mitochondrial Purification buffer
- Mitochondrial Storage buffer
- Protease inhibitor solution (100x)
- Pre-label microtubes: whole cell, cytosolic, nuclear, mitochondrial, ER

3. Mitochondrial fractionation protein extracts (Q-proteome high purity-mitochondrial isolation kit, Qiagen)

- Aspirate off media. Wash cells and collect in 1ml PBS^+ by gentle scrapping. Pellet cells by centrifugation at 1000 x g for 10 min at 4C.
- Optional: if whole cell protein lysates are needed, remove supernatant, resuspend pellet in PBS+ and aliquot a portion into a separate pre-labeled tube (whole cell protein extract). Re-centrifuge remaining cells at 1000 x g for 10 min at 4C.
- Remove supernatant and resuspend pellet in 1.0 ml of lysis buffer by pipetting up and down. Incubate for 10 min at 4C on end-over-end shaker. Centrifuge at 1000x g for 10 min at 4C.
- Pipette supernatant into new tube (cytosolic extract); place on ice. Resuspend pellet in 1.5 ml disruption buffer.

- Using a blunt-ended needle and syringe, disrupt remaining cell contents by passing lysate through the needle 10 – 20 times using vigorous force. Centrifuge lysate 1000x g for 10 min at 4C.
- Transfer supernatant into new tube. Pellet contains nuclei, cell debris, and unbroken cells (nuclear extract); store pellet at 4C.
- Centrifuge supernatant at 6000 x g for 10 min at 4C. Transfer supernatant into new tube (ER or microsomal extract) and store at 4C. Pellet contains mitochondria.
- Resuspend pellet in 750 ul of Mitochondrial Purification buffer by carefully triturating with a 1 ml pipette tip, creating a mitochondrial suspension.
- In a new 2 ml microcentrifuge tube, pipette fresh 750 ul Mitochondrial Purification buffer. In same 2 ml tube, slowly pipette 500 ul Disruption buffer into the bottom of the tube, so it is under the Mitochondrial Purification buffer.
- Carefully pipette the mitochondrial suspension and deliver on top of the Mitochondrial Purification buffer. Due to solution viscosity, the Disruption and Mitochondria Purification buffer do not readily mix, thus creating three layers, in which the mitochondrial suspension layer is on top.
- Centrifuge at 14,000 x g for 15 min at 4C.
- Carefully remove 1.2 ml of supernatant without disturbing mitochondrial pellet/band at bottom. Save supernatant of mitochondrial crude extract for further analysis.
- Carefully remove the mitochondrial pellet (~0.5 ml) by pipetting from the bottom of the tube, and transfer to fresh 2 ml microcentrifuge tube.

- Dilute this clear mitochondrial pellet in 1.5 ml Mitochondrial Storage buffer. Centrifuge at 8000 x g for 10 min at 4C. Repeat until you can visualize a pellet at bottom of the tube. (centrifuge around 2-3 times).
- Based on pellet size, resuspend pellet in same weight:volume ratio of Mitochondrial storage buffer. If pellet is around 100 ul in size, add 100 ul buffer. Store all extracts for immediate (4C) or long term analysis (-80C freezer).
- Determine protein concentration by Bradford assay and analyze samples on protein gel.

Nuclear and cytoplasmic protein extracts were made using the NE-PER Kit (Pierce). Add protease inhibitors as described in protein extract section to solutions CER I, CER II, and NER. Keep all reagents on ice unless stated otherwise as per manufacturer's procedure.

Reagents:

- PBS
- CER I ,CER II and NER
- Lysis Buffer
- Disruption Buffer

<u>4. Nuclear and cytoplasmic fractionation protein Extracts (NE-PER Kit)</u>

- Aspirate media and wash with PBS. Gently scrape cells into pre-labeled microtube; pellet by centrifugation at 1500 x g for 5 min at 4C.
- Remove supernatant and add 200 ul ice-cold CER I to cell pellet. Vortex microtube to break apart pellet for 15 sec and then incubate for 10 min on ice.
- Add 11 µl cold CER II; vortex microtube for 5 sec on the highest setting and then incubate for 1 min on ice. Vortex tube for 5 seconds and then centrifuge at 13000 x g for 5 min at

4C.

- Immediately transfer the supernatant (cytoplasmic extract) fraction to a clean pre-chilled tube. Place this tube on ice until use or storage.
- Resuspend the insoluble pellet fraction in 100 µl of ice-cold NER. Vortex on the highest setting for 15 seconds every 10 min for 40 min. Centrifuge the tube at 13000 x g for 10 min at 4C.
- Transfer supernatant (nuclear extract) fraction to a clean pre-chilled tube. Place this tube on ice until use or storage.
- Determine protein concentration by Bradford assay and analyze samples on protein gel.

8.7 Co-Immunoprecipitation

- Prepare cell lysates as described in protein extracts section.
- Dilute protein extract 1:10 in lysis buffer.
- To 1 ml of cell lysate (250-1000µg total protein) add 1-5 µg of primary antibody and nutate at 4C for 1 hour.
- Add 30-50 µl of Protein G-Agarose beads (Santa Cruz) to immunoprecipitation (IP) reaction; nutate 4-16 hours at 4C.
- Pellet IP reaction by centrifugation at 1000 x g for 30 seconds. Wash pellet with 1 ml of lysis buffer.
- Repeat steps 5 and 6 two more times.
- Resuspend pellet in 40 µl of 2x SDS sample buffer; boil for 5 min.
- Transfer supernatant to new tube. Analyze sample by SDS-PAGE and Western immunoblot analysis.

8.8 Sodium dodecyl sulfate polyacrylamide gel electrophoresis (SDS-PAGE)

Whole cell or fractionation protein extracts were analyzed by SDS-PAGE. The polyacrylamide gels were prepared as followed:

Reagents (for one gel):

- 10% Resolving gel (15ml)
  - ddH_2O 5.9 ml
  - 1.5M Tris (pH 8.8) 3.8 ml
  - 30% acrylamide mix 5 ml
  - 10% SDS 0.15 ml
  - 10% APS 0.15 ml
  - TEMED .006 ml
- Stacking gel (4ml)
  - ddH_2O 2.7 ml
  - 1.5 M Tris pH (6.8) 0.5 ml
  - 30% acrylamide mix 0.67 ml
  - 10% SDS 0.04 ml
  - 10% APS 0.04 ml
  - TEMED 0.004 ml
- 5x Running buffer (1 L):
  - 15.1 g Tris
  - 12.0 g Glycine
  - 5.0 g SDS
  - 1 L ddH_2O

1. PAGE

- Prepare 1.5 mm resolving gel and stacking gel with appropriate comb inserted in BioRad mini-gel apparatus.
- Fill BioRad mini-gel apparatus with 1x Running buffer.
- Load protein samples on gel and run gel at 80 volts.

8.9 Western immunoblot

For detecting total protein, protein extracts run on SDS-PAGE were subjected to Western immunoblot analysis. Prepare polyvinylidene difluoride (PVDF) membrane, blocking buffer, washing solutions, enhanced chemiluminescence (ECL), and antibody diluent as per manufacturer's instruction.

Reagents:

- 5x TBST (2 L)
  - 73.1 g NaCl
  - 31.0 g Tris
  - 10.0 ml Tween-20
  - Adjust pH to 8.0 before adding Tween-20
- 10x CAPS (1 L)
  - 17.71 g CAPS
  - 2.40 NaOH
- Transfer buffer (1 L)
  - Methanol 100 ml
  - 10x CAPS 100 ml
  - ddH_2O 800 ml

- Blocking buffer (5% (w/v) skim milk powder in TBST)
- Primary antibody solution (5% bovine serum albumin in TBST, Sigma)
- Secondary antibody solution (1-5% (w/v) skim milk powder in TBST or 5% bovine serum albumin in TBST, Sigma)
- Ponceau-S solution (Sigma)
- ECL (Pierce)

1. Immunoblot

- Following SDS-PAGE, transfer protein to PVDF membrane by wet transfer: 20 volts for 16-20 hours at room temperature.
- Add 20 ml Ponceau-S stain to visualize protein bands on membrane. Wash with 1x TBST (3 X 5 min) to remove stain.
- Apply blocking buffer to membrane; incubate for 1-2 hours at room temperature.
- Incubate membrane with primary antibody diluted 1:100-1:10 000 in solution overnight at 4C.
- Wash membrane with 1x TBST (4 X 15 min).
- Incubate membrane with secondary antibody 1:1000-1:100 000 in solution for 1 hour at room temperature.
- Wash membrane with 1x TBST (4 X 15 min).
- Develop membrane (immunoblot) with ECL, expose blot to film, and develop.

8.10 Immunofluorescence

Reagents:

- PBS
- Fixing buffer (4% Paraformaldehyde in PBS)

- Blocking buffer (5% serum in 3% Triton-X in PBS)
- Serum (matching species that secondary antibody was raised in)
- Antibody buffer (1% BSA in 3% Triton-X in PBS)
- Fluorophore-conjugated secondary antibody (light sensitive)
- Hoechst 33342 fluorescent dye (Biotium)
- Fluorosave

1. Fixing cells

- Following experimental procedure of cells seeded in a 24-well plate, wash cells twice with PBS
- Add 0.5 ml warm fixing buffer per well for 15 minutes at room temperature.
- Aspirate and wash cells 3 times with PBS (5 min each wash).

2. Immunostaining

- Add 0.5 ml blocking buffer (contains 5% serum) per well and incubate for 1 hour at room temperature.
- Incubate cells with primary antibody diluted (1:50 – 1:1000) in antibody buffer for 16-20 hours at 4C.
- Wash cells 3 times with PBS (5 min each wash).
- Incubate cells with fluorophores-conjugated secondary antibody diluted (1:50 – 1:1000) in antiody buffer; directed against IgG from species the primary antibody was raised in. Incubate in dark for 1-2 hours at room temperature. Wash cells 3 times with PBS (5 min each wash).

3. Counterstain (Hoechst)

- Dilute Hoechst (1:2000) in PBS and incubate for 20 minutes at room temperature.

- Wash cells 3 times with PBS (5 min each wash).
- Aspirate carefully. Leave cells in PBS and image. If necessary, add 1-2 drops of fluorosave and sterile glass coverslip; use suction to remove bubbles. Let it dry for 2-3 hours at room temperature and store at 4C in dark until ready to image.

8.11 Cell viability assay

Colorimetric assay used to determine cell viability or cytotoxicity by measuring reduction of MTT (3-(4,5-Dimethylthiazol-2-yl)-2,5-diphenyltetrazolium bromide) reagent.

Reagents:

- Growth media: DMEM with 10% FBS and Penicillin-Streptomycin
- MTT reagent (Biotium)
- DMSO (non-sterile, Sigma)

<u>1. MTT Assay</u>

- Aspirate media from cells seeded on a 96-well plate. Replace with 100 ul fresh growth media per well.
- Add in 10 ul DMSO and mix gently with pipette tip. Incubate 96-well plate in the dark for 2 hours at 37C.
- Aspirate media. Add 50 ul DMSO per well. Incubate 96-well plate in the dark for 10 minutes at 37C.
- Measure optical density at 540 nm wavelength with a spectrophotometer and record absorbance values.

8.12 Live Cell Fluorescent Imaging

Cells were stained with fluorescent dyes as per manufacturer's guidelines and recommendations. Images were captured using an Olympus IX70 inverted microscope equipped with Q-Imaging Retiga SRV Fast 1394 camera and NIS Elements AR 3.0 software. Image J software was used for processing images including fluorescent quantification, scale bars and background subtraction. The following are steps are general procedures adhered to for all cell lines.

Reagents

- Growth media: DMEM with 10% FBS and Penicillin-Streptomycin
- Calcein-AM (Biotium)
- Ethidium homodimer-1 (Biotium)
- Hoechst 33342 (Biotium)
- MitoTracker Red CMXRos (Cell Signaling Technology)
- Tetramethylrhodamine-methylester (TMRM; Biotium)
- MitoSox Red (Life Technologies)
- Cobalt chloride ($CoCl_2$)

Staining Cells:

- Dilute fluorescent dye in appropriate amount of growth media and apply to cells. Incubate in the dark at 37C for 30 minutes (unless stated otherwise); replace with fresh growth media and image live cells.

<u>1. Cell viability (Calcein-AM + ethidium homodimer-1)</u>

- Apply 2 uM calcein-AM (1:500 dilution of 1 mM stock) with 2 uM ethidium-homodimer-1 (1:1000 dilution of 1 mM stock). Calcein-AM stains viable cells green while ethidium homodimer-1 stains membrane ruptured cells red, or cells exhibiting necrosis. Ethidium

homodimer-1 positive cells in comparison to calcein-AM determine percentage of necrosis.

2. Counterstains

- Nuclear stain: apply 8 uM Hoechst (1:2000 dilution of 16 mM stock)
- Mitochondrial stain: apply 50 nM of MitoTracker Red CMXRos (1:2000 dilution of 100 uM stock)

3. Mitochondrial membrane potential

- Apply 100 nM TMRM (1:1000 dilution of 100 uM stock) with 8 uM Hoechst. The change in integrated fluorescent intensity of TMRM is an index of mitochondrial membrane potential.

4. Mitochondrial permeability transition pore assay

- Apply 2 uM calcein-AM (1:500 dilution of 1 mM stock) with 5 mM $CoCl_2$ (1:500 dilution of 500 mM stock) with 8 uM Hoechst. Calcein-AM will stain viable cells green and in the presence of $CoCl_2$, this signal is quenched, resulting in green fluorescent punctate cells. The change in integrated fluorescent intensity or loss of puncta is an index of permeability transition pore opening.

5. Mitochondrial oxidative stress (MitoSox)

- Apply 5 uM MitoSox Red (1:1000 dilution of 5 mM stock) in warm growth media and incubate cells in the dark at 37C for 10 minutes. Wash cells 3 times with warm PBS. Apply Hoechst counterstain, as indicated above. The change in integrated fluorescent intensity of MitoSox is an index of mitochondrial oxidative stress.

8.13 Mitochondrial Respiration

An XF Cell Mitochondria (Mito) Stress Assay on was used to determine mitochondrial respiration on a Seahorse XF24 Extracellular Flux Analyzer (Seahorse Biosciences) in differentiated H9c2 cells or isolated primary ventricular neonatal cardiomyocytes (PVNM). Cells are seeded in a specialized XF24 microplate that analyzes oxygen consumption rate (OCR).

Reagents:

- XF24 Flux Pack Mini (Seahorse Bioscience #100867-100)
  - Cartridge lid
  - Sensor cartridge
  - Hydrobooster
  - Utility Plate
  - XF Calibrant solution
  - Cell Culture Microplates
- 1% Fibronectin (in 0.02% sterile gelatin; Sigma #F1141)
- XF Assay Media (modified DMEM with no glucose; Seahorse Bioscience #102365-100)
- Glucose (Sigma #G7021)
- Sodium Pyruvate (100 mM liquid, Life Technologies #11360-070)
- Mito Stress inhibitors (1 mM stock; Sigma)
  - FCCP (#C2920)
  - Oligomycin (#O4876)
  - Antimycin A (A8674)
  - Rotenone (R8875)

XF24 Mito Stress Assay and Analyzer Procedure

1. Seeding cells on XF24 Microplates

- Deliver 100 ul cell suspension twice: the two-step delivery method allows for uniform cell density; cell suspension delivery in one step is not recommended.
- H9c2: seed cells at a density of 100,000 cells/well. Leave one well in each row as a background control with no cells. Perform experiment.
- PVNM: Day before isolating primary cardiomyocytes, coat each well (including background wells) with 100 ul of 1% Fibronectin; incubate overnight at 37C. Day of PVNM isolation, aspirate Fibronectin solution and seed 100,000 cells/well. Perform experiment.

2. Hydrate Cartridge

- Prior to respiration assay, add 1 mL of XF24 Calibrant solution to each well in the Sensor cartridge; incubate overnight in a non-CO_2 incubator at 37C.

3. Mito Stress Assay: XF Media

- Prepare fresh media day of analysis
- Measure 100 mL of XF Media and add 1 mL of sodium pyruvate (1 mM final concentration) and 0.45 g glucose (25 mM final concentration).
- Set pH to 7.4; sterilize and keep at 37C

4. XF Media change

- Aspirate media off of cells (H9c2 or PVNM) and replace with 550 ul of XF Media per well (including empty background wells).
- Incubate cells in a non-CO_2 incubator at 37C for 1 hour.

5. Mito Stress Inhibitors

- Prepare while cells are in non-CO_2 incubator
- Label 3 x 15 ml falcon tubes A, B, C, and dilute inhibitors (1:100 dilution of 1mM stock) in XF Media; keep warm at 37C:

- A = Oligomycin: 40 ul of stock + 3960 ul XF Media
- B = FCCP: 40 ul of stock + 3960 ul XF Media
- C = R/A 40 ul of Rotenone stock + 40 ul Antimycin A stock + 3920 ul XF Media.

- Carefully pipette (as indicated) diluted inhibitor solution into appropriate drug ports in sensor cartridge:
  - First injection Port A = 55 ul Oligomycin
    - After establishing basal respiration, Oligomycin A inhibits ATP synthase, thus reducing ATP synthesis that is linked to a reduction in oxygen consumption rate.
  - Second injection Port B = 61 ul FCCP
    - FCCP uncouples respiration from ATP synthesis, thus causing an increase in OCR, reflecting maximal respiration.
  - Third injection Port C = 68 ul R/A
    - Combination of Rotenone (complex I inhibitor) and Antimycin A (complex III inhibitor) block the electron transport chain, thus decreasing OCR at cytochrome c oxidase. The remaining OCR is due to non-mitochondrial respiration.
  - Port D = empty
- When inhibitors are injected into wells during Mito Stress assay, the final concentration of each inhibitor is 1 uM.
- If sensor cartridge cools down, allow it to warm up in non-CO_2 incubator at 37C prior to calibrating the XF24 Flux Analyzer machine.

6. Calibration
   - Load XF Mito Stress template onto XF24 software: set established assay with optimal mix, wait and measure cycles. Select experimental conditions and set background control wells.
   - Once warm, load both sensor cartridge and utility plate on the right side of the tray, in the correct orientation without a lid, into the XF24 Flux Analyzer.
   - Follow software prompts and start calibration (~25 minutes)
7. Run Mito Stress protocol
   - After calibration, remove utility plate and replace with pre-incubated cell plate from non-CO_2 incubator.
   - Run XF Mito Stress protocol (~120 minutes).
   - Save experimental results and analyze respiration.

CHAPTER IX: References

1. Gilboa, S. M., Devine, O. J., Kucik, J. E., Oster, M. E., Riehle-Colarusso, T., Nembhard, W. N., Xu, P., Correa, A., Jenkins, K., and Marelli, A. J. (2016) Congenital Heart Defects in the United StatesClinical Perspective. *Circulation* **134**, 101-109
2. Marelli, A. J., Ionescu-Ittu, R., Mackie, A. S., Guo, L., Dendukuri, N., and Kaouache, M. (2014) Lifetime Prevalence of Congenital Heart Disease in the General Population From 2000 to 2010. *Circulation* **130**, 749-756
3. Vinge, L. E., Raake, P. W., and Koch, W. J. (2008) Gene Therapy in Heart Failure. *Circulation Research* **102**, 1458-1470
4. Barry, S. P., and Townsend, P. A. (2010) What Causes a Broken Heart: Molecular Insights into Heart Failure. in *International Review of Cell and Molecular Biology*, Elsevier
5. Olson, E. N. (2006) Gene Regulatory Networks in the Evolution and Development of the Heart. *Science* **313**, 1922-1927
6. Srivastava, D. (2006) Making or Breaking the Heart: From Lineage Determination to Morphogenesis. *Cell* **126**, 1037-1048
7. Xin, M., Olson, E. N., and Bassel-Duby, R. (2013) Mending broken hearts: cardiac development as a basis for adult heart regeneration and repair. *Nature Reviews Molecular Cell Biology* **14**, 529-541
8. Budts, W., Roos-Hesselink, J., Radle-Hurst, T., Eicken, A., McDonagh, T. A., Lambrinou, E., Crespo-Leiro, M. G., Walker, F., and Frogoudaki, A. A. (2016) Treatment of heart failure in adult congenital heart disease: a position paper of the Working Group of Grown-Up Congenital Heart Disease and the Heart Failure Association of the European Society of Cardiology. *European Heart Journal* **37**, 1419-1427
9. Srivastava, D., and Olson, E. N. (2000) A genetic blueprint for cardiac development. *Nature* **407**, 221
10. Dunwoodie, S. L. (2007) Combinatorial signaling in the heart orchestrates cardiac induction, lineage specification and chamber formation. *Seminars in Cell & Developmental Biology* **18**, 54-66
11. Meulemans, D., and Bronner-Fraser, M. (2004) Gene-Regulatory Interactions in Neural Crest Evolution and Development. *Developmental Cell* **7**, 291-299
12. Garg, V., Kathiriya, I. S., Barnes, R., Schluterman, M. K., King, I. N., Butler, C. A., Rothrock, C. R., Eapen, R. S., Hirayama-Yamada, K., Joo, K., Matsuoka, R., Cohen, J. C., and Srivastava, D. (2003) GATA4 mutations cause human congenital heart defects and reveal an interaction with TBX5. *Nature* **424**, 443-447
13. Qian, L., Huang, Y., Spencer, C. I., Foley, A., Vedantham, V., Liu, L., Conway, S. J., Fu, J.-d., and Srivastava, D. (2012) In vivo reprogramming of murine cardiac fibroblasts into induced cardiomyocytes. *Nature* **485**, 593-598
14. Protze, S., Khattak, S., Poulet, C., Lindemann, D., Tanaka, E. M., and Ravens, U. (2012) A new approach to transcription factor screening for reprogramming of fibroblasts to cardiomyocyte-like cells. *Journal of Molecular and Cellular Cardiology* **53**, 323-332
15. Fu, J.-D., Stone, N., nbsp, R, Liu, L., Spencer, C., nbsp, Ian, Qian, L., Hayashi, Y., Delgado-Olguin, P., Ding, S., Bruneau, B., nbsp, G, and Srivastava, D. (2013) Direct

Reprogramming of Human Fibroblasts toward a Cardiomyocyte-like State. *Stem Cell Reports* **1**, 235-247
16. Cao, N., Huang, Y., Zheng, J., Spencer, C. I., Zhang, Y., Fu, J.-D., Nie, B., Xie, M., Zhang, M., Wang, H., Ma, T., Xu, T., Shi, G., Srivastava, D., and Ding, S. (2016) Conversion of human fibroblasts into functional cardiomyocytes by small molecules. *Science* **352**, 1216
17. Belian, E., Noseda, M., Abreu Paiva, M. S., Leja, T., Sampson, R., and Schneider, M. D. (2015) Forward Programming of Cardiac Stem Cells by Homogeneous Transduction with MYOCD plus TBX5. *PLOS ONE* **10**, e0125384
18. Shi, Z., and Rockey, D. C. (2017) Upregulation of the actin cytoskeleton via myocardin leads to increased expression of type 1 collagen. *Laboratory Investigation* **97**, 1412
19. Abdalla, M., Goc, A., Segar, L., and Somanath, P. R. (2013) Akt1 Mediates α-Smooth Muscle Actin Expression and Myofibroblast Differentiation via Myocardin and Serum Response Factor. *Journal of Biological Chemistry* **288**, 33483-33493
20. Wang, D. Z., Li, S., Hockemeyer, D., Sutherland, L., Wang, Z., Schratt, G., Richardson, J. A., Nordheim, A., and Olson, E. N. (2002) Potentiation of serum response factor activity by a family of myocardin-related transcription factors. *Proceedings of the National Academy of Sciences* **99**, 14855-14860
21. Small, E. M., Thatcher, J. E., Sutherland, L. B., Kinoshita, H., Gerard, R. D., Richardson, J. A., DiMaio, J. M., Sadek, H., Kuwahara, K., and Olson, E. N. (2010) Myocardin-Related Transcription Factor-A Controls Myofibroblast Activation and Fibrosis in Response to Myocardial Infarction. *Circulation Research* **107**, 294
22. Miano, J. M. (2015) Myocardin in biology and disease. *Journal of biomedical research*, 3-19
23. Wang, D.-Z., Chang, P. S., Wang, Z., Sutherland, L., Richardson, J. A., Small, E., Krieg, P. A., and Olson, E. N. (2001) Activation of Cardiac Gene Expression by Myocardin, a Transcriptional Cofactor for Serum Response Factor. *Cell* **105**, 851-862
24. Parlakian, A., Tuil, D., Hamard, G., Tavernier, G., Hentzen, D., Concordet, J. P., Paulin, D., Li, Z., and Daegelen, D. (2004) Targeted Inactivation of Serum Response Factor in the Developing Heart Results in Myocardial Defects and Embryonic Lethality. *Molecular and Cellular Biology* **24**, 5281-5289
25. Coletti, D., Daou, N., Hassani, M., Li, Z., and Parlakian, A. (2016) Serum Response Factor in muscle tissues: from development to ageing. *European Journal of Translational Myology* **26**
26. Creemers, E. E., Sutherland, L. B., Oh, J., Barbosa, A. C., and Olson, E. N. (2006) Coactivation of MEF2 by the SAP Domain Proteins Myocardin and MASTR. *Molecular Cell* **23**, 83-96
27. Imamura, M., Long, X., Nanda, V., and Miano, J. M. (2010) Expression and functional activity of four myocardin isoforms. *Gene* **464**, 1-10
28. Chen, J., Kitchen, C. M., Streb, J. W., and Miano, J. M. (2002) Myocardin: A Component of a Molecular Switch for Smooth Muscle Differentiation. *Journal of Molecular and Cellular Cardiology* **34**, 1345-1356
29. Du, K. L., Ip, H. S., Li, J., Chen, M., Dandre, F., Yu, W., Lu, M. M., Owens, G. K., and Parmacek, M. S. (2003) Myocardin Is a Critical Serum Response Factor Cofactor in the Transcriptional Program Regulating Smooth Muscle Cell Differentiation. *Molecular and Cellular Biology* **23**, 2425-2437

30. Li, S., Wang, D. Z., Wang, Z., Richardson, J. A., and Olson, E. N. (2003) The serum response factor coactivator myocardin is required for vascular smooth muscle development. *Proceedings of the National Academy of Sciences* **100**, 9366-9370
31. Small, E. M. (2005) Myocardin is sufficient and necessary for cardiac gene expression in Xenopus. *Development* **132**, 987-997
32. Vantuyn, J., Knaanshanzer, S., Vandewatering, M., Degraaf, M., Vanderlaarse, A., Schalij, M., Vanderwall, E., Devries, A., and Atsma, D. (2005) Activation of cardiac and smooth muscle-specific genes in primary human cells after forced expression of human myocardin. *Cardiovascular Research* **67**, 245-255
33. Long, X., Creemers, E. E., Wang, D.-Z., Olson, E. N., and Miano, J. M. (2007) Myocardin is a bifunctional switch for smooth versus skeletal muscle differentiation. *Proceedings of the National Academy of Sciences* **104**, 16570-16575
34. Pipes, G. C., Creemers, E. E., and Olson, E. N. (2006) The myocardin family of transcriptional coactivators: versatile regulators of cell growth, migration, and myogenesis. *Genes Dev* **20**, 1545-1556
35. Miralles, F., Posern, G., Zaromytidou, A.-I., and Treisman, R. (2003) Actin Dynamics Control SRF Activity by Regulation of Its Coactivator MAL. *Cell* **113**, 329-342
36. Vartiainen, M. K., Guettler, S., Larijani, B., and Treisman, R. (2007) Nuclear Actin Regulates Dynamic Subcellular Localization and Activity of the SRF Cofactor MAL. *Science* **316**, 1749
37. Du, K. L., Chen, M., Li, J., Lepore, J. J., Mericko, P., and Parmacek, M. S. (2004) Megakaryoblastic leukemia factor-1 transduces cytoskeletal signals and induces smooth muscle cell differentiation from undifferentiated embryonic stem cells. *J Biol Chem* **279**, 17578-17586
38. Li, S., Chang, S., Qi, X., Richardson, J. A., and Olson, E. N. (2006) Requirement of a myocardin-related transcription factor for development of mammary myoepithelial cells. *Mol Cell Biol* **26**, 5797-5808
39. Li, J., Zhu, X., Chen, M., Cheng, L., Zhou, D., Lu, M. M., Du, K., Epstein, J. A., and Parmacek, M. S. (2005) Myocardin-related transcription factor B is required in cardiac neural crest for smooth muscle differentiation and cardiovascular development. *Proceedings of the National Academy of Sciences of the United States of America* **102**, 8916-8921
40. Trembley, M. A., Velasquez, L. S., de Mesy Bentley, K. L., and Small, E. M. (2015) Myocardin-related transcription factors control the motility of epicardium-derived cells and the maturation of coronary vessels. *Development* **142**, 21
41. Mokalled, M. H., Carroll, K. J., Cenik, B. K., Chen, B., Liu, N., Olson, E. N., and Bassel-Duby, R. (2015) Myocardin-related transcription factors are required for cardiac development and function. *Developmental Biology* **406**, 109-116
42. Cenik, B. K., Liu, N., Chen, B., Bezprozvannaya, S., Olson, E. N., and Bassel-Duby, R. (2016) Myocardin-related transcription factors are required for skeletal muscle development. *Development* **143**, 2853-2861
43. Creemers, E. E., Sutherland, L. B., McAnally, J., Richardson, J. A., and Olson, E. N. (2006) Myocardin is a direct transcriptional target of Mef2, Tead and Foxo proteins during cardiovascular development. *Development* **133**, 4245-4256
44. Meadows, S. M., Warkman, A. S., Salanga, M. C., Small, E. M., and Krieg, P. A. (2008) The myocardin-related transcription factor, MASTR, cooperates with MyoD to activate

skeletal muscle gene expression. *Proceedings of the National Academy of Sciences* **105**, 1545-1550
45. Mokalled, M. H., Johnson, A. N., Creemers, E. E., and Olson, E. N. (2012) MASTR directs MyoD-dependent satellite cell differentiation during skeletal muscle regeneration. *Genes Dev* **26**, 190-202
46. Olson, E. N., and Nordheim, A. (2010) Linking actin dynamics and gene transcription to drive cellular motile functions. *Nature Reviews Molecular Cell Biology* **11**, 353-365
47. Swärd, K., Stenkula, K. G., Rippe, C., Alajbegovic, A., Gomez, M. F., and Albinsson, S. (2016) Emerging roles of the myocardin family of proteins in lipid and glucose metabolism. *The Journal of Physiology* **594**, 4741-4752
48. Chen, J.-F., Wang, S., Wu, Q., Cao, D., Nguyen, T., Chen, Y., and Wang, D.-Z. (2008) Myocardin Marks the Earliest Cardiac Gene Expression and Plays an Important Role in Heart Development. *The Anatomical Record: Advances in Integrative Anatomy and Evolutionary Biology* **291**, 1200-1211
49. Huang, J., Cheng, L., Li, J., Chen, M., Zhou, D., Lu, M. M., Proweller, A., Epstein, J. A., and Parmacek, M. S. (2008) Myocardin regulates expression of contractile genes in smooth muscle cells and is required for closure of the ductus arteriosus in mice. *Journal of Clinical Investigation*
50. Malina, R. M. (1993) The developing human: Clinically oriented embryology (5th edition). xi + 493 pp. By Keith L. Moore and T.V.N. Persaud. Philadelphia: W. B. Saunders, 1993. . *American Journal of Human Biology* **5**, 507-507
51. Huang, J., Elicker, J., Bowens, N., Liu, X., Cheng, L., Cappola, T. P., Zhu, X., and Parmacek, M. S. (2012) Myocardin regulates BMP10 expression and is required for heart development. *Journal of Clinical Investigation* **122**, 3678-3691
52. Huang, J., Min Lu, M., Cheng, L., Yuan, L. J., Zhu, X., Stout, A. L., Chen, M., Li, J., and Parmacek, M. S. (2009) Myocardin is required for cardiomyocyte survival and maintenance of heart function. *Proceedings of the National Academy of Sciences* **106**, 18734-18739
53. Wang, Z., Wang, D. Z., Pipes, G. C. T., and Olson, E. N. (2003) Myocardin is a master regulator of smooth muscle gene expression. *Proceedings of the National Academy of Sciences* **100**, 7129-7134
54. Ueyama, T., Kasahara, H., Ishiwata, T., Nie, Q., and Izumo, S. (2003) Myocardin Expression Is Regulated by Nkx2.5, and Its Function Is Required for Cardiomyogenesis. *Molecular and Cellular Biology* **23**, 9222-9232
55. Oh, J., Wang, Z., Wang, D. Z., Lien, C. L., Xing, W., and Olson, E. N. (2004) Target Gene-Specific Modulation of Myocardin Activity by GATA Transcription Factors. *Molecular and Cellular Biology* **24**, 8519-8528
56. Wang, C., Cao, D., Wang, Q., and Wang, D.-Z. (2011) Synergistic Activation of Cardiac Genes by Myocardin and Tbx5. *PLoS ONE* **6**, e24242
57. Dreßen, M., Lahm, H., Lahm, A., Wolf, K., Doppler, S., Deutsch, M.-A., Cleuziou, J., Pabst von Ohain, J., Schön, P., Ewert, P., Malcic, I., Lange, R., and Krane, M. (2016) A novel de novo TBX5 mutation in a patient with Holt–Oram syndrome leading to a dramatically reduced biological function. *Molecular Genetics & Genomic Medicine* **4**, 557-567
58. Mullard, A. (2015) The Roadmap Epigenomics Project opens new drug development avenues. *Nature Reviews Drug Discovery* **14**, 223-225

59. Baccarelli, A., Rienstra, M., and Benjamin, E. J. (2010) Cardiovascular Epigenetics: Basic Concepts and Results From Animal and Human Studies. *Circulation: Cardiovascular Genetics* **3**, 567-573
60. Smith, Z. D., and Meissner, A. (2013) DNA methylation: roles in mammalian development. *Nature Reviews Genetics* **14**, 204-220
61. Chaturvedi, P., and Tyagi, S. C. (2014) Epigenetic mechanisms underlying cardiac degeneration and regeneration. *International Journal of Cardiology* **173**, 1-11
62. Zhuang, J., Luan, P., Li, H., Wang, K., Zhang, P., Xu, Y., and Peng, W. (2016) The Yin-Yang Dynamics of DNA Methylation Is the Key Regulator for Smooth Muscle Cell Phenotype Switch and Vascular RemodelingHighlights. *Arteriosclerosis, Thrombosis, and Vascular Biology* **37**, 84-97
63. Portela, A., and Esteller, M. (2010) Epigenetic modifications and human disease. *Nature Biotechnology* **28**, 1057-1068
64. Cao, D., Wang, Z., Zhang, C. L., Oh, J., Xing, W., Li, S., Richardson, J. A., Wang, D. Z., and Olson, E. N. (2004) Modulation of Smooth Muscle Gene Expression by Association of Histone Acetyltransferases and Deacetylases with Myocardin. *Molecular and Cellular Biology* **25**, 364-376
65. McKinsey, T. A., Zhang, C.-L., Lu, J., and Olson, E. N. (2000) Signal-dependent nuclear export of a histone deacetylase regulates muscle differentiation. *Nature* **408**, 106
66. Berdeaux, R., Goebel, N., Banaszynski, L., Takemori, H., Wandless, T., Shelton, G. D., and Montminy, M. (2007) SIK1 is a class II HDAC kinase that promotes survival of skeletal myocytes. *Nature Medicine* **13**, 597-603
67. Gordon, J. W., Pagiatakis, C., Salma, J., Du, M., Andreucci, J. J., Zhao, J., Hou, G., Perry, R. L., Dan, Q., Courtman, D., Bendeck, M. P., and McDermott, J. C. (2009) Protein Kinase A-regulated Assembly of a MEF2¬ Σ HDAC4 Repressor Complex Controls c-Jun Expression in Vascular Smooth Muscle Cells. *Journal of Biological Chemistry* **284**, 19027-19042
68. Czubryt, M. P., McAnally, J., Fishman, G. I., and Olson, E. N. (2003) Regulation of peroxisome proliferator-activated receptor   coactivator 1 (PGC-1) and mitochondrial function by MEF2 and HDAC5. *Proceedings of the National Academy of Sciences* **100**, 1711-1716
69. Vega , R., Harrison , B., E, M., CR, R., PJ, P., EN, O., and TA., M. (2004) Protein kinases C and D mediate agonist-dependent cardiac hypertrophy through nuclear export of histone deacetylase 5. *Mol Cell Biol* **24**, 8374-8385.
70. Fielitz, J., Kim, M.-S., Shelton, J. M., Qi, X., Hill, J. A., Richardson, J. A., Bassel-Duby, R., and Olson, E. N. (2008) Requirement of protein kinase D1 for pathological cardiac remodeling. *Proceedings of the National Academy of Sciences of the United States of America* **105**, 3059-3063
71. Bossuyt, J., Helmstadter, K., Wu, X., Clements-Jewery, H., Haworth, R. S., Avkiran, M., Martin, J. L., Pogwizd, S. M., and Bers, D. M. (2008) Calcium/Calmodulin-Dependent Protein Kinase IIδ and Protein Kinase D Overexpression Reinforce the Histone Deacetylase 5 Redistribution in Heart Failure. *Circulation Research* **102**, 695
72. Cao, D., Wang, C., Tang, R., Chen, H., Zhang, Z., Tatsuguchi, M., and Wang, D.-Z. (2012) Acetylation of Myocardin Is Required for the Activation of Cardiac and Smooth Muscle Genes. *Journal of Biological Chemistry* **287**, 38495-38504

73. Liu, Z.-P., Wang, Z., Yanagisawa, H., and Olson, E. N. (2005) Phenotypic Modulation of Smooth Muscle Cells through Interaction of Foxo4 and Myocardin. *Developmental Cell* **9**, 261-270
74. Yoshida, T., Yamashita, M., Horimai, C., and Hayashi, M. (2014) Kruppel-like Factor 4 Protein Regulates Isoproterenol-induced Cardiac Hypertrophy by Modulating Myocardin Expression and Activity. *Journal of Biological Chemistry* **289**, 26107-26118
75. McDonald, O. G. (2005) Control of SRF binding to CArG box chromatin regulates smooth muscle gene expression in vivo. *Journal of Clinical Investigation* **116**, 36-48
76. Ma, Y., Li, Q., Li, A., Wei, Y., Long, P., Jiang, X., Sun, F., Weiskirchen, R., Wu, B., Liang, C., Grötzinger, J., Wei, Y., Yu, W., Mercola, M., Huang, Y., Wang, J., Yu, Y., and Schwartz, R. J. (2017) The CSRP2BP histone acetyltransferase drives smooth muscle gene expression. *Nucleic Acids Research* **45**, 3046-3058
77. Sun, X., Hota, S. K., Zhou, Y.-Q., Novak, S., Miguel-Perez, D., Christodoulou, D., Seidman, C. E., Seidman, J. G., Gregorio, C. C., Henkelman, R. M., Rossant, J., and Bruneau, B. G. (2017) Cardiac-enriched BAF chromatin-remodeling complex subunit Baf60c regulates gene expression programs essential for heart development and function. *Biology Open*
78. Rosales, W., Carulla, J., Garc, #xed, a, J., Vargas, D., and Lizcano, F. (2016) Role of Histone Demethylases in Cardiomyocytes Induced to Hypertrophy. *BioMed Research International* **2016**, 7
79. Zhang, Q.-J., and Liu, Z.-P. (2015) Histone methylations in heart development, congenital and adult heart diseases. *Epigenomics* **7**, 321-330
80. Agger, K., Cloos, P. A. C., Christensen, J., Pasini, D., Rose, S., Rappsilber, J., Issaeva, I., Canaani, E., Salcini, A. E., and Helin, K. (2007) UTX and JMJD3 are histone H3K27 demethylases involved in HOX gene regulation and development. *Nature* **449**, 731-734
81. Lee, S., Lee, J., nbsp, W, and Lee, S.-K. (2012) UTX, a Histone H3-Lysine 27 Demethylase, Acts as a Critical Switch to Activate the Cardiac Developmental Program. *Developmental Cell* **22**, 25-37
82. Lockman, K., Taylor, J. M., and Mack, C. P. (2007) The Histone Demethylase, Jmjd1a, Interacts With the Myocardin Factors to Regulate SMC Differentiation Marker Gene Expression. *Circulation Research* **101**, e115-e123
83. Gray, S. G., Iglesias, A. H., Lizcano, F., Villanueva, R., Camelo, S., Jingu, H., Teh, B. T., Koibuchi, N., Chin, W. W., Kokkotou, E., and Dangond, F. (2005) Functional Characterization of JMJD2A, a Histone Deacetylase- and Retinoblastoma-binding Protein. *Journal of Biological Chemistry* **280**, 28507-28518
84. Zhang, Q.-J., Chen, H.-Z., Wang, L., Liu, D.-P., Hill, J. A., and Liu, Z.-P. (2011) The histone trimethyllysine demethylase JMJD2A promotes cardiac hypertrophy in response to hypertrophic stimuli in mice. *Journal of Clinical Investigation* **121**, 2447-2456
85. Wang, Z., Wang, D.-Z., Hockemeyer, D., McAnally, J., Nordheim, A., and Olson, E. N. (2004) Myocardin and ternary complex factors compete for SRF to control smooth muscle gene expression. *Nature* **428**, 185-189
86. Yin, F., and Herring, B. P. (2004) GATA-6 Can Act as a Positive or Negative Regulator of Smooth Muscle-specific Gene Expression. *Journal of Biological Chemistry* **280**, 4745-4752

87. Proweller, A., Pear, W. S., and Parmacek, M. S. (2005) Notch Signaling Represses Myocardin-induced Smooth Muscle Cell Differentiation. *Journal of Biological Chemistry* **280**, 8994-9004
88. Penton, A. L., Leonard, L. D., and Spinner, N. B. (2012) Notch signaling in human development and disease. *Seminars in Cell & Developmental Biology* **23**, 450-457
89. Doi, H. (2005) HERP1 Inhibits Myocardin-Induced Vascular Smooth Muscle Cell Differentiation by Interfering With SRF Binding to CArG Box. *Arteriosclerosis, Thrombosis, and Vascular Biology* **25**, 2328-2334
90. Qiu, P. (2005) Myocardin Enhances Smad3-Mediated Transforming Growth Factor- 1 Signaling in a CArG Box-Independent Manner: Smad-Binding Element Is an Important cis Element for SM22 Transcription In Vivo. *Circulation Research* **97**, 983-991
91. Xie, W.-B., Li, Z., Miano, J. M., Long, X., and Chen, S.-Y. (2011) Smad3-mediated Myocardin Silencing. *Journal of Biological Chemistry* **286**, 15050-15057
92. Li, H. J., Haque, Z., Lu, Q., Li, L., Karas, R., and Mendelsohn, M. (2007) Steroid receptor coactivator 3 is a coactivator for myocardin, the regulator of smooth muscle transcription and differentiation. *Proceedings of the National Academy of Sciences* **104**, 4065-4070
93. Liao, X.-H., Wang, N., Zhao, D.-W., Zheng, D.-L., Zheng, L., Xing, W.-J., Ma, W.-J., Bao, L.-Y., Dong, J., and Zhang, T.-C. (2015) STAT3 Protein Regulates Vascular Smooth Muscle Cell Phenotypic Switch by Interaction with Myocardin. *Journal of Biological Chemistry* **290**, 19641-19652
94. Tang, R.-h., Zheng, X.-L., Callis, T. E., Stansfield, W. E., He, J., Baldwin, A. S., Wang, D.-Z., and Selzman, C. H. (2008) Myocardin inhibits cellular proliferation by inhibiting NF-κB(p65)-dependent cell cycle progression. *Proceedings of the National Academy of Sciences* **105**, 3362-3367
95. Singh, P., and Zheng, X.-L. (2014) Dual Regulation of Myocardin Expression by Tumor Necrosis Factor-α in Vascular Smooth Muscle Cells. *PLOS ONE* **9**, e112120
96. Song, S.-H., Kim, K., Jo, E.-K., Kim, Y.-W., Kwon, J.-S., Bae, S. S., Sung, J.-H., Park, S. G., Kim, J. T., and Suh, W. (2016) Fibroblast Growth Factor 12 Is a Novel Regulator of Vascular Smooth Muscle Cell Plasticity and Fate<span hwp:id="article-title-24" class="sub-article-title">Highlights</span&gt. *Arteriosclerosis, Thrombosis, and Vascular Biology* **36**, 1928
97. Hu, G., Wang, X., Saunders, D. N., Henderson, M., Russell, A. J., Herring, B. P., and Zhou, J. (2010) Modulation of Myocardin Function by the Ubiquitin E3 Ligase UBR5. *Journal of Biological Chemistry* **285**, 11800-11809
98. Taurin, S., Sandbo, N., Yau, D. M., Sethakorn, N., Kach, J., and Dulin, N. O. (2009) Phosphorylation of Myocardin by Extracellular Signal-regulated Kinase. *Journal of Biological Chemistry* **284**, 33789-33794
99. Yin, H., Jiang, Y., Li, H., Li, J., Gui, Y., and Zheng, X.-L. (2011) Proteasomal degradation of myocardin is required for its transcriptional activity in vascular smooth muscle cells. *Journal of Cellular Physiology* **226**, 1897-1906

100. Singh P; Li, D. G., Y; Zheng, XL. (2017) Atrogin-1 increases smooth muscle contractility through myocardin degradation. . *Journal of Cellular Physiology* **232**, 3195-3196
101. Badorff, C. (2005) Glycogen Synthase Kinase 3 Inhibits Myocardin-Dependent Transcription and Hypertrophy Induction Through Site-Specific Phosphorylation. *Circulation Research* **97**, 645-654
102. Callis, T. E. (2005) Bone Morphogenetic Protein Signaling Modulates Myocardin Transactivation of Cardiac Genes. *Circulation Research* **97**, 992-1000
103. Wang, J., Li, A., Wang, Z., Feng, X., Olson, E. N., and Schwartz, R. J. (2006) Myocardin Sumoylation Transactivates Cardiogenic Genes in Pluripotent 10T1/2 Fibroblasts. *Molecular and Cellular Biology* **27**, 622-632
104. Islam, S., Yasui, Y., Kaul, P., Marelli, A. J., and Mackie, A. S. (2016) Congenital Heart Disease Hospitalizations in Canada: A 10-Year Experience. *Canadian Journal of Cardiology* **32**, 197-203
105. Torrado, M., Lopez, E., Centeno, A., Medrano, C., Castro-Beiras, A., and Mikhailov, A. T. (2003) Myocardin mRNA is augmented in the failing myocardium: expression profiling in the porcine model and human dilated cardiomyopathy. *Journal of Molecular Medicine* **81**, 566-577
106. Xing, W. (2006) Myocardin Induces Cardiomyocyte Hypertrophy. *Circulation Research* **98**, 1089-1097
107. Wang, K., Long, B., Zhou, J., and Li, P.-F. (2010) miR-9 and NFATc3 Regulate Myocardin in Cardiac Hypertrophy. *Journal of Biological Chemistry* **285**, 11903-11912
108. Ransom, J. F., King, I. N., Garg, V., and Srivastava, D. (2008) A Rare Human Sequence Variant Reveals Myocardin Autoinhibition. *Journal of Biological Chemistry* **283**, 35845-35852
109. Torrado, M., Iglesias, R., Centeno, A., Lopez, E., and Mikhailov, A. T. (2011) Targeted Gene-Silencing Reveals the Functional Significance of Myocardin Signaling in the Failing Heart. *PLoS ONE* **6**, e26392
110. Nam, Y.-J., Song, K., Luo, X., Daniel, E., Lambeth, K., West, K., Hill, J. A., DiMaio, J. M., Baker, L. A., Bassel-Duby, R., and Olson, E. N. (2013) Reprogramming of human fibroblasts toward a cardiac fate. *Proceedings of the National Academy of Sciences* **110**, 5588-5593
111. Christoforou, N., Chakraborty, S., Kirkton, R. D., Adler, A. F., Addis, R. C., and Leong, K. W. (2017) Core Transcription Factors, MicroRNAs, and Small Molecules Drive Transdifferentiation of Human Fibroblasts Towards The Cardiac Cell Lineage. *Sci Rep* **7**, 40285
112. Latronico, M. V. G., Catalucci, D., and Condorelli, G. (2007) Emerging Role of MicroRNAs in Cardiovascular Biology. *Circulation Research* **101**, 1225-1236
113. Wang, H., and Cai, J. (2017) The role of microRNAs in heart failure. *Biochimica et Biophysica Acta (BBA) - Molecular Basis of Disease* **1863**, 2019-2030
114. Olson, E. N. (2014) MicroRNAs as Therapeutic Targets and Biomarkers of Cardiovascular Disease. *Science Translational Medicine* **6**, 239ps233-239ps233
115. Cordes, K. R., Sheehy, N. T., White, M. P., Berry, E. C., Morton, S. U., Muth, A. N., Lee, T.-H., Miano, J. M., Ivey, K. N., and Srivastava, D. (2009) miR-145 and miR-143 regulate smooth muscle cell fate and plasticity. *Nature*

116. Jiang, Y., Yin, H., and Zheng, X.-L. (2010) MicroRNA-1 inhibits myocardin-induced contractility of human vascular smooth muscle cells. *Journal of Cellular Physiology* **225**, 506-511
117. Chen, J., Yin, H., Jiang, Y., Radhakrishnan, S. K., Huang, Z.-P., Li, J., Shi, Z., Kilsdonk, E. P. C., Gui, Y., Wang, D.-Z., and Zheng, X.-L. (2011) Induction of MicroRNA-1 by Myocardin in Smooth Muscle Cells Inhibits Cell Proliferation. *Arteriosclerosis, Thrombosis, and Vascular Biology* **31**, 368
118. Wystub, K., Besser, J., Bachmann, A., Boettger, T., and Braun, T. (2013) miR-1/133a Clusters Cooperatively Specify the Cardiomyogenic Lineage by Adjustment of Myocardin Levels during Embryonic Heart Development. *PLoS Genetics* **9**, e1003793
119. Liao, X.-H., Wang, N., Zhao, D.-W., Zheng, D.-L., Zheng, L., Wen-Jing, X., Zhou, H., Cao, D.-S., and Zhang, T.-C. (2015) NF-KB (p65) negatively regulates myocardin-induced cardiomyocyte hypertrophy through multiple mechanisms. *Cellular Signalling* **27**, 1021-1022
120. Castaldi, A., Zaglia, T., Di Mauro, V., Carullo, P., Viggiani, G., Borile, G., Di Stefano, B., Schiattarella, G. G., Gualazzi, M. G., Elia, L., Stirparo, G. G., Colorito, M. L., Pironti, G., Kunderfranco, P., Esposito, G., Bang, M. L., Mongillo, M., Condorelli, G., and Catalucci, D. (2014) MicroRNA-133 Modulates the 1-Adrenergic Receptor Transduction Cascade. *Circulation Research* **115**, 273-283
121. Whelan, R. S., Kaplinskiy, V., and Kitsis, R. N. (2010) Cell Death in the Pathogenesis of Heart Disease: Mechanisms and Significance. *Annual Review of Physiology* **72**, 19-44
122. Taylor, R. C., Cullen, S. P., and Martin, S. J. (2008) Apoptosis: controlled demolition at the cellular level. *Nature Reviews Molecular Cell Biology* **9**, 231-241
123. Suzanne, M., and Steller, H. (2013) Shaping organisms with apoptosis. *Cell Death and Differentiation* **20**, 669-675
124. Ashkenazi, A., and Salvesen, G. (2014) Regulated Cell Death: Signaling and Mechanisms. *Annual Review of Cell and Developmental Biology* **30**, 337-356
125. Berghe, T. V., Linkermann, A., Jouan-Lanhouet, S., Walczak, H., and Vandenabeele, P. (2014) Regulated necrosis: the expanding network of non-apoptotic cell death pathways. *Nature Reviews Molecular Cell Biology* **15**, 135-147
126. Dorn, G. W. (2012) Molecular Mechanisms That Differentiate Apoptosis from Programmed Necrosis. *Toxicologic Pathology* **41**, 227-234
127. Galluzzi, L., Vitale, I., Aaronson, S. A., Abrams, J. M., Adam, D., Agostinis, P., Alnemri, E. S., Altucci, L., Amelio, I., Andrews, D. W., Annicchiarico-Petruzzelli, M., Antonov, A. V., Arama, E., Baehrecke, E. H., Barlev, N. A., Bazan, N. G., Bernassola, F., Bertrand, M. J. M., Bianchi, K., Blagosklonny, M. V., Blomgren, K., Borner, C., Boya, P., Brenner, C., Campanella, M., Candi, E., Carmona-Gutierrez, D., Cecconi, F., Chan, F. K. M., Chandel, N. S., Cheng, E. H., Chipuk, J. E., Cidlowski, J. A., Ciechanover, A., Cohen, G. M., Conrad, M., Cubillos-Ruiz, J. R., Czabotar, P. E., D'Angiolella, V., Dawson, T. M., Dawson, V. L., De Laurenzi, V., De Maria, R., Debatin, K.-M., DeBerardinis, R. J., Deshmukh, M., Di Daniele, N., Di Virgilio, F., Dixit, V. M., Dixon, S. J., Duckett, C. S., Dynlacht, B. D., El-Deiry, W. S., Elrod, J. W., Fimia, G. M., Fulda, S., García-Sáez, A. J., Garg, A. D., Garrido, C., Gavathiotis, E., Golstein, P., Gottlieb, E., Green, D. R., Greene, L. A., Gronemeyer, H., Gross, A., Hajnoczky, G., Hardwick, J. M., Harris, I. S., Hengartner, M. O., Hetz, C., Ichijo, H., Jäättelä, M., Joseph, B., Jost, P. J., Juin, P. P., Kaiser, W. J., Karin, M., Kaufmann, T.,

Kepp, O., Kimchi, A., Kitsis, R. N., Klionsky, D. J., Knight, R. A., Kumar, S., Lee, S. W., Lemasters, J. J., Levine, B., Linkermann, A., Lipton, S. A., Lockshin, R. A., López-Otín, C., Lowe, S. W., Luedde, T., Lugli, E., MacFarlane, M., Madeo, F., Malewicz, M., Malorni, W., Manic, G., Marine, J.-C., Martin, S. J., Martinou, J.-C., Medema, J. P., Mehlen, P., Meier, P., Melino, S., Miao, E. A., Molkentin, J. D., Moll, U. M., Muñoz-Pinedo, C., Nagata, S., Nuñez, G., Oberst, A., Oren, M., Overholtzer, M., Pagano, M., Panaretakis, T., Pasparakis, M., Penninger, J. M., Pereira, D. M., Pervaiz, S., Peter, M. E., Piacentini, M., Pinton, P., Prehn, J. H. M., Puthalakath, H., Rabinovich, G. A., Rehm, M., Rizzuto, R., Rodrigues, C. M. P., Rubinsztein, D. C., Rudel, T., Ryan, K. M., Sayan, E., Scorrano, L., Shao, F., Shi, Y., Silke, J., Simon, H.-U., Sistigu, A., Stockwell, B. R., Strasser, A., Szabadkai, G., Tait, S. W. G., Tang, D., Tavernarakis, N., Thorburn, A., Tsujimoto, Y., Turk, B., Vanden Berghe, T., Vandenabeele, P., Vander Heiden, M. G., Villunger, A., Virgin, H. W., Vousden, K. H., Vucic, D., Wagner, E. F., Walczak, H., Wallach, D., Wang, Y., Wells, J. A., Wood, W., Yuan, J., Zakeri, Z., Zhivotovsky, B., Zitvogel, L., Melino, G., and Kroemer, G. (2018) Molecular mechanisms of cell death: recommendations of the Nomenclature Committee on Cell Death 2018. *Cell Death & Differentiation* **25**, 486-541

128. Wu, C.-C., Lee, S., Malladi, S., Chen, M.-D., Mastrandrea, N. J., Zhang, Z., and Bratton, S. B. (2016) The Apaf-1 apoptosome induces formation of caspase-9 homo- and heterodimers with distinct activities. *Nature Communications* **7**, 13565
129. Basso, E., Fante, L., Fowlkes, J., Petronilli, V., Forte, M. A., and Bernardi, P. (2005) Properties of the Permeability Transition Pore in Mitochondria Devoid of Cyclophilin D. *Journal of Biological Chemistry* **280**, 18558-18561
130. Hom, J., nbsp, R, Quintanilla, R., nbsp, A, Hoffman, D., nbsp, L, de, nbsp, Mesy, nbsp, Bentley, K., nbsp, L, Molkentin, J., nbsp, D, Sheu, S.-S., Porter, G., nbsp, and A. (2011) The Permeability Transition Pore Controls Cardiac Mitochondrial Maturation and Myocyte Differentiation. *Developmental Cell* **21**, 469-478
131. Alavian, K. N., Beutner, G., Lazrove, E., Sacchetti, S., Park, H. A., Licznerski, P., Li, H., Nabili, P., Hockensmith, K., Graham, M., Porter, G. A., and Jonas, E. A. (2014) An uncoupling channel within the c-subunit ring of the F1FO ATP synthase is the mitochondrial permeability transition pore. *Proceedings of the National Academy of Sciences* **111**, 10580-10585
132. Clarke, S. J., McStay, G. P., and Halestrap, A. P. (2002) Sanglifehrin A Acts as a Potent Inhibitor of the Mitochondrial Permeability Transition and Reperfusion Injury of the Heart by Binding to Cyclophilin-D at a Different Site from Cyclosporin A. *Journal of Biological Chemistry* **277**, 34793-34799
133. Scaffidi, P., Misteli, T., and Bianchi, M. E. (2010) Release of chromatin protein HMGB1 by necrotic cells triggers inflammation. *Nature* **467**, 622
134. Andrassy, M., Volz, H. C., Igwe, J. C., Funke, B., Eichberger, S. N., Kaya, Z., Buss, S., Autschbach, F., Pleger, S. T., Lukic, I. K., Bea, F., Hardt, S. E., Humpert, P. M., Bianchi, M. E., Mairbäurl, H., Nawroth, P. P., Remppis, A., Katus, H. A., and Bierhaus, A. (2008) High-Mobility Group Box-1 in Ischemia-Reperfusion Injury of the Heart. *Circulation* **117**, 3216
135. Silke, J., Rickard, J. A., and Gerlic, M. (2015) The diverse role of RIP kinases in necroptosis and inflammation. *Nature Immunology* **16**, 689-697

136. Cai, Z., and Liu, Z.-G. (2014) Execution of RIPK3-regulated necrosis. *Molecular & Cellular Oncology* **1**, e960759
137. Aglietti, R. A., and Dueber, E. C. (2017) Recent Insights into the Molecular Mechanisms Underlying Pyroptosis and Gasdermin Family Functions. *Trends in Immunology* **38**, 261-271
138. Dixon, S., nbsp, J, Lemberg, K., nbsp, M, Lamprecht, M., nbsp, R, Skouta, R., Zaitsev, E., nbsp, M, Gleason, C., nbsp, E, Patel, D., nbsp, N, Bauer, A., nbsp, J, Cantley, A., nbsp, M, Yang, W., nbsp, Seok, Morrison, B., Stockwell, B., nbsp, and R. (2012) Ferroptosis: An Iron-Dependent Form of Nonapoptotic Cell Death. *Cell* **149**, 1060-1072
139. Ghavami, S., Yeganeh, B., Stelmack, G. L., Kashani, H. H., Sharma, P., Cunnington, R., Rattan, S., Bathe, K., Klonisch, T., Dixon, I. M. C., Freed, D. H., and Halayko, A. J. (2012) Apoptosis, autophagy and ER stress in mevalonate cascade inhibition-induced cell death of human atrial fibroblasts. *Cell Death and Disease* **3**, e330
140. Green, D. R., and Victor, B. (2012) The pantheon of the fallen: why are there so many forms of cell death? *Trends in Cell Biology* **22**, 555-556
141. Boatright, K. M., Renatus, M., Scott, F. L., Sperandio, S., Shin, H., Pedersen, I. M., Ricci, J.-E., Edris, W. A., Sutherlin, D. P., Green, D. R., and Salvesen, G. S. (2003) A Unified Model for Apical Caspase Activation. *Molecular Cell* **11**, 529-541
142. Tait, S. W. G., and Green, D. R. (2010) Mitochondria and cell death: outer membrane permeabilization and beyond. *Nature Reviews Molecular Cell Biology* **11**, 621-632
143. Danial, N. N., and Korsmeyer, S. J. (2004) Cell Death: critical control points. *Cell* **116**, 205-219
144. Youle, R. J., and Strasser, A. (2008) The BCL-2 protein family: opposing activities that mediate cell death. *Nature Reviews Molecular Cell Biology* **9**, 47-59
145. Kharbanda, S., Pandey, P., Schofield, L., Israels, S., Roncinske, R., Yoshida, K., Bharti, A., Yuan, Z. M., Saxena, S., Weichselbaum, R., Nalin, C., and Kufe, D. (1997) Role for Bcl-xL as an inhibitor of cytosolic cytochrome C accumulation in DNA damage-induced apoptosis. *Proceedings of the National Academy of Sciences* **94**, 6939-6942
146. Kluck, R. M. (1997) The Release of Cytochrome c from Mitochondria: A Primary Site for Bcl-2 Regulation of Apoptosis. *Science* **275**, 1132-1136
147. Wei, M. C. (2001) Proapoptotic BAX and BAK: A Requisite Gateway to Mitochondrial Dysfunction and Death. *Science* **292**, 727-730
148. Cheng, E. H. Y. A., Wei, M. C., Weiler, S., Flavell, R. A., Mak, T. W., Lindsten, T., and Korsmeyer, S. J. (2001) BCL-2, BCL-XL Sequester BH3 Domain-Only Molecules Preventing BAX- and BAK-Mediated Mitochondrial Apoptosis. *Molecular Cell* **8**, 705-711
149. Zhou, L., and Chang, D. C. (2008) Dynamics and structure of the Bax-Bak complex responsible for releasing mitochondrial proteins during apoptosis. *Journal of Cell Science* **121**, 2186-2196
150. Dewson, G. (2015) Investigating the Oligomerization of Bak and Bax during Apoptosis by Cysteine Linkage: Figure 1. *Cold Spring Harbor Protocols* **2015**, pdb.prot086470
151. Dewson, G., Kratina, T., Czabotar, P., Day, C. L., Adams, J. M., and Kluck, R. M. (2009) Bak Activation for Apoptosis Involves Oligomerization of Dimers via Their Œ±6 Helices. *Molecular Cell* **36**, 696-703
152. Kalkavan, H., and Green, D. R. (2017) MOMP, cell suicide as a BCL-2 family business. *Cell Death and Differentiation* **25**, 46-55

153. Shiozaki, E. N., Chai, J., and Shi, Y. (2002) Oligomerization and activation of caspase-9, induced by Apaf-1 CARD. *Proceedings of the National Academy of Sciences* **99**, 4197-4202
154. Korsmeyer, S. J., Wei, M. C., Saito, M., Weiler, S., Oh, K. J., and Schlesinger, P. H. (2000) Pro-apoptotic cascade activates BID, which oligomerizes BAK or BAX into pores that result in the release of cytochrome c. *Cell Death and Differentiation* **7**, 1166-1173
155. Moldoveanu, T., Grace, C. R., Llambi, F., Nourse, A., Fitzgerald, P., Gehring, K., Kriwacki, R. W., and Green, D. R. (2013) BID-induced structural changes in BAK promote apoptosis. *Nature Structural & Molecular Biology* **20**, 589-597
156. Huang, K., Zhang, J., O'Neill, K. L., Gurumurthy, C. B., Quadros, R. M., Tu, Y., and Luo, X. (2016) Cleavage by Caspase 8 and Mitochondrial Membrane Association Activate the BH3-only Protein Bid during TRAIL-induced Apoptosis. *Journal of Biological Chemistry* **291**, 11843-11851
157. Wang, Y., Kim, N. S., Haince, J.-F., Kang, H. C., David, K. K., Andrabi, S. A., Poirier, G. G., Dawson, V. L., and Dawson, T. M. (2011) Poly(ADP-Ribose) (PAR) Binding to Apoptosis-Inducing Factor Is Critical for PAR Polymerase-1–Dependent Cell Death (Parthanatos). *Science Signaling* **4**, ra20
158. Fatokun, A. A., Dawson, V. L., and Dawson, T. M. (2014) Parthanatos: mitochondrial-linked mechanisms and therapeutic opportunities. *British Journal of Pharmacology* **171**, 2000-2016
159. Wu, X. N., Yang, Z. H., Wang, X. K., Zhang, Y., Wan, H., Song, Y., Chen, X., Shao, J., and Han, J. (2014) Distinct roles of RIP1-RIP3 hetero- and RIP3-RIP3 homo-interaction in mediating necroptosis. *Cell Death and Differentiation* **21**, 1709-1720
160. Sun, L., and Wang, X. (2014) A new kind of cell suicide: mechanisms and functions of programmed necrosis. *Trends in Biochemical Sciences* **39**, 587-593
161. Cai, Z., Jitkaew, S., Zhao, J., Chiang, H.-C., Choksi, S., Liu, J., Ward, Y., Wu, L.-g., and Liu, Z.-G. (2013) Plasma membrane translocation of trimerized MLKL protein is required for TNF-induced necroptosis. *Nature Cell Biology* **16**, 55-65
162. Shulga, N., and Pastorino, J. G. (2012) GRIM-19-mediated translocation of STAT3 to mitochondria is necessary for TNF-induced necroptosis. *Journal of Cell Science* **125**, 2995-3003
163. Marshall, K. D., and Baines, C. P. (2014) Necroptosis: is there a role for mitochondria? *Frontiers in Physiology* **5**
164. Kung, G., Konstantinidis, K., and Kitsis, R. N. (2011) Programmed Necrosis, Not Apoptosis, in the Heart. *Circulation Research* **108**, 1017-1036
165. Kwong, J., nbsp, Q, Molkentin, J., nbsp, and D. (2015) Physiological and Pathological Roles of the Mitochondrial Permeability Transition Pore in the Heart. *Cell Metabolism* **21**, 206-214
166. Halestrap, A. P. (2009) What is the mitochondrial permeability transition pore? *Journal of Molecular and Cellular Cardiology* **46**, 821-831
167. Bernardi, P., Rasola, A., Forte, M., and Lippe, G. (2015) The Mitochondrial Permeability Transition Pore: Channel Formation by F-ATP Synthase, Integration in Signal Transduction, and Role in Pathophysiology. *Physiological Reviews* **95**, 1111-1155
168. Nakagawa, T., Shimizu, S., Watanabe, T., Yamaguchi, O., Otsu, K., Yamagata, H., Inohara, H., Kubo, T., and Tsujimoto, Y. (2005) Cyclophilin D-dependent mitochondrial

permeability transition regulates some necrotic but not apoptotic cell death. *Nature* **434**, 652-658
169. Ma, S., Boerner, J. E., TiongYip, C., Weidmann, B., Ryder, N. S., Cooreman, M. P., and Lin, K. (2006) NIM811, a Cyclophilin Inhibitor, Exhibits Potent In Vitro Activity against Hepatitis C Virus Alone or in Combination with Alpha Interferon. *Antimicrobial Agents and Chemotherapy* **50**, 2976-2982
170. Baines, C. P., Kaiser, R. A., Sheiko, T., Craigen, W. J., and Molkentin, J. D. (2007) Voltage-dependent anion channels are dispensable for mitochondrial-dependent cell death. *Nature Cell Biology* **9**, 550-555
171. Kokoszka, J. E., Waymire, K. G., Levy, S. E., Sligh, J. E., Cai, J., Jones, D. P., MacGregor, G. R., and Wallace, D. C. (2004) Erratum: The ADP/ATP translocator is not essential for the mitochondrial permeability transition pore. *Nature* **427**, 461-465
172. Richardson, A. P., and Halestrap, A. P. (2016) Quantification of active mitochondrial permeability transition pores using GNX-4975 inhibitor titrations provides insights into molecular identity. *Biochemical Journal* **473**, 1129-1140
173. Karch, J., and Molkentin, J. D. (2014) Identifying the components of the elusive mitochondrial permeability transition pore. *Proceedings of the National Academy of Sciences* **111**, 10396-10397
174. Giorgio, V., Bisetto, E., Soriano, M. E., Dabbeni-Sala, F., Basso, E., Petronilli, V., Forte, M. A., Bernardi, P., and Lippe, G. (2009) Cyclophilin D Modulates Mitochondrial F0F1-ATP Synthase by Interacting with the Lateral Stalk of the Complex. *Journal of Biological Chemistry* **284**, 33982-33988
175. Giorgio, V., von Stockum, S., Antoniel, M., Fabbro, A., Fogolari, F., Forte, M., Glick, G. D., Petronilli, V., Zoratti, M., Szabo, I., Lippe, G., and Bernardi, P. (2013) Dimers of mitochondrial ATP synthase form the permeability transition pore. *Proceedings of the National Academy of Sciences* **110**, 5887-5892
176. Bonora, M., Bononi, A., De Marchi, E., Giorgi, C., Lebiedzinska, M., Marchi, S., Patergnani, S., Rimessi, A., Suski, J. M., Wojtala, A., Wieckowski, M. R., Kroemer, G., Galluzzi, L., and Pinton, P. (2013) Role of the c subunit of the FOATP synthase in mitochondrial permeability transition. *Cell Cycle* **12**, 674-683
177. Gálvez, A. S., Brunskill, E. W., Marreez, Y., Benner, B. J., Regula, K. M., Kirschenbaum, L. A., and Dorn, G. W. (2006) Distinct Pathways Regulate Proapoptotic Nix and BNip3 in Cardiac Stress. *Journal of Biological Chemistry* **281**, 1442-1448
178. Zhang, L., Li, L., Liu, H., Borowitz, J. L., and Isom, G. E. (2009) BNIP3 mediates cell death by different pathways following localization to endoplasmic reticulum and mitochondrion. *The FASEB Journal* **23**, 3405-3414
179. Dobson, C. M. (2004) Principles of protein folding, misfolding and aggregation. *Seminars in Cell & Developmental Biology* **15**, 3-16
180. Ron, D., and Walter, P. (2007) Signal integration in the endoplasmic reticulum unfolded protein response. *Nature Reviews Molecular Cell Biology* **8**, 519
181. Shimazaki, H., Watanabe, K., Veeraveedu, P. T., Harima, M., Thandavarayan, R. A., Arozal, W., Tachikawa, H., Kodama, M., and Aizawa, Y. (2010) The antioxidant edaravone attenuates ER-stress-mediated cardiac apoptosis and dysfunction in rats with autoimmune myocarditis. *Free Radical Research* **44**, 1082-1090
182. Rao, R. V., Ellerby, H. M., and Bredesen, D. E. (2004) Coupling endoplasmic reticulum stress to the cell death program. *Cell Death And Differentiation* **11**, 372

183. Janssen, K., Horn, S., Niemann, M. T., Daniel, P. T., Schulze-Osthoff, K., and Fischer, U. (2009) Inhibition of the ER Calcium pump forces multidrug-resistant cells deficient in Bak and Bax into necrosis. *Journal of Cell Science* **122**, 4481
184. Ullman, E., Fan, Y., Stawowczyk, M., Chen, H. M., Yue, Z., and Zong, W. X. (2008) Autophagy promotes necrosis in apoptosis-deficient cells in response to ER stress. *Cell death and differentiation* **15**, 422-425
185. Naya, F. J., Black, B. L., Wu, H., Bassel-Duby, R., Richardson, J. A., Hill, J. A., and Olson, E. N. (2002) Mitochondrial deficiency and cardiac sudden death in mice lacking the MEF2A transcription factor. *Nature Medicine* **8**, 1303
186. Miano, J. M., N, R., Georger, M. A., de Mesy Bentley, K. L., Emerson, R. L., Balza, R. O., Jr., Xiao, Q., Weiler, H., Ginty, D. D., and Misra, R. P. (2004) Restricted inactivation of serum response factor to the cardiovascular system. *Proc Natl Acad Sci USA* **101**, 17132–17137
187. Liu, N., Williams AH, Kim Y, McAnally J, Bezprozvannaya S, Sutherland LB, Richardson JA, and Bassel-Duby R, O. E. (2007) An intragenic MEF2-dependent enhancer directs muscle-specific expression of microRNAs 1 and 133. *Proc Natl Acad Sci USA* **104**, 20844–20849
188. Liu, N., Shelton, J. M., Frisard, M. I., Hulver, M. W., McMillan, R. P., Wu, Y., Voelker, K. A., Grange, R. W., Richardson, J. A., Bassel-Duby, R., and Olson, E. N. (2011) Mice lacking microRNA 133a develop dynamin 2-dependent centronuclear myopathy. *J Clin Invest* **121**, 3258–3268
189. Liu, N., Bezprozvannaya, S., Williams, A., Qi, X., Richardson, J., R, B.-D., and EN., O. (2008) microRNA-133a regulates cardiomyocyte proliferation and suppresses smooth muscle gene expression in the heart. *Genes Dec* **22**, 3242-3254
190. Wang, N. S., Unkila, M. T., Reineks, E. Z., and Distelhorst, C. W. (2001) Transient Expression of Wild-type or Mitochondrially Targeted Bcl-2 Induces Apoptosis, whereas Transient Expression of Endoplasmic Reticulum-targeted Bcl-2 Is Protective against Bax-induced Cell Death. *Journal of Biological Chemistry* **276**, 44117-44128
191. Potthoff, M. J., and Olson, E. N. (2007) MEF2: a central regulator of diverse developmental programs. *Development* **134**, 4131–4140
192. Li, S., McAnally, J., Bassel-Duby, R., Richardson, J. A., Wiebel, F. F., Nordheim, A., and Olson, E. N. (2005) Requirement for serum response factor for skeletal muscle growth and maturation revealed by tissue-specific gene deletion in mice. *Proc Natl Acad Sci USA* **102**, 1082–1087
193. Florini, J. R., Ewton DZ Fau - Magri, K. A., and Magri, K. A. (1991) Hormones, growth factors, and myogenic differentiation. *Annu Rev Physiol* **53**, 201–216
194. Harvey, R. P. (2002) Patterning the vertebrate heart. *Nat Rev Genet* 544–556
195. Owens, G. K., Kumar MS and Wamhoff, B. R., and Wamhoff, B. R. (2004) Molecular regulation of vascular smooth muscle cell differentiation in development and disease. *Physiol Rev* **84**, 767–801
196. Bayol, S. A., Simbi BH Stickland, N C. (2005) A maternal cafeteria diet during gestation and lactation promotes adiposity and impairs skeletal muscle development and metabolism in rat offspring at weaning. *The Journal of Physiology* 951-956
197. Pereira, T. J., Fonseca, M. A., Campbell, K. E., Moyce, B. L., Cole, L. K., Hatch, G. M., Doucette, C. A., Klein, J., Aliani, M., and Dolinsky, V. W. (2015) Maternal obesity characterized by gestational diabetes increases the susceptibility of rat offspring to

hepatic steatosis via a disrupted liver metabolome. *The Journal of Physiology*, **593**, 3181-3197
198. Parker, M. H., Seale P, and Rudnicki, M. A. (2003) Looking back to the embryo: defining transcriptional networks in adult myogenesis. *Nat Rev Genet* **4**, 497–507
199. Kelly, R. G. (2005) Molecular inroads into the anterior heart field. *Trends Cardiovasc Med* **14**, 51-56
200. Majesky, M. W. (2007) Developmental basis of vascular smooth muscle diversity. *Arterioscler Thromb Vasc Biol* **27**, 1248-1258
201. Potthoff, M. J., H., W., Arnold, M. A., Shelton, J. M., Backs, J., McAnally, John, Richardson, J. A., and Bassel-Duby, R. O., Eric N. (2007) Histone deacetylase degradation and MEF2 activation promote the formation of slow-twitch myofibers. *J Clin Invest* **117**, 2459–2467
202. Cox, DM., Du, M., Marback, M., Yang, EC.,Chan, J., Siu, KW., and McDermott, JC. (2003) Phosphorylation motifs regulating the stability and function of myocyte enhancer factor 2A. *J Biol Chem* **278**, 15297–15303
203. Rampalli, S., F, L. L., Mak, E., Ge, K., Brand, M., Tapscott, S. J., and Dilworth, F. J. (2007) p38 MAPK signaling regulates recruitment of Ash2L-containing methyltransferase complexes to specific genes during differentiation. *Nat Struct Mol Biol* **14**, 1150–1156
204. Miano, J. M. (2003) Serum response factor: toggling between disparate programs of gene expression. *J Mol Cell Cardiol* **35**, 577-593
205. Torella, D., Catalucci, D., Ellison, G. M., Leone, A., Waring, C. D., Bochicchio, A., Vicinanza, C., Aquila, I., Curcio, A., Condorelli, G., and Indolfi, C. (2011) MicroRNA-133 controls vascular smooth muscle cell phenotypic switch in vitro and vascular remodeling in vivo. *Circ Res* **106**, 880- 893
206. Coll, T., Rodriguez-Calvo, R., Eyre, E., Palomer, X., Sanchez, R. M., Merlos, M., Laguna, J. C., and Vazquez-Carrera, M. (2006) Palmitate-mediated downregulation of peroxisome proliferator-activated receptor-gamma coactivator 1alpha in skeletal muscle cells involves MEK1/2 and nuclear factor-kappaB activation. *55*, 2779-2787
207. Gordon JW, D. V., Mughal W, Gordon GRJ, McGavock J. (2015) **Targeting skeletal muscle mitochondria to prevent type 2 diabetes in youth.** . *Biochem Cell Biol*, 1-14
208. Wheaton, K., and Riabowol, K. (2004) Protein kinase C delta blocks immediate-early gene expression in senescent cells by inactivating serum response factor. *Mol Cell Biol* **24**, 7298-7311
209. Zhang, J., and Ney, P. A. (2009) Role of BNIP3 and NIX in cell death, autophagy, and mitophagy. *Cell Death Differ* **16**, 939-946
210. Zhang, W., Morris, Q. D., Chang, R., Shai, O., Bakowski, M. A., Mitsakakis, N., Mohammad, N., Robinson, M. D., Zirngibl, R., Somogyi, E., Laurin, N., Eftekharpour, E., Sat, E., Grigull, J., Pan, Q., Peng, W.-T., Krogan, N., Greenblatt, J., Fehlings, M., van der Kooy, D., Aubin, J., Bruneau, B. G., Rossant, J., Blencowe, B. J., Frey, B. J., and Hughes, T. R. (2004) The functional landscape of mouse gene expression. *Journal of Biology* **3**, 21
211. RL, P., C, Y., N, S., J, S., M, M., L, N., H, I., J, C., JW, G., and JC., M. (2009) Direct interaction between myocyte enhancer factor 2 (MEF2) and protein phosphatase 1alpha represses MEF2-dependent gene expression. *Mol Cell Biol* **29**, 3355-3366

212. McDermott, J. C., Cardoso Mc Fau - Yu, Y. T., Yu Yt Fau - Andres, V., Andres V Fau - Leifer, D., Leifer D Fau - Krainc, D., Krainc D Fau - Lipton, S. A., Lipton Sa Fau - Nadal-Ginard, B., and Nadal-Ginard, B. (1993) hMEF2C gene encodes skeletal muscle- and brain-specific transcription factors. *Mol Cell Biol* **13**, 2564-2577
213. Pagiatakis, C., JW, G., Ehyai, S., and McDermott, J. C. (2012) A novel RhoA/ROCK-CPI-17-MEF2C signaling pathway regulates vascular smooth muscle cell gene expression. *J Biol Chem* **287**, 8361-8370
214. Chiang, H. R., Schoenfeld Lw Fau - Ruby, J. G., Ruby Jg Fau - Auyeung, V. C., Auyeung Vc Fau - Spies, N., Spies N Fau - Baek, D., Baek D Fau - Johnston, W. K., Johnston Wk Fau - Russ, C., Russ C Fau - Luo, S., Luo S Fau - Babiarz, J. E., Babiarz Je Fau - Blelloch, R., Blelloch R Fau - Schroth, G. P., Schroth Gp Fau - Nusbaum, C., Nusbaum C Fau - Bartel, D. P., and Bartel, D. P. (2010) Mammalian microRNAs: experimental evaluation of novel and previously annotated genes. *Genes Dev* **24**, 992-1009
215. Medjkane, S., Perez-Sanchez C Fau - Gaggioli, C., Gaggioli C Fau - Sahai, E., Sahai E Fau - Treisman, R., and Treisman, R. (2009) Myocardin-related transcription factors and SRF are required for cytoskeletal dynamics and experimental metastasis. *Nat Cell Biol* **11**, 257-268
216. Fei, P., Wang W Fau - Kim, S.-h., Kim Sh Fau - Wang, S., Wang S Fau - Burns, T. F., Burns Tf Fau - Sax, J. K., Sax Jk Fau - Buzzai, M., Buzzai M Fau - Dicker, D. T., Dicker Dt Fau - McKenna, W. G., McKenna Wg Fau - Bernhard, E. J., Bernhard Ej Fau - El-Deiry, W. S., and El-Deiry, W. S. (2004) Bnip3L is induced by p53 under hypoxia, and its knockdown promotes tumor growth. *Cancer Cell* **6**, 597-609
217. Wang, N. S., Unkila Mt Fau - Reineks, E. Z., Reineks Ez Fau - Distelhorst, C. W., and Distelhorst, C. W. (2001) Transient expression of wild-type or mitochondrially targeted Bcl-2 induces apoptosis, whereas transient expression of endoplasmic reticulum-targeted Bcl-2 is protective against Bax-induced cell death. *J Biol Chem* **276**, 44117-44128
218. Gosens, R., Gl, S., Dueck, G., McNeill, K. D., Yamasaki, A., Gerthoffer, W. T., Unruh, H., Gounni, A. S., Zaagsma, J., and Halayko, A. J. Role of caveolin-1 in p42/p44 MAP kinase activation and proliferation of human airway smooth muscle. *Am J Physiol Lung Cell Mol Physiol* L523-534
219. Chavez, J. A., and Summers, S. A. (2003) Characterizing the effects of saturated fatty acids on insulin signaling and ceramide and diacylglycerol accumulation in 3T3-L1 adipocytes and C2C12 myotubes. *Archives of Biochemistry and Biophysics* **419**, 101-109
220. Cheung, K., LK, C., B, X., K2, C., X, M., Y, M., GM1, H., Q, T., and VW, D. (2015) Sirtuin-3 (SIRT3) Protein Attenuates Doxorubicin-induced Oxidative Stress and Improves Mitochondrial Respiration in H9c2 Cardiomyocytes. *J Biol Chem* **290**, 10981-10993
221. Dolinsky, V. W., CF, R.-C., Morton, J. S., Davidge, S. T., and Dyck, J. R. B. (2011) Continued postnatal administration of resveratrol prevents diet-induced metabolic syndrome in rat offspring born growth restricted. *Diabetes* **60**, 2274-2284
222. Du, M., R, P., Nowacki, N. B., Gordon, J. W., Salma, J., Zhao, J., Aziz, A., Chan, J., Siu, K. W. M., and McDermott, J. C. (2008) Protein kinase A represses skeletal myogenesis by targeting myocyte enhancer factor 2D. *Mol Cell Biol* **28**, 2952-2970

223. Chen, S., P, P., Feng, B., Matkovich, S. J., Dorn, G. W., 2nd, and Chakrabarti, S. (2014) Cardiac miR-133a overexpression prevents early cardiac fibrosis in diabetes. *J Cell Mol Med* **18**, 415-421
224. Chen, J.-F., Mandel, E. M., Thomson, J. M., Wu, Q., Callis, T. E., Hammond, S. M., Conlon, F. L., and Wang, D.-Z. (2005) The role of microRNA-1 and microRNA-133 in skeletal muscle proliferation and differentiation. *Nature Genetics* **38**, 228
225. Clark, Rebecca I., Tan, Sharon W., Péan, Claire B., Roostalu, U., Vivancos, V., Bronda, K., Pilátová, M., Fu, J., Walker, David W., Berdeaux, R., Geissmann, F., and Dionne, Marc S. (2013) MEF2 Is an In Vivo Immune-Metabolic Switch. *Cell* **155**, 435-447
226. Ornatsky, O., DM, C., P, T., JJ, A., ZA, Q., JL, W., R, P., YT, Y., and JC., M. (1999) Post-translational control of the MEF2A transcriptional regulatory protein. *Nuclei Acids Res* **27**, 2646-2654
227. Chen, Y., Lewis, W., Diwan, A., Cheng, E., SJ, M., and 2nd., D. G. (2010) Dual autonomous mitochondrial cell death pathways are activated by Nix/BNip3L and induce cardiomyopathy. . *Proc Natl Acad Sci USA* **107**, 9035-9042
228. Schweers, R., Zhang, J., Randall, M., Loyd, M., W, L., FC, D., M, K., JT, O., JL, C., JL, M., and PA., N. (2007) NIX is required for programmed mitochondrial clearance during reticulocyte maturation. . *Proc Natl Acad Sci USA* **104**, 19500-19505
229. Matkovich, S. J., W, W., Tu, Y., Eschenbacher, W. H., Dorn, L. E., Condorelli, G., Diwan, A., Nerbonne, J. M., and Dorn, G. W., 2nd. (2010) MicroRNA-133a protects against myocardial fibrosis and modulates electrical repolarization without affecting hypertrophy in pressure-overloaded adult hearts. *Circ Res* **106**, 166-175
230. Yussman, M. G., T, T., Odley, A., Lynch, R. A., Wu, G., Colbert, M. C., Aronow, B. J., Lorenz, J. N., and Dorn, G. W., 2nd. (2002) Mitochondrial death protein Nix is induced in cardiac hypertrophy and triggers apoptotic cardiomyopathy. *Nat Med*
231. Carè, A., Catalucci, D., Felicetti, F., Bonci, D., Addario, A., Gallo, P., Bang, M.-L., Segnalini, P., Gu, Y., Dalton, N. D., Elia, L., Latronico, M. V. G., Høydal, M., Autore, C., Russo, M. A., Dorn Ii, G. W., Ellingsen, Ø., Ruiz-Lozano, P., Peterson, K. L., Croce, C. M., Peschle, C., and Condorelli, G. (2007) MicroRNA-133 controls cardiac hypertrophy. *Nature Medicine* **13**, 613
232. Gordon, J. (2017) Regulation of cardiac myocyte cell death and differentiation by myocardin. *Mol Cell Biochem*
233. Ieda, M., Fu, J.-D., Delgado-Olguin, P., Vedantham, V., Hayashi, Y., Bruneau, B. G., and Srivastava, D. (2010) Direct Reprogramming of Fibroblasts into Functional Cardiomyocytes by Defined Factors. *Cell* **142**, 375-386
234. Barth, E., Stämmler, G., Speiser, B., and Schaper, J. Ultrastructural quantitation of mitochondria and myofilaments in cardiac muscle from 10 different animal species including man. *Journal of Molecular and Cellular Cardiology* **24**, 669-681
235. Izzo, V., Bravo-San Pedro, J. M., Sica, V., Kroemer, G., and Galluzzi, L. (2016) Mitochondrial Permeability Transition: New Findings and Persisting Uncertainties. *Trends in Cell Biology* **26**, 655-667
236. Karch, J., Kwong, J. Q., Burr, A. R., Sargent, M. A., Elrod, J. W., Peixoto, P. M., Martinez-Caballero, S., Osinska, H., Cheng, E. H. Y., Robbins, J., Kinnally, K. W., and Molkentin, J. D. (2013) Bax and Bak function as the outer membrane component of the mitochondrial permeability pore in regulating necrotic cell death in mice. *eLife* **2**, e00772

237. Pérez, M. J., and Quintanilla, R. A. (2017) Development or disease: duality of the mitochondrial permeability transition pore. *Developmental Biology* **426**, 1-7
238. Baines, C. P., Kaiser, R. A., Purcell, N. H., Blair, N. S., Osinska, H., Hambleton, M. A., Brunskill, E. W., Sayen, M. R., Gottlieb, R. A., Dorn Ii, G. W., Robbins, J., and Molkentin, J. D. (2005) Loss of cyclophilin D reveals a critical role for mitochondrial permeability transition in cell death. *Nature* **434**, 658
239. Kwong, Jennifer Q., Lu, X., Correll, Robert N., Schwanekamp, Jennifer A., Vagnozzi, Ronald J., Sargent, Michelle A., York, Allen J., Zhang, J., Bers, Donald M., and Molkentin, Jeffery D. (2015) The Mitochondrial Calcium Uniporter Selectively Matches Metabolic Output to Acute Contractile Stress in the Heart. *Cell Reports* **12**, 15-22
240. Luongo, Timothy S., Lambert, Jonathan P., Yuan, A., Zhang, X., Gross, P., Song, J., Shanmughapriya, S., Gao, E., Jain, M., Houser, Steven R., Koch, Walter J., Cheung, Joseph Y., Madesh, M., and Elrod, John W. (2015) The Mitochondrial Calcium Uniporter Matches Energetic Supply with Cardiac Workload during Stress and Modulates Permeability Transition. *Cell Reports* **12**, 23-34
241. Dorn, G. W., II. (2011) Nix Nought Nothing: Fairy tale or real deal. *Journal of Molecular and Cellular Cardiology* **51**, 497-500
242. Dorn Ii, G. W., and Kirshenbaum, L. A. (2009) Cardiac reanimation: targeting cardiomyocyte death by BNIP3 and NIX/BNIP3L. *Oncogene* **27**, S158
243. Chen, G., Cizeau, J., Vande Velde, C., Park, J. H., Bozek, G., Bolton, J., Shi, L., Dubik, D., and Greenberg, A. (1999) Nix and Nip3 Form a Subfamily of Pro-apoptotic Mitochondrial Proteins. *Journal of Biological Chemistry* **274**, 7-10
244. Vande Velde, C., Cizeau, J., Dubik, D., Alimonti, J., Brown, T., Israels, S., Hakem, R., and Greenberg, A. H. (2000) BNIP3 and Genetic Control of Necrosis-Like Cell Death through the Mitochondrial Permeability Transition Pore. *Molecular and Cellular Biology* **20**, 5454-5468
245. Diwan, A., Matkovich, S. J., Yuan, Q., Zhao, W., Yatani, A., Brown, J. H., Molkentin, J. D., Kranias, E. G., and Dorn, G. W. (2008) Endoplasmic reticulum-mitochondria crosstalk in NIX-mediated murine cell death. *Journal of Clinical Investigation*
246. Mughal, W., Nguyen, L., Pustylnik, S., da Silva Rosa, S. C., Piotrowski, S., Chapman, D., Du, M., Alli, N. S., Grigull, J., Halayko, A. J., Aliani, M., Topham, M. K., Epand, R. M., Hatch, G. M., Pereira, T. J., Kereliuk, S., McDermott, J. C., Rampitsch, C., Dolinsky, V. W., and Gordon, J. W. (2015) A conserved MADS-box phosphorylation motif regulates differentiation and mitochondrial function in skeletal, cardiac, and smooth muscle cells. *Cell Death & Disease* **6**, e1944
247. Yoshida, T., Sinha, S., Dandré, F., Wamhoff, B. R., Hoofnagle, M. H., Kremer, B. E., Wang, D.-Z., Olson, E. N., and Owens, G. K. (2003) Myocardin Is a Key Regulator of CArG-Dependent Transcription of Multiple Smooth Muscle Marker Genes. *Circulation Research* **92**, 856
248. Kotera, I., Iwasaki, T., Imamura, H., Noji, H., and Nagai, T. (2010) Reversible Dimerization of Aequorea victoria Fluorescent Proteins Increases the Dynamic Range of FRET-Based Indicators. *ACS Chemical Biology* **5**, 215-222
249. Wu, J., Prole, David L., Shen, Y., Lin, Z., Gnanasekaran, A., Liu, Y., Chen, L., Zhou, H., Chen, S. R W., Usachev, Yuriy M., Taylor, Colin W., and Campbell, Robert E. (2014) Red fluorescent genetically encoded Ca(2+) indicators for use in mitochondria and endoplasmic reticulum. *Biochemical Journal* **464**, 13-22

250. Wu, J., Liu, L., Matsuda, T., Zhao, Y., Rebane, A., Drobizhev, M., Chang, Y.-F., Araki, S., Arai, Y., March, K., Hughes, T. E., Sagou, K., Miyata, T., Nagai, T., Li, W.-h., and Campbell, R. E. (2013) Improved Orange and Red Ca2+ Indicators and Photophysical Considerations for Optogenetic Applications. *ACS Chemical Neuroscience* **4**, 963-972
251. Ghavami, S., Cunnington, R. H., Gupta, S., Yeganeh, B., Filomeno, K. L., Freed, D. H., Chen, S., Klonisch, T., Halayko, A. J., Ambrose, E., Singal, R., and Dixon, I. M. C. (2015) Autophagy is a regulator of TGF-β1-induced fibrogenesis in primary human atrial myofibroblasts. *Cell Death &Amp; Disease* **6**, e1696
252. Dixon, I. M., Lee, S. L., and Dhalla, N. S. (1990) Nitrendipine binding in congestive heart failure due to myocardial infarction. *Circulation Research* **66**, 782
253. Zong, W. X., and Thompson, C. B. (2009) Necrotic death as a cell fate. *Genes Dev* **20**, 1-15
254. Rong, Y.-P., Aromolaran, A. S., Bultynck, G., Zhong, F., Li, X., McColl, K., Matsuyama, S., Herlitze, S., Roderick, H. L., Bootman, M. D., Mignery, G. A., Parys, J. B., De Smedt, H., and Distelhorst, C. W. (2008) Targeting Bcl-2-IP3 Receptor Interaction to Reverse Bcl-2's Inhibition of Apoptotic Calcium Signals. *Molecular cell* **31**, 255-265
255. Chen, R., Valencia, I., Zhong, F., McColl, K. S., Roderick, H. L., Bootman, M. D., Berridge, M. J., Conway, S. J., Holmes, A. B., Mignery, G. A., Velez, P., and Distelhorst, C. W. (2004) Bcl-2 functionally interacts with inositol 1,4,5-trisphosphate receptors to regulate calcium release from the ER in response to inositol 1,4,5-trisphosphate. *The Journal of Cell Biology* **166**, 193
256. Diwan, A., Wansapura, J., Syed, F. M., Matkovich, S. J., Lorenz, J. N., and Dorn, G. W. (2008) Nix-Mediated Apoptosis Links Myocardial Fibrosis, Cardiac Remodeling, and Hypertrophy Decompensation. *Circulation*
257. Murgia, M., Giorgi C Fau - Pinton, P., Pinton P Fau - Rizzuto, R., and Rizzuto, R. (2009) Controlling metabolism and cell death: at the heart of mitochondrial calcium signalling. *J Mol Cell Cardiol* **46**
258. Pinton, P., Giorgi, C., Siviero, R., Zecchini, E., and Rizzuto, R. (2008) Calcium and apoptosis: ER-mitochondria Ca2+ transfer in the control of apoptosis. *Oncogene* **27**, 6407
259. Sardão, V. A., Oliveira, P. J., Holy, J., Oliveira, C. R., and Wallace, K. B. (2007) Vital imaging of H9c2 myoblasts exposed to tert-butylhydroperoxide – characterization of morphological features of cell death. *BMC Cell Biology* **8**, 11
260. Watkins, S. J., Borthwick, G. M., and Arthur, H. M. (2011) The H9C2 cell line and primary neonatal cardiomyocyte cells show similar hypertrophic responses in vitro. *In Vitro Cellular & Developmental Biology - Animal* **47**, 125-131
261. Zordoky, B. N. M., and El-Kadi, A. O. S. (2007) H9c2 cell line is a valuable in vitro model to study the drug metabolizing enzymes in the heart. *Journal of Pharmacological and Toxicological Methods* **56**, 317-322
262. Hashimoto, H., Olson, E. N., and Bassel-Duby, R. (2018) Therapeutic approaches for cardiac regeneration and repair. *Nature Reviews Cardiology*
263. Burridge, P. W., and Zambidis, E. T. (2013) Highly Efficient Directed Differentiation of Human Induced Pluripotent Stem Cells into Cardiomyocytes. in *Pluripotent Stem Cells: Methods and Protocols* (Lakshmipathy, U., and Vemuri, M. C. eds.), Humana Press, Totowa, NJ. pp 149-161
264. Deng, Z., Chen, J.-F., and Wang, D.-Z. (2011) Transgenic overexpression of miR-133a in skeletal muscle. *BMC Musculoskeletal Disorders* **12**, 115

265. Koutsoulidou, A., Mastroyiannopoulos, N. P., Furling, D., Uney, J. B., and Phylactou, L. A. (2011) Expression of miR-1, miR-133a, miR-133b and miR-206 increases during development of human skeletal muscle. *BMC Developmental Biology* **11**, 34
266. Shen, X., Soibam, B., Benham, A., Xu, X., Chopra, M., Peng, X., Yu, W., Bao, W., Liang, R., Azares, A., Liu, P., Gunaratne, P. H., Mercola, M., Cooney, A. J., Schwartz, R. J., and Liu, Y. (2016) miR-322/-503 cluster is expressed in the earliest cardiac progenitor cells and drives cardiomyocyte specification. *Proceedings of the National Academy of Sciences* **113**, 9551
267. Malhotra, J. D., and Kaufman, R. J. (2011) ER Stress and Its Functional Link to Mitochondria: Role in Cell Survival and Death. *Cold Spring Harbor Perspectives in Biology* **3**, a004424
268. Wang, C.-H., and Wei, Y.-H. (2017) Role of mitochondrial dysfunction and dysregulation of Ca(2+) homeostasis in the pathophysiology of insulin resistance and type 2 diabetes. *Journal of Biomedical Science* **24**, 70
269. Deegan, S., Koryga, I., Glynn, S. A., Gupta, S., Gorman, A. M., and Samali, A. (2015) A close connection between the PERK and IRE arms of the UPR and the transcriptional regulation of autophagy. *Biochemical and Biophysical Research Communications* **456**, 305-311
270. Huang, J., Wang, T., Wright, A. C., Yang, J., Zhou, S., Li, L., Yang, J., Small, A., and Parmacek, M. S. (2015) Myocardin is required for maintenance of vascular and visceral smooth muscle homeostasis during postnatal development. *Proceedings of the National Academy of Sciences* **112**, 4447
271. Thomas, R. L., and Gustafsson, Å. B. (2013) MCL1 is critical for mitochondrial function and autophagy in the heart. *Autophagy* **9**, 1902-1903
272. Masters, S. C., Yang, H., Datta, S. R., Greenberg, M. E., and Fu, H. (2001) 14-3-3 Inhibits Bad-Induced Cell Death through Interaction with Serine-136. *Molecular Pharmacology* **60**, 1325
273. Clapp, C., Portt, L., Khoury, C., Sheibani, S., Norman, G., Ebner, P., Eid, R., Vali, H., Mandato, C. A., Madeo, F., and Greenwood, M. T. (2012) 14-3-3 Protects against stress-induced apoptosis. *Cell Death &Amp; Disease* **3**, e348
274. Jasinski-Bergner, S., Stehle, F., Gonschorek, E., Kalich, J., Schulz, K., Huettelmaier, S., Braun, J., and Seliger, B. (2014) Identification of 14-3-3β Gene as a Novel miR-152 Target Using a Proteome-based Approach. *The Journal of Biological Chemistry* **289**, 31121-31135
275. Otsu, K., Murakawa, T., and Yamaguchi, O. (2015) BCL2L13 is a mammalian homolog of the yeast mitophagy receptor Atg32. *Autophagy* **11**, 1932-1933
276. Nakazawa, M., Matsubara, H., Matsushita, Y., Watanabe, M., Vo, N., Yoshida, H., Yamaguchi, M., and Kataoka, T. (2016) The Human Bcl-2 Family Member Bcl-rambo Localizes to Mitochondria and Induces Apoptosis and Morphological Aberrations in Drosophila. *PLoS ONE* **11**, e0157823
277. Luo, Y., Xu, Y., Liang, C., Xing, W., and Zhang, T. (2018) The mechanism of myocardial hypertrophy regulated by the interaction between mhrt and myocardin. *Cellular Signalling* **43**, 11-20
278. Garcia-Vargas, L., Addison, S. S., Nistala, R., Kurukulasuriya, D., and Sowers, J. R. (2012) Gestational Diabetes and the Offspring: Implications in the Development of the Cardiorenal Metabolic Syndrome in Offspring. *Cardiorenal Medicine* **2**, 134-142

279. Lacroix, M., Kina, E., and Hivert, M.-F. (2013) Maternal/Fetal Determinants of Insulin Resistance in Women During Pregnancy and in Offspring Over Life. *Current Diabetes Reports* **13**, 238-244
280. Symonds, M. E., Mendez, M. A., Meltzer, H. M., Koletzko, B., Godfrey, K., Forsyth, S., and van der Beek, E. M. (2013) Early Life Nutritional Programming of Obesity: Mother-Child Cohort Studies. *Annals of Nutrition and Metabolism* **62**, 137-145
281. Vegter Eline, L., van der Meer, P., de Windt Leon, J., Pinto Yigal, M., and Voors Adriaan, A. (2016) MicroRNAs in heart failure: from biomarker to target for therapy. *European Journal of Heart Failure* **18**, 457-468
282. Suh, D. H., Kim, M.-K., Kim, H. S., Chung, H. H., and Song, Y. S. (2013) Mitochondrial permeability transition pore as a selective target for anti-cancer therapy. *Frontiers in Oncology* **3**, 41
283. Yuan, Y., Yao, Y. F., Hu, S. N., Gao, J., and Zhang, L.-L. (2015) MiR-133a Is Functionally Involved in Doxorubicin-Resistance in Breast Cancer Cells MCF-7 via Its Regulation of the Expression of Uncoupling Protein 2. *PLoS ONE* **10**, e0129843
284. Boon, R. A., Iekushi, K., Lechner, S., Seeger, T., Fischer, A., Heydt, S., Kaluza, D., Tréguer, K., Carmona, G., Bonauer, A., Horrevoets, A. J. G., Didier, N., Girmatsion, Z., Biliczki, P., Ehrlich, J. R., Katus, H. A., Müller, O. J., Potente, M., Zeiher, A. M., Hermeking, H., and Dimmeler, S. (2013) MicroRNA-34a regulates cardiac ageing and function. *Nature* **495**, 107
285. Grueter, Chad E., van Rooij, E., Johnson, Brett A., DeLeon, Susan M., Sutherland, Lillian B., Qi, X., Gautron, L., Elmquist, Joel K., Bassel-Duby, R., and Olson, Eric N. A Cardiac MicroRNA Governs Systemic Energy Homeostasis by Regulation of MED13. *Cell* **149**, 671-683